Connections Between Inositol Phosphate Signaling and Energy Responses in Plants

Sarah Phoebe Williams

Dissertation submitted to the faculty of the Virginia Polytechnic Institute and State University in partial fulfillment of the requirements for the degree of

Doctor of Philosophy
In
Biochemistry

Glenda Gillaspy, Chair
Eric Beers
Maria Belen Cassera
Zhijian Tu

October 28, 2015
Blacksburg, VA

Keywords:
Energy, $InsP_6$, $InsP_7$, Inositol, Inositol Phosphate, Inositol Pyrophosphate, Phytic Acid, Sucrose Non-Fermenting Related Kinase (SnRK1), sugar-sensing, VIP

Connections Between Inositol Phosphate Signaling and Energy Responses in Plants

Sarah Phoebe Williams

ABSTRACT

The ability for an organism to sense and respond appropriately to its environment is often critical for survival. One mechanism for this is the inositol phosphate (InsP) signaling pathway. This work focuses on the role of InsP signaling in maintaining energy homeostasis in the plant. InsP signaling is connected to energy sensing in plants via a protein complex containing both the inositol polyphosphate 5-phosphatases (5PTase13) and the Sucrose non-Fermenting Related Kinase 1 (SnRK1). SnRK1 is considered a fuel gauge for the plant cell that senses energy status and reprograms growth appropriately. While the *SnRK1.1* gene has been well studied, the role other SnRK1 isoforms play in energy or stress signaling is less well understood. This work examined the role of 3 SnRK1 isoforms in energy signaling, finding that SnRK1.1 and SnRK1.2 are regulated and function differently in Arabidopsis. The second part of this work focuses on the inositol pyrophosphates, which are a novel group of InsP signaling molecules containing diphosphate or triphosphate chains (i.e. PPx) attached to the inositol ring. These PPx-InsPs are emerging as critical players in the integration of cellular metabolism and stress signaling in non-plant eukaryotes. Most eukaryotes synthesize the precursor molecule, *myo*-inositol (1,2,3,4,5,6)-hexakisphosphate ($InsP_6$), which can serve as a signaling molecule or as storage compound of inositol, phosphorus, and minerals. Even though plants produce huge amounts of $InsP_6$ in seeds, almost no attention has been paid to whether PPx-InsPs exist in plants, and if so, what roles these

molecules play. This work details the presence of PPx-InsPs in plants and delineates two Arabidopsis gene products (*AtVip1* and *AtVip2*) capable of PP-$InsP_5$ synthesis. We further examined the subcellular location of enzymes connected to PPx-InsP synthesis as well as the developmental and tissue specific patterns of expression of the genes that encode these enzymes. We localized the enzymes involved in $InsP_6$ and PPx-InsP production to the nucleus and endoplasmic reticulum (ER). The subcellular compartmentalization of PPx-InsP signaling may be unique to plants. An increased understanding in the pathways involved in energy sensing and metabolic response may reveal novel strategies to improve crops for yield and viability in the future.

ACKNOWLEDGEMENTS

I would like to gratefully acknowledge the following people:

Glenda Gillaspy for her mentorship both as a scientist and as an educator. The Gillaspy lab members, especially Janet, Jiun, and Padma, for both good times and hard work in the lab. The Molecular Plant Sciences Community and the Biochemistry department for providing just a supportive environment. Our collaborators, Imara Perera and Victoy Raboy for sharing their expertise.

FUNDING

I would like to acknowledge the following sources of support for my graduate education:

the Institute for Critical Technology and Applied Sciences (ICTAS) Doctoral Fellowship, the Department of Biochemistry, and the Molecular Plant Sciences Program.

I would like to acknowledge the following sources of support for this research:

Chapter I: This work was supported by a NSF collaborative grant (MCB1051646 to GG and MCB 1052034 to IYP) and a NIFA award (2013-02277 to GG and IYP).

Chapter II: This work was supported by a NSF grant (MCB1051646) and a NIFA award (2013-67013-21356) to GG

Chapter III: This research was supported by an NSF collaborative grant to GG, IYP and VR (MCB1051646), and a NIFA award to GG, IYP and BP (2013-02277), as well as an NSF-REU supplement (to PS).

Chapter IV: This work is supported by an NSF collaborative grant (MCB1051646).

ATTRIBUTIONS

Several colleagues contributed to the writing and research in several manuscripts presented as chapters in this dissertation.

Chapter I: "Biosynthesis and Possible Functions of Inositol Pyrophosphates in Plants", published in Frontiers in Plant Science, 2015.

Glenda Gillaspy, PhD (Gillaspy Lab, Department of Biochemistry) is currently head of the Biochemistry department at Virginia Tech. Dr. Gillaspy is a co-author on the paper, co-principal investigator for the grant supporting this work and contributed editorial comments on the manuscript.

Imara Perera, PhD (Perera Lab, Department of Plant and Microbial Biology, NCSU) is currently a professor at North Carolina State University. Dr. Perera was a co-author on this paper, co-principal investigator for the grant supporting this work and contributed editorial comments to the manuscript.

Chapter II: "Regulation of Sucrose Non-Fermenting Related Kinase 1 Genes in *Arabidopsis thaliana*", published in Frontiers in Plant Science, 2014.

Padma Rangarajan, MS (Gillaspy Lab, Department of Biochemistry) was a Masters student at Virginia Tech. Mrs. Rangarajan is a co-author on the paper and contributed to the molecular techniques used.

Janet Donahue, MS (Gillaspy Lab, Department of Biochemistry) is currently a senior Laboratory Specialist at Virginia Tech. Ms. Donahue is a co-author on the paper and contributed to the molecular techniques used.

Jenna Hess, MS (Gillaspy Lab, Department of Biochemistry) is currently the Director of Operations, Biosafety at WIRB-Copernicus Group. Ms. Hess is a co-author on the paper and contributed to the molecular techniques used.

Glenda Gillaspy, PhD (Gillaspy Lab, Department of Biochemistry) is currently head of the Biochemistry department at Virginia Tech. Dr. Gillaspy is a co-author on the paper, principal investigator for the grant supporting this work and wrote the manuscript.

Chapter III: "Two Inositol Hexakisphosphate Kinases Drive Inositol Pyrophosphate Synthesis in Plants", published in The Plant Journal, 2014.

Mintu Desai, PhD (Perera Lab, Department of Plant and Microbial Biology, NCSU) is currently a Research Scientist at Tyton BioEnergy Systems. Dr. Desai is a co-author on the paper and contributed to the molecular techniques used.

Padma Rangarajan, MS (Gillaspy Lab, Department of Biochemistry) was a Masters student at Virginia Tech. Mrs. Rangarajan is a co-author on the paper and contributed to the molecular techniques used.

Janet Donahue, MS (Gillaspy Lab, Department of Biochemistry) is currently a senior Laboratory Specialist at Virginia Tech. Mrs. Donahue is a co-author on the paper and contributed to the molecular techniques used.

Eric Land (Perera Lab, Department of Plant and Microbial Biology, NCSU) is currently a Laboratory Specialist at North Carolina State University. Mr. Land is a co-author on the paper and contributed to the molecular techniques used.

Mihir Mandal, PhD (Gillaspy Lab, Department of Biochemistry) is currently a Post-Doctoral Researcher at Virginia Tech in the lab of Jason Holliday. Dr. Mandal is a co-author on the paper and contributed to the molecular techniques used.

Brian Phillippy, PhD (Perera Lab, Department of Plant and Microbial Biology, NCSU) is a research scientist at North Carolina State University. Dr. Phillippy is a co-author on the paper and measured the mass levels on inositol phosphates in plants.

Victor Raboy, PhD (Raboy Lab, Agricultural Research Service-USDA) is currently a Research Geneticist with the ARS-USDA, Aberdeen, ID. Dr. Raboy is a co-author on the paper, co-principal investigator for the grant supporting this work and contributed to the molecular techniques used.

Imara Perera PhD (Perera Lab, Department of Plant and Microbial Biology) is currently a professor at North Carolina State University. Dr. Perera is a co-author on the paper and co-principal investigator for the grant supporting this work.

Glenda Gillaspy, PhD (Gillaspy Lab, Department of Biochemistry) is currently head of the Biochemistry department at Virginia Tech. Dr. Gillaspy is a co-author on the paper, co-principal investigator for the grant supporting this work and wrote the manuscript.

TABLE OF CONTENTS

LIST OF FIGURES

Chapter I:

Chapter II:

Chapter III:

Chapter IV:

LIST OF TABLES

TABLE OF ABBREVIATIONS

Ins	*myo*-inositol
PtdIns	Phosphatidylinositol
PtdInsP	Phosphatidylinositol Phosphate
PPx-InsP	Diphosphorylinositol Polyphosphates
InsP	Inositol Phosphate
Glu	Glucose
Suc	Sucrose
Man	Mannitol
Tre	Trehalose
SnRK1	Sucrose Non-Fermenting-1-Related Kinase
Snf1	Sucrose Non-Fermenting-1
WT	Wild Type
Ler	*Landsburg erecta*
qPCR	Quantitative PCR
qRT-PCR	Quantitative Real-Time Polymerase Chain Reaction
GFP	Green Fluorescent Protein
MS	Murashige & Skoog (plant culture salts)
GUS	β-glucuronidase
CaMV	Cauliflower Mosaic Virus
$InsP_6$	Inositol Hexakisphosphate, Phytate, Phytic Acid
$InsP_7$	Diphosphoinositol Pentakisphosphate
$InsP_8$	Bidiphosphoinositol Tetrakisphosphate, Triphosphoinositol Pentakisphosphate
PPx-InsP	Inositol Pyrophosphate
PLC	Phospholypase C
$Ins(1,4,5)P_3$	*myo*-Inositol-(1,4,5)-Triphosphate
HPLC	High-Performance Liquid Chromatography
ScVIP	Very Important Protein, HsPPIP5K, ScASP1, AtVIP
ScKSC1	Protein Kinase C Suppressor 1, HsIP6K
PAGE	Polyacrylamide Gel Electrophoresis
SDS-PAGE	Sodium Dodecyl Sulfate Polyacrylamide Gel Electrophoresis
ER	Endoplasmic Reticulum

CHAPTER I:

RATIONALE

Inherent to a plant's survival is its ability to sense and respond to its environment. As a sessile organism, this ability to respond appropriately to environmental and nutritional stress is vital to its ability to grow, develop and reproduce. Two potential regulators of energy homeostasis are the AMP-activated protein kinase (AMPK) and the inositol phosphate (InsP) signaling pathway. Understanding the function of these potential regulators in the sensing and response of plants to changing energy status can help identify targets for novel ways to increase plant survival, yield and even valued metabolite production.

The Sucrose-non-fermenting related kinase 1 (SnRK1) in plants (*1, 2*), and sucrose non-fermenting 1 (*SNF1*) and AMP-activated protein kinase (*AMPK*) in yeast and animals respectively, are considered as fuel gauge sensors of the eukaryotic cell (*3*). Much data in plants has suggested that the SnRK1 protein kinase functions in low energy conditions to reprogram metabolism through regulation of enzyme activity and transcription of target genes (*2*). In this way, SnRK1 functions as a regulator of the internal energy environment. Work from the Gillaspy lab has identified cross talk between the SnRK1 pathway and the InsP signaling pathway through the interaction of SnRK1 and inositol polyphosphate phosphatase 13 (5PTase13) (*4*). 5PTase13 dephosphorylates Ins(1,4,5)P_3, a product of phospholipase C (PLC). PLC and Ins(1,4,5)P_3 have been identified as critical players in the response to many stimuli , including, gravity (*5*), light (*6*) water (*7*), and energy status (*8, 9*).

The InsP signaling pathway consists of either soluble or lipid-bound species of *myo*-inositol, a 6 carbon ring, distinct in the number and position of phosphates on that ring (*10*). Each species is a specific signaling molecule, unique in the information it conveys (*10*). New players in InsP signaling are the inositol pyrophosphates (PPx-InsP). These molecules have diphosphate or triphosphate moieties on the inositol ring. This work delineates and measures the accumulation of PPx-InsPs in plants, as well as characterizing one class of enzymes capable of PPx-InsP synthesis. While the function of PPx-InsPs in plants is currently being investigated, in other eukaryotes these important signaling molecules are known to play a role in maintaining metabolic homeostasis (*11*).

OBJECTIVES

This work has four objectives: the first is to characterize the role of the SnRK1 isoforms in plant growth and energy response; the second is to identify inositol pyrophosphates in plants; the third is to characterize the enzymes that synthesize PPx-InsP in plants; and the fourth is to examine the spatial and temporal location of InsP signaling. The first objective is addressed in Chapter II, "Regulation of Sucrose Non-Fermenting Related Kinase 1 Genes in *Arabidopsis thaliana*". This chapter examines the differential expression of SnRK1.1 and SnRK1.2 in plants and investigates how different SnRK1 isoforms reprogram growth and development. The second and third objectives are addressed in Chapter III, "Two Inositol Hexakisphosphate Kinases Drive Inositol Pyrophosphate Synthesis in Plants". This chapter quantifies PPx-InsPs in plants, and characterizes a family of kinases (AtVIPs) capable of catalyzing PPx-InsP synthesis. The fourth objective is addressed in Chapter IV, "Distribution of PPx-InsP Synthesis and Degradation

Enzymes Across Cell Compartments". This chapter investigates the spatial regulation of the PPx-InsP synthesis and degradation pathways.

LITERATURE REVIEW

"Biosynthesis and Possible Functions of Inositol Pyrophosphates in Plants"

Adapted from: Sarah P. Williams, Glenda E. Gillaspy, Imara Y. Perera,

Frontiers in Plant Science (2015) vol 6:67. doi:10.3389/fpls.2015.00067

Contribution of Authors: Manuscript written by SPW, edited by GEG and IYP

Overview of Inositol Phosphate (InsP) Signaling

Myo-inositol (inositol) signaling is much like a language in that each molecular species used in the pathway, whether lipid or soluble in nature, can convey specific information to the cell, like a word. In this analogy, each combination of different numbers and positions of phosphates on the inositol ring and the presence of diacylglycerol linked via the C1 of inositol, also convey unique information (see **Figure 1.1**). Comprehensive analyses of both inositol and inositol phospholipids in signaling have been previously reviewed (*10, 12, 13*), so this review focuses on new InsP signaling molecules, the di- phospho (PP) and tri-phospho (PPP) inositol phosphates (PPx-InsPs), also known as inositol pyrophosphates. These high-energy molecules have been studied in non-plant eukaryotes, however, their existence and role in plants is newly emerging. The main questions regarding PPx-InsPs are: can these molecules be detected in plants, how are they synthesized and what type of information do they convey? Recent work addressing these questions will be discussed in the broader context of understanding how PPx-InsPs function in eukaryotes.

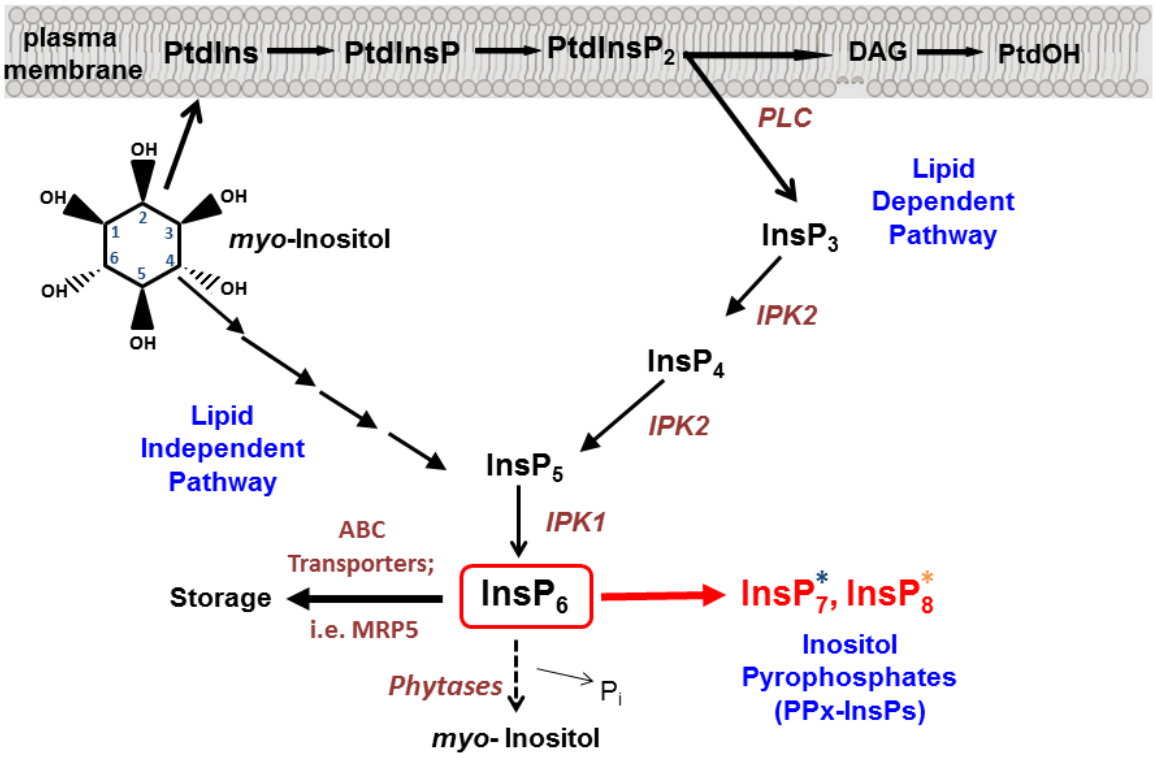

Figure 1.1. Synthesis of Inositol Pyrophosphates

Overview of the InsP signaling pathway, including both lipid dependent and lipid independent routes for synthesis of $InsP_6$. Inositol Pyrophosphate (PPx-InsP) synthesis is indicated in red. Major lipid and inositol species are indicated in black and key enzymes are indicated in brown. A more detailed outline of PPx-InsP synthesis is depicted in **Figure 1.2**. The blue and orange asterisks correspond to the colored boxes in **Figure 1.2**.

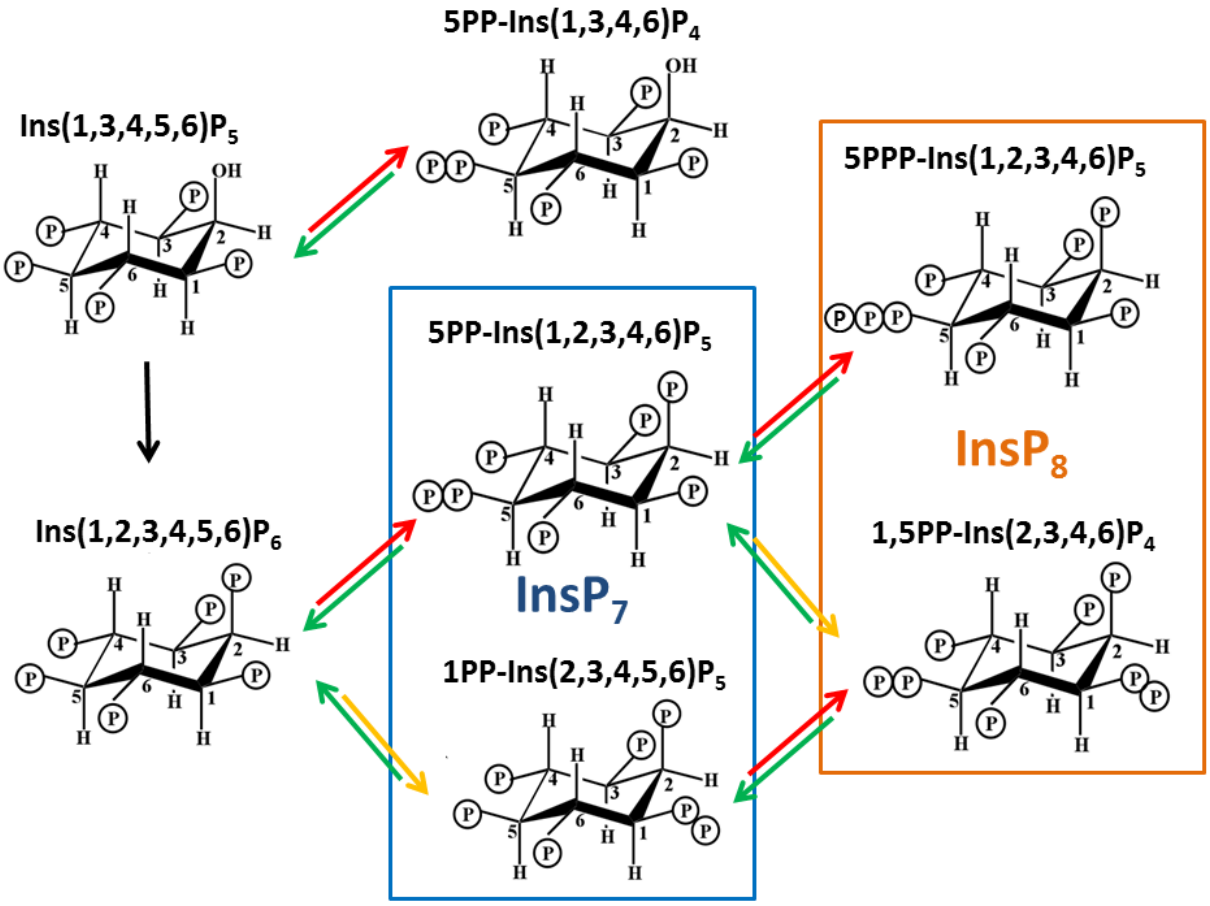

Figure 1.2. Structure of PPx-InsPs and Pathway of Proposed Synthesis

The unboxed area is the last step in $InsP_6$ synthesis, catalyzed by the IPK1 enzyme in plants. The boxed areas in blue and orange indicate $InsP_7$ and $InsP_8$ synthesis. The colored arrows indicate known enzymes in yeast. Red arrows indicate KCS1 activity, while yellow arrows indicate VIP activity. The green arrows indicate phosphatase activity by DDP1.

History and Structure of PPx-InsPs

PPx-InsPs were first identified in Dictyostelium in 1993 (*14-17*). They are similar to ATP and polyphosphates in that they contain a linear chain of two (PP) or three (PPP) phosphates separated by pyrophosphate bonds, linked to an InsP molecule (see **Figure 1.2**).

The PPx moieties at one or more positions on the inositol ring in PPx-InsPs are synthesized from $InsP_5$ or $InsP_6$ (*17, 18*), resulting in InsPs containing seven or eight phosphates (i.e. $InsP_7$ and $InsP_8$). The high energy pyrophosphate bonds present in PPx-InsPs may serve as a way to store energy in the cell, with the standard free energy of hydrolysis of $InsP_7$ and $InsP_8$ higher than that of ADP and ATP, respectively (*16*). Indeed, the initial role proposed for PPx-InsPs was simply as a high energy molecules, as they can be broken down to generate ATP (*19, 20*). However, PPx-InsPs are present at very low amounts and they have high turnover rates, suggesting that they serve as more than energy storage molecules (*14, 17*). Recently new physiological roles have been discovered for PPx-InsPs, supporting their role as dynamic and important signaling molecules.

Only a few of the theoretically possible PPx-InsP structures have been confirmed. The naming convention is to describe the position and number of the pyrophosphates first, followed by the name of the InsP. For example, Dictyostelium contains 6PP-$InsP_5$ and 5PP-$InsP_5$, and these contain a pyrophosphate on the 6th and 5th carbons of $InsP_5$, respectively. Dictyostelium also contains 5,4/6$(PP)_2$-$InsP_4$ or 1/3,5$(PP)_2$-$InsP_4$, and in these cases the slash indicates one of the pyrophosphates present can occur at *either* of two carbons (i.e. at the C4 or C6 position, or at C1 or C3, respectively). The ratios of these different PPx-InsPs differ in various Dictyostelium species examined (*21, 22*). Another member of the Amoebazoa kingdom, *Entamoeba histolytica*,

has further diversity in that a PPx-InsP was identified containing *neo*-inositol, rather than *myo*-inositol (*23*). This difference could produce even more diversity in the language of InsPs, but it is not yet known if this occurs in other organisms.

In Dictyostelium and the animal kingdom, PPx-InsPs synthesized from $InsP_5$ exist (*21, 22, 24*), however at present there is no data indicating they are found in plants. This review will focus on the PPx-InsP species synthesized from $InsP_6$. The most abundant $InsP_7$ isomer has been confirmed through NMR as 5PP-$InsP_5$ (*24, 25*). A second $InsP_7$ was first speculated to be pyrophosphorylated at C4 or C6 (i.e. 4/6), but was later conclusively identified as 1/3PP-$InsP_5$ (*26*). Recent work in animals has shown that the 1- rather than 3- position is phosphorylated, thus 1PP-$InsP_5$ is likely to be the second type of $InsP_7$ present in animals (*27*). Given this, we use 1PP-$InsP_5$ as the updated nomenclature for this second molecular species of $InsP_7$. Studies in yeast and humans identified that both of these $InsP_7$ molecules are present. The $InsP_8$ species confirmed are 1,5$(PP)_2$-$InsP_4$ (*in vivo*) and 5PPP-$InsP_5$ (*in vitro*) (*24, 26*).

Methods Used to Detect PPx-InsPs

Several methods have been used to detect PPx-InsPs, each having distinct strengths and limitations. The most common method is to introduce a radiolabeled precursor, often ^{3}H-*myo*-inositol or ^{3}H-$InsP_6$, followed by HPLC separation of InsP species produced after a given time (*28*). This method is very sensitive, but labor-intensive, and while it can resolve isomers of the lower InsPs, currently it is not possible to separate different PPx-InsP isomers. As well, one is limited to analysis of cells/tissues that can take up the radiolabeled precursor. However, this

method has an advantage in that one can be fairly certain of the identity of the resulting labeled peaks on the HPLC chromatograms. A nonradioactive high-performance anion-exchange chromatographic method based on metal dye detection (MDD)-HPLC can also be used to detect PPx-InsPs. The advantage of this method is that it can separate different isomers of $InsP_7$, however this method requires a 3 pump HPLC unit which increases the complexity of the system and limits its use (*29*). Another method of separation of InsPs is thin layer chromatography, which utilizes either radiolabeling or dye for detection of InsP species (*30*). This method, in general, does not have great sensitivity, and is most often used with purified PPx-InsPs.

Since acidic conditions can cause the degradation of PPx-InsPs, HPLC analyses may underestimate the amount of PPx-InsPs present (*31*). A new method developed to limit exposure of extracted PPx-InsPs to acid buffers is polyacrylamide gel separation by electrophoresis (PAGE), and subsequent staining with either DAPI or toluidine blue to detect InsPs (*31*). The PAGE technique is sensitive enough to visualize PPx-InsPs from cell/tissue extracts, and it can separate different $InsP_7$ and $InsP_8$ isomers. However, its distinct advantage is that it may allow for a better estimation of PPx-InsP abundance because of the speed of analysis. The disadvantage of using PAGE is that conclusive identification of stained “bands” as PPx-InsPs is best verified with a separate technology, as other molecules could be present and give rise to bands. It is important to note that co-migration with InsP and PPx-InsP standards is required for all of these methods, and follow-up NMR is needed to conclusively identify the specific structure of PPx-InsP species.

Plants Contain PPx-InsPs

Plants have large amounts of one of the precursors to PPx-InsPs, $InsP_6$, which is well studied as a phosphorous storage molecule (*32*). Given this, it seems likely that plants also synthesize the PPx-InsPs. Previous studies had noted InsP molecules more polar than $InsP_6$ in barley, duckweed, and potato (*33-36*). Acting on this information, we recently utilized both HPLC separation of radiolabeled plant tissues and PAGE to delineate the presence of $InsP_7$ and $InsP_8$ in higher plants including Arabidopsis, *Camelina sativa*, cotton, and maize (*37*). These two methods provided a complementary analysis of higher phosphorylated InsPs, including the PPx-InsPs. Since PPx-InsPs are low abundance molecules, it is not surprising that Arabidopsis seeds were found to contain less than 2% of the total inositol pool as inositol pyrophosphates (1.33% $InsP_7$, 0.24% $InsP_8$). Vegetative tissue from Arabidopsis was also analyzed and PPx-InsPs were found in both seedlings (0.64% $InsP_7$, 0.14% $InsP_8$) and mature leaves (1.00% $InsP_7$). $InsP_7$ was detected in other plant species as well, including another member of the Brassica family, *Camelina sativa* (1.40% in seedlings), and an unrelated dicot, cotton (*Gossypium hirsutum*) in the leaves and in shoots and roots of seedlings. PAGE analysis was used to detect PPx-InsPs in both Arabidopsis and maize seed in this same work (*37*). These findings indicate that PPx-InsPs may play a role during the plant life cycle throughout the plant kingdom, both in monocots and dicots.

Critical to our detection of the PPx-InsPs in plants was the use of a mutant containing elevated $InsP_7$ and $InsP_8$. The Multidrug Resistance associated Protein 5 (MRP5) is a high affinity ABC-binding cassette transporter that specifically binds to $InsP_6$ (*38*) (**Figure 1.1**). Studies on MRP5 have indicated the likely role of this transporter is in moving $InsP_6$ into the storage vacuole (*38*).

The subcellular localization of MRP5 has been reported as both the plasma membrane (*39*) and the vacuolar membrane (*38*), however it has been suggested that the plasma membrane localization is an artifact resulting from ectopic expression (*38*). MRP5 was first identified as an important player in stomatal responses, since guard cells of the loss-of-function *mrp5* mutant are insensitive to ABA and Ca^{2+} (*40*). This alteration in guard cell function results in reduction of water loss and use, allowing *mrp5* mutants some resistance to drought (*40*). The maize paralogue of MRP5 (called MRP4), results in decreased levels of $InsP_6$ in seeds when mutated (*38, 41*). Our recent study showed that in addition to decreased levels of $InsP_6$, *mrp5* mutants have elevated levels of $InsP_7$ and $InsP_8$ in seeds (*37*). These changes are less striking in vegetative tissue, perhaps as a result of overall lower levels of $InsP_6$ (*37*), or reduced MRP5 expression (*38*) in vegetative tissues. The guard cell phenotype of *mrp5* mutants has been attributed to an increase in cytosolic $InsP_6$, which could mobilize Ca^{2+}, leading to inhibition of inward rectifying K^+ channels, and changes in turgor pressure resulting in a decreased stomatal aperture (*36, 38, 42*). With the identification of elevated PPx-InsPs in *mrp5* mutants, an alternative hypothesis for alterations in *mrp5* guard cell signaling is that changes in $InsP_7$ and $InsP_8$ may be involved.

It should be noted that the recent study identifying PPx-InsPs in plants was not able to discern the enantiomers present (*37*). Thus it is not known whether plants contain 5PP-$InsP_7$ or 1PP-$InsP_7$ similar to yeast and animals, or (4/6)PP-$InsP_7$, similar to Dictyostelium. Efforts were made to purify the plant PPx-InsPs, however no informative NMR data was obtained (*37*). The identity of the plant isomers is key, and in itself may yield insights into the pathway, as different types of enzymes in other organisms give rise to specific PPx-InsP isomers. The following section describes this relationship between PPx-InsP synthesis and isomers in detail.

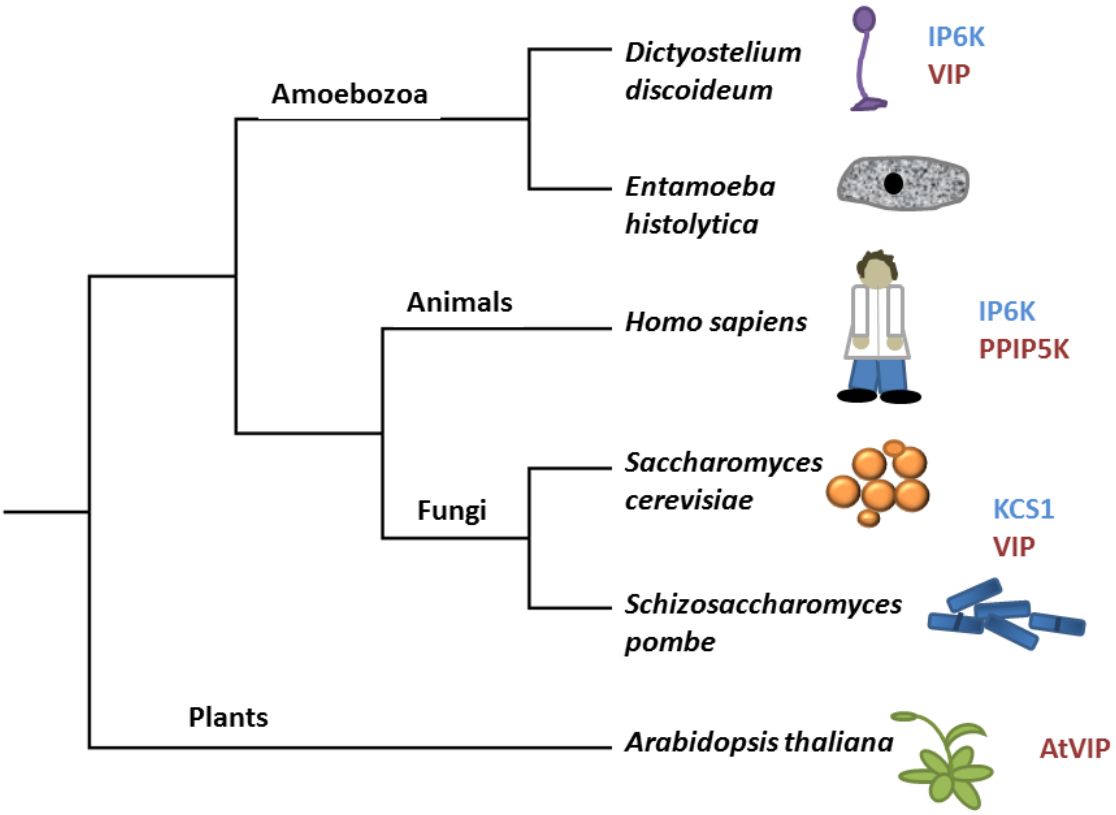

Figure 1.3. A Modified Tree of Life Indicating $InsP_6$ Kinases

A modified tree of life indicating composition of genes in different species that encode kinases capable of phosphorylating $InsP_6$. Genes in blue have sequence identity with *KCS1*, whereas genes in red have sequence identity with *Vip*. The tree depicts evolutionary relationships between groups discussed in the review.

Synthesis of PPx-InsPs by KCS1/IP6K Enzymes

There are two classes of genes shown to encode enzymes required for synthesis of PPx-InsPs. **Figure 1.3** shows the presence and names of these genes in species relevant to this review. These two classes of genes encode distinct enzymes that catalyze the addition of pyrophosphates at specific positions on the inositol ring (**Figure 1.2**). The first class is named the $InsP_6$ kinases (IP6Ks), and the kinase activity of these enzymes phosphorylates the 5-position of $InsP_5$, $InsP_6$, and $InsP_7$, yielding 5PP-$InsP_4$ or 5PP-$InsP_5$ and two possible forms of $InsP_8$: 1/3,5PP-$InsP_5$ and 5PPP-$InsP_5$ (*24*). In yeast, this class of enzymes is named KCS1, and was first identified in a suppressor screen of the yeast Protein Kinase C (*pkc1*) mutant (*43*). *Kcs1* encodes a protein closely related to the bZIP family of transcription factors, although analysis of its two potential leucine zipper motifs indicates the secondary alpha-helical structure for DNA binding is not formed (*43*). Instead, the altered structure of this alpha helix in addition to a two-turn 3_{10} helix, forms a pocket for $InsP_6$ binding (*44*).

Under low energy conditions, KCS1 can generate ATP from $InsP_6$ (*45*). This dual function of KCS1 to both degrade $InsP_6$ and generate $InsP_7$ presents the possibility of KCS1 acting as an ATP/ADP ratio sensor (*45*). Given the considerable amount of $InsP_6$ in plants, if present, a KCS1-like enzyme could generate a significant source of ATP under low energy conditions. However, sequence homology searches using the yeast KCS1 and human IP6K proteins indicate that there are no KCS1/IP6K homologues in plants (*11*, *37*).

In the absence of a plant KCS1/IP6K, one might expect that 5PP-$InsP_5$ could not be synthesized. However, there is the possibility of another InsP kinase in plants acting as a KCS1/IP6K in the

synthesis of 5PP-$InsP_5$. The larger InsP kinase family (Pfam PF03770) has a PxxxDxKxG ('PDKG') catalytic motif and includes the $InsP_3$ kinases (IP3Ks), IP6K, and inositol polyphosphate multikinases (IPMKs). Recent phylogenetic studies on these enzymes has suggested that the InsP kinase family common ancestor is an IP6K precursor (*11*). The rationale is that the substrate-binding pocket for $InsP_6$ is larger, and from this common ancestor, the binding pocket would shrink to become more specific for other InsPs (*44*). Not all extant species have developed kinases solely acting on $InsP_3$: *Entamoeba histolytica* still has an IP3K which retains IP6K activity (*44*), presenting the possibility that if plants have a KCS1/IP6K, it may be distinct from that of yeast and mammals.

Synthesis of PPx-InsPs by VIP/PPIP5K Enzymes

The second class of enzymes capable of synthesizing PPx-InsPs are the VIPs, which are also known as diphosphoinositol pentakisphosphate kinases (PPIP5Ks) in animals (*46*) (**Figures 1.2, 1.3**). In quick succession, two groups identified VIPs in yeast and mammalian cells (*25*, *47*, *48*). The name PPIP5K originated as scientists were looking for an enzyme capable of phosphorylating PP-$InsP_5$ to produce the $InsP_8$, which had been observed in mammalian cell extracts (*16*). The PPIP5K that was identified has a higher affinity for $InsP_7$ than $InsP_6$ (*47*). These enzymes produce a structurally distinct $InsP_7$ with recent NMR work delineating 1PP-$InsP_7$ as the product (*27*). These enzymes can also phosphorylate 5PP-$InsP_5$ to produce 1,5$(PP)_2$-$InsP_4$ (**Figure 1.2**) or speculatively, even 1PPP-$InsP_5$.

The *Vip* genes are conserved across eukaryotes, including plants (*25, 37*). They have a dual domain structure consisting of an N-terminal ATP grasp domain with kinase activity and a C-terminal histidine acid phosphatase domain or "phytase" domain (*25*) (see **Figure 1.4**). The human PPIP5K1 phosphatase domain is not active with $InsP_5$, $InsP_6$, PP-$InsP_4$, or PP-$InsP_5$ as the substrate or even *p*-nitrophenyl phosphate, a generic substrate for acid phosphatases (*49*). This is probably due to the fact that PPIP5Ks lack a conserved histidine essential for phosphatase activity. In addition, the phosphatase catalytic region is interrupted by a Pleckstrin Homology (PH) domain (*49*). The PH domain is found in signaling proteins and is responsible for binding phospholipids or molecules derived from their head group (*50*). The hybrid PH domain in PPIP5K1 preferentially binds PtdIns(3,4,5)P_3 and can also bind $InsP_6$ allowing PPIP5K1 to translocate from the cytoplasm to the plasma membrane when the PtdIns(3,4,5)P_3 signaling pathway is activated (*49*). Critical to ligand binding is arginine 417 in the PH domain of PPIP5K1 (*49*).

All plant species searched through BLAST contained multiple expressed Vip homologues (*37*). Arabidopsis contains two conserved *Vip* genes, *AtVip1* (At3g01310) and *AtVip2* (At5g15070) and the encoded proteins have 94% similarity to each other, but only 50% and 59% similarity to yeast ScVIP1 and human HsVIP1 respectively (*37*). As with yeast and human VIPs, Arabidopsis VIP1 and VIP2 contain a RimK/ATP-Grasp domain (kinase domain) and a histidine acid-phosphatase domain (**Figure 1.4**). A BLAST analysis identifies potential *Vip* genes in several other plant species indicating that PPx-InsP synthesis is conserved across the plant kingdom. The kinase domain of the Arabidopsis VIPs contains a conserved aspartic acid (D), which as in yeast and humans, is necessary for activity (*25, 37, 47*). This residue is also conserved in mouse and

Drosophila VIPs, however its role in activity has yet to be confirmed (*48*). The AtVIP1 and AtVIP2 phosphatase domains are also interrupted with a putative PH domain (*49*), (**Figure 1.4**), however binding to PtdInsPs has not been tested to date. The arginine residue required for PtdInsP-binding of the human PPIP5K is not conserved in the AtVIPs, however, the substituted lysine at this position provides a similar charge as arginine and there are other arginine residues located nearby (**Figure 1.4**). Phosphoproteomics has shown that AtVIPs have a serine adjacent to the phosphatase domain that is phosphorylated. This is not conserved in ScVIP and HsVIP (http://phosphat.mpimp-golm.mpg.de) and may represent a unique mechanism for regulation of VIP activity specific to plants (*37*).

Importantly, both *AtVip*s encode catalytically active proteins that allow specific yeast mutants to synthesize $InsP_7$ (*37*). There appears to be an intriguing difference in the AtVIPs as compared to the human and yeast VIPs. In the human PPIP5K and yeast VIPs the kinase domain alone is more active than the full-length protein (*25, 48*), while both full-length AtVIPs are more active than their kinase domains alone (*37*). One explanation for this difference is that the phosphatase domain in the yeast VIP and human PPIP5K may auto-inhibit the kinase activity, and this control may be missing in the AtVIPs. Data from yeast supports this idea of auto-inhibition (*48*). A second explanation is that the unique presence of a phosphorylated serine in the AtVIPs might provide regulatory control.

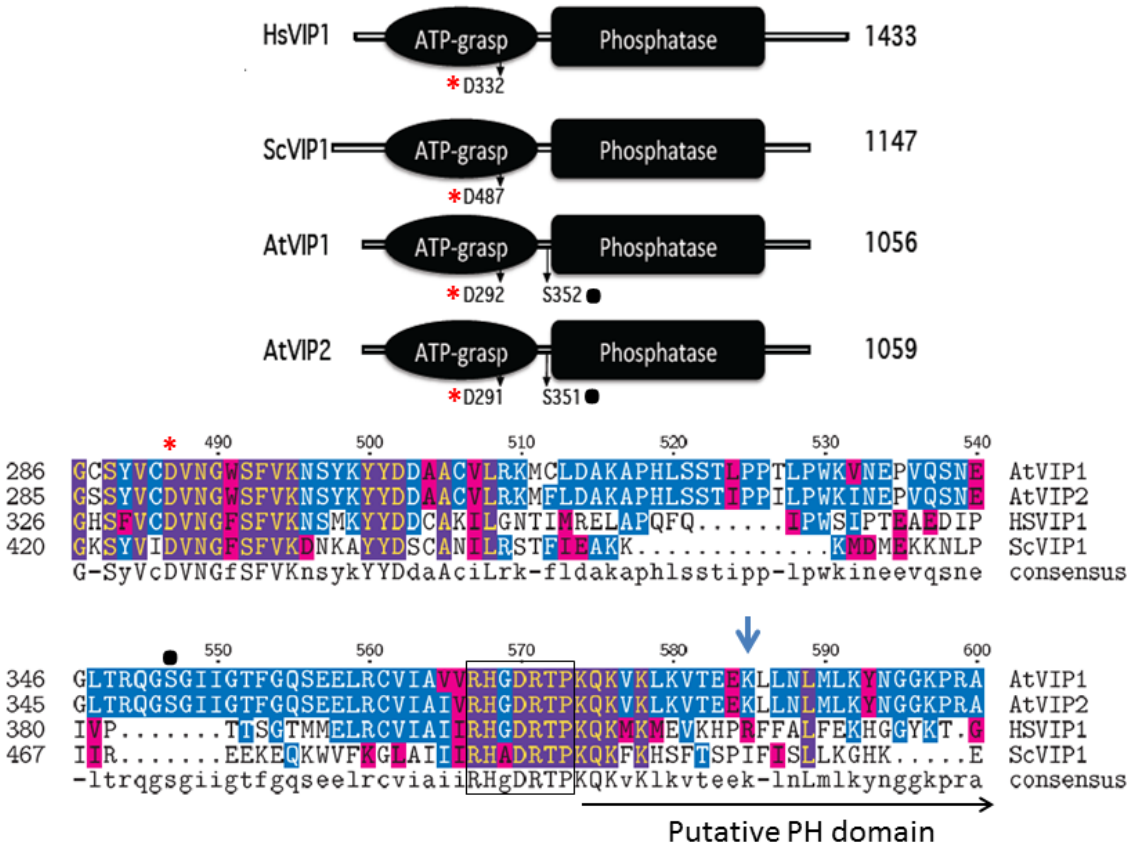

Figure 1.4. Schematic Alignment of the Kinase and Phosphatase Domains of VIPs

The ATP grasp/RimK/ kinase (ATP-grasp) and the histidine acid Phosphatase (Phosphatase) domains within the VIP proteins from *Homo sapiens* (Hs: Genbank AAH57395), *Saccharomyces cerevisiae* (Sc: NP_013514) and *Arabidopsis thaliana* (*AtVip1* Gene ID: 821297; *AtVip2* Gene ID: 831359). The red asterisks denotes in both panels the conserved aspartic acid residue (D) required for kinase activity, and the black dot, the known phosphorylated serine residues within the Arabidopsis VIPs. The lower panel contains the amino acid alignment of the boundary region between the ATP-Grasp and Phosphatase domains. The beginning of the Histidine Acid phosphatase domain is boxed, followed by the PH domain and Arg417 is marked by the blue arrow.

Although NMR data on the plant PPx-InsPs is not yet available, it seems reasonable to speculate that only the 1PP-PPx-InsPs should be synthesized in plants, since VIP enzymes are known to phosphorylate at this position. Indeed, the architecture of the VIP catalytic site is what determines the position of phosphorylation (*46*), and as discussed above, 5PP-InsPs may not be synthesized. Intriguing however, both $InsP_7$ and $InsP_8$ have been found in plants (*37*). This argues for the presence of a plant enzyme capable of 5PP-InsP synthetic ability, since the only structurally verified isomers of $InsP_8$ in any organism, 1,5$(PP)_2$-$InsP_4$ and 5PPP-$InsP_5$, both require phosphorylation at a C5 position (*21, 22, 24, 26*). Further, in yeast, KCS1 and VIP are known to act sequentially to phosphorylate each other's $InsP_7$ product, resulting in 1,5$(PP)_2$-$InsP_4$ synthesis (**Figure 1.2**). Alternatively, the plant $InsP_8$ molecule may be unique in nature and may not require phosphorylation at the 5-position. Thus, either the plant VIPs are different enough that they can phosphorylate a different position, or there are other enzymes in the plant that can phosphorylate $InsP_6$ or $InsP_7$. It is important to note one final structural implication of PPx-InsPs: $InsP_7$ produced by either IP6K or VIP may not be equivalent since the charge from phosphate is distributed differently in each, and the shapes are not superimposable. As a result, different $InsP_7$ enantiomers may interact with different proteins and act in different signaling conditions or pathways.

The similarity of AtVIP1 and AtVIP2 proteins (94% similarity), and the ability of each gene product to restore $InsP_7$ synthesis in yeast, suggests that these two genes function similarly at the biochemical level. Thus, the expression patterns of each gene may provide information on where and when $InsP_7$ is synthesized. Recent studies showed that *AtVip1* expression is high in vegetative tissues, including shoot of seedlings as well as mature leaf and stem. In contrast,

AtVip2 is most abundantly expressed in roots and reproductive tissues (*37*) suggesting differential spatial regulation. Additionally, since both *AtVip1* and *AtVip2* are expressed together in some vegetative tissues, they may be differentially regulated at a subcellular level. Using subcellular prediction tools, we found compelling predictions for AtVIP1 nuclear localization and an AtVIP2 cytosolic location within the plant cell. Discerning whether the two AtVIPs really do function in these compartments will require experimental validation.

Meaning of PPx-InsPs: How are they likely to function in plants?

If we continue the analogy of InsP as words, our next challenge will be to understand what these words mean and what information they convey. We will describe how $InsP_7$ is known to modify or interact with proteins in other model systems, and how these actions lead to changes in known signaling functions in yeast and animals. Although little is known about PPx-InsPs function in plants and mechanisms regulating InsP signaling differ between plants and animals, it is likely that $InsP_7$ conveys plant signaling information by virtue of modifying or interacting with proteins. Drawing parallels from the known and hypothesized roles of $InsP_7$ in other organisms, we speculate that PPx-InsPs function in several plant signaling pathways, including, but not limited to energy homeostasis, phosphate (P_i) sensing, and immune responses. In the following sections, we will elaborate on published data from other model systems that indicates a role for PPx-InsPs in these pathways.

Energy Homeostasis

PPx-InsPs are involved in energy homeostasis both at the cellular and organismal level. Maintaining energy homeostasis, or the balance of intake/production, storage and use of energy often in the form of ATP or sugar, is essential for all living organism. In animals, the AMP Kinase (AMPK) is often named as an energy sensor. Under low energy conditions, AMP is bound, activating the AMP kinase and reprograming the cell to maximize energy acquisition and minimize energy use (*51*). In opposition is mammalian Target Of Rapamycin (mTOR), which under high energy conditions promotes growth and cell division (*52*). In plants, these two enzymes also form the base for maintaining energy homeostasis.

At the cellular level, PPx-InsPs regulate ATP levels through what has been referred to as the "glycolic/mitochondrial metabolic ratio" in yeast (*53*). Yeast mutants lacking KCS1 have up to 5 fold higher level of ATP than their wild type controls while overexpression of KCS1 results in a decrease of ATP (*53*). A similar result is seen with *kcs1* mutant mouse embryonic fibroblast (MEF) cells, where levels of ADP and AMP are low. Further studies showed that the yeast *kcs1* and *kcs1/vip1* mutants as well as MEF *ip6k* mutants have reduction or loss of functional mitochondria. This loss of mitochondrial function with high ATP levels can be explained by an increase in glycolysis and a reduction of ATP used in metabolic pathways. Thus, the lack of $InsP_7$ synthesis in these mutants leads to changes in ATP synthesis and utilization. $InsP_7$ in this system most likely affects ATP levels by altering transcription of genes that control glycolysis. Specifically, in yeast promoters of glycolytic regulatory genes have a CT-box that binds to the General Control Response 1 (GCR1) transcription factor. $InsP_7$ may function to regulate GCR1 directly by a non-catalytic transfer of the β-phosphate from $InsP_7$ to an already phosphorylated

serine residue in GCR1, resulting in a pyrophosphorylated serine. This modification likely causes a conformational change in GCR1, allowing it to bind the CT-box, thereby regulating the expression of glycolytic regulatory genes (*53*).

This addition of a new pyrophosphate bond on an already phosphorylated serine residue in a target substrate protein is a proposed mechanism unique to $InsP_7$. First demonstrated in yeast, $InsP_7$ was shown to modify proteins important for ribosomal biogenesis and endosomal trafficking (*54*). The pyrophosphorylated serine in target proteins is surrounded by acidic residues, possibly enhancing the recruitment of Mg^{2+} as a cofactor. This modification would be more permanent than phosphorylation by ATP (*55*), as no known enzymes exist to remove the pyrophosphate. One limitation to acceptance of this mechanism is that it has been difficult to verify whether such pyrophosphorylated serines occur in *vivo*.

At the whole organism level, $InsP_7$ functions in sugar homeostasis through regulating insulin release and glucose uptake in animals. In mammals, $InsP_7$ acts as an inhibitor of the Protein Kinase B (also known as Akt) pathway, reducing glucose uptake, insulin sensitivity and protein translation. In response to growth factors, Akt is normally phosphorylated by a protein kinase named PDK1 (3-phosphoinositide-dependent protein kinase 1), which activates the GSK3β (Glycogen synthase kinase 3) and mTOR signaling pathways. Activation of Akt requires binding of its PH domain to $PtdIns(3,4,5)P_3$, associated with the plasma membrane. When bound to $PtdIns(3,4,5)P_3$, Akt undergoes a conformational change which exposes its activation domain, allowing Akt to be phosphorylated and activated by PDK1 (*56*). $InsP_7$, produced by IP6K1, acts as an inhibitor of Akt by competing for binding to the PH domain within Akt. This effectively

prevents the phosphorylation of T308 of Akt (*57*), and dampens Akt signaling. *ip6k1* loss-of-function mutant mice are smaller than their wild type littermates and have lower circulating levels of insulin, but are not diabetic and they have normal blood glucose levels (*58*). These genetic data underscore the role of $InsP_7$ in global metabolic control.

While insulin is not made by plants, gene homologues functioning in the Akt, GSK3β, and mTOR pathways exist in plants, and have been implicated in growth control pathways. Plants contain homologues of both Akt (i.e. Adi3: AvrPto-dependent Pto-interacting protein 3) and the kinase that activates Akt, PDK1. Most studies indicate that plants do not synthesize $PtdIns(3,4,5)P_3$, however plant PDK1 is known to bind phosphatidic acid via its PH domain, allowing membrane localization (*59*) and the subsequent activation of Adi3 (*60*). Adi3 can suppress the activity of a major regulator of plant metabolism and AMPK homolog, SnRK1 (Sucrose non-fermenting Related Kinase 1), through phosphorylation of a SnRK1 multiple subunit complex (*61*). GSK-3 kinases are negative regulators of signal transduction pathways controlling metabolism and developmental events across the animal kingdom. In plants, GSK3 homologues are involved in brassinosteroid (BR) signaling pathways. Specifically, the brassinosteroid insensitive 2 (BIN2) protein is a GSK-3 that functions as a negative regulator of BR signal transduction (*62, 63*). As with the animal GSK-3 signaling, BR signal transduction is required for proper metabolic and developmental control throughout the life of a plant. In the case of mTOR, the Arabidopsis gene homologues are known to be important regulators of metabolic changes in response to glucose. Arabidopsis TOR signaling has been linked to transcriptional reprogramming of central and secondary metabolism and other processes within plants (*64*).

We do not yet know whether $InsP_7$ in plants regulates transcription via pyrophosphorylation or whether $InsP_7$ can compete with binding to PH domains of plant proteins, however, both are potential mechanisms by which $InsP_7$ could act. Determining whether plants use $InsP_7$ to regulate metabolism or growth, and the mechanistic details of such regulation will benefit from the development of genetic resources to examine *Atvip* loss-of-function mutants. In addition, we need to know whether PPx-InsPs levels are altered by changes in energy or metabolic status. Answering these questions is now possible as the basis for detecting and measuring PPx-InsPs in plants has been established, and the *AtVip* genes have been cloned and shown to encode active proteins.

P_i Sensing

PPx-InsPs are also involved in perceiving and maintaining P_i levels and numerous studies link PPx-InsPs to low P_i responses in other organisms. Plant P_i homeostasis is a highly regulated process (*65*) and it is important to consider whether PPx-InsPs play a role in this process in plants. P_i sensing involves the perception of P_i present in the environment, followed by acquisition, remobilization and recycling of P_i to maintain P_i homeostasis. In yeast, the response to P_i starvation is regulated by the P_i-responsive (PHO) signaling pathway, including the Pho80-Pho85 cyclin-CDK (cyclin dependent kinase) complex (*66, 67*). When P_i levels are low, the Pho80-Pho85 protein complex is inactive. As a result, the Pho4 transcription factor is not phosphorylated and remains in the nucleus where it acts to activate PHO genes (*68, 69*).

Though there is some lack of consensus for the exact mechanism by which PPx-InsPs control P_i sensing, it is clear that they play a role in P_i homeostasis. One group found that low P_i elevates $InsP_7$, and genetic evidence suggested that it was 1PP-$InsP_5$, although this was not experimentally confirmed (*70*). This group showed that $InsP_7$ physically interacts with Pho81, inactivating the Pho80-Pho85 complex, and ultimately leading to changes in gene expression required to maintain metabolic homeostasis under low P_i conditions. In addition, this pathway was dependent on the activity of the yeast *Vip* genes (*70*). The finding that $InsP_7$ is elevated in yeast in response to low P_i has been contested by other investigators. Exposure of wild type yeast to P_i-free medium for 20 min resulted in a decrease of intracellular PPx-InsPs levels by 80%, without affecting $InsP_6$ levels (*71*).

The change in $InsP_7$ levels is not the only phenotype that suggests KCS1 is involved in the yeast low P_i response. An intriguing connection between KCS1 and P_i sensing comes from recent studies that found that Pho4 binds to intragenic regions of the *Kcs1* gene, promoting the transcription of intragenic and antisense RNA. The authors suggested that the truncated KCS1 protein produced could down-regulate KCS1 function (*72*). An alternative hypothesis is that this truncated KCS1 protein has an altered enzymatic property yet to be determined (*73*). Further work is needed to examine these possibilities and determine the function of intragenic and antisense *Kcs1* RNA. In addition, recent work examining the lipidome of numerous yeast mutants found similarities in changes in sphingolipids of *pho85* and *kcs1*, but not *vip1* mutants, suggesting that similar metabolic changes take place in *pho85* and *kcs1* mutants (*74*). Together

these data suggest that either *Vip* or *Kcs1* genes, or possibly both, are linked to P_i sensing and sphingolipid homeostasis in yeast.

In animal cells, IP6K has been identified as a stimulator of P_i uptake in response to low nutrients. A study found that the mRNAs expressed in rabbit duodenum from a rabbit fed a low P_i diet can stimulate Na^+-dependent P_i uptake when injected into *Xenopus* oocytes (*75*). From this pool of mRNAs, the P_i uptake stimulator (PiUS) gene was isolated and confirmed to increase P_i uptake when expressed in *Xenopus* oocytes (*76*). The *PiUS* gene was later found to encode an IP6K, and the gene is now known as *Ip6k2* (*77*).

In plants, InsPs are essential for P_i response and homeostasis. Arabidopsis mutants in *ipk1*, which catalyzes the addition of a phosphate at the 2-position to select substrates, have a 83% reduction in $InsP_6$ levels compared to wild type, and are hypersensitive to P_i (*78*). These mutants have increased uptake of P_i and root to shoot translocation of P_i (*79*). Many plant responses to P_i starvation (PSR) are regulated at a transcriptional and post-transcriptional level. A recent study has shown that a sub set of PSR genes involved in P_i uptake, translocation and remobilization are up regulated in the *ipk1* mutant under P_i sufficient conditions (*79*). Additionally, increased expression of a subset of PSR genes was shown to correlate with a reduction of histone H2A.Z occupancy (*80*) and interestingly, H2A.Z occupancy at chromatin sites associated with several PSR genes was found to be significantly reduced in *ipk1* (under both sufficient and low P_i) compared to wild type (*79*). However, Arabidopsis mutants with lower $InsP_6$ levels including *mips1* (*myo*-inositol 1-phosphate synthase), do not show an accumulation of P_i, indicating that $InsP_6$ *per se* is probably not the molecule utilized for sensing P_i (*79*). This implicates other InsPs

or the PPx-InsPs as controllers of P_i sensing. In particular, since PPx-InsPs are synthesized from $InsP_6$ substrates, these molecules might serve as critical players in sensing P_i. We note that the conversion between $InsP_6$ and the PPx-InsPs might be important as $InsP_6$ serves an important function in phosphorous storage (*32*).

Studies on yeast and animal mutant responses to low P_i were among the first to highlight a specific property of InsPs that may be especially important for understanding PPx-InsP function. Response to environmental stress, including P_i starvation, requires the fine tuning of TOR and the TORC1 complex activity. This results in the down regulation of ribosomal and protein synthesis regulatory genes, as well as the up regulation of stress response genes (*81*). Working in parallel with the inactivation of TORC1, the histone deacetylase (HDAC) enzyme is recruited to turn off expression of ribosomal and protein synthesis regulatory genes (*82*). This HDAC activity is dependent on $InsP_4$, which is known to act as a "molecular glue" allowing the HDAC Rpd3L complex to interact with its co-repressor, SMRT (silencing mediator of retinoic acid and thyroid hormone receptor) (*83*). $InsP_7$ has been hypothesized to interact with this same complex (*84*), suggesting that PPx-InsPs may play a role in chromatin remodeling thereby regulating gene expression.

There are other known cases of InsPs serving a role as a type of molecular glue, and these bear mentioning. $InsP_6$ and $InsP_5$ have been found in the auxin (TIR1; Transport Inhibitor Response 1) (*85*) and jasmonic acid receptor, COI1 (Coronatine Insensitive 1) (*86, 87*), respectively. In both of these examples, InsPs are lodged between the F-Box and the repressor protein target in the E3 ubiquitin ligase complex. When the hormone is present, the repressors for auxin and

jasmonic acid, Aux/IAA (Auxin inducible) and JAZ (Jasmonate Zim-domain protein) respectively, are degraded, allowing for transcription of hormone responsive genes. TIR1 is a member of a family of F-box proteins whose five members differ slightly in expression, biochemical activity or function (*88*) and Aux/IAA belongs to an even larger family of 29 proteins (*89*). Like TIR1, COI1 is a member of the F-Box family while JAZ is a 12 member subgroup of TIFY (named for the shared TIF[F/Y]XG motif) (*90, 91*). With all the potential combinations of hormone receptors and repressor proteins, it is interesting to speculate whether other InsPs, including PPx-InsPs, may function as cofactors in hormone signaling to regulate transcription.

Immune Response

The innate immune system is the first line of defense in both plants and animals. The first step in the innate immune response pathway involves the recognition of pathogen-associated molecular patterns (PAMPs) by the host pattern recognition receptors (PRRs) on the cell surface or cytoplasm. In plants, pathogen detection, signaling, and immune response takes place in most cells, while animal immune systems have evolved specialized mobile immune cells. Detection of PAMPs by PRRs initiate signaling cascades which can result in Ca^{2+} release, activation of kinases, and transcription factors, production of reactive oxygen species and alterations in other signaling pathways within the organism (*92*). In animals, RIG-1 (retinoic acid-inducible gene 1) is a PRR in the cytoplasm, which detects double stranded viral DNA and activates a signaling cascade in which the transcription factor IRF3 (Interferon regulatory factor 3) is phosphorylated. IFR3 then moves into the nucleus and promotes the expression of type-1 interferon genes. The

interferon proteins then stimulate anti-viral or anti-bacterial activity in leukocytes (*93*). Recently, this innate response pathway was linked to PPx-InsPs. An *in vitro* study found both $InsP_7$ and $InsP_8$ are capable of inducing an interferon response through the RIG-1 signaling pathway. The authors of this study speculated that 1PP-$InsP_5$ is the physiologically relevant molecule and acts a co-factor for protein interactions or by β-phosphorylation of a serine residue on IRF3, a type of PPx-InsP-driven protein pyrophosphorylation event that we have previously discussed (*94*).

The innate immune system in plants and animals share many similarities in the use of PAMPs and PRR as a method of detecting pathogens. Plants have a large diversity of PRR and Resistance (R) genes, however homologues of the RIG-1/IRF3 pathway have not been found in plants. Therefore, while it is interesting to speculate that PPx-InsPs may regulate specific defense transcription factors in plants, the lack of RIG-1 and IRF-3 homologues suggests that this pathway may be unique to animal innate immunity signaling.

A second role of PPx-InsPs in the animal innate immune response involves the afore-mentioned PDK1/Akt signaling pathway. This complex pathway regulates multiple central biological processes including cell survival, proliferation, growth, and metabolism (*95*). In the immune system, neutrophil activation is tightly controlled, with 5PP-$InsP_5$ acting as a negative regulator. As described previously, 5PP-$InsP_5$ competes for binding with Akt through the PH domain. Upon infection, 5PP-$InsP_5$ levels drop allowing Akt to translocate to the membrane and allow for the induction of PtdIns(3,4,5)P_3 signaling, leading to neutrophil activation and superoxide production. *ip6k* mutant neutrophils have increased bactericidal activity and ROS production (*96*). Akt triggers reactive oxygen species and nitric oxide production, and is not limited to

neutrophils, it can also regulate programmed cell death in other cell types (*97*). The inhibition of Akt signaling by $InsP_7$ is a general phenomenon, however, the mechanism of regulation and the biological outcome may differ depending on tissue and signaling context (*96*).

A common characteristic of the innate immune response is the programed cell death of infected cells to reduce the spread of disease. In plants, localized programed cell death stimulated by the hypersensitive response occurs rapidly in response to pathogen infection (*98*). As mentioned previously, plants have a homologous pathway to the PDK1/Akt pathway in mammals. In plants, the homolog to Akt is Adi3, which acts in the immune response as a negative regulator of cell death through the MAPK kinase cascade. Akt and Adi3 kinases may be a target for pathogen manipulation of the host In the case of *Pseudomonas* infection of tomato, the bacterial effector protein AvrPto interacts with the Adi3 presumably to manipulate cell death (*99*). It is intriguing to speculate whether PPx-InsPs may serve as innate immunity signaling molecules in plants, perhaps by acting to antagonize Adi3 signaling. However, it should be noted that although functionally similar, Akt and Adi3 share only 21.4% amino acid identity, suggesting differences in regulation and possibly function (*99*).

A final connection between PPx-InsPs and plant innate immune signaling involves plant mutants defective in the synthesis or metabolism of InsPs. Transgenic plants constitutively expressing the human type 1 inositol polyphosphate 5-phosphatase (InsP 5-ptase, the enzyme which dephosphorylates $InsP_3$), showed a compromised defense response, including decreased expression of defense genes and a reduction in the systemic acquired immunity in response to a bacterial pathogen (*100*). Furthermore, plants defective in synthesis of *myo*-inositol and $InsP_6$

were also more susceptible to disease, including viral, bacterial and fungal pathogen infection (*101*). It was concluded that $InsP_6$ and not its precursors is the critical InsP for this phenotype, however, the authors of this study could not rule out a role for PPx-InsPs in this process due to the difficulty in detection (*101*). Crops with altered InsP profiles, specifically low $InsP_6$, have been developed to combat issues of nutrition and P_i pollution (*102*). If $InsP_6$ or PPx-InsPs play a role in pathogen resistance and immune response, it could negatively impact the performance of these so-called low phytate crops.

Concluding Remarks

PPx-InsPs have recently been identified in higher plants, adding new molecular players in the plant InsP signaling pathway. Both $InsP_7$ and $InsP_8$ have been detected in a handful of plant species. With two *Vip*/*PPIP5K* gene homologues as the only identified kinase to synthesize PPx-InsPs, the predicted species are 1PP-$InsP_5$ and either 1,3$(PP)_2$-$InsP_4$ or 1PPP-$InsP_5$. Further work is needed to identify the stereochemistry of plant PPx-InsPs and to clarify the regulatory components involved in their synthesis and metabolism. Drawing parallels to known roles of PPx-InsPs in other eukaryotes, plant PPx-InsPs may have a role in energy, P_i sensing, and innate immunity signaling pathways. Thus, identification of PPx-InsPs in plants presents a new avenue and tool that may be useful for improving crop yield, reduced fertilizer demand, and improved growth under stress.

REFERENCES

1. P. Coello, S. J. Hey, N. G. Halford, The sucrose non-fermenting-1-related (SnRK) family of protein kinases: potential for manipulation to improve stress tolerance and increase yield. *J Exp Bot* **62**, 883 (Jan, 2011).
2. E. Baena-Gonzalez, F. Rolland, J. M. Thevelein, J. Sheen, A central integrator of transcription networks in plant stress and energy signalling. *Nature* **448**, 938 (Aug 23, 2007).
3. R. Ghillebert *et al.*, The AMPK/SNF1/SnRK1 fuel gauge and energy regulator: structure, function and regulation. *Febs j* **278**, 3978 (Nov, 2011).
4. E. A. Ananieva, G. E. Gillaspy, A. Ely, R. N. Burnette, F. L. Erickson, Interaction of the WD40 domain of a myoinositol polyphosphate 5-phosphatase with SnRK1 links inositol, sugar, and stress signaling. *Plant Physiol* **148**, 1868 (Dec, 2008).
5. I. Y. Perera, C.-Y. Hung, S. Brady, G. K. Muday, W. F. Boss, A Universal Role for Inositol 1,4,5-Trisphosphate-Mediated Signaling in Plant Gravitropism. *Plant Physiology* **140**, 746 (12/05/2006).
6. X. Chen, W. H. Lin, Y. Wang, S. Luan, H. W. Xue, An inositol polyphosphate 5-phosphatase functions in PHOTOTROPIN1 signaling in Arabidopis by altering cytosolic Ca2+. *Plant Cell* **20**, 353 (Feb, 2008).
7. T. Munnik, J. E. Vermeer, Osmotic stress-induced phosphoinositide and inositol phosphate signalling in plants. *Plant, cell & environment* **33**, 655 (Apr, 2010).
8. E. A. Ananieva, G. E. Gillaspy, Switches in nutrient and inositol signaling. *Plant Signaling & Behavior* **4**, 304 (01/31/2009).
9. S. R. Alford, P. Rangarajan, P. Williams, G. E. Gillaspy, myo-Inositol Oxygenase is Required for Responses to Low Energy Conditions in Arabidopsis thaliana. *Frontiers in plant science* **3**, 69 (04/19/2012).
10. G. E. Gillaspy, The cellular language of myo-inositol signaling. *New Phytol* **192**, 823 (Dec, 2011).
11. M. Bennett, S. M. Onnebo, C. Azevedo, A. Saiardi, Inositol pyrophosphates: metabolism and signaling. *Cell Mol Life Sci* **63**, 552 (Mar, 2006).
12. W. van Leeuwen, L. Okresz, L. Bogre, T. Munnik, Learning the lipid language of plant signalling. *Trends Plant Sci* **9**, 378 (Aug, 2004).
13. M. Heilmann, I. Heilmann, Plant phosphoinositides-complex networks controlling growth and adaptation. *Biochim Biophys Acta*, (Oct 2, 2014).
14. M. C. Glennon, S. B. Shears, Turnover of inositol pentakisphosphates, inositol hexakisphosphate and diphosphoinositol polyphosphates in primary cultured hepatocytes. *Biochem J* **293 (Pt 2)**, 583 (Jul 15, 1993).
15. P. T. Hawkins, L. R. Stephens, J. R. Piggott, Analysis of inositol metabolites produced by Saccharomyces cerevisiae in response to glucose stimulation. *The Journal of biological chemistry* **268**, 3374 (Feb 15, 1993).
16. L. Stephens *et al.*, The detection, purification, structural characterization, and metabolism of diphosphoinositol pentakisphosphate(s) and bisdiphosphoinositol tetrakisphosphate(s). *J Biol Chem* **268**, 4009 (Feb 25, 1993).

17. F. S. Menniti, R. N. Miller, J. W. Putney, Jr., S. B. Shears, Turnover of inositol polyphosphate pyrophosphates in pancreatoma cells. *J Biol Chem* **268**, 3850 (Feb 25, 1993).
18. S. B. Shears, N. A. Gokhale, H. Wang, A. Zaremba, Diphosphoinositol polyphosphates: what are the mechanisms? *Advances in enzyme regulation* **51**, 13 (2011).
19. S. M. Voglmaier *et al.*, Purified inositol hexakisphosphate kinase is an ATP synthase: diphosphoinositol pentakisphosphate as a high-energy phosphate donor. *Proc Natl Acad Sci U S A* **93**, 4305 (Apr 30, 1996).
20. C. F. Huang, S. M. Voglmaier, M. E. Bembenek, A. Saiardi, S. H. Snyder, Identification and purification of diphosphoinositol pentakisphosphate kinase, which synthesizes the inositol pyrophosphate bis(diphospho)inositol tetrakisphosphate. *Biochemistry* **37**, 14998 (Oct 20, 1998).
21. T. Laussmann, K. M. Reddy, K. K. Reddy, J. R. Falck, G. Vogel, Diphospho-myo-inositol phosphates from Dictyostelium identified as D-6-diphospho-myo-inositol pentakisphosphate and D-5,6-bisdiphospho-myo-inositol tetrakisphosphate. *Biochem J* **322 (Pt 1)**, 31 (Feb 15, 1997).
22. T. Laussmann *et al.*, Diphospho-myo-inositol phosphates in Dictyostelium and Polysphondylium: identification of a new bisdiphospho-myo-inositol tetrakisphosphate. *FEBS Lett* **426**, 145 (Apr 10, 1998).
23. J. B. Martin, T. Laussmann, T. Bakker-Grunwald, G. Vogel, G. Klein, neo-inositol polyphosphates in the amoeba Entamoeba histolytica. *J Biol Chem* **275**, 10134 (Apr 7, 2000).
24. P. Draskovic *et al.*, Inositol hexakisphosphate kinase products contain diphosphate and triphosphate groups. *Chem Biol* **15**, 274 (Mar, 2008).
25. S. Mulugu *et al.*, A conserved family of enzymes that phosphorylate inositol hexakisphosphate. *Science* **316**, 106 (Apr 6, 2007).
26. H. Lin *et al.*, Structural analysis and detection of biological inositol pyrophosphates reveal that the family of VIP/diphosphoinositol pentakisphosphate kinases are 1/3-kinases. *J Biol Chem* **284**, 1863 (Jan 16, 2009).
27. H. Wang, J. R. Falck, T. M. Hall, S. B. Shears, Structural basis for an inositol pyrophosphate kinase surmounting phosphate crowding. *Nat Chem Biol* **8**, 111 (Jan, 2012).
28. C. Azevedo, A. Saiardi, Extraction and analysis of soluble inositol polyphosphates from yeast. *Nat Protoc* **1**, 2416 (2006).
29. G. W. Mayr, A novel metal-dye detection system permits picomolar-range h.p.l.c. analysis of inositol polyphosphates from non-radioactively labelled cell or tissue specimens. *Biochem J* **254**, 585 (Sep 1, 1988).
30. J. C. Otto *et al.*, Biochemical analysis of inositol phosphate kinases. *Methods Enzymol* **434**, 171 (2007).
31. O. Losito, Z. Szijgyarto, A. C. Resnick, A. Saiardi, Inositol pyrophosphates and their unique metabolic complexity: analysis by gel electrophoresis. *PLoS One* **4**, e5580 (2009).
32. V. Raboy, myo-Inositol-1,2,3,4,5,6-hexakisphosphate. *Phytochemistry* **64**, 1033 (Nov, 2003).
33. J. A. Dorsch *et al.*, Seed phosphorus and inositol phosphate phenotype of barley low phytic acid genotypes. *Phytochemistry* **62**, 691 (Mar, 2003).

34. C. A. Brearley, D. E. Hanke, Inositol phosphates in barley (Hordeum vulgare L.) aleurone tissue are stereochemically similar to the products of breakdown of InsP6 in vitro by wheat-bran phytase. *Biochem J* **318 (Pt 1)**, 279 (Aug 15, 1996).
35. S. Flores, C. C. Smart, Abscisic acid-induced changes in inositol metabolism in Spirodela polyrrhiza. *Planta* **211**, 823 (Nov, 2000).
36. F. Lemtiri-Chlieh, E. A. MacRobbie, C. A. Brearley, Inositol hexakisphosphate is a physiological signal regulating the K+-inward rectifying conductance in guard cells. *Proc Natl Acad Sci U S A* **97**, 8687 (Jul 18, 2000).
37. M. Desai *et al.*, Two Inositol Hexakisphosphate Kinases Drive Inositol Pyrophosphate Synthesis in Plants. *Plant J*, (Sep 17, 2014).
38. R. Nagy *et al.*, The Arabidopsis ATP-binding cassette protein AtMRP5/AtABCC5 is a high affinity inositol hexakisphosphate transporter involved in guard cell signaling and phytate storage. *J Biol Chem* **284**, 33614 (Nov 27, 2009).
39. S. J. Suh *et al.*, The ATP binding cassette transporter AtMRP5 modulates anion and calcium channel activities in Arabidopsis guard cells. *J Biol Chem* **282**, 1916 (Jan 19, 2007).
40. M. Klein *et al.*, The plant multidrug resistance ABC transporter AtMRP5 is involved in guard cell hormonal signalling and water use. *Plant J* **33**, 119 (Jan, 2003).
41. J. Shi *et al.*, Embryo-specific silencing of a transporter reduces phytic acid content of maize and soybean seeds. *Nat Biotechnol* **25**, 930 (Aug, 2007).
42. F. Lemtiri-Chlieh *et al.*, Inositol hexakisphosphate mobilizes an endomembrane store of calcium in guard cells. *Proc Natl Acad Sci U S A* **100**, 10091 (Aug 19, 2003).
43. K. N. Huang, L. S. Symington, Suppressors of a Saccharomyces cerevisiae pkc1 mutation identify alleles of the phosphatase gene PTC1 and of a novel gene encoding a putative basic leucine zipper protein. *Genetics* **141**, 1275 (Dec, 1995).
44. H. Wang, E. F. DeRose, R. E. London, S. B. Shears, IP6K structure and the molecular determinants of catalytic specificity in an inositol phosphate kinase family. *Nat Commun* **5**, 4178 (2014).
45. T. Wundenberg, N. Grabinski, H. Lin, G. W. Mayr, Discovery of InsP6-kinases as InsP6-dephosphorylating enzymes provides a new mechanism of cytosolic InsP6 degradation driven by the cellular ATP/ADP ratio. *Biochem J* **462**, 173 (Aug 15, 2014).
46. S. B. Shears, J. D. Weaver, H. Wang, Structural insight into inositol pyrophosphate turnover. *Adv Biol Regul* **53**, 19 (Jan, 2013).
47. J. H. Choi, J. Williams, J. Cho, J. R. Falck, S. B. Shears, Purification, sequencing, and molecular identification of a mammalian PP-InsP5 kinase that is activated when cells are exposed to hyperosmotic stress. *J Biol Chem* **282**, 30763 (Oct 19, 2007).
48. P. C. Fridy, J. C. Otto, D. E. Dollins, J. D. York, Cloning and characterization of two human VIP1-like inositol hexakisphosphate and diphosphoinositol pentakisphosphate kinases. *J Biol Chem* **282**, 30754 (Oct 19, 2007).
49. N. A. Gokhale, A. Zaremba, S. B. Shears, Receptor-dependent compartmentalization of PPIP5K1, a kinase with a cryptic polyphosphoinositide binding domain. *Biochem J* **434**, 415 (Mar 15, 2011).
50. K. Scheffzek, S. Welti, Pleckstrin homology (PH) like domains - versatile modules in protein-protein interaction platforms. *FEBS Lett* **586**, 2662 (Aug 14, 2012).
51. D. G. Hardie, AMPK and autophagy get connected. *EMBO J* **30**, 634 (Feb 16, 2011).

52. E. A. Dunlop, A. R. Tee, Mammalian target of rapamycin complex 1: signalling inputs, substrates and feedback mechanisms. *Cell Signal* **21**, 827 (Jun, 2009).
53. Z. Szijgyarto, A. Garedew, C. Azevedo, A. Saiardi, Influence of inositol pyrophosphates on cellular energy dynamics. *Science* **334**, 802 (Nov 11, 2011).
54. A. Saiardi, R. Bhandari, A. C. Resnick, A. M. Snowman, S. H. Snyder, Phosphorylation of proteins by inositol pyrophosphates. *Science* **306**, 2101 (Dec 17, 2004).
55. R. Bhandari *et al.*, Protein pyrophosphorylation by inositol pyrophosphates is a posttranslational event. *Proc Natl Acad Sci U S A* **104**, 15305 (Sep 25, 2007).
56. V. Calleja *et al.*, Intramolecular and intermolecular interactions of protein kinase B define its activation in vivo. *PLoS Biol* **5**, e95 (Apr, 2007).
57. A. Chakraborty *et al.*, Inositol pyrophosphates inhibit Akt signaling, thereby regulating insulin sensitivity and weight gain. *Cell* **143**, 897 (Dec 10, 2010).
58. R. Bhandari, K. R. Juluri, A. C. Resnick, S. H. Snyder, Gene deletion of inositol hexakisphosphate kinase 1 reveals inositol pyrophosphate regulation of insulin secretion, growth, and spermiogenesis. *Proc Natl Acad Sci U S A* **105**, 2349 (Feb 19, 2008).
59. R. G. Anthony *et al.*, A protein kinase target of a PDK1 signalling pathway is involved in root hair growth in Arabidopsis. *EMBO J* **23**, 572 (Feb 11, 2004).
60. T. P. Devarenne, G. B. Martin, Manipulation of plant programmed cell death pathways during plant-pathogen interactions. *Plant Signal Behav* **2**, 188 (May, 2007).
61. J. Avila *et al.*, The beta-subunit of the SnRK1 complex is phosphorylated by the plant cell death suppressor Adi3. *Plant Physiol* **159**, 1277 (Jul, 2012).
62. Z. Yan, J. Zhao, P. Peng, R. K. Chihara, J. Li, BIN2 functions redundantly with other Arabidopsis GSK3-like kinases to regulate brassinosteroid signaling. *Plant Physiol* **150**, 710 (Jun, 2009).
63. S. D. Clouse, Brassinosteroid signal transduction: from receptor kinase activation to transcriptional networks regulating plant development. *Plant Cell* **23**, 1219 (Apr, 2011).
64. Y. Xiong, J. Sheen, The role of target of rapamycin signaling networks in plant growth and metabolism. *Plant Physiol* **164**, 499 (Feb, 2014).
65. Z. Zhang, H. Liao, W. J. Lucas, Molecular mechanisms underlying phosphate sensing, signaling, and adaptation in plants. *J Integr Plant Biol* **56**, 192 (Mar, 2014).
66. M. E. Lenburg, E. K. O'Shea, Signaling phosphate starvation. *Trends Biochem Sci* **21**, 383 (Oct, 1996).
67. A. S. Carroll, E. K. O'Shea, Pho85 and signaling environmental conditions. *Trends Biochem Sci* **27**, 87 (Feb, 2002).
68. A. Kaffman, I. Herskowitz, R. Tjian, E. K. O'Shea, Phosphorylation of the transcription factor PHO4 by a cyclin-CDK complex, PHO80-PHO85. *Science* **263**, 1153 (Feb 25, 1994).
69. E. M. O'Neill, A. Kaffman, E. R. Jolly, E. K. O'Shea, Regulation of PHO4 nuclear localization by the PHO80-PHO85 cyclin-CDK complex. *Science* **271**, 209 (Jan 12, 1996).
70. Y. S. Lee, S. Mulugu, J. D. York, E. K. O'Shea, Regulation of a cyclin-CDK-CDK inhibitor complex by inositol pyrophosphates. *Science* **316**, 109 (Apr 6, 2007).
71. A. Lonetti *et al.*, Identification of an evolutionarily conserved family of inorganic polyphosphate endopolyphosphatases. *J Biol Chem* **286**, 31966 (Sep 16, 2011).

72. M. Nishizawa, T. Komai, N. Morohashi, M. Shimizu, A. Toh-e, Transcriptional repression by the Pho4 transcription factor controls the timing of SNZ1 expression. *Eukaryot Cell* **7**, 949 (Jun, 2008).
73. A. Saiardi, How inositol pyrophosphates control cellular phosphate homeostasis? *Adv Biol Regul* **52**, 351 (May, 2012).
74. A. X. da Silveira Dos Santos *et al.*, Systematic lipidomic analysis of yeast protein kinase and phosphatase mutants reveals novel insights into regulation of lipid homeostasis. *Mol Biol Cell* **25**, 3234 (Oct 15, 2014).
75. A. Yagci, A. Werner, H. Murer, J. Biber, Effect of rabbit duodenal mRNA on phosphate transport in Xenopus laevis oocytes: dependence on 1,25-dihydroxy-vitamin-D3. *Pflugers Arch* **422**, 211 (Dec, 1992).
76. F. Norbis *et al.*, Identification of a cDNA/protein leading to an increased Pi-uptake in Xenopus laevis oocytes. *J Membr Biol* **156**, 19 (Mar 1, 1997).
77. A. Saiardi, H. Erdjument-Bromage, A. M. Snowman, P. Tempst, S. H. Snyder, Synthesis of diphosphoinositol pentakisphosphate by a newly identified family of higher inositol polyphosphate kinases. *Current biology : CB* **9**, 1323 (Nov 18, 1999).
78. J. Stevenson-Paulik, R. J. Bastidas, S. T. Chiou, R. A. Frye, J. D. York, Generation of phytate-free seeds in Arabidopsis through disruption of inositol polyphosphate kinases. *Proc Natl Acad Sci U S A* **102**, 12612 (Aug 30, 2005).
79. H. F. Kuo *et al.*, Arabidopsis inositol pentakisphosphate 2-kinase, AtIPK1, is required for growth and modulates phosphate homeostasis at the transcriptional level. *Plant J* **80**, 503 (Nov, 2014).
80. A. P. Smith *et al.*, Histone H2A.Z regulates the expression of several classes of phosphate starvation response genes but not as a transcriptional activator. *Plant Physiol* **152**, 217 (Jan, 2010).
81. R. Loewith *et al.*, Two TOR complexes, only one of which is rapamycin sensitive, have distinct roles in cell growth control. *Mol Cell* **10**, 457 (Sep, 2002).
82. A. L. Alejandro-Osorio *et al.*, The histone deacetylase Rpd3p is required for transient changes in genomic expression in response to stress. *Genome Biol* **10**, R57 (2009).
83. P. J. Watson, L. Fairall, G. M. Santos, J. W. Schwabe, Structure of HDAC3 bound to co-repressor and inositol tetraphosphate. *Nature* **481**, 335 (Jan 19, 2012).
84. J. Worley, X. Luo, A. P. Capaldi, Inositol pyrophosphates regulate cell growth and the environmental stress response by activating the HDAC Rpd3L. *Cell Rep* **3**, 1476 (May 30, 2013).
85. X. Tan *et al.*, Mechanism of auxin perception by the TIR1 ubiquitin ligase. *Nature* **446**, 640 (Apr 5, 2007).
86. L. B. Sheard *et al.*, Jasmonate perception by inositol-phosphate-potentiated COI1-JAZ co-receptor. *Nature* **468**, 400 (Nov 18, 2010).
87. A. Mosblech, C. Thurow, C. Gatz, I. Feussner, I. Heilmann, Jasmonic acid perception by COI1 involves inositol polyphosphates in Arabidopsis thaliana. *Plant J* **65**, 949 (Mar, 2011).
88. G. Parry *et al.*, Complex regulation of the TIR1/AFB family of auxin receptors. *Proc Natl Acad Sci U S A* **106**, 22540 (Dec 29, 2009).

89. D. L. Remington, T. J. Vision, T. J. Guilfoyle, J. W. Reed, Contrasting modes of diversification in the Aux/IAA and ARF gene families. *Plant Physiol* **135**, 1738 (Jul, 2004).
90. A. Chini *et al.*, The JAZ family of repressors is the missing link in jasmonate signalling. *Nature* **448**, 666 (Aug 9, 2007).
91. B. Vanholme, W. Grunewald, A. Bateman, T. Kohchi, G. Gheysen, The tify family previously known as ZIM. *Trends Plant Sci* **12**, 239 (Jun, 2007).
92. J. D. Jones, J. L. Dangl, The plant immune system. *Nature* **444**, 323 (Nov 16, 2006).
93. G. Trinchieri, Type I interferon: friend or foe? *J Exp Med* **207**, 2053 (Sep 27, 2010).
94. N. K. Pulloor *et al.*, Human genome-wide RNAi screen identifies an essential role for inositol pyrophosphates in Type-I interferon response. *PLoS Pathog* **10**, e1003981 (Feb, 2014).
95. B. A. Hemmings, D. F. Restuccia, PI3K-PKB/Akt pathway. *Cold Spring Harb Perspect Biol* **4**, a011189 (Sep, 2012).
96. A. Prasad *et al.*, Inositol hexakisphosphate kinase 1 regulates neutrophil function in innate immunity by inhibiting phosphatidylinositol-(3,4,5)-trisphosphate signaling. *Nat Immunol* **12**, 752 (Aug, 2011).
97. E. Lam, Controlled cell death, plant survival and development. *Nat Rev Mol Cell Biol* **5**, 305 (Apr, 2004).
98. J. B. Morel, J. L. Dangl, The hypersensitive response and the induction of cell death in plants. *Cell Death Differ* **4**, 671 (Dec, 1997).
99. T. P. Devarenne, S. K. Ekengren, K. F. Pedley, G. B. Martin, Adi3 is a Pdk1-interacting AGC kinase that negatively regulates plant cell death. *EMBO J* **25**, 255 (Jan 11, 2006).
100. C. Y. Hung, P. Aspesi, Jr., M. R. Hunter, A. W. Lomax, I. Y. Perera, Phosphoinositide-signaling is one component of a robust plant defense response. *Front Plant Sci* **5**, 267 (2014).
101. A. M. Murphy, B. Otto, C. A. Brearley, J. P. Carr, D. E. Hanke, A role for inositol hexakisphosphate in the maintenance of basal resistance to plant pathogens. *Plant J* **56**, 638 (Nov, 2008).
102. V. Raboy, The ABCs of low-phytate crops. *Nat Biotechnol* **25**, 874 (Aug, 2007).

CHAPTER II

"Regulation of Sucrose Non-Fermenting Related Kinase 1 Genes in *Arabidopsis thaliana*"

Adapted from: Sarah P. Williams, Padma Rangarajan, Janet L. Donahue, Jenna E. Hess and Glenda E. Gillaspy, *Frontiers in Plant Science* (2014) vol5:324. doi:10.3389/fpls.2014.00324

Contribution of Authors: SPW did confocal imaging and plant growth experiment, SPW and PR did promoter:Gus experiments, JH generated promoter:Gus Arabidopsis lines, JD did IP, protein activity assays and RT-PCR, GG directed the research, GG and SPW wrote the manuscript

Keywords:
SnRK1, trehalose, sugar-sensing, energy, gene expression

ABSTRACT

The Sucrose non-Fermenting Related Kinase 1 (SnRK1) proteins have been linked to regulation of energy and stress signaling in eukaryotes. In plants, there is a small *SnRK1* gene family. While the *SnRK1.1* gene has been well studied, the role other SnRK1 isoforms play in energy or stress signaling is less well understood. We used promoter:GUS analysis and found *SnRK1.1* is broadly expressed, while *SnRK1.2* is spatially restricted. *SnRK1.2* is expressed most abundantly in hydathodes, at the base of leaf primordia, and in vascular tissues within both shoots and roots.

We examined the impact that sugars have on *SnRK1* gene expression and found that trehalose induces *SnRK1.2* expression. Given that the SnRK1.1 and SnRK1.2 proteins are very similar at the amino acid level, we sought to address whether SnRK1.2 is capable of re-programming growth and development as has been seen previously with SnRK1.1 overexpression. While gain-of-function transgenic plants overexpressing two different isoforms of SnRK1.1 flower late as seen previously in other SnRK1.1 overexpressors, SnRK1.2 overexpressors flower early. In addition, SnRK1.2 overexpressors have increased leaf size and rosette diameter during early development, which is the opposite of SnRK1.1 overexpressors. We also investigated whether SnRK1.2 was localized to similar subcellular compartments as SnRK1.1, and found that both accumulate in the nucleus and cytoplasm in transient expression assays. In addition, we found SnRK1.1 accumulates in small puncta that appear after a mechanical wounding stress. Together, these data suggest key differences in regulation of the *SnRK1.1* and *SnRK1.2* genes in plants, and highlights differences overexpression of each gene has on the development of Arabidopsis.

INTRODUCTION

The Sucrose non-Fermenting Related Kinase 1 (SnRK1) family of proteins has been linked to regulation of energy metabolism and stress signaling in diverse types of eukaryotes (*1-3*). All plants surveyed contain *SnRK1* genes that are structurally and functionally analogous to their yeast and mammalian counterparts, sucrose non-fermenting 1 (*SNF1*) and AMP-activated protein kinase (*AMPK*), respectively. SNF1, AMPK and SnRK1 are Ser/Thr protein kinases that are considered to function as fuel gauge sensors that sense cellular carbohydrate status and/or AMP/ATP levels in order to maintain growth in response to available energy (*4-7*). SnRK1

proteins carry out their function as part of heterotrimeric protein complexes, binding to β and γ subunits (*8-10*) or to a hybrid βγ subunit in plants (*11-13*).

The small Arabidopsis *SnRK1* gene family is composed of three genes, *SnRK1.1*, *SnRK1.2*, and *SnRK1.3* (*14*). While *SnRK1.3* is considered a non-expressed pseudogene, the roles of *SnRK1.1* and *SnRK1.2* were delineated in seminal work by Baena-Gonzalez using a genetics approach in *Arabidopsis thaliana.* Overexpression of the *SnRK1.1* gene re-programs metabolism such that flowering and senescence of mature plants is delayed (*14*). The delay in flowering and senescence effectively lengthens the lifespan of the plant, most likely through the combined direct protein phosphorylation of SnRK1 substrates, regulation of transcription in the nucleus (*14*), and post-transcriptional regulation of target genes (*15*). Some of the known SnRK1 substrates are key metabolic enzymes such as sucrose phosphate synthase, nitrate reductase and HMG-CoA reductase (*16*), while others such as FUS3 are transcription factors (*17*). FUS3 and SnRK1.1 interact to regulate embryonic-to-vegetative and vegetative-to reproductive phase transitions and lateral organ development (*17*). *FUS3*-overexpression delays vegetative growth and flowering by increasing levels of ABA, while repressing GA biosynthesis and ethylene signaling (*18*). Therefore, SnRK1 may regulate post-embryonic development through regulation of hormone biosynthesis and signaling. Analysis of *SnRK1* genetic mutants in Arabidopsis showed that *SnRK1.1* and *SnRK1.2* genes have partially redundant functions, and when expression of both genes are reduced, seedling growth under low energy conditions is compromised and mature plants undergo growth deprivation, early flowering and early senescence (*14*). Comparable phenotypes were also shown in moss (*Physcomitrella patens*), in

which a double mutant lacking the two *SnRK1* genes has accelerated development and early senescence (*19*).

Other gain-of-function studies have shown that SnRK1.1 overexpressors are altered in ABA as well as sugar signaling pathways (*20*). Recent work has shown that SnRK1.1 and SnRK1.2 interact with two clade A type 2C protein phosphatases, established repressors of the ABA signaling pathway. Inactivation of SnRK1.1 by these phosphatases may allow for the coordinated activation of ABA and energy signaling (*21*). The SnRK1.1 and SnRK1.2 proteins are 81% identical and contain a similar arrangement of functional domains including an N-terminal kinase domain, a Ubiquitin associated (UBA) domain, and a C-terminal kinase associated domain. The regions outside the kinase domain have been shown to facilitate SnRK1 protein interactions with various proteins, indicating that SnRK1 proteins may be part of several different protein complexes (*22-25*).

Interestingly, biochemical data has indicated that SnRK1 activity in plant cells is mostly a function of the SnRK1.1 gene product (*20*), thus the *SnRK1.2* gene may play a minor or restricted role in regulating most plant metabolism, stress and/or energy sensing. The Arabidopsis *SnRK1.2* gene has been overexpressed in *N. benthamiana*, where overexpression leads to enhanced resistance to geminiviral infection, although at the cost of adverse effects on plant growth (*22*). Although the network of genes regulated by SnRK1 has been elucidated (*14*), our understanding of how the *SnRK1.1* and *SnRK1.2* genes themselves are regulated and function with respect to one another has not been addressed. The *SnRK1* genes have been shown to be expressed throughout development, including within the meristem and leaf primordial (*26-30*),

however very little spatial information on the expression of different *SnRK1* genes within a species exists.

Given that there are multiple cDNAs of both *SnRK1* genes expressed in plants, we sought to address the spatial regulation of *SnRK1.1* and *SnRK1.2* in Arabidopsis, how different sugars impact expression of these genes, and how different SnRK1 protein isoforms alter plant growth and development when overexpressed. Our data show that *SnRK1.2* gene expression is spatially restricted within Arabidopsis, and can be induced by trehalose, but not other sugars. When overexpressed, a SnRK1.2-green fluorescent protein (GFP) gene fusion alters development in a manner opposite in nature to overexpression of *SnRK1.1-GFP*. These data suggest that *SnRK1.2* may have a unique function in plants that warrants further investigation.

RESULTS

Developmental Regulation of SnRK1.1 and SnRK1.2 Expression

To explore the role SnRK1 may play in plant growth and development, we examined the spatial and temporal regulation of expression of the *SnRK1.1* and *SnRK1.2* genes. Promoter:gene reporter transgenic plants were constructed using 0.8 kB and 4.3 kB of the *SnRK1.1* and *SnRK1.2* promoters, respectively. Multiple lines of *SnRK1.1p:GUS* and *SnRK1.2p:GUS* seedlings were identified, and homozygous lines were isolated and studied to verify reproducibility of GUS staining patterns. When *SnRK1.1p:GUS* and *SnRK1.2p:GUS* seedlings are grown on MS agar without an added carbon source, a striking difference in GUS expression is noted (**Figure 2.1 A-D**). The *SnRK1.1* promoter drives expression throughout the seedling, with highest expression in

leaf primordia and vascular tissue (**Figure 2.1A**), and the seedling root tip (**Figure 2.1 C**). In contrast, expression of the *SnRK1.2* promoter is restricted to only a few cells at this stage including hydathodes, leaf primordia and in portions of the cotyledon vascular tissue (**Figure 2.1 B,D**). At ten days both promoters drive strong expression in developing leaves (**Figure 2.1 E, F**), with the *SnRK1.2* promoter restricted to the base of the leaf, the vascular tissue and the hydathodes (**Figure 2.1F**). Soil-grown plants were analyzed and indicate that *SnRK1.1* continues to be broadly expressed in the shoot (**Figure 2.1G**), whereas, activity of the *SnRK1.2* promoter is restricted to the base of newly developing leaves and hydathodes (**Figure 2.1H**). In roots, expression of *SnRK1.1* is abundant in vascular tissue and developing lateral root primordia with no added carbon source (**Figure 2.1J, K, 2.2A,B**), and in soil (**Figure 2.1K**). *SnRK1.2* is not abundantly expressed in roots until 10 d, at which time its expression is similar to that of *SnRK1.1* (**Figure 2.2A,B**). *SnRK1.1* is expressed in developing embryos within siliques, but *SnRK1.2* is not (**Figure 2.1L-O**). We conclude that *SnRK1.1* is more abundant and broadly expressed in plant tissues, whereas *SnRK1.2* expression is more spatially restricted.

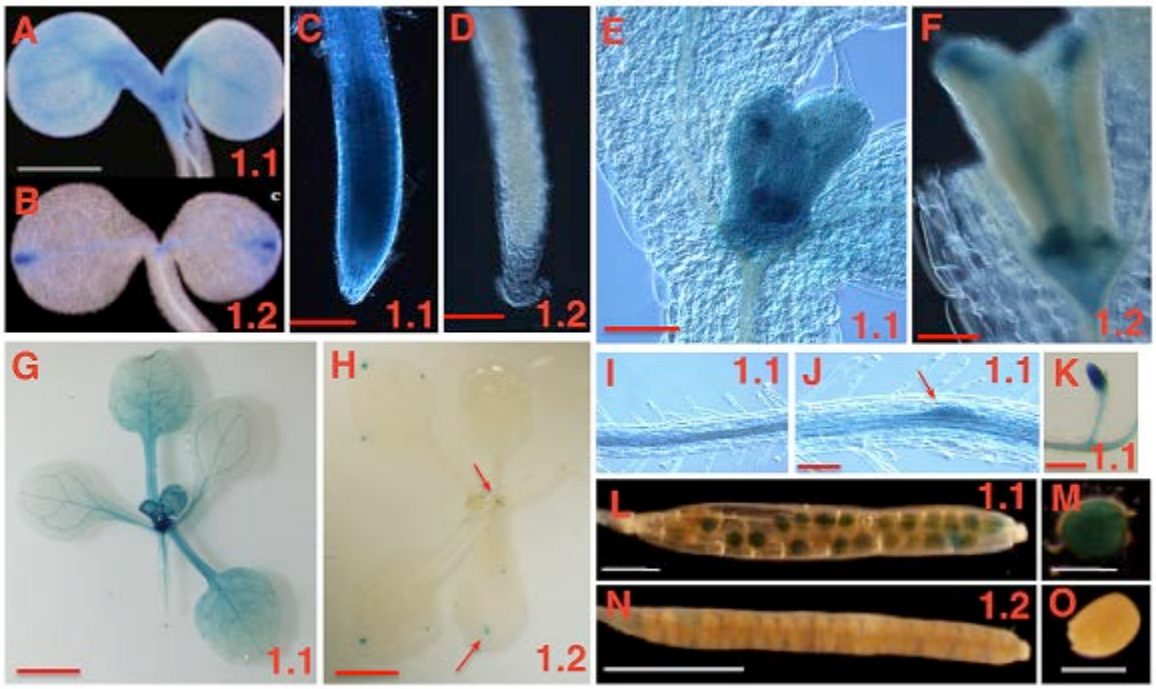

Figure 2.1. Spatial Expression Patterns of *SnRK1.1* and *SnRK1.2* Genes

The promoters from *SnRK1.1* (1.1 shown in A,C,E,G,I-K,L,M) or *SnRK1.2* (1.2 shown in B,D,F,H,N,O) were used to drive GUS expression in transgenic plants. (A-F, I, J) are from plants grown on MS agar with no added sugar, and (G, H, L-O) are from soil-grown plants. (A, B) 5 d cotyledons, bar = 1 mm. (C, D) 5 d roots, bar = 100 µM. (E, F) 10 d leaf primordia, bar = 100 µM. (G, H, and K) 15 d plants and roots, bar = 2 mm. (I, J) 10 d roots, bar = 100 µM; (L, M) siliques, (N, O) developing seed, bar = 500 µM.

Regulation of SnRK1.1 and SnRK1.2 Expression by Sugars

Because of the role of SnRK1 in carbon sensing and allocation in plants (*14, 20, 31*), we investigated whether different carbon sources would alter the patterning of *SnRK1* expression as measured in *SnRK1.1p:GUS* and *SnRK1.2p:GUS* plants. In addition, we used quantitative RT-PCR (Q-PCR) to determine whether the abundance of *SnRK1.1* and *SnRK1.2* transcripts in wildtype plants were increased by sugar treatment. Seedlings grown for 5 and 10 d in the presence of trehalose, sucrose, glucose, fructose or mannitol, did have small alterations in expression of *SnRK1.1* in the shoot, but these changes may be indicative of changes in the developmental state (see GUS staining in cotyledons and new leaves in **Figure 2.2A,B** top panels). When a shorter-term treatment of sugar (24 hr) is given to 9 d seedlings and *SnRK1.1* expression is measured by Q-PCR, we find that *SnRK1.1* expression is slightly, but significantly, decreased by treatment with fructose, glucose, sucrose, but not trehalose or mannitol (**Figure 2.3**). In contrast, trehalose increases *SnRK1.2* expression, as seen by changes in GUS staining of *SnRK1.2p:GUS* seedlings grown for 5 or 10 d in trehalose (**Figure 2.2A,B**). Specifically, trehalose induced expression of *SnRK1.2* in 5 d seedling roots that extended to the top of the root tip (**Figure 2A**, bottom panel). Trehalose also elevated *SnRK1.2* expression in 10 d seedling roots, hydathodes, vascular tissue and the base of the leaf (**Figure 2.2B**, bottom panel). This increase in *SnRK1.2* expression is also noted when a shorter-term treatment of sugar (24 hr) is given to 9 d seedlings (**Figure 2.3**). In this short-term sugar treatment, mannitol also decreased *SnRK1.2* expression to small degree (**Figure 2.3**). We conclude that trehalose increases *SnRK1.2* expression, while mannitol decreases *SnRK1.2* expression. Regulation of *SnRK1.1* differs as other sugars such as sucrose, glucose and fructose result in a small decline in *SnRK1.1* expression in seedlings.

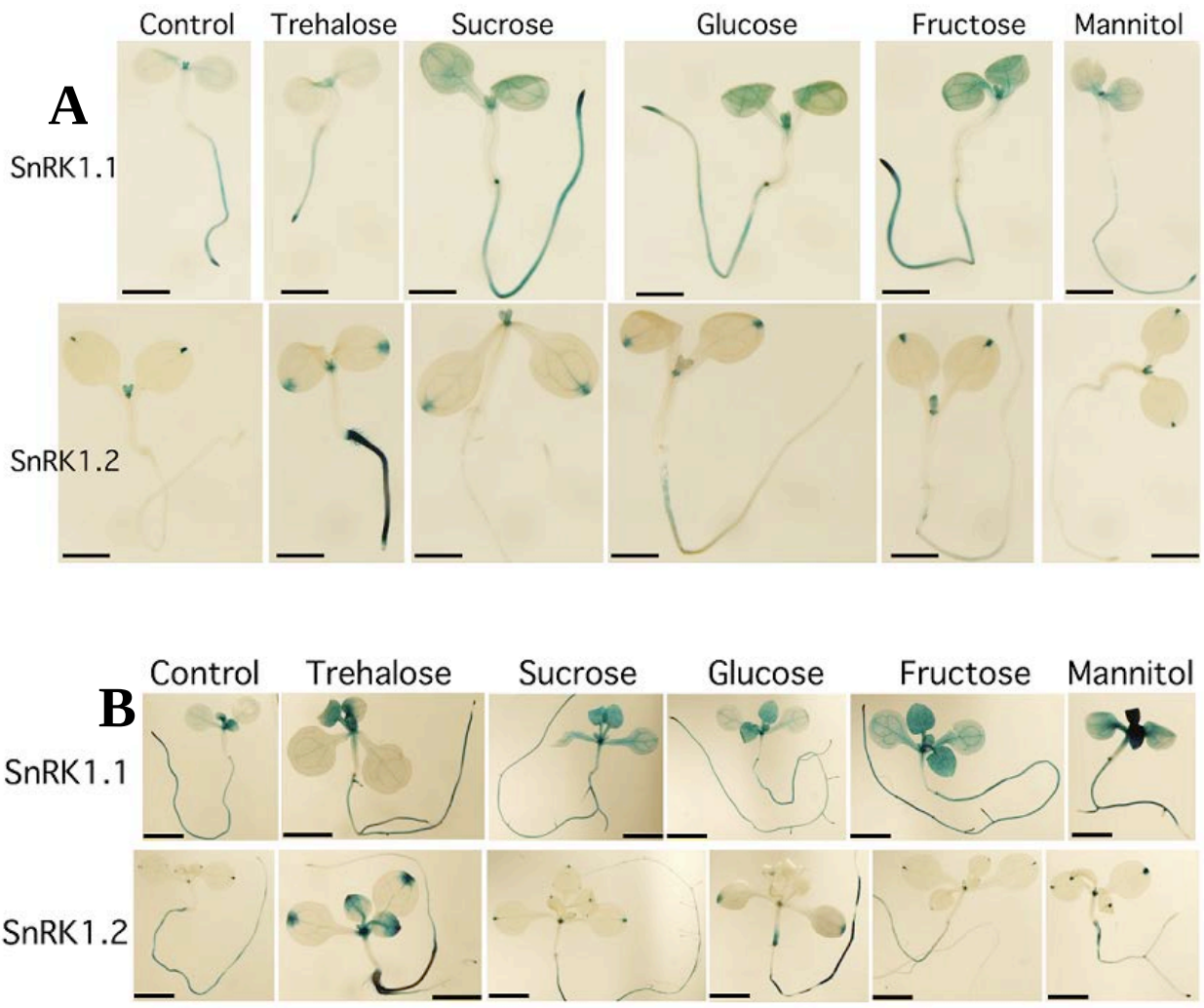

Figure 2.2. Effects of Sugars on the Expression of *SnRK1.1* and *SnRK1.2*

(A) 5 d seedlings grown with 1% trehalose, 3% sucrose,1.5% glucose, 1.5% fructose or 3% mannitol. Bar = 1 mm. (B) 10 d seedlings grown with the same sugars as in A. Bar = 2 mM.

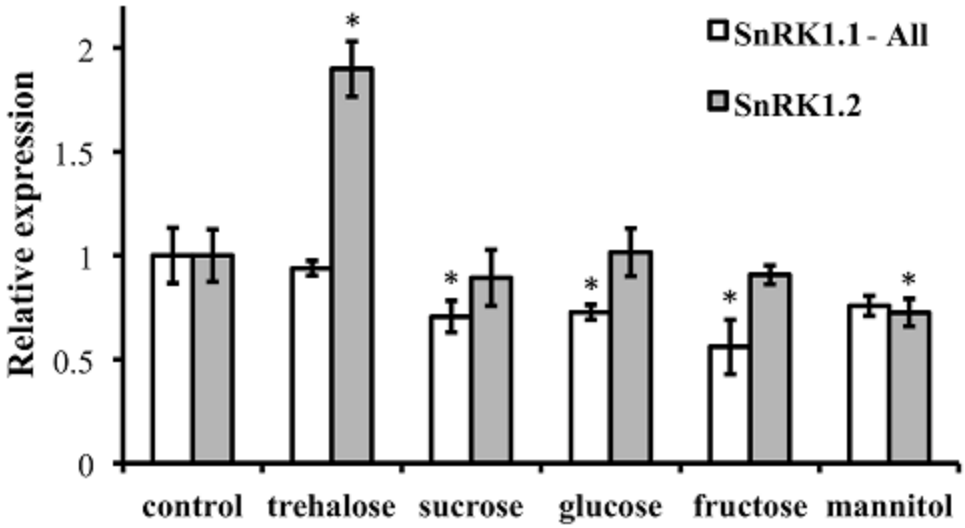

Figure 2.3. RNA Levels of *SnRK1.1* and *SnRK1.2* in Sugar-treated Seedlings

Wildtype seedlings were grown for 9 days and then treated with no sugar (control), 1% trehalose, 1.5% sucrose, 1.5% fructose, or 3% mannitol. *SnRK1.1* and *SnRK1.2* expression was measured with real-time PCR and was normalized to *SnRK1.1* control and *SnRK1.2* control levels, respectively, which are set to 1. SnRK1.1-All primers amplify all SnRK1.1 cDNAs, including those that encode SnRK1.1 and SnRK1.1T proteins. Means of triplicate reactions $\pm$ SE are presented. *, p value ≤ 0.05 when compared to the control.

SnRK1.1 and SnRK1.2 cDNAs and SnRK1 Protein Isoforms

After noticing significant differences in a group of so-called full-length *SnRK1.1* cDNAs, we compared the structures of different *SnRK1.1* and *SnRK1.2* cDNAs (**Figure 2.4A**). For this analysis we focused solely on verified full-length cDNAs. Both *SnRK1* genes are predicted to undergo differential splicing of a non-coding exon located at the 5'end, and in the case of *SnRK1.1*, alterations in splicing can result in two SnRK1.1 protein isoforms differing in a 23 amino acid extension at the N-terminus (**Figure 2.4A,B**). We have named the shorter truncated protein SnRK1.1T, while we call the longer protein SnRK1.1 (**Figure 2.4B**). Comparison of SnRK1.1, SnRK1.1T and SnRK1.2 predicted proteins shows that the 23 amino acid extension is unique to SnRK1.1, while all three proteins contain highly similar sequences and protein domains (**Figure 2.4B**, **Supp. Figure 2.11**). It is important to note that most investigations on *SnRK1.1* focus on the SnRK1.1T isoform, including the complementation of the yeast *snf1* mutant (*32*), and re-programming of Arabidopsis growth and ABA responses by overexpression (*14, 20*).

We first used quantitative PCR to confirm the developmental expression patterns noted with promoter-GUS constructs, and to confirm that cDNAs capable of encoding the SnRK1.1 and SnRK1.1T proteins were expressed in Arabidopsis. For this work we designed oligonucleotide primers to amplify the unique 5'end of the longer *SnRK1.1* cDNA that can encode the extra 23 amino acids (SnRK1.1), as well as the set of primers we previously used to amplify ***all*** *SnRK1.1* cDNAs (called SnRK1.1-All), plus a set to amplify *SnRK1.2*. We found very little expression of the longer SnRK1.1 isoform in all tissues examined (**Figure 2.5**). In contrast, our SnRK1.1-All primers detected expression at fairly high levels in seedlings, leaves, roots, cauline leaves,

flowers and siliques (**Figure 2.5**), indicating that the majority of SnRK1.1 expressed in these tissues has the ability to encode the SnRK1.1T protein isoform. *SnRK1.2* was also expressed in these tissues, but at a lower level as compared to *SnRK1.1* (**Figure 2.5**).

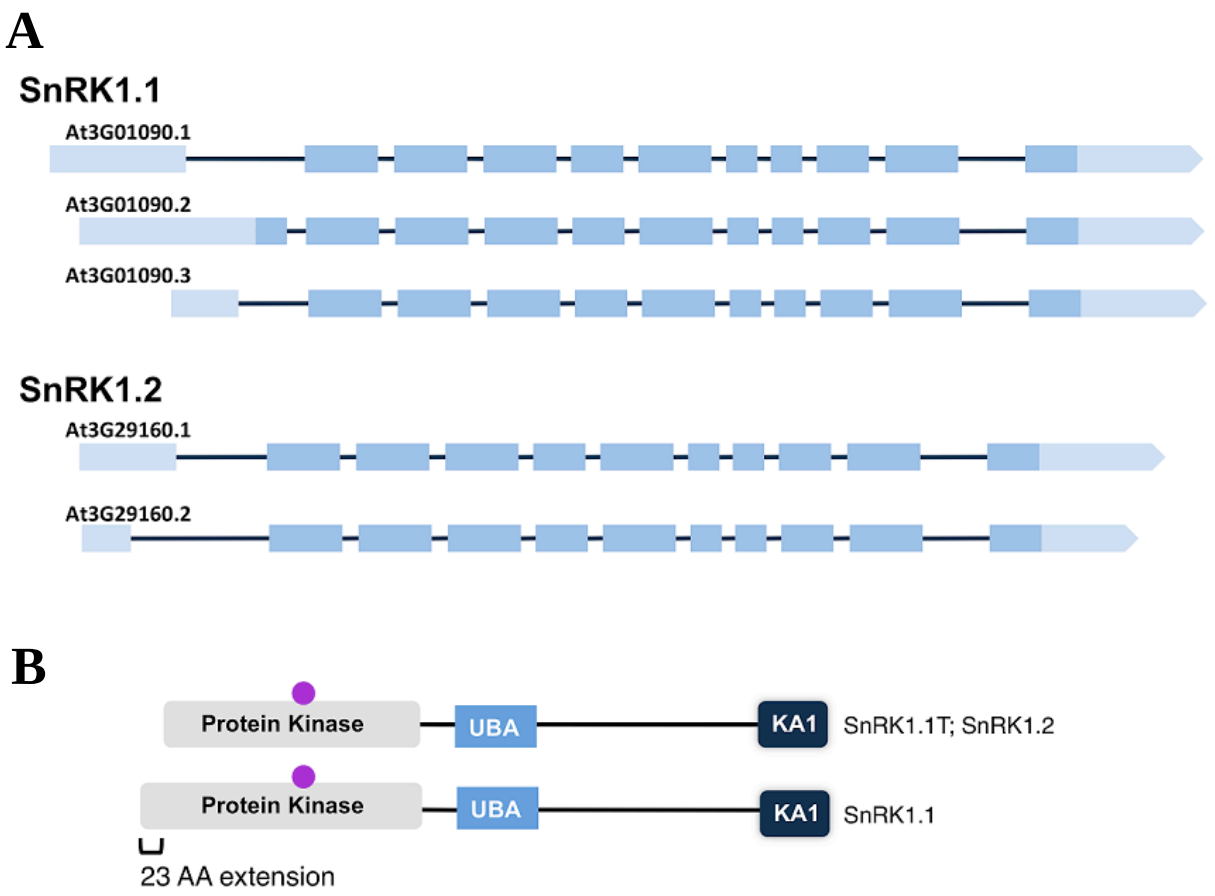

Figure 2.4. Map of SnRK1 Isoforms and Domain Structures

(A) The reported intron-exon maps of *SnRK1* genes. Dark boxes denote exons while light boxes denote 5' and 3' UTRs. (B) SnRK1 kinases contain 3 domains: Protein Kinase, Ubiquitin Associated (UBA), and Kinase Associated 1 (KA1). The location of the active site residues are indicated by a purple circle.

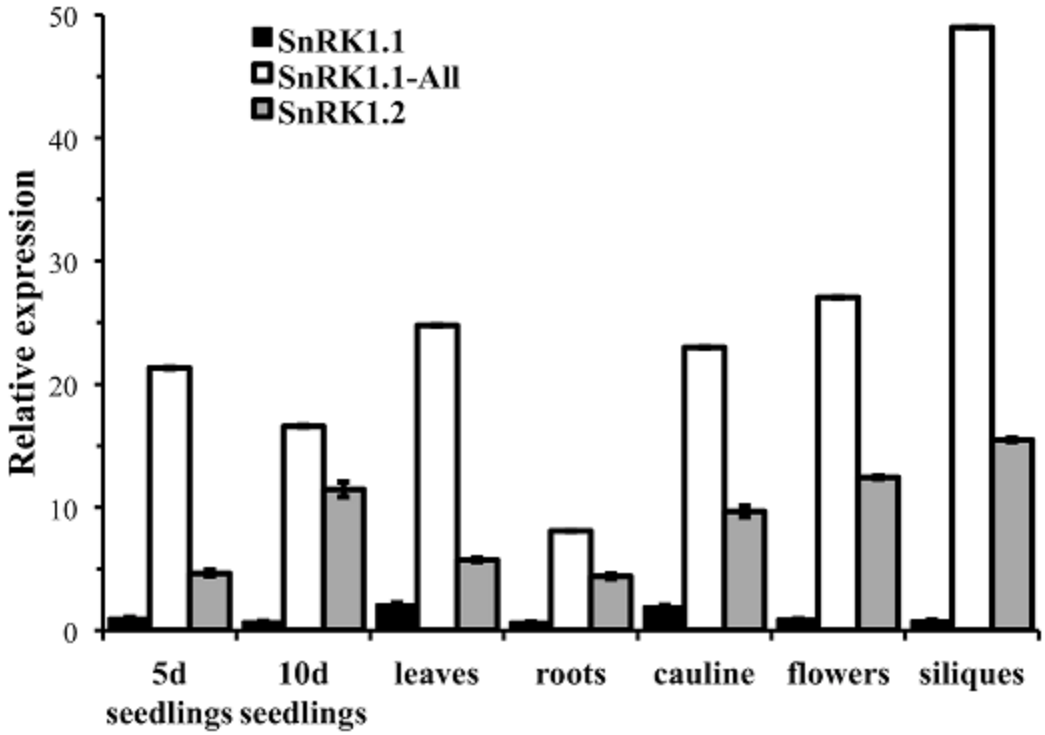

Figure 2.5. Relative Expression of *SnRK1* Genes as Determined by Real-Time PCR

Primers specific for amplifying the longer cDNA clone that encodes the SnRK1.1 protein (SnRK1.1), all SnRK1.1 cDNAs (SnRK1.1 - All), and SnRK1.2 were used to measure expression in 5 d and 10 d seedlings (seedlings), and tissues from 6 week-old soil-grown plants: rosette leaves, roots, cauline leaves, flowers, and green siliques. *SnRK1* expression was compared to *PEX4* to generate relative expression levels. Means of triplicate reactions are presented.

Overexpression of Different SnRK1 Proteins *in Planta*

To determine whether the three SnRK1 protein isoforms (SnRK1.1, SnRK1.1T and SnRK1.2) are each capable of altering plant growth and development, we compared the impact of overexpression of each. We used the 35S CaMV promoter to drive SnRK1-green fluorescent protein (GFP*)* gene fusions, and identified two independent lines with ectopic expression of *SnRK1.1*, *SnRK1.1T* and *SnRK1.2*. Transgenic plants were characterized with respect to transgene expression using real time PCR. **Figure 2.6** shows that our SnRK1.1-GFP, SnRK1.1T-GFP and SnRK1.2-GFP plants accumulate transgenic RNA (**Figure 2.6A-C** respectively). In addition, we examined total *SnRK1.1* and *SnRK1.2* RNAs in these lines to confirm overexpression (**Figure 2.6D-G**). This analysis also showed that overexpression of the transgene was greater in some lines as compared to others, and could vary during development. For example, SnRK1.1a contains higher expression of *SnRK1.1* than SnRK1.1b in seedlings, but not leaves (**Figure 2.6A,B,D,E**). Interestingly, *SnRK1.2* levels were increased in SnRK1.1T-GFP plants (**Figure 2.6E**). Panels F and G in **Figure 2.6** indicate that SnRK1.2-GFP overexpression seedlings have a 2.4- and 2.9-fold increase in *SnRK1.2* RNA (**Figure 2.6F**), while leaves from these same plants indicate a 4.5- and 3.6-fold increase in *SnRK1.2* expression (**Figure 2.6G**).

We also wanted to verify that our SnRK1 transgenic plants accumulated active SnRK1 protein. Since removal of other contaminating kinases present in plant extracts is key to examining SnRK1 activity, we used immunoprecipitation of tagged SnRK1 proteins from plant extracts, followed by SnRK1 activity assays for this verification. Previously characterized Arabidopsis SnRK1 overexpressors constructed in the *Landsberg erecta* (Ler) ecotype (herein called SnRK1.1T-HA plants) were utilized as a positive control, and wildtype Arabidopsis Col and Ler

plants were used as negative controls. Crude protein extracts from leaves were incubated with either anti-GFP agarose or anti-HA antibodies coupled to Protein A sepharose beads, and bound, washed proteins were incubated in SnRK1 activity assays with the SPS substrate peptide and γ-P^{32}-ATP as described previously (*33*) (**Figure 2.7A**). In addition, bound and washed proteins were analyzed by western blotting with anti-SnRK1.1, anti-GFP or anti-HA antibodies to examine the immunoprecipitated proteins (**Figure 2.7B**). The anti-SnRK1 antibody is described in detail in the Methods. As expected, we found that wildtype Col and Ler extracts had minimal (i.e. background) levels of SnRK1 activity (measured by the pmoles of P^{32} added to the SPS substrate peptide) (**Figure 2.7A**). In contrast, immunoprecipitated proteins from SnRK1.1-GFP, SnRK1.1T-GFP and SnRK1.1T-HA plants indicated that all transgenic SnRK1.1 proteins are catalytically active (**Figure 2.7A**). However, immunoprecipitated SnRK1.1-GFP has 57%, and SnRK1.1T-GFP has 80%, respectively, of the activity of SnRK1.1T-HA, suggesting that both GFP-tagged proteins have a reduction in their SnRK1 activity as compared to the HA-tagged protein. Western blotting with an anti-SnRK1 antibody verifies that proteins of the correct size were present in the immunoprecipitation, that anti-GFP and anti-SnRK1 antibodies detect similarly sized proteins, and that the SnRK1.1T protein is slightly decreased in size from the larger, SnRK1.1 protein (**Figure 2.7B**). It is important to note that we tried several times to immunoprecipitate SnRK1.2-GFP from transgenic extracts, but could not obtain enough protein to do reliable activity assays. We could detect a faint band corresponding to SnRK1.2-GFP in both crude plant extracts and immunoprecipitations, so we conclude that SnRK1.2-GFP protein is being synthesized, however, the levels of this protein are very low, and preclude measuring enzyme activity.

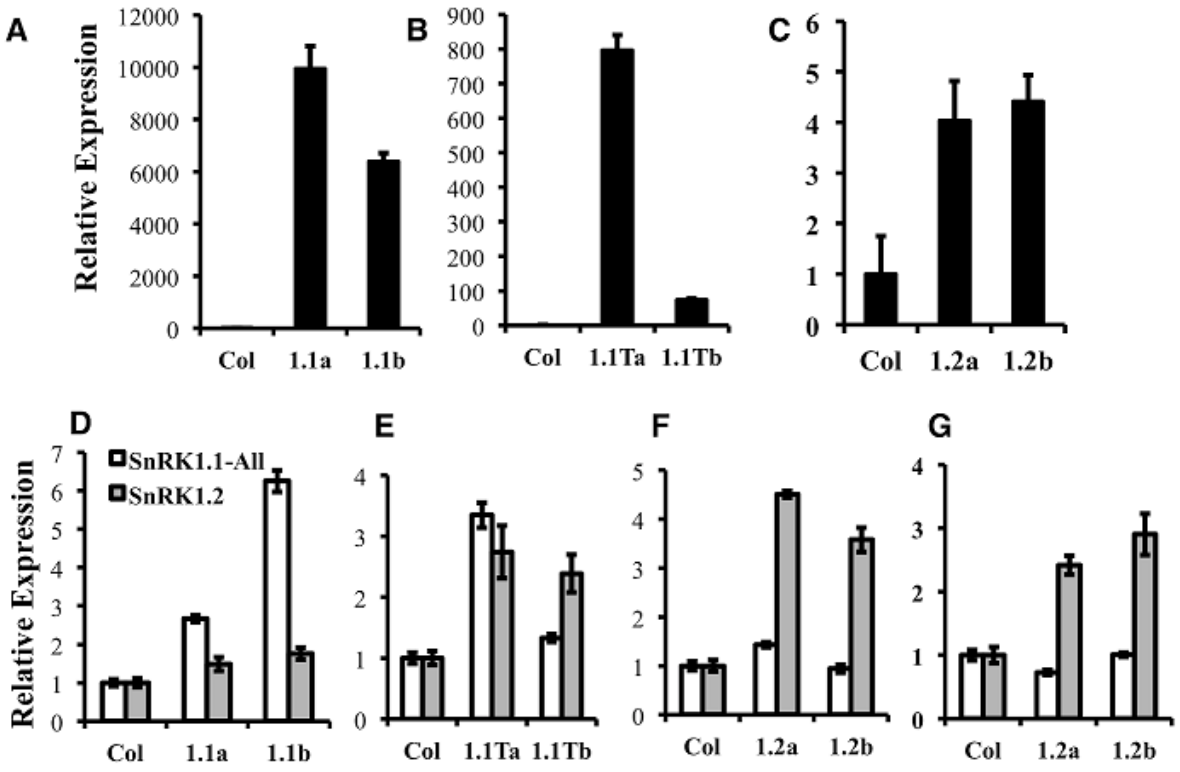

Figure 2.6. Expression of Transgenes in SnRK1 Transgenic Plants

(A-C) Relative levels of *GFP* expression in 10 d seedlings of wild type (Col), SnRK1.1-GFP, SnRK1.1T-GFP and SnRK1.2-GFP. (D-G) Relative levels of *SnRK1.1* and *SnRK1.2* expression in the indicated lines with RNA extracted from (D-F) rosette leaves of 60 d soil-grown plants, and (E) 10 d seedlings. Means of triplicate reactions ± SE are presented. Two or more biological replicates were performed for each.

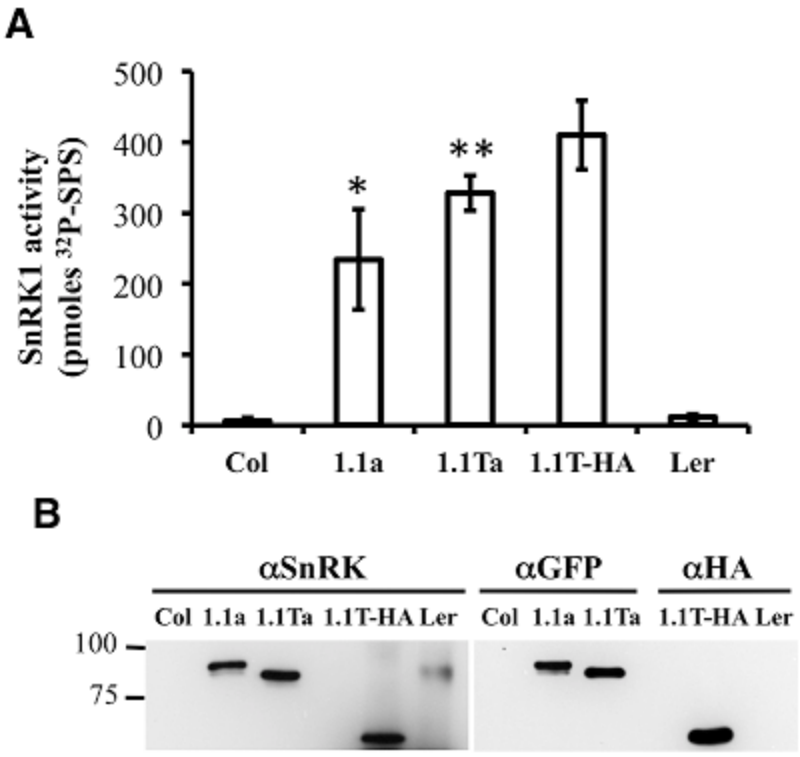

Figure 2.7. SnRK1 Activity in Transgenic Plants

(A) SnRK1 proeins were immunoprecipitated as described in the Methods, and kinase assays were performed. Means of 3 triplicate reactions ± SE are presented. *, p value ≤ 0.01, and ** indicates a p value less than 0.05 as compared to the 1.1T-HA sample. (B) An equal amount of sample was detected by western analysis with anti-SnRK, anti-GFP, or anti-HA antibody.

Overexpression of SnRK1.2 Decreases Time to Flowering

Previously characterized Arabidopsis SnRK1 overexpressers (SnRK1.1T-HA plants constructed in the Ler background) (*14*), and SnRK1.1-HA plants constructed in the Col background (*17*), flower late, due to delayed developmental transitions throughout the life of the plant (*34*). This suggests that the 23 amino acid N-terminal extension missing in the SnRK1.1T protein does not impact function. Whether or not overexpression of SnRK1.2 has a similar effect on delaying developmental transitions has not been reported. To address these issues, we compared our SnRK1.1-GFP, SnRK1.1T-GFP and SnRK1.2-GFP plants to the previously characterized SnRK1.1T-HA plants (see **Figure 2.13**). We grew each transgenic line and matched wildtypes in different growth rooms and chambers set to standard long-day conditions in three separate experiments, and measured the days to flowering (**Figure 2.8**). As shown previously by others, SnRK1.1T-HA plants are significantly delayed in their flowering, by 3.3 d (**Figure 2.8A**). Both SnRK1.1-GFP lines also consistently flower late by app. 1 d, and this difference is statistically significant for the SnRK1.1b line (**Figure 2.8A**). The SnRK1.1T-GFP lines also flower late by 1.9 and 1.2 d respectively (**Figure 2.8A**). Unexpectedly, both SnRK1.2-GFP lines flower early with a 3.6 and 4.5 d difference in days to flowering, respectively (**Figure 2.8A**). These same trends in flowering time were also seen when the number of leaves to flowering were measured, although in some cases the differences were not statistically significant (**Figure 2.8B**). We conclude that overexpression of SnRK1.2 has the opposite impact on flowering time as compared to that of SnRK1.1 overexpression. We also conclude that the reduction in SnRK1 activity caused by the GFP tag and the extra 23 aa present in SnRK1.1-GFP do not alter the ability of these proteins to induce late flowering when overexpressed, however, these changes may decrease the degree to which flowering time is delayed.

In addition to flowering early, we also noticed that SnRK1.2-GFP plants tend to have flatter leaves (**Figure 2.8C**), that are ~120% longer and 108% wider as compared to wildtype leaves (**Figure 2.14**). Thus, overall, the appearance of SnRK1.2-GFP plants is altered when compared to wildtype or the other SnRK1.1-GFP lines (**Figure 2.14**). It is interesting to note that in our hands, the SnRK1.1T-HA plants are developmentally delayed until flowering, and then after flowering vegetative biomass increases, which is a potentially valuable trait (**Figure 2.14**). To compare the growth and development of all SnRK1 transgenic lines, we examined growth throughout development, using rosette diameter as one indicator of organism size (**Figure 2.9**). This analysis shows that SnRK1.1T-HA plants have a smaller rosette size through 28 d, and by 35 d their rosette diameter is larger (**Figure 2.9**). SnRK1.1-GFP and SnRK1.1T-GFP lines have a similar trend up to 28 d, with both lines of each type showing smaller rosette diameter (**Figure 2.9**). In contrast, both SnRK1.2-GFP lines have a larger rosette diameter until 28 d (**Figure 2.9**). After 28 d, data on rosette width starts to vary within each set of lines (**Figure 2.9**). Even though we tried to tightly control these experiments and repeated them with 3 biological replicates (N= 100-120 plants of each type), we have been unable to obtain consistent results on organism size of SnRK1-GFP plants during late stages of development. This is in stark contrast to the SnRK1.1T-HA plants that show very consistent increases in organismal size post-flowering (**Figure 2.9** and **Figure 2.14**).

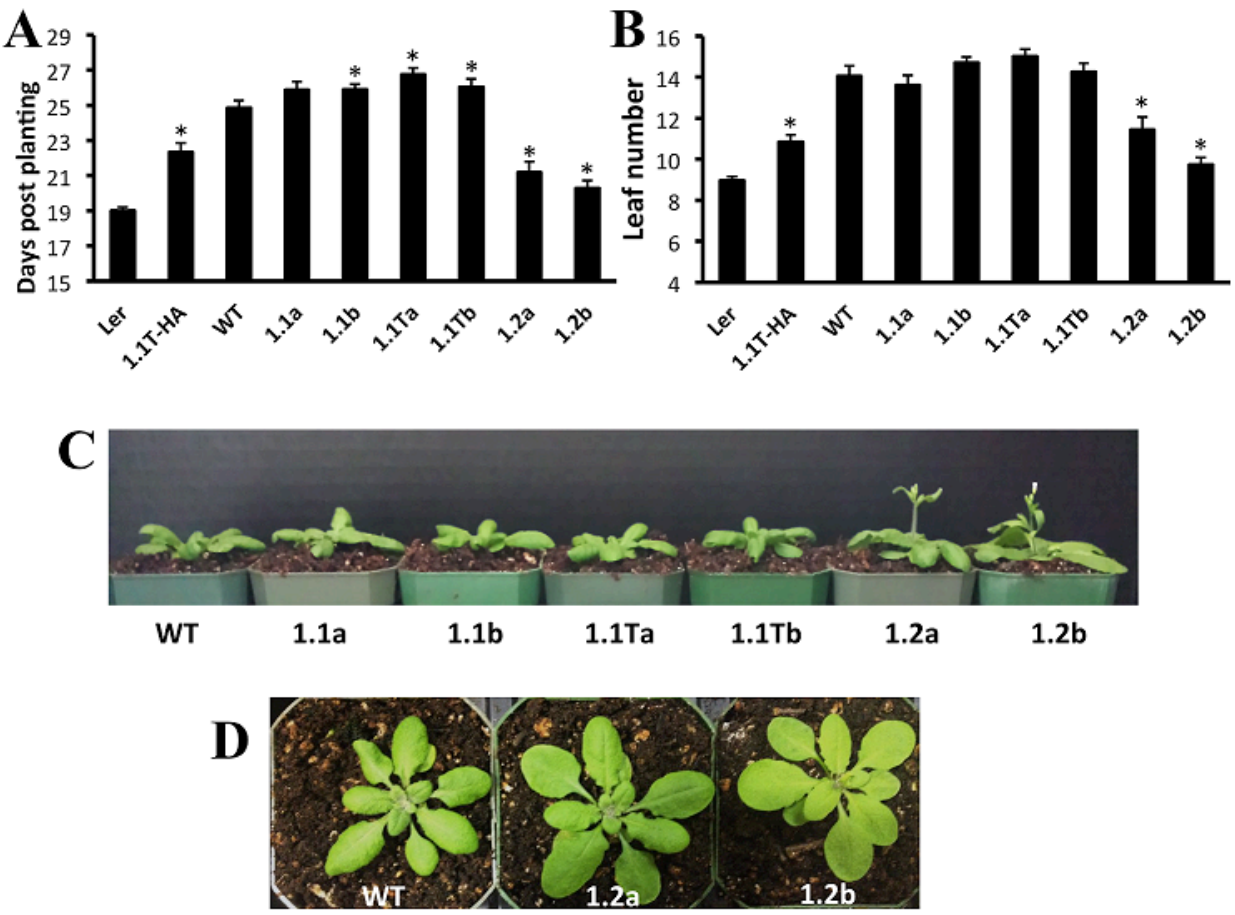

Figure 2.8. Flowering Time Alterations in SnRK1 Transgenic Plants

(A) Days to flowering and (B) Number of leaves at flowering of soil-grown Arabidopsis wild type and SnRK1 overexpressing lines. (C) 21 d plants (D) 23 d plants. N = 30 plants for each genotype. Means $\pm$ SD are presented. *, p value ≤ 0.05 when compared to the wildtype control. This experiment was replicated three times.

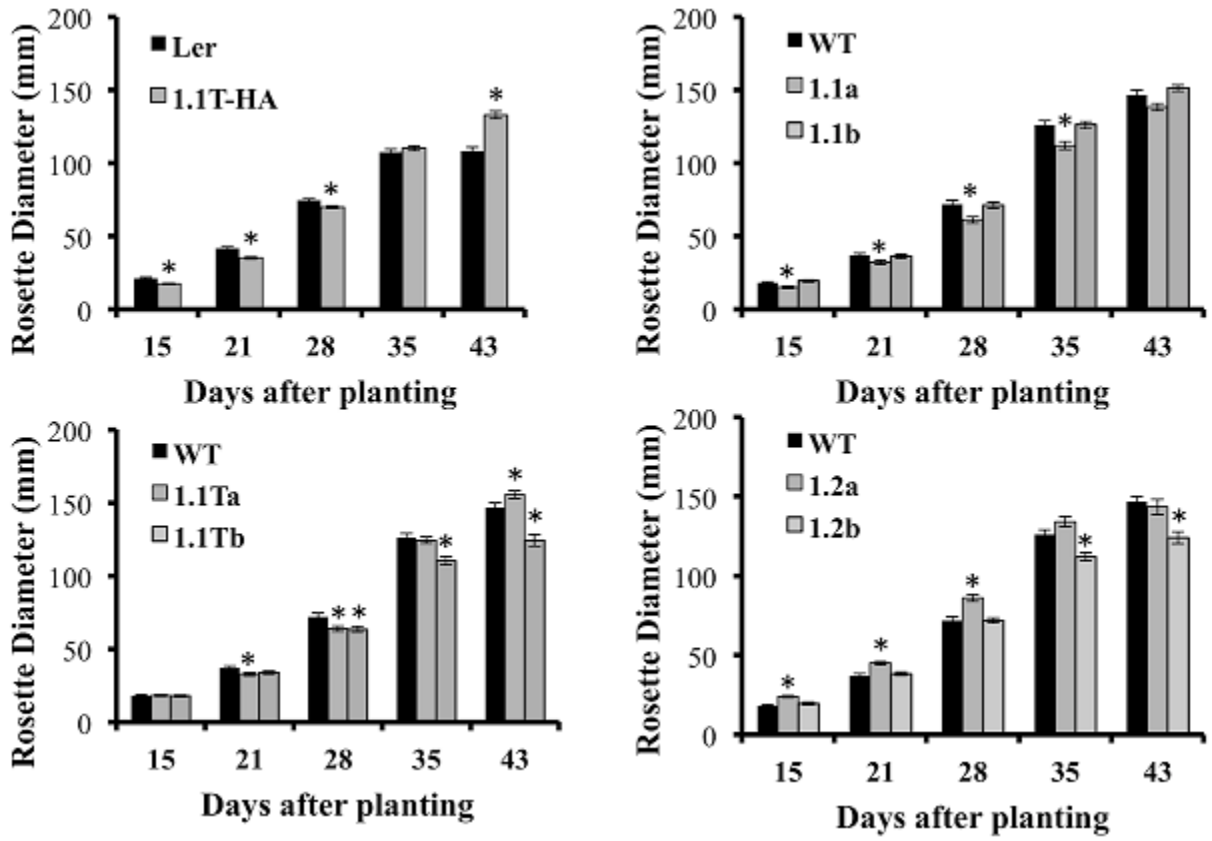

Figure 2.9. Rosette Diameter Measurements

Rosette diameter of soil-grown plants grown under long day conditions for the indicated number of days. Means ± SD are presented. *, p value ≤ 0.05 when compared to the wildtype control.

Subcellular Localization of SnRK1.1, SnRK1.1T and SnRK1.2

To investigate the subcellular location of SnRK1.1, SnRK1.1T and SnRK1.2, we first expressed each construct in *N. benthamiana* leaves in transient expression assays. To ensure the patterns observed were not due to overexpression and off-target accumulation, we used confocal microscopy to image cells at 12, 24, 48 and 72 hours after infiltration (data not shown). We found each SnRK1-GFP isoform was expressed and accumulated stably as measured by protein blotting (**Figure 2.10**, Top). 48 hours after agro-infiltration, SnRK1.1-GFP localizes to the cytoplasm and nucleus, however the most striking signal is from large puncta that do not co-localize with chloroplasts (**Figure 2.10A**). To further investigate these puncta we transiently expressed SnRK1.1-GFP with mCherry organelle markers in *N. benthamiana.* The SnRK1.1-GFP puncta do not co-localize with Golgi, peroxisomes or mitochondria (**Figure 2.15A-C**). We found that SnRK1.1T-GFP localizes to the cytoplasm and nucleus as does SnRK1.2-GFP (**Figure 2.10B, C** respectively). While performing localization experiments, it was observed that SnRK1.1T-GFP plants form very small puncta in addition to the prior nuclear and cytoplasmic signal. The small puncta first appear in cells near the cut margin of the leaf, and increased over time after cutting and preparing samples for microscopy (**Figure 2.10E**). Similar smaller puncta were observed in SnRK1.1-GFP cells, however they took on the order of 30 more minutes to appear (**Figure 2.10D**). No large accumulation of puncta were observed in SnRK1.2-GFP cells, although there were areas in these cells close to the plasma membrane with a spotty pattern that appear to be distinct from the smaller puncta seen in SnRK1.1T-GFP and SnRK1.1-GFP samples (**Figure 2.10F**). To determine the identity of these small puncta, co-localization experiments were performed with mCherry organelle markers. Small puncta from SnRK1-1T-GFP cells do not co-localize with Golgi, peroxisomal, or mitochondrial markers (**Figure 2.15D-F**).

This pattern was confirmed in Arabidopsis with confocal imaging of homozygous progeny of two different overexpressing lines of SnRK1.1-GFP and SnRK1.1T-GFP plants. We found prominent large puncta in the SnRK1.1a line (**Figure 2.16A**), and cytoplasmic localization in both lines (**Figure 2.16A,B**). SnRK1.1a is the line with more abundant expression (**Figure 2.6**). In SnRK1.1T-GFP plants we found that GFP fluorescence was cytoplasmic. Interestingly, small puncta began to appear in SnRK1.1Ta cells 60 minutes after mechanical wounding (i.e. cutting of the leaf margin) (**Figure 2.15E**). We did not see the consistent nuclear signal observed in *N. benthamiana* for either Arabidopsis SnRK1.1 construct (compare **Figure 2.10** and **Figure 2.15**). We could not detect reliable GFP fluorescence in any of our SnRK1.2:GFP lines, thus we conclude that the SnRK1.2-GFP protein is most likely below the level of detection using our confocal imaging conditions.

From both the *N. benthamiana* and Arabidopsis work we conclude that the SnRK1.1T isoform can localize to both the nucleus and cytoplasm, as well as being contained in small puncta of unknown origin. These puncta are stimulated by mechanical wounding and/or the stress of preparing samples, and may indicate that the SnRK1.1T isoform is dynamic and moves within the cell. The extra 23 amino acids on the N-terminus of SnRK1.1-GFP are associated with the unique appearance of larger puncta that also are not part of a known organelle. Lastly, the SnRK1.2 isoform has a similar nuclear and cytoplasmic location, but does not accumulate in small puncta after wounding.

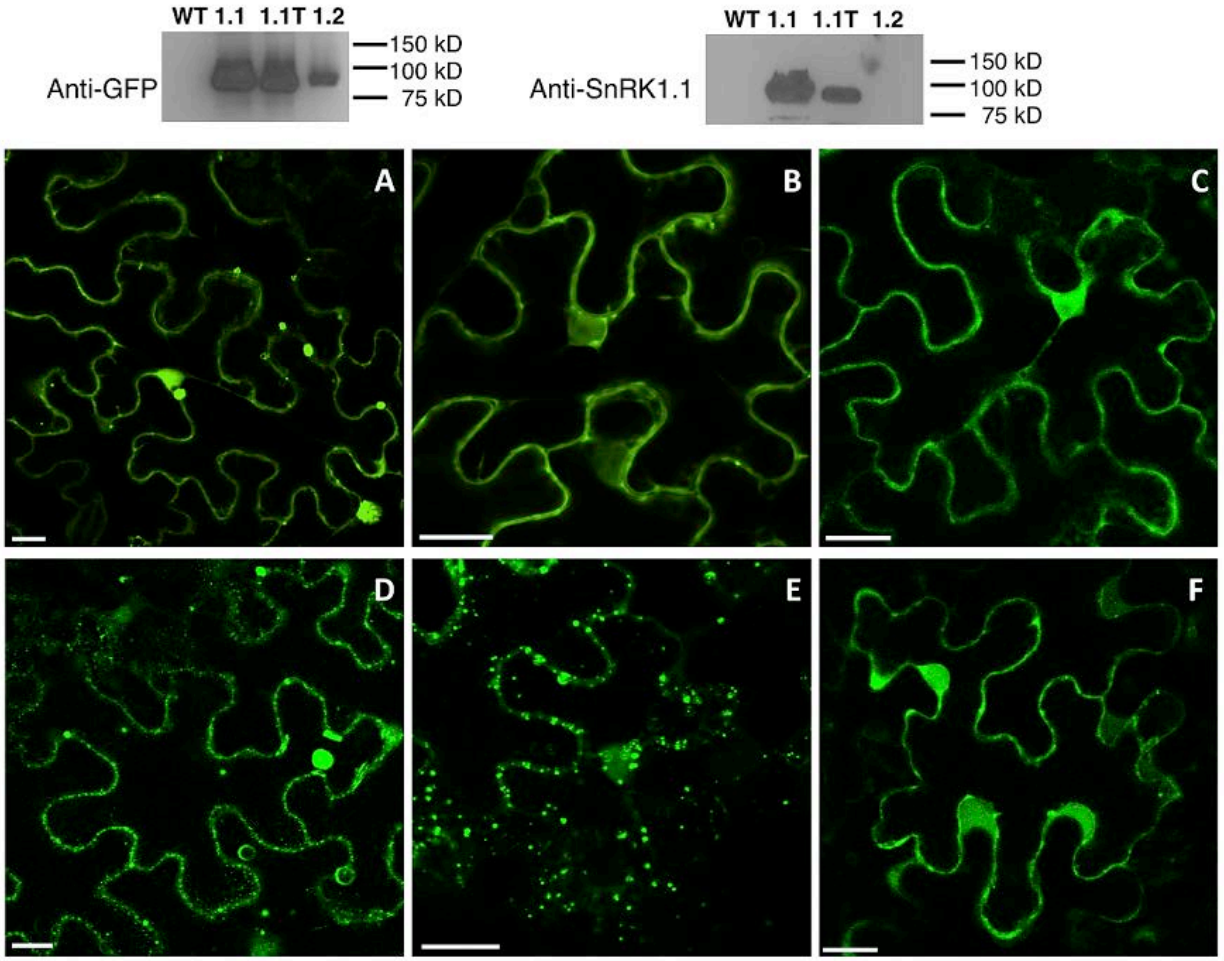

Figure 2.10. Subcellular Location of SnRK1.1-, SnRK1.1T-, and SnRK1.2-GFP Proteins

Upper: Leaves of *N. benthamiana* transiently expressing SnRK1.1-GFP, SnRK1.1T-GFP, and SnRK1.2-GFP were analyzed by protein blotting with the indicated antiserum. Lower: Single optical sections of *N. benthamiana* transiently expressing SnRK1.1-GFP (A, D), SnRK1.1T-GFP (B, E), and SnRK1.2-GFP (C, F). A small section of mature leaves were removed and epidermal cells imaged using confocal microscopy at 0 min (A-C) and 30 min (D-F). Scale Bar = 20 µm

DISCUSSION

The SnRK1 protein is a major regulator of plant growth and development, and when overexpressed it can re-program metabolism (*14, 20*) and delay developmental transitions (*17*). Since most previous work has focused on the *SnRK1.1* gene, we sought to understand how *SnRK1.1* and *SnRK1.2* are regulated, and whether ectopic expression of each has the same or different consequences on plant growth and development. Our work provides key insights into spatial patterns of *SnRK1.1* and *SnRK1.2* expression, and also in the ability of *SnRK1.2* to impact plant growth when overexpressed.

We used promoter:GUS transgenic plants and quantitative PCR to show that *SnRK1.2* is much less abundantly expressed as compared to the *SnRK1.1* gene (**Figures 2.1-2.2**). In addition, although *SnRK1.1* is broadly expressed in both shoot and root tissues, *SnRK1.2* expression is restricted to the hydathodes, cells at the base of leaf primordia, and some portions of vascular tissues. *SnRK1.2* is also expressed in roots throughout development past 5 d (**Figures 2.1-2.2**). Given the previous biochemical and genetic studies by others showing that the SnRK1.2 is a protein kinase implicated in energy regulation (*14*), we speculate that SnRK1.2 acts within a limited number of cells in the plant. We note here that this pattern of expression is similar to that from some genes involved in nutrient transport/sensing (*35, 36*). Our finding of restricted SnRK1.2 expression agrees with previous observations that SnRK1.1 is responsible for the major part of SnRK1 activity in Arabidopsis suspension cells (*20*).

We also found that *SnRK1.2* expression is elevated by trehalose (**Figures. 2.2-2.3**). Careful work by others has shown that trehalose mediates its effects via elevation of trehalose 6 phosphate

(T6P) levels within plant cells (*37*), where T6P is thought to communicate sugar or stress status (*38-40*). Previous microarray experiments have shown that *SnRK1.2* expression is elevated by trehalose, which suggested that SnRK1.2 participates in the signaling pathway to sense sugar or stress (*37*). Our results bring spatial information to the trehalose regulation of SnRK1.2, indicating that this induction occurs primarily in the root area closest to the root-shoot junction. We speculate that roots, a sink tissue, may have a special need for responding to trehalose and T6P, as trehalose stimulates accumulation of ~5-fold more starch in source tissues such as the cotyledons and a corresponding decrease in starch in root columella cells (*41*). Interestingly T6P is a regulator of flowering time (*42*) and can also act as an inhibitor of SnRK1.1 and SnRK1.2 enzyme activity (*43, 44*). Although it seems counter intuitive for T6P to increase SnRK1.2 transcription and decrease SnRK1.2 activity, it should be noted that T6P inhibition of SnRK1 activity requires an intermediary factor (*43*). Thus it is possible that T6P dependence on this intermediary factor allows T6P to elevate *SnRK1.2* transcription in the root, while decreasing activity elsewhere.

One of the most compelling reasons to study SnRK1 function in plants is the alteration of growth and development conferred by overexpression of SnRK1 (*14, 17, 45*) (Supp. **Figure 2.14**), which could be a useful tool for engineering desirable traits (*1*). Specifically, others have shown that overexpression of SnRK1.1 delays developmental transitions, such as the vegetative to reproductive transition, which manifests as a delay in time to flowering (*17*). This delay effectively decreases the size of SnRK1.1 overexpressors early in development, as measured by a smaller rosette width (**Figure 2.9**). Similarly, we found that SnRK1.1-GFP and SnRK1.1T-GFP plants flowered late and had smaller rosettes up to 28 d (**Figure 2.8-2.9**). In contrast,

overexpression of SnRK1.2, which was accompanied by increased levels of *SnRK1.2* RNA (**Figure 2.6**), resulted in early flowering (**Figure 2.8**), and larger rosettes and leaves prior to day 28 (**Figure 2.9**, **Figure 2.14**). These data indicate that SnRK1.2, when overexpressed, has the opposite impact on flowering time as compared to SnRK1.1 overexpression. Previous biochemical studies have supported a similar enzyme activity for SnRK1.1 and SnRK1.2 proteins (*14, 20*), and knockdown of SnRK1.1 and SnRK1.2 in Arabidopsis also support a redundant role for these two proteins. The mechanism for how overexpression of SnRK1.2 leads to a change in growth and shortens time to flowering is unknown at present. We speculate that the *SnRK1.2* gene, which is normally restricted in expression (in hydathodes, at the base of leaf primordia, and in vascular tissues within both seedling shoots and roots), could impact changes in flowering time gene regulation. As we see very little SnRK1.2:GFP protein accumulation in our overexpression lines, we suggest that a small difference in SnRK1.2 expression may have significant effects due to elevated protein kinase activity and impact on signaling. This concept of slight changes in kinase activity triggering significant downstream effects by amplifying signals has been discussed previously (*46*).

Another possibility for the seemingly opposite impact of SnRK1.1 and SnRK1.2 overexpression, is that SnRK1.1 and SnRK1.2 physically interact with different protein partners in the cell, and such interactors could be key for driving different biological outcomes in SnRK1 overexpression plants. In support of this, a recent query of String proteome-wide binary protein-protein interactions (*47*) indicated that SnRK1.1 and SnRK1.2 have some novel interactors. These include two different senescence-associated proteins, along with FUS3 and FUS5 for SnRK1.1, and JAZ3, the TOE2 transcription factor, and Starch Excess 4 (SEX4) for SnRK1.2. It is

interesting to note that *sex4* mutants show a prolonged juvenile stage, and flower late (*48*), thus this potentially novel SnRK1.2 interactor has a known connection to regulation of flowering time.

To further understand SnRK1.2 function, we performed subcellular localization studies using both a transient expression assay, and by examining transformed Arabidopsis. We found SnRK1.2 localized to both the nucleus and cytoplasm, which is the same location we and others have documented for SnRK1.1 (*13, 17, 22, 30*). An intriguing finding is that SnRK1.1T-GFP is stimulated by mechanical wounding to localize in small puncta (**Figure 2.9**, **Figure 2.16**). These small puncta are not part of known organelles such as chloroplasts, mitochondria, peroxisomes or the Golgi apparatus (**Figure 2.15**). These puncta have been previously noted by others (*13, 17, 30*), but our report is the first to connect these to a mechanical wounding stimulus. It is known that rice SnRK1.1T-GFP most likely moves between the nucleus and cytoplasm (*31*). We found SnRK1.1T in both the nucleus and cytoplasm in transient expression assays, but could not confirm the nuclear location in mature Arabidopsis leaves. Others reported SnRK1.1T-GFP in the chloroplast of stably transformed Arabidopsis (*27*). While we cannot rule out that some portion of SnRK1.1T-GFP localized to chloroplasts and it was below our limits of detection in our studies, our data strongly support the cytoplasm and small puncta as areas of the cell where SnRK1.1T-GFP accumulates to the highest degree. We speculate that the small puncta allow for movement of SnRK1.1T between compartments in response to stress. In addition, since we never observed SnRK1.2-GFP in small puncta or formation in response to wounding, we hypothesize that movement within the cell is unique to SnRK1.1 isoforms.

We also addressed the existence of a longer *SnRK1.1* cDNA that is predicted to encode a SnRK1.1 protein with 23 extra amino acids at the N-terminus. We found only minimal expression of this SnRK1.1 cDNA (**Figure 2.5**), and the SnRK1.1-GFP encoded by this cDNA had an additional subcellular location of accumulation within large puncta (**Figure 2.9**). SnRK1.1-GFP transiently expressed also localized to small puncta after wounding, although there was a delay in appearance of these puncta. Understanding what role, if any, this SnRK1.1 isoform plays in plants awaits purification of native SnRK1.1 isoforms and analysis via mass spectrometry.

In conclusion, the data reported here support a role for *SnRK1.2* as a spatially restricted *SnRK1* isoform that is capable of inducing early flowering when overexpressed. In addition, our results indicate an intriguing new possibility that certain stresses, such as mechanical wounding, induce movement or redistribution of SnRK1.1T protein in the cell.

MATERIALS AND METHODS

Plant Growth Conditions

Arabidopsis thaliana ecotype Columbia and Landsberg erecta (Ler) plants were used for all experiments. For seedling growth experiments, seeds were surface-sterilized and plated on 0.5x Murashige and Skoog (MS) salts + 0.8 % agar medium plus the indicated sugars. Seed were stratified at 4°C for three days and grown under 120-130 μE m^{-2} s^{-1} light under long day (16 h light) conditions with a mixture of fluorescent and incandescent lamps. All plant growth analyses were performed with at least three different biological replicates.

Construction of Promoter-Reporter Transgenic Plants and Imaging

The promoter sequences of *SnRK1.1* (At3g01090) and *SnRK1.2* (At3g29160) were analyzed using tools available from the web site Plant Cis-Acting Regulatory Element (P.L.A.C.E.) (*49*). We focused on using the native, intergenic regions of *SnRK1.1* and *SnRK1.2* genes, which is approximately 0.8 kB and 4.3 kB of the *SnRK1.1* and *SnRK1.2* 5' upstream sequences (i.e. promoters, respectively). These were amplified from CS60000 genomic DNA by PCR using the primers indicated in **Supplemental Table 2.1**, and were cloned via the Gateway system into plasmid pBGWFS7 (*50*) containing an *eGFP:uidA* gene fusion. GUS constructs were transformed into Arabidopsis using *Agrobacterium* transformation (*51*). Homozygous lines were obtained through BASTA resistance screening. GUS staining of 3-10 day-old seedlings grown on 0.5x MS agar plates + indicated sugars or of plant tissues from soil grown plants has been described (*52*), and staining was observed using an Olympus SZX16 and Zeiss Axiophot microscope. At least 3 biological replicates of different developmental stage and sugar-treated

seedlings were performed.

Quantitative PCR

Conditions have been previously described (*53*). Briefly, RNA was purified using a Qiagen RNeasy kit with DNase treatment, from 6 week-old soil-grown plants (roots, leaves, cauline leaves, flowers, siliques). Silique RNAs were initially extracted with phenol/chloroform and precipitated with LiCl before RNeasy purification. RNA was also extracted from seedlings grown on 0.5x MS agar plates for 5 days or 10 days. cDNA was synthesized from RNA using a Bio-Rad iScript cDNA synthesis kit. Reactions containing cDNA, Sybr Green MasterMix (Applied Biosystems) and primers, were performed in triplicate (61^{o} C annealing temperature) and monitored with Applied Biosystems 7300 Real-Time PCR instrumentation outfitted with SDS software version 1.4. Primers were designed to detect the longest SnRK1.1 cDNA (Accession no. AY093170), all known cDNAs encoding SnRK1.1, SnRK1.2 cDNA, and PEX4 cDNA (At5g25760) (Supp. **Table 2.1**). For all experiments, at least two biological replicates were performed.

Flowering Time and Leaf Size Assays

WT and mutant plants were grown as described previously under long-day (16 hr days) conditions. Careful attention was given to growing plants side-by-side or in the same pot for comparison. Plants were examined at the point of inflorescence emergence and leaves were counted. Three biological replicates were analyzed. For leaf measurements the length and width

of the largest leaf on each 27 d soil-grown plant was measured (N = 100-120 plants per genotype).

Protein Blot Analyses

Conditions have been previously reported (*54*). Briefly, tissues were ground in liquid nitrogen, homogenized and resuspended with a pestle in SDS-bromophenol blue loading dye, boiled, and the supernatant was loaded onto a polyacrylamide gel for separation. Equal amounts of protein were loaded onto gels. SDS-PAGE was followed by western blotting with a 1:20,000 dilution of rabbit anti-GFP antibody (Invitrogen Molecular Probes, Eugene, OR) or an anti-SnRK1.1 antibody. This antibody was produced by CoCalico, Inc. by injecting rabbits with a SnRK1.1-V5 recombinant protein (*54*) purified by ion-metal affinity (IMAC) and size exclusion chromatography (**Figure 2.12**). Sera from rabbits was purified by affinity-blot purification (as described in (*55*) and then tested for specificity with protein blots containing recombinant SnRK1.1, or extracts from SnRK1.1T-HA and previously characterized SnRK1.1 RNAi knock-down lines (*14*) (**Figure. 2.12**). This anti-SnRK1.1 antibody does not cross-react with SnRK1.2-GFP. A secondary goat, anti-rabbit horseradish peroxidase antibody (Bio-Rad Laboratories, Hercules, CA) was used at a 1:2,500 dilution. Immunoreactive bands were detected using an ECL Plus Western Blotting Detection System (Amersham, Buckinghamshire, UK). Ponceau S staining of blots was performed to ensure that equal amounts of protein within extracts were analyzed.

SnRK1 Activity Assays

The immunoprecipitation reactions were carried out as described (*56*) with the following modifications: leaves from mature 60 d plants were ground in liquid nitrogen and resuspended in extraction buffer (50 mM Tris-Cl, pH7.5, 150 mM NaCl, 1 mM EDTA, 10 mM $MgCl_2$, 0.1% Triton X-100, 10% glycerol) containing protease inhibitor (Sigma 9599), 10.5 µM MG132 (proteasome inhibitor), and 10 mM DTT). After centrifugation at 13.2 rpm for 15 min the supernatant was incubated with either anti-GFP agarose or anti-HA antibody bound to protein A sepharose beads. Extracts and beads were rocked for 3 h at 4^o C, then washed 4x with Buffer A and 2x with 50 mM HEPES, pH 7, 1 mM DTT. After washing, these beads were incubated in SnRK1 activity assays as described in (*33*). Briefly, beads were incubated in kinase buffer (50 mM Tris-HCl and 1 mM DTT, pH 7.0), with SPS substrate peptide and γ-^{32}P-ATP, unlabeled ATP, and $MgCl_2$. Samples were incubated for 30 min at 30 degrees C, and spotted onto P81 paper and washed in 125 mM phosphoric acid as described. A reaction control with no SPS peptide to correct for autophosphorylation, and a no protein extract control were included. Activity is expressed as pmoles of phosphate incorporated into peptide per reaction. The assay was performed using two biologically independent extracts and three replicates of each extract. An initial time course with immunoprecipitated proteins indicated that product accumulation was linear over 45 minutes in these assay conditions (**Figure 2.12**). Two biological replicates were analyzed.

GFP Localization and Imaging

The coding regions of *SnRK1.1*, *SnRK1.1T*, and *SnRK1.2* were amplified from plasmids or 7 d seedlings using the primers indicated in Supp. **Table 2.1**, and were recombined into vector pK7FWG2 (Karimi et al. 2002) containing the 35S Cauliflower Mosaic virus promoter and a C-terminal *GFP* gene. Transformation of Arabidopsis was as described (*57*). Mature leaves of homozygous Arabidopsis lines were used for GFP fluorescence detection using a Zeiss LSM 510 laser-scanning microscope (Carl Zeiss) with an inverted Axio Observer Z1 base. GFP excitation was done using a 488-nm argon laser and fluorescence detected using 505- to 550-nm band-pass emission filter. Slides were examined with x40 C-Apochromat water immersion lens. *Nicotiana benthamiana* plants were agro-infiltrated as previously described (*58*). A set of mCherry tagged organelle markers were used for co-localization experiments (*59*). Leaf sections were imaged 48 hours post infiltration using the confocal microscope described above. mCherry was imaged using excitation with a 543-nm HeNe laser and 560-nm band-pass emission filter. At least three biological replicates were analyzed for each.

Acknowledgements

The Virginia Agricultural Experiment Research Station is also acknowledged. We also thank Elena Baena-Gonzalez and Filip Rolland for making 35S-SnRK1.1T-HA plants available, and Elitsa Ananieva for construction of clones and helpful advice.

REFERENCES

1. P. Coello, S. J. Hey, N. G. Halford, The sucrose non-fermenting-1-related (SnRK) family of protein kinases: potential for manipulation to improve stress tolerance and increase yield. *J Exp Bot* **62**, 883 (Jan, 2011).
2. N. G. Halford, S. J. Hey, Snf1-related protein kinases (SnRKs) act within an intricate network that links metabolic and stress signalling in plants. *The Biochemical journal* **419**, 247 (Apr 15, 2009).
3. A. Y. Tsai, S. Gazzarrini, Trehalose-6-phosphate and SnRK1 kinases in plant development and signaling: the emerging picture. *Front Plant Sci* **5**, 119 (2014).
4. R. Ghillebert *et al.*, The AMPK/SNF1/SnRK1 fuel gauge and energy regulator: structure, function and regulation. *Febs J* **278**, 3978 (Nov, 2011).
5. N. G. Halford, M. J. Paul, Carbon metabolite sensing and signalling. *Plant Biotechnol J* **1**, 381 (Nov, 2003).
6. S. J. Hey, E. Byrne, N. G. Halford, The interface between metabolic and stress signalling. *Ann Bot* **105**, 197 (Feb, 2010).
7. F. Rolland, E. Baena-Gonzalez, J. Sheen, Sugar sensing and signaling in plants: conserved and novel mechanisms. *Annu Rev Plant Biol* **57**, 675 (2006).
8. V. Lumbreras, M. M. Alba, T. Kleinow, C. Koncz, M. Pages, Domain fusion between SNF1-related kinase subunits during plant evolution. *EMBO Rep* **2**, 55 (Jan, 2001).
9. L. Gissot *et al.*, AKINbetagamma contributes to SnRK1 heterotrimeric complexes and interacts with two proteins implicated in plant pathogen resistance through its KIS/GBD sequence. *Plant Physiol* **142**, 931 (Nov, 2006).
10. C. Polge, M. Jossier, P. Crozet, L. Gissot, M. Thomas, Beta-subunits of the SnRK1 complexes share a common ancestral function together with expression and function specificities; physical interaction with nitrate reductase specifically occurs via AKINbeta1-subunit. *Plant Physiol* **148**, 1570 (Nov, 2008).
11. M. Ramon *et al.*, The hybrid four-CBS-domain KINbetagamma subunit functions as the canonical gamma subunit of the plant energy sensor SnRK1. *Plant J* **75**, 11 (Jul, 2013).
12. T. Kleinow *et al.*, Functional identification of an Arabidopsis snf4 ortholog by screening for heterologous multicopy suppressors of snf4 deficiency in yeast. *Plant J* **23**, 115 (Jul, 2000).
13. C. Lopez-Paz, B. Vilela, M. Riera, M. Pages, V. Lumbreras, Maize AKINbetagamma dimerizes through the KIS/CBM domain and assembles into SnRK1 complexes. *FEBS letters* **583**, 1887 (Jun 18, 2009).
14. E. Baena-Gonzalez, F. Rolland, J. M. Thevelein, J. Sheen, A central integrator of transcription networks in plant stress and energy signalling. *Nature* **448**, 938 (Aug 23, 2007).
15. A. Confraria, C. Martinho, A. Elias, I. Rubio-Somoza, E. Baena-Gonzalez, miRNAs mediate SnRK1-dependent energy signaling in Arabidopsis. *Front Plant Sci.* **4**, 197 (2014).
16. N. G. Halford *et al.*, Metabolic signalling and carbon partitioning: role of Snf1-related (SnRK1) protein kinase. *J Exp Bot* **54**, 467 (Jan, 2003).
17. A. Y. Tsai, S. Gazzarrini, AKIN10 and FUSCA3 interact to control lateral organ development and phase transitions in Arabidopsis. *Plant J* **69**, 809 (Mar, 2012).

18. S. Gazzarrini, Y. Tsuchiya, S. Lumba, M. Okamoto, P. McCourt, The transcription factor FUSCA3 controls developmental timing in Arabidopsis through the hormones gibberellin and abscisic acid. *Dev Cell* **7**, 373 (Sep, 2004).
19. M. Thelander, T. Olsson, H. Ronne, Snf1-related protein kinase 1 is needed for growth in a normal day-night light cycle. *Embo J* **23**, 1900 (Apr 21, 2004).
20. M. Jossier *et al.*, SnRK1 (SNF1-related kinase 1) has a central role in sugar and ABA signalling in Arabidopsis thaliana. *Plant J* **59**, 316 (Jul, 2009).
21. A. Rodrigues *et al.*, ABI1 and PP2CA phosphatases are negative regulators of Snf1-related protein kinase1 signaling in Arabidopsis. *The Plant cell* **25**, 3871 (Oct, 2013).
22. G. Mohannath *et al.*, A complex containing SNF1-related kinase (SnRK1) and adenosine kinase in Arabidopsis. *PLoS One* **9**, e87592 (2014).
23. S. Ng *et al.*, Cyclin-dependent kinase E1 (CDKE1) provides a cellular switch in plants between growth and stress responses. *The Journal of biological chemistry* **288**, 3449 (Feb 1, 2013).
24. B. Singh, H. D. Cheek, C. H. Haigler, A synthetic auxin (NAA) suppresses secondary wall cellulose synthesis and enhances elongation in cultured cotton fiber. *Plant Cell Rep* **28**, 1023 (Jul, 2009).
25. C. R. Lin *et al.*, SnRK1A-interacting negative regulators modulate the nutrient starvation signaling sensor SnRK1 in source-sink communication in cereal seedlings under abiotic stress. *The Plant cell* **26**, 808 (Feb, 2014).
26. K. J. Bradford *et al.*, Abscisic acid and gibberellin differentially regulate expression of genes of the SNF1-related kinase complex in tomato seeds. *Plant Physiol* **132**, 1560 (Jul, 2003).
27. S. Fragoso *et al.*, SnRK1 isoforms AKIN10 and AKIN11 are differentially regulated in Arabidopsis plants under phosphate starvation. *Plant Physiol* **149**, 1906 (Apr, 2009).
28. S. Pien, J. Wyrzykowska, A. J. Fleming, Novel marker genes for early leaf development indicate spatial regulation of carbohydrate metabolism within the apical meristem. *Plant J* **25**, 663 (Mar, 2001).
29. M. Takano, H. Kajiya-Kanegae, H. Funatsuki, S. Kikuchi, Rice has two distinct classes of protein kinase genes related to SNF1 of Saccharomyces cerevisiae, which are differently regulated in early seed development. *Mol Gen Genet* **260**, 388 (Nov, 1998).
30. M. Bitrian, F. Roodbarkelari, M. Horvath, C. Koncz, BAC-recombineering for studying plant gene regulation: developmental control and cellular localization of SnRK1 kinase subunits. *Plant J* **65**, 829 (Mar, 2011).
31. Y. H. Cho, J. W. Hong, E. C. Kim, S. D. Yoo, Regulatory functions of SnRK1 in stress-responsive gene expression and in plant growth and development. *Plant Physiol* **158**, 1955 (Apr, 2012).
32. A. Alderson *et al.*, Complementation of snf1, a mutation affecting global regulation of carbon metabolism in yeast, by a plant protein kinase cDNA. *Proc Natl Acad Sci U S A* **88**, 8602 (Oct 1, 1991).
33. E. A. Ananieva, G. E. Gillaspy, A. Ely, R. N. Burnette, F. L. Erickson, Interaction of the WD40 domain of a myoinositol polyphosphate 5-phosphatase with SnRK1 links inositol, sugar, and stress signaling. *Plant Physiol* **148**, 1868 (Dec, 2008).

34. A. Y. Tsai, S. Gazzarrini, Overlapping and distinct roles of AKIN10 and FUSCA3 in ABA and sugar signaling during seed germination. *Plant Signal Behav* **7**, 1238 (Oct 1, 2012).
35. G. Pilot *et al.*, Overexpression of GLUTAMINE DUMPER1 leads to hypersecretion of glutamine from Hydathodes of Arabidopsis leaves. *The Plant cell* **16**, 1827 (Jul, 2004).
36. L. Barker *et al.*, SUT2, a putative sucrose sensor in sieve elements. *The Plant cell* **12**, 1153 (Jul, 2000).
37. H. Schluepmann *et al.*, Trehalose mediated growth inhibition of Arabidopsis seedlings is due to trehalose-6-phosphate accumulation. *Plant Physiol* **135**, 879 (Jun, 2004).
38. J. Lastdrager, J. Hanson, S. Smeekens, Sugar signals and the control of plant growth and development. *J Exp Bot*, (Jan 22, 2014).
39. H. Schluepmann, T. Pellny, A. van Dijken, S. Smeekens, M. Paul, Trehalose 6-phosphate is indispensable for carbohydrate utilization and growth in Arabidopsis thaliana. *Proc Natl Acad Sci U S A* **100**, 6849 (May 27, 2003).
40. L. E. O'Hara, M. J. Paul, A. Wingler, How do sugars regulate plant growth and development? New insight into the role of trehalose-6-phosphate. *Mol Plant* **6**, 261 (Mar, 2013).
41. M. Aghdasi, H. Schluepmann, S. Smeekens, Characterization of Arabidopsis seedlings growthand development under trehalose feeding. *Journal of Cell and Molecular Research* **1**, 1 (2010).
42. V. Wahl *et al.*, Regulation of flowering by trehalose-6-phosphate signaling in Arabidopsis thaliana. *Science* **339**, 704 (Feb 8, 2013).
43. Y. Zhang *et al.*, Inhibition of SNF1-related protein kinase1 activity and regulation of metabolic pathways by trehalose-6-phosphate. *Plant Physiol* **149**, 1860 (Apr, 2009).
44. T. L. Delatte *et al.*, Growth arrest by trehalose-6-phosphate: an astonishing case of primary metabolite control over growth by way of the SnRK1 signaling pathway. *Plant Physiol* **157**, 160 (Sep, 2011).
45. R. S. McKibbin *et al.*, Production of high-starch, low-glucose potatoes through over-expression of the metabolic regulator SnRK1. *Plant Biotechnol J* **4**, 409 (Jul, 2006).
46. P. B. Chock, E. R. Stadtman, Covalently interconvertible enzyme cascade systems. *Methods Enzymol* **64**, 397 (1980).
47. D. Szklarczyk *et al.*, The STRING database in 2011: functional interaction networks of proteins, globally integrated and scored. *Nucleic Acids Res* **39**, D561 (Jan, 2011).
48. I. G. Matsoukas, A. J. Massiah, B. Thomas, Starch metabolism and antiflorigenic signals modulate the juvenile-to-adult phase transition in Arabidopsis. *Plant Cell Environ* **36**, 1802 (Oct, 2013).
49. K. Higo, Y. Ugawa, M. Iwamoto, T. Korenaga, Plant cis-acting regulatory DNA elements (PLACE) database: 1999. *Nucleic Acids Res* **27**, 297 (January 1, 1999, 1999).
50. M. Karimi, D. Inze, A. Depicker, GATEWAY vectors for Agrobacterium-mediated plant transformation. *Trends in plant science* **7**, 193 (May, 2002).
51. N. Bechtold, J. Ellis, G. Pelletier, In planta Agrobacterium mediated gene transfer by infiltration of adult *Arabidopsis thaliana* plants. *Comptes Rendus De L'academic Des Sciences Serie Iii Sciences De La Vie* **316**, 1194 (1993).

52. J. C. Styer, J. Keddie, J. Spence, G. E. Gillaspy, Genomic organization and regulation of the LeIMP-1 and LeIMP-2 genes encoding myo-inositol monophosphatase in tomato. *Gene* **326**, 35 (Feb 4, 2004).
53. J. L. Donahue *et al.*, The Arabidopsis thaliana Myo-inositol 1-phosphate synthase1 gene is required for Myo-inositol synthesis and suppression of cell death. *The Plant cell* **22**, 888 (Mar, 2010).
54. R. N. Burnette, B. M. Gunesekera, G. E. Gillaspy, An Arabidopsis inositol 5-phosphatase gain-of-function alters abscisic acid signaling. *Plant Physiol* **132**, 1011 (Jun, 2003).
55. E. Harlow, D. Lane, *Antibodies a laboratory manual.* (Cold Spring Harbor Laboratory, 1988), pp. 726.
56. M. E. Ercetin *et al.*, A phosphatidylinositol phosphate-specific myo-inositol polyphosphate 5-phosphatase required for seedling growth. *Plant Mol Biol*, (Apr 8, 2008).
57. N. Bechtold, J. Ellis, G. Pelletier, In planta Agrobacterium mediated gene transfer by infiltration of adult Arabidopsis thaliana plants. *Comptes rendus de l'Académie des sciences. Série 3, Sciences de la vie* **316**, 1194 (1993).
58. J. Kapila, R. DeRycke, M. Van Montagu, G. Angenon, An Agrobacterium-mediated transient gene expression system for intact leaves. *Plant Sci* **122**, 101 (1997).
59. B. K. Nelson, X. Cai, A. Nebenfuhr, A multicolored set of in vivo organelle markers for co-localization studies in Arabidopsis and other plants. *Plant J* **51**, 1126 (Sep, 2007).

APPENDIX TO CHAPTER II

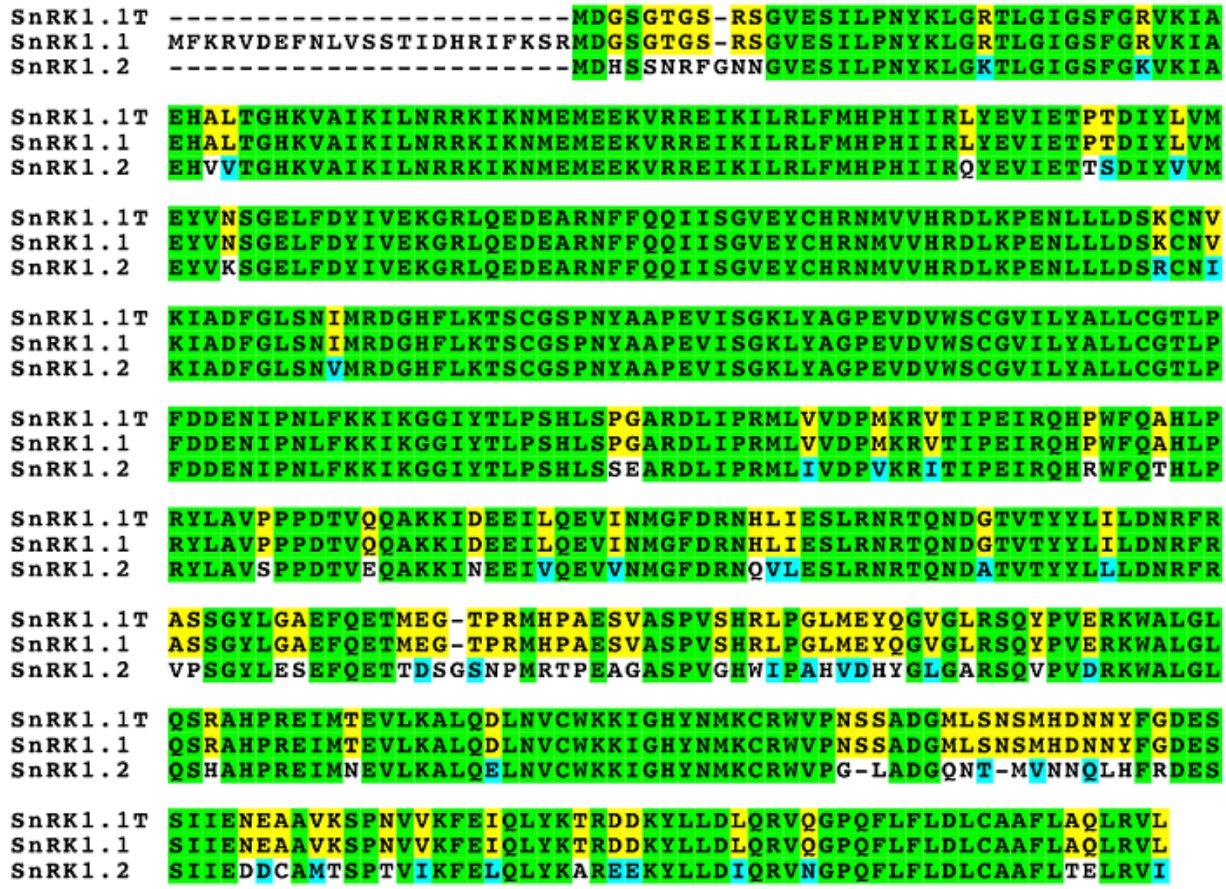

Figure 2.11. Supplemental Data: Amino Acid Alignment of SnRK1 Proteins

Predicted amino acid sequences of SnRK1.1, SnRK1.1T and SnRK1.2 were aligned with ClustalW.

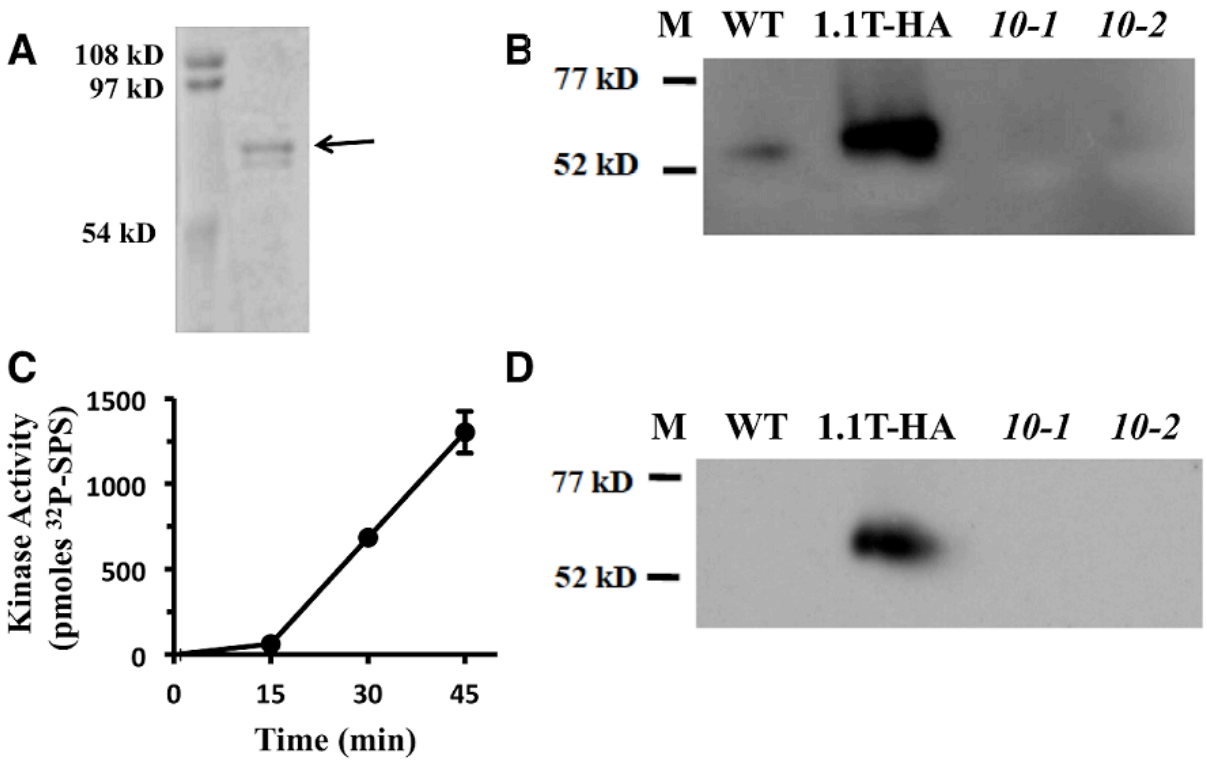

Figure 2.12. Supplemental Data: Anti-SnRK1 Antibody and Activity Assay

(A) Purified SnRK1.1-V5 recombinant protein was separated by SDS-PAGE. (B, D) Immunoreactivity of anti-SnRK1.1 with native SnRK1.1. Plant extracts were made from wildtype Ler plants (WT), SnRK1.1.T-HA (1.1T-HA), and SnRK1.1 RNAi knock-down lines 10-1 and 10-2 (*14*). Protein blots were probed with a 1:1,500 dilution of purified anti-SnRK1.1 (B) or 1:2,500 dilution of a commercial anti-HA antibody (D). (C) Linearity of SnRK1 activity assay conditions. Means ± SE are presented.

Figure 2.13. Supplemental Data: Overexpression of SnRK1.1 in Ler

Transgenic plants overexpressing SnRK1.1T-HA (SnRK1-Ox) and matched control WT (Ler) were grown under LD conditions.

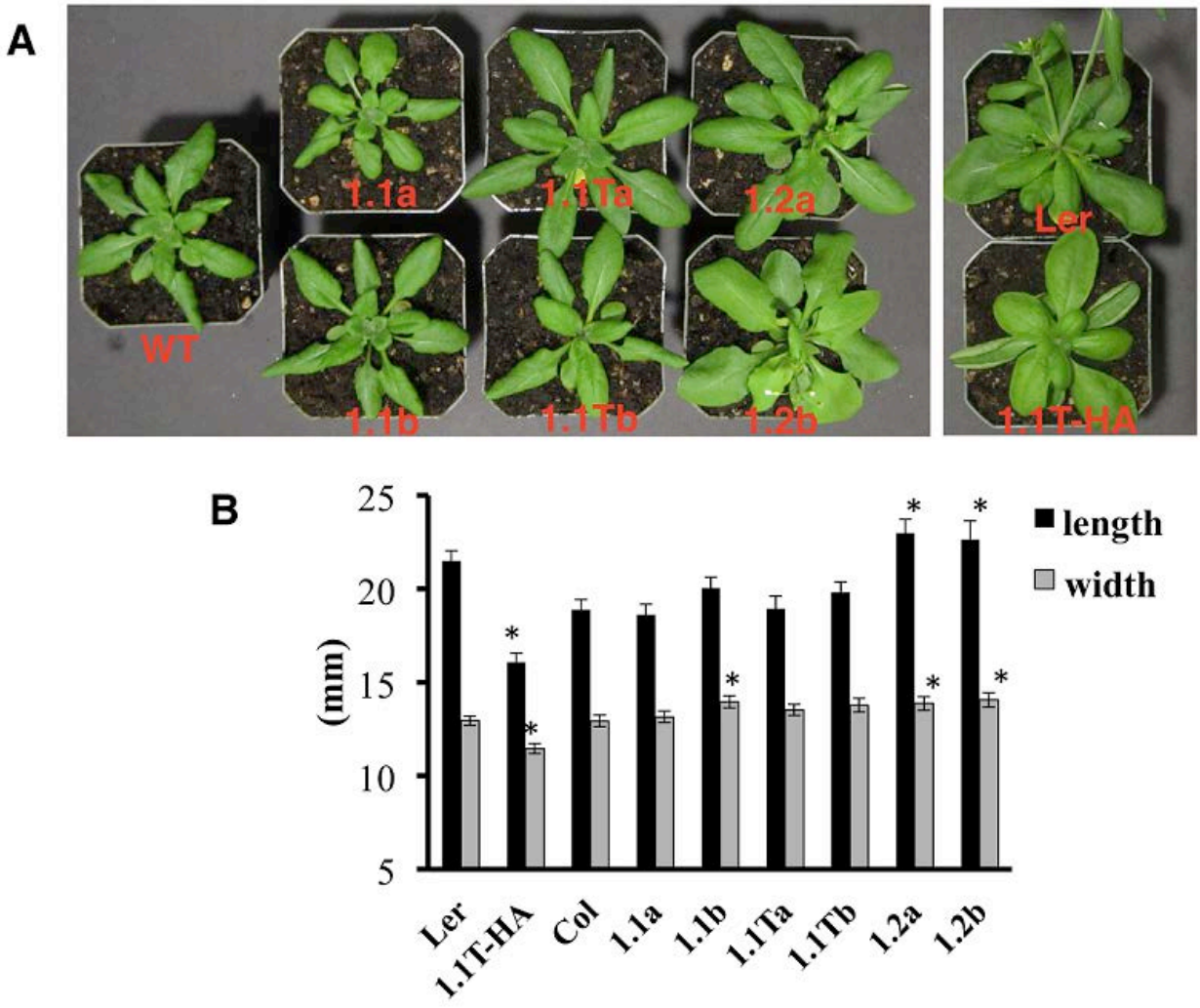

Figure 2.14. Supplemental Data: Appearance and Leaf Size of SnRK1 Transgenic Plants

(A) 30 d wildtype and transgenic plants. (B) Leaf length and width measurements taken at 27 d.

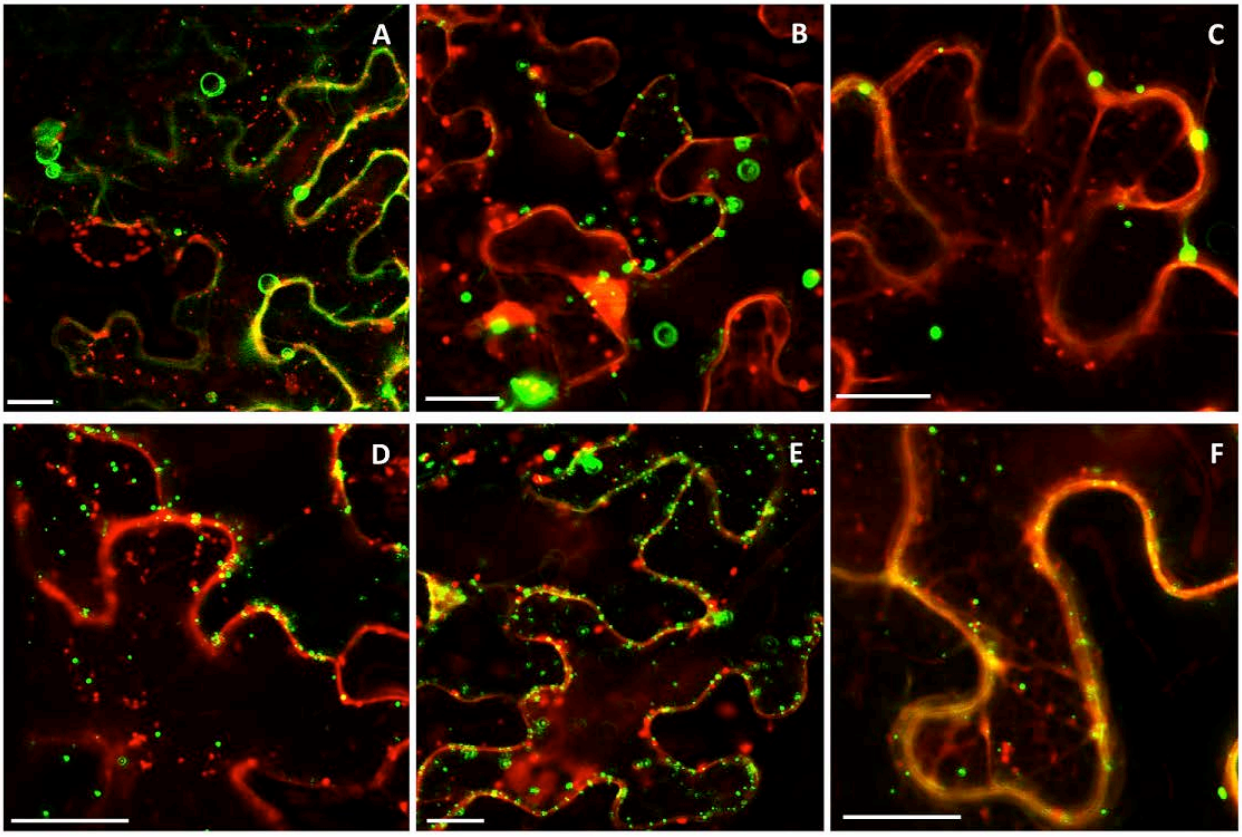

Figure 2.15. Supplemental Data: Co-localization of SnRK-GFP with Organelle Markers

Single optical sections of *N benthamiana* transiently expressing SnRK1.1-GFP (A-C) and SnRK1.1T-GFP (D, E). SnRK-GFP was co-expressed with a set of mCherry tagged organelle markers, golgi (A, D), peroxisome (B, E), and mitochondria (C, F). Epidermal cells of mature leaves were imaged using confocal microscopy. Bar = 20 µm

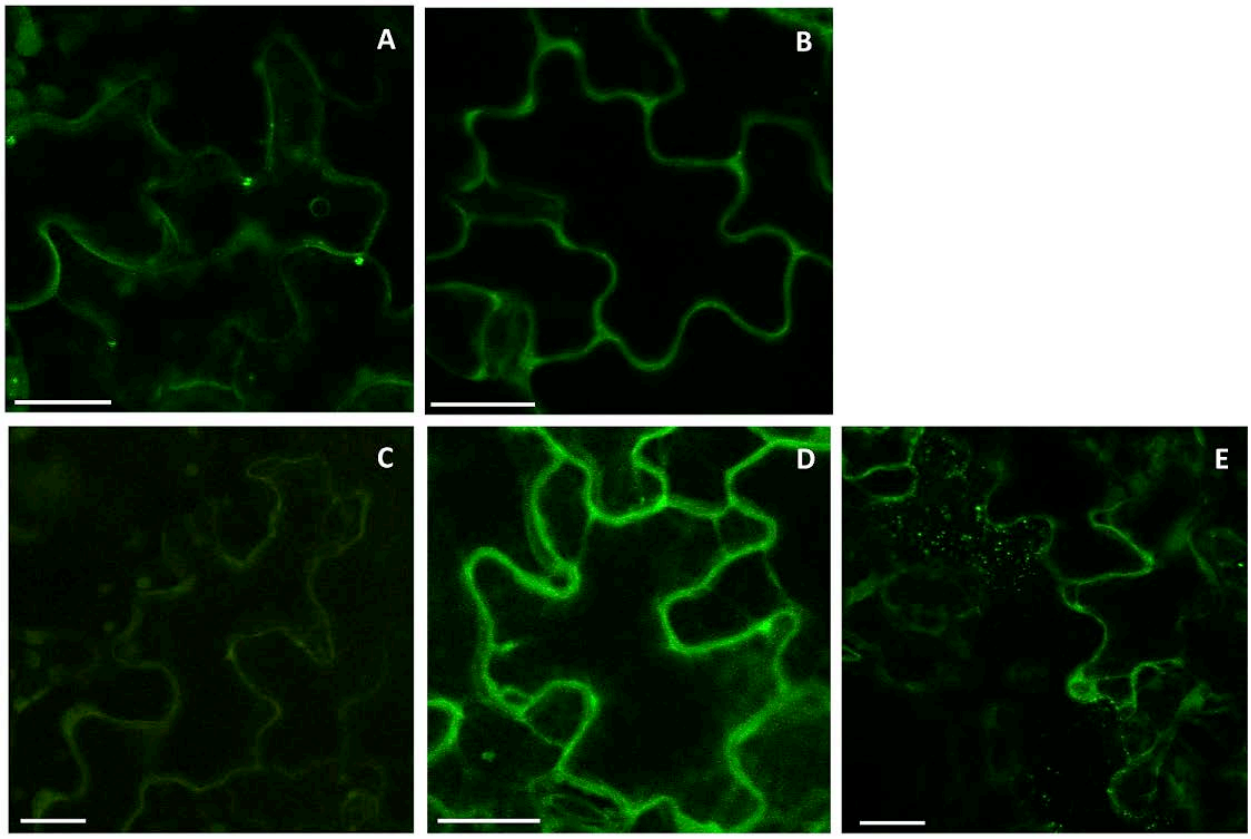

Figure 2.16. Supplemental Data: Subcellular Localization of SnRK1.1 and SnRK1.1T in Arabidopsis

Epidermal cells of mature leaves of soil grown Arabidopsis plants imaged with confocal microscopy. Two independent lines of SnRK1.1:GFP (1.1a [A] and 1.1b [B]) and SnRK1.1T:GFP (1.1Tb [C] and 1.1Ta [D]) were imaged immediately after cutting leaf sections. The two lines of SnRK1.2:GFP gave no detectable signal. Leaf sections were imaged again after 30 and 60 min. The SnRK 1.1Ta contain small fluorescent puncta ~60 min after wounding (E). Bar = 20 µm

Table 2.1. Supplemental Data: Sequences and Names of Primers Used in this Work

RT-PCR	qSnRK1.1*for*[1]	CCGAATTGGGGATAGTCTGAAAATTGC
	qSnRK1.1*rev*[1]	CTCATCTACTCGTTTGAACATGAGAATTTAGCG
	qSnRK1.1-All*for*[2]	GGAGATGGAGGAGAAAGTGAG
	qSnRK1.1-All*rev*[2]	GAGTTCACATACTCCATGACAAG
	qSnRK1.2*for*	GAACTTCAGCTATACAAAGC
	qSnRK1.2*rev*	GCGCATAGATCCAAGAAG
	qPEX4*for*	CTTAACTGCGACTCAGGGAATCTTCTAAG
	qPEX4*rev*	TCATCCTTTCTTAGGCATAGCGGC
	qGFP*for*	GCACCATCTTCTTCAAGGACGA
	qGFP*rev*	TGTGGCTGTTGTAGTTGTACTCCAG
Cloning	SnRK1.1*for*	ATGTTCAAACGAGTAGATGA
	SnRK1.1*rev*	GAGGACTCGGAGCTGAGCAAG
	SnRK1.1T*for*	ATGGATGGATCAGGCACAGG
	SnRK1.1T*rev*	GAGGACTCGGAGCTGAGCAAG
	SnRK1.2*for*	ATGGATCATTCATCAAATAG
	SnRK1.2*rev*	CACACGAAGCTCTGTAAG
GUS Cloning	SnRK1.1GUS*for*	GATGACCTTTTTACTTGAGCTATTGAAG
	SnRK1.1GUS*rev*	GAGAATTTAGCGAGAATTAGGATCCCTTTTA
	SnRK1.2GUS*for*	GACAGATAAAAGCTTGGATTATAGAGATACAG
	SnRK1.2GUS*rev*	CGTCTTGGAGTAGATCCGAGAATC

[1] Primers detect Accession #AY093170 and TAIR Accession At3g01090.2.

[2] Primers detect Accession #AY093170 and TAIR Accessions At3g01090.1, At3g01090.2 and At3g01090.3.

CHAPTER III

"Two Inositol Hexakisphosphate Kinases Drive Inositol Pyrophosphate Synthesis in Plants"

Adapted from: Mintu Desai, Padma Rangarajan, Janet L. Donahue, Sarah P. Williams, Eric S. Land, Mihir K. Mandal, Brian Q. Phillippy, Imara Y. Perera, Victor Raboy, and Glenda E. Gillaspy, *The Plant Journal* (2014) 80, 642–653.

Contribution of Authors: PR, MM, JD, BP profiled InsP in plants, SPW and VR ran PAGE gels, MD generated yeast clones, JD ran RT-PCR analysis, JD profiled InsPs in yeast, MD did yeast growth experiments, MD and SPW imaged yeast, GG and IP directed the research, GG wrote the manuscript.

Key words: *Arabidopsis thaliana*, At3g01310, At5g15070, inositol pyrophosphate, inositol kinase, $InsP_6$

ABSTRACT

Inositol pyrophosphates are unique cellular signaling molecules with recently discovered roles in energy sensing and metabolism. Studies in eukaryotes have revealed that these compounds turn over rapidly, and thus only small amounts accumulate. Inositol pyrophosphates have not been the subject of investigation in plants even though seeds produce large amounts of their precursor, *myo*-inositol hexakisphosphate ($InsP_6$). Here, we report that Arabidopsis and maize $InsP_6$

transporter mutants have elevated levels of inositol pyrophosphates in their seed, providing unequivocal identification of their presence in plant tissues. We also show that plant seeds store a little over 1% of their inositol phosphate pool as $InsP_7$ and $InsP_8$. Many tissues, including, seed, seedlings, roots and leaves accumulate $InsP_7$ and $InsP_8$, thus synthesis is not confined to tissues with high $InsP_6$. We identified two highly similar Arabidopsis genes, *AtVip1* and *AtVip2*, which are orthologous to the yeast and mammalian VIP kinases. Both *AtVip1* and *AtVip2* encode proteins capable of restoring $InsP_7$ synthesis in yeast mutants, thus *AtVip1* and *AtVip2* can function as bonafide $InsP_6$ kinases. *AtVip1* and *AtVip2* are differentially expressed in plant tissues, suggesting non-redundant or non-overlapping functions in plants. These results contribute to our knowledge of inositol phosphate metabolism and will lay a foundation for understanding the role of $InsP_7$ and $InsP_8$ in plants.

INTRODUCTION

The *myo*-inositol phosphates (InsPs) are signaling molecules that are critically important in eukaryotes, functioning in a wide array of processes such as hormonal signaling, stress responses, telomere maintenance, vesicular trafficking, phosphorus sensing, homeostasis and storage (*1-4*). In plants, several signals such as gravitropism, drought and salt treatment perturb levels of InsPs, which are thought to provide a chemical code critical for plant response to these signals (*5-9*). A unique group of InsP signaling molecules containing diphosphate or triphosphate chains (i.e. PPx-InsPs) are emerging as critical players in various signaling processes in eukaryotes, and are synthesized from higher InsP precursors (**Figure 3.1**) (*10-12*). PPx-InsPs are thought of as “energy-rich” molecules because pyrophosphate moieties have a free energy of

hydrolysis comparable to that of ATP (*13*). PPx-InsPs have recently been shown to be critical for metabolic reprogramming by influencing ATP homeostasis and mitochondrial function in yeast (*14*), during hyperosmotic stress (*15*), insulin signaling (*16*), histone demethylation (*17*), and DNA recombination (*18*).

One precursor to PPx-InsPs is *myo*-inositol (1,2,3,4,5,6)-hexakisphosphate ($InsP_6$), which also is a potential signaling molecule (**Figure 3.1**) (*19*). In plants, an additional role of $InsP_6$ is as a seed storage compound of inositol, phosphorus, and minerals. $InsP_6$ accumulates during seed development via synthesis followed by storage as mixed "phytin" salts in discrete inclusions referred to as globoids, that in turn are found within a specialized subset of protein storage microvacuoles (*20*). In fact, plant seeds are amongst the top $InsP_6$ producers on the planet, synthesizing large amounts of $InsP_6$ that is later hydrolyzed during seed germination (*21*). This abundance of seed $InsP_6$ becomes problematic in US agriculture as non-ruminant animals fed seed meal do not digest $InsP_6$ resulting in phosphate "pollution" from manure run-off (*22, 23*). Given the importance of $InsP_6$ and phosphate in plants, it is surprising that the synthesis and accumulation of potential energy signaling molecules like PPx-InsPs has not been investigated.

Synthesis of InsPs and PPx-InsP molecules is catalyzed by different classes of evolutionarily conserved $InsP_6$ kinases (**Figure 3.1**) (*24*). Two lineages of genes have been shown to encode enzymes that phosphorylate $InsP_6$, resulting in PP-$InsP_5$ synthesis, a molecule containing 7 phosphates (also known as $InsP_7$). The $InsP_6$ kinases (IP6Ks) phosphorylate the 5-position of $InsP_6$ resulting in 5PP-Ins(1,2,3,4,6)P_5 (*25*). $InsP_6$ kinase-encoding genes have been described in humans (*HsIP6K1,2,3*) (*26*) and yeast (*ScKcs1*) (*27*). The second lineage of genes are the yeast

Vip genes and human *PPIP5K1* genes that phosphorylate the 1- or 3-position of $InsP_6$ to form 1/3PP-Ins(2,3,4,5,6)P_5 (**Figure 3.1**) (*28*). In addition, both types of enzymes can phosphorylate each other's products, resulting in 1,5PP_2-$InsP_4$, which is also referred to as $InsP_8$ (**Figure 3.1**) (*29, 30*). Other enantiomers of $InsP_8$, such as 1/3PPP-$InsP_5$ and/or 1,3PP_2-$InsP_4$ are theoretically possible as recombinant IP6Ks and VIPs, alone, result in $InsP_8$ synthesis, *in vitro (29)*. VIPs are conserved throughout eukaryotes, including higher plants, and contain a widely-conserved dual domain structure; an N-terminal ATP grasp domain that has kinase activity and a C-terminal histidine acid phosphatase domain (*28*). Given that plant genomes contain conserved VIP-like genes (*28*), it seems likely that plants synthesize $InsP_7$ and $InsP_8$. Indeed, studies reported over 15 years ago alluded to a molecule more polar than $InsP_6$ from plant extracts (*31-33*). Given the potential role of $InsP_7$ and $InsP_8$ in energy regulation, and the abundance of $InsP_6$ in plants, we investigated whether these molecules are present in plants, and whether the predicted Arabidopsis *Vip* genes function in $InsP_7$ synthesis. Here we report accumulation of $InsP_7$ and $InsP_8$ in different types of plants and in both vegetative and seed tissues. Further we show that seed from $InsP_6$ transporter mutants in Arabidopsis and maize have elevated $InsP_7$ and $InsP_8$ levels. We also show that plants contain paralogues of the yeast *Vip* genes that encode enzymes that can catalyze the synthesis of $InsP_7$ and correct the phenotypic consequences of a yeast *vip1* null mutation. Our work represents a significant advance for understanding the potential roles of $InsP_7$ and $InsP_8$ in plants.

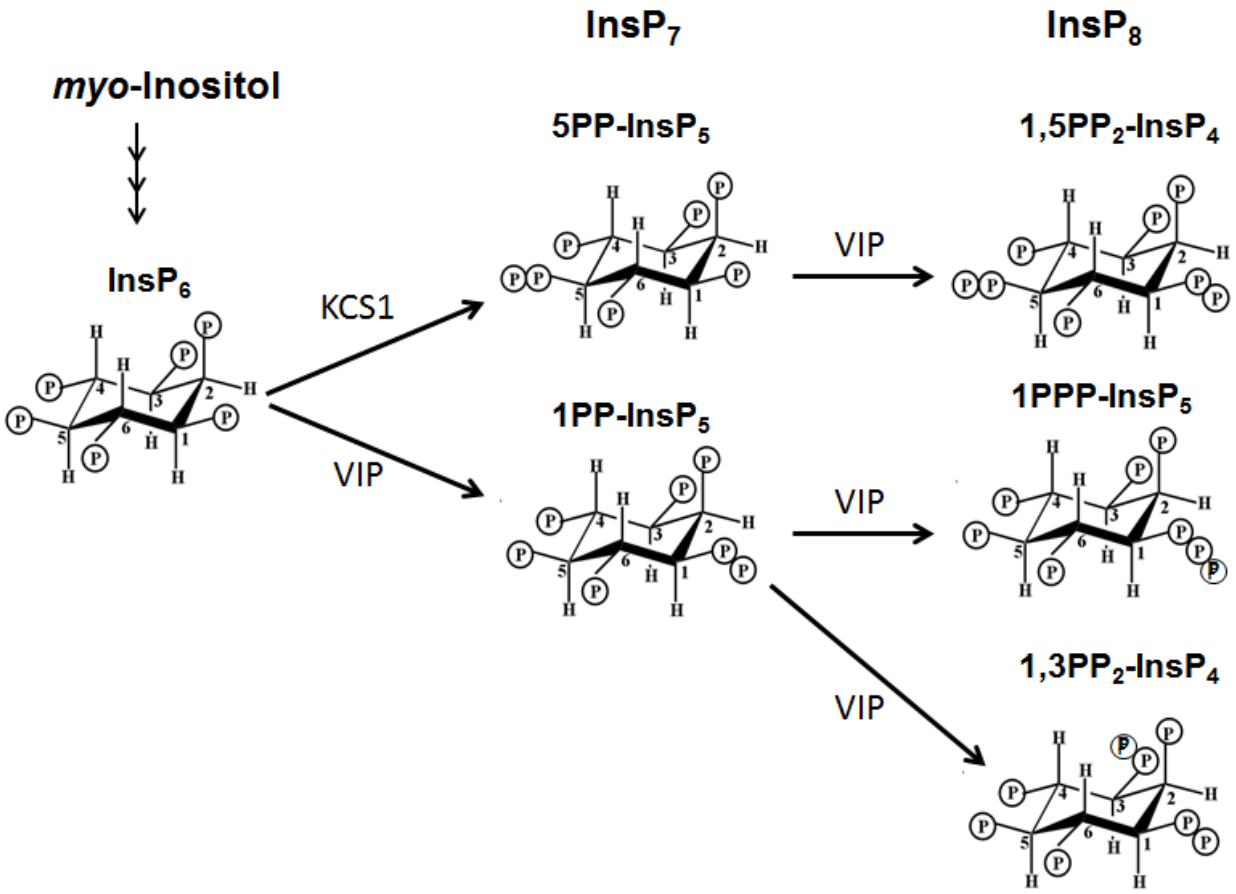

Figure 3.1. Pathways to Inositol Polyphosphate Containing Diphosphate and Triphosphate Moieties

The numbering of the *myo*-inositol backbone follows the "D"-numbering convention. P = H_2PO_4. Note that VIP is a 1/3 kinase and a 3PP-InsP_5 product is also possible. Accumulation of 1,5PP_2-InsP_4 in yeast and animal cells has been verified, while 1,3PP_2-InsP_4 and 1PPP-InsP_5 have been found only *in vitro*.

RESULTS

Seeds of Higher Plants Contain $InsP_7$ and $InsP_8$

Previous studies noted the presence of a ^{3}H-*myo*-inositol labeled compound that is more highly retained by anion exchange HPLC columns than $InsP_6$ in plant extracts (*31-33*). However, to date, these compounds have not been characterized further. We sought definitive evidence for compounds more polar than $InsP_6$, which would indicate that plants synthesize $InsP_7$. We used PAGE analyses of seed extracts from *Arabidopsis thaliana* mutants with null or recessive alleles of four genes known to perturb seed $InsP_6$ accumulation to test the hypothesis that higher plant cells can synthesize $InsP_7$ (**Figure 3.2A**). These mutants have a block in $InsP_6$ synthesis (*ipk2β* and *ipk1*, lanes 6, 7), an unknown defect that impacts seed $InsP_6$ (At3g45090, lane 8), or a block in $InsP_6$ transport (*At mrp5*; lane 9) (*34-36*). We reasoned that alterations in $InsP_6$ in these mutants might alter the pool of $InsP_6$ available to $InsP_6$ kinases, and thus manifest differences in $InsP_7$ levels. Seeds homozygous for *Atipk2β, Atipk1* or *At3g45090* revealed the reduced seed $InsP_6$ phenotype that has been previously reported, but no clearly visible accumulation of $InsP_7$ (**Figure 3.2A**). In contrast, *Atmrp5* mutant seed contain reduced $InsP_6$, as compared with wildtype, accompanied by increases in molecules co-migrating with authentic 1/3 or 5PP-$InsP_5$ and $InsP_8$ (**Figure 3.2A**). We also observed a similar phenotype in seed homozygous for a recessive allele of maize MRP4, the maize orthologue of Arabidopsis *mrp5* (*35, 37*) (Supp. **Figure 3.8**). We observed a similar accumulation of molecules co-migrating with authentic 1/3 or 5PP-$InsP_5$ and $InsP_8$ standards in maize *mrp4*, suggesting altered accumulation of $InsP_7$ and $InsP_8$ in this species as well. In addition, we observed the presence of faint bands in wildtype maize co-migrating with PP-$InsP_5$ standards, suggesting that small amounts of $InsP_7$ may be

synthesized in wildtype maize seeds (**Figure 3.8**). As a second test to confirm the presence of $InsP_7$ in plants using PAGE, we utilized a ferric precipitation/concentration procedure with *Atmrp*5 seed as source material (**Figure 3.2B**). The results clearly illustrate that *Atmrp5* mutant seed contain compounds with mobility in PAGE gels similar to $InsP_7$ and $InsP_8$ (**Figure 3.2B**).

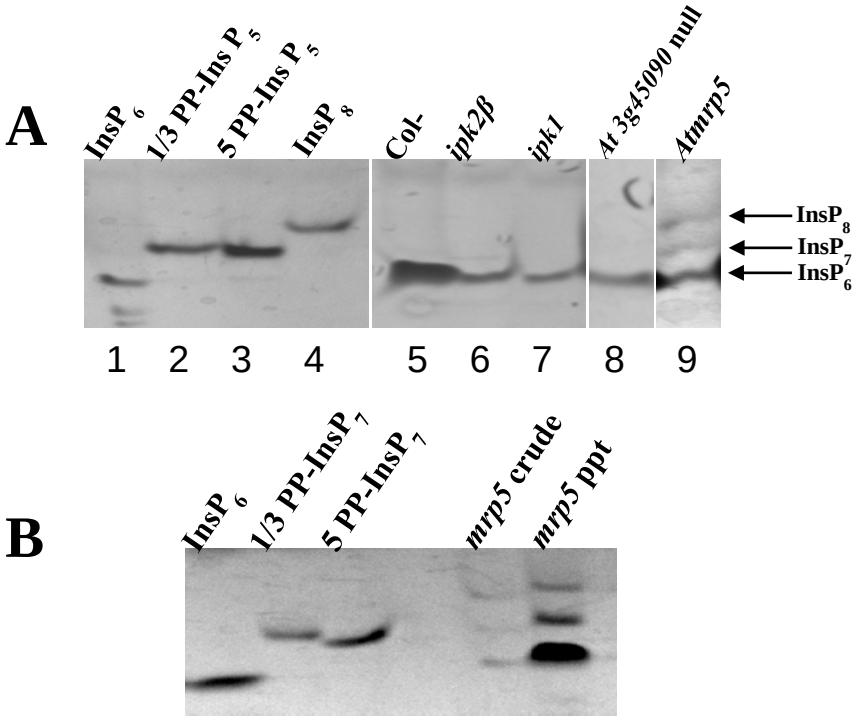

Figure 3.2. PAGE Analyses of Inositol Polyphosphates in Seed

(A) InsPs from mature dry seeds of *Arabidopsis thaliana* lines homozygous for recessive alleles of genes known to impact seed $InsP_6$ synthesis or accumulation were extracted and analyzed via PAGE as described in the methods. Gels were stained with toluidine blue. Col-1 is the wildtype control. Standards lanes contain 2.5 nmoles of each indicated compound.
(B) Crude extracts or those treated with ferric precipitation (ppt) and concentration from *Atmrp5* seed analyzed via PAGE. Standards lanes contain 5.0 nmoles of $InsP_6$ and 1.0 nmole of 1/3 or 5PP-$InsP_5$. The number of independent biological replicates for each extract is *ipk2β*, *ipk1*, and At3g45090 (N=3); Col-1 and *mrp5* (N= 5).

HPLC Analysis of $InsP_7$ and $InsP_8$ in Higher Plants

To confirm our results with PAGE, we used radiolabeling with ^{3}H-*myo*-Ins followed by extraction and separation by HPLC. We first examined developing seed labeled within the Arabidopsis silique for four days using methods described by others (*38*) and diagrammed in **Figure 3.9**. An average HPLC elution profile of higher inositol phosphates from wild-type Arabidopsis developing seed is shown in **Figure 3.3A**. Co-elution with InsP standards indicated that the higher InsPs ($InsP_5$, $InsP_6$ and $InsP_7$) can be separated. As $InsP_7$ and $InsP_8$ are noted to be unstable under most conditions, we also collected HPLC fractions and used scintillation counting to enhance detection and to quantify the counts per minute (CPM) of $InsP_5$, $InsP_6$, $InsP_7$ and $InsP_8$ that accumulated under our labeling conditions (**Figure 3.3A** inset). We accounted for differences in ^{3}H-*myo*-Ins uptake and during extraction by normalizing data. Specifically, we pooled CPM for each individual InsP peak and compared this to the CPM incorporated into the total InsP pool, as described in the Experimental procedures. Using these conditions we found on average 25-40% of the ^{3}H-*myo*-Ins was incorporated into the developing seed. **Table 3.1** contains the relative percentages of InsPs as a ratio of total InsPs from each sample. As expected, $InsP_6$ was the most abundant InsP, constituting 35.56% of labeled InsPs within seeds. Three isomers of $InsP_5$ were detectable, and when combined, these constitute 4.23% of InsPs. Notably, we also found a small, but very reproducible peak of $InsP_7$, which comprised 1.33% of InsPs in developing seed. This $InsP_7$ peak co-eluted with $InsP_7$ from labeled yeast mutants defective in breaking down $InsP_7$. Lastly, we identified an even smaller pool of putative $InsP_8$ in developing seed, comprising only 0.24% of labeled InsPs (**Table 3.1**), which is only apparent as a peak with scintillation counting (shown in **Figure 3.3B** and **Figure 3.10**). When the siliques chosen for labeling are older, the total percentage of $InsP_6$ increased to 75.23 +/- 2.5%, and PP-$InsP_5$

increased to 2.63 +/- 0.77%, in alignment with the known higher accumulation of $InsP_6$ in developing seed. $InsP_5$ levels were not appreciably altered in older, radiolabeled developing seed (4.16% +/- 0.50%). We conclude that wildtype Arabidopsis developing seed accumulate molecules with the properties of $InsP_7$ and $InsP_8$. Together with our PAGE analyses, these data confirm the presence of the "pyrophosphorylated" InsPs in plants.

To quantify higher InsPs in *mrp5* mutants, we also labeled *Atmrp5* developing seed within siliques. Our results show that *Atmrp5* developing seed from siliques accumulate significantly more $InsP_5$, $InsP_7$ and $InsP_8$, but have a decrease in $InsP_6$ (**Table 3.1**, **Figure 3.11**). A similar finding of decreased $InsP_6$ in these mutants has been reported (*35*), but the elevation in $InsP_7$ seen here is the first reported. Together our data support the role of the MRP5 transporter as key for limiting $InsP_7$ and $InsP_8$ in Arabidopsis developing seed.

We wanted to ascertain whether $InsP_7$ and $InsP_8$ were also present in vegetative tissues, which could support a role in signal transduction for these molecules. To determine whether vegetative plant tissues also accumulate $InsP_7$, we similarly analyzed 7-day old Arabidopsis seedlings and found detectable levels of $InsP_5$, $InsP_6$, $InsP_7$ and $InsP_8$ (**Figure 3.3B**). The seedling $InsP_5$, $InsP_6$, $InsP_7$, and $InsP_8$ peaks comprise 2.70%, 27.82% and 0.64%, and 0.14% of all InsPs (**Table 3.1**). We compared these data to those from radiolabeled *Atmrp5* seedlings and found significant differences in $InsP_5$, $InsP_6$ and $InsP_7$ levels within these mutants, but not in $InsP_8$ (**Table 3.1**). Together these data show that Arabidopsis seedlings accumulate molecules with the properties of $InsP_7$ and $InsP_8$, and that *Atmrp5* seedlings have alterations in $InsP_5$, $InsP_6$ and $InsP_7$ levels.

To determine if plants other than Arabidopsis accumulate $InsP_7$, we used this same approach to analyze *Camelina sativa* seedlings, leaves from Arabidopsis and cotton plants, and shoots and roots from cotton seedlings. These tissues contained on average 1.40%, 1.00%, 1.30 to 2.0%, 0.80% and 0.90% of their InsP pool as $InsP_7$, respectively (data for Camelina in **Figure 3.10**). We conclude that $InsP_7$ and $InsP_8$ comprise a small portion of the InsP pool in plants, and are not restricted to seed tissue, but instead accumulate in many different tissues within plants.

Table 3.1. Higher InsP Levels in Arabidopsis Siliques and Seedlings

	Siliques		Seedling	
	WT	***mrp5***	**WT**	***mrp5***
$InsP_5$	4.23 + 0.23	*9.40 ± 0.10	2.70 ± 0.10	*2.30 ± 0.09
$InsP_6$	35.56 ± 0.41	*30.90 ± 3.30	27.82 ± 1.59	*15.60 ± 0.55
$InsP_7$	1.33 ± 0.04	*2.90 ± 0.11	0.64 ± 0.05	*0.50 ± 0.01
$InsP_8$	0.24 ± 0.02	*0.55 ± 0.01	0.14 ± 0.01	0.15 ± 0.01

The relative percentages of InsPs in wildtype (WT) or *mrp5* mutant tissues are presented as a ratio of total InsPs plus or minus the standard deviation. Three biological replicates of seedlings and five biological replicates of siliques were analyzed. The * indicates p value less than 0.05 as compared to the wildtype (WT).

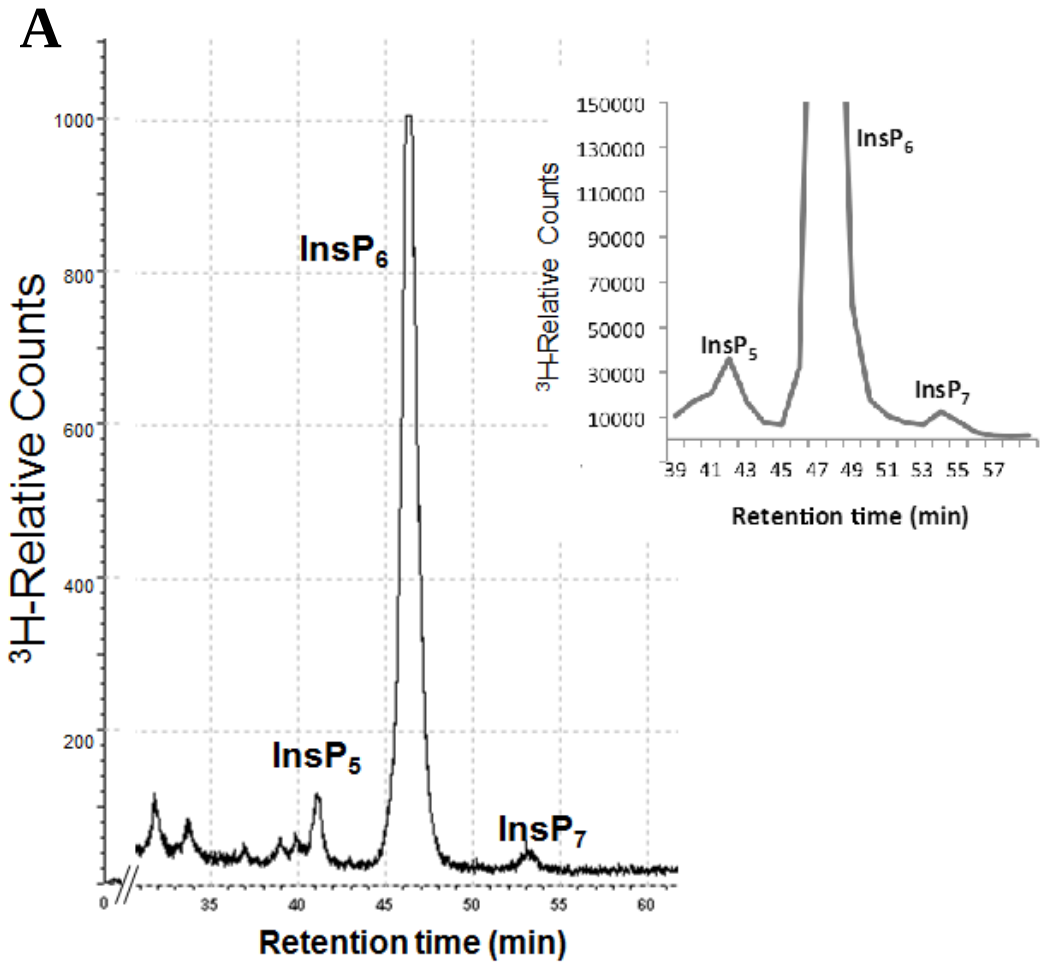
A
^{3}H-Relative Counts
1000
800
600
400
200
0
35
40
45
50
55
60
InsP$_6$
InsP$_5$
InsP$_7$
Retention time (min)
^{3}H-Relative Counts
150000
130000
110000
90000
70000
50000
30000
10000
39 41 43 45 47 49 51 53 55 57
InsP$_6$
InsP$_5$
InsP$_7$
Retention time (min)

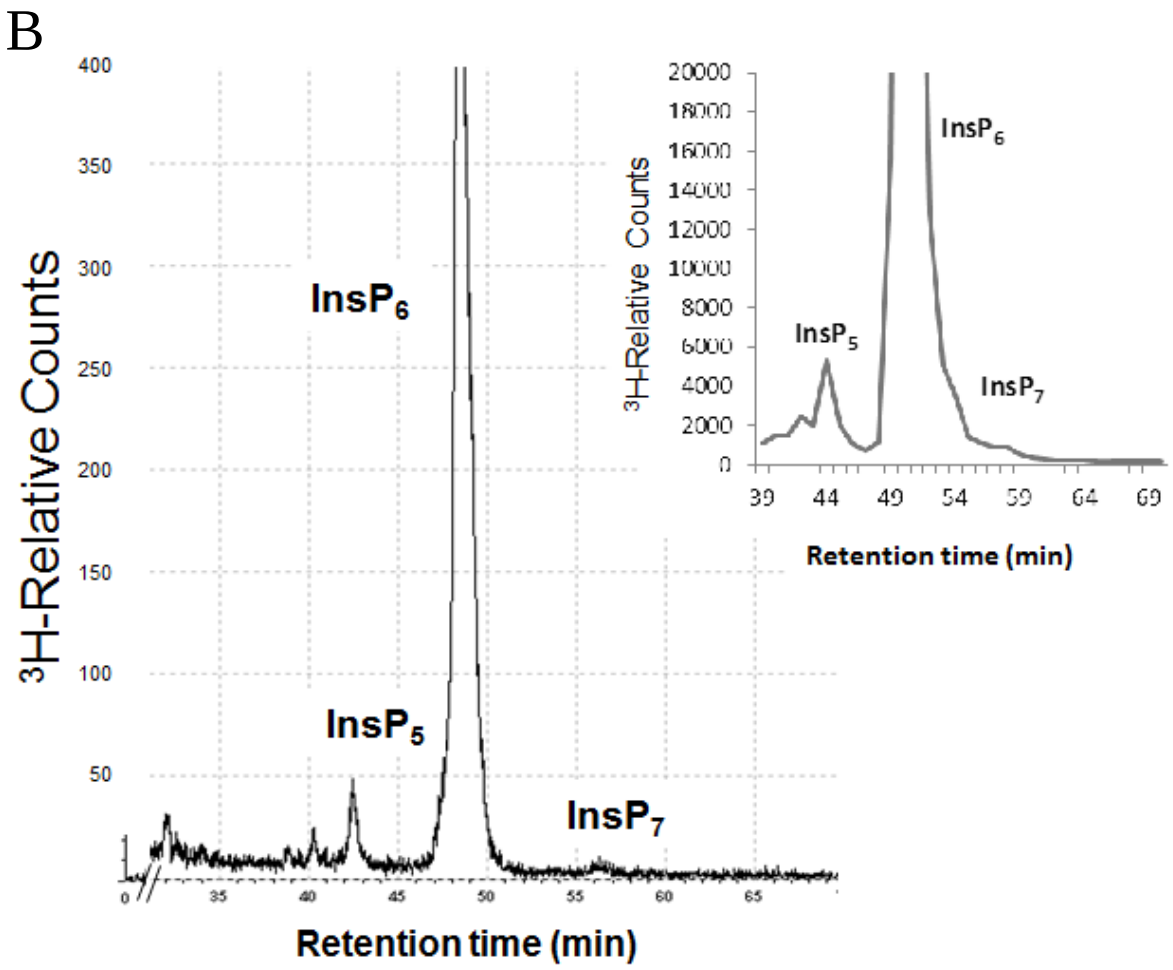

Figure 3.3. HPLC Analysis of InsPs in Arabidopsis

(A) Developing seeds within siliques were radiolabeled with ^{3}H-*myo*-inositol for four days. InsPs were extracted, separated using anion exchange, and quantified via an in-line radioisotope detector. A discrete peak for $InsP_7$ was identified by co-migration with $InsP_7$ from yeast. The inset shows relative counts obtained from scintillation counting of eluted HPLC fractions. The data are representative of 7 biological replicates.
(B) Seedlings were radiolabeled ^{3}H-*myo*-inositol for six days and analyzed as described for (A). Data are representative of 15 biological replicates.

Two Arabidopsis Genes are Similar to the Human and Yeast Vip kinases

Two types of kinases in eukaryotes are capable of phosphorylating $InsP_6$, the VIP kinases and the $InsP_6$ kinases (IP6Ks) (*11, 39*). Although we could not identify a reasonable Arabidopsis gene homologue of the $InsP_6$ kinase using BLAST searches, we did identify two potential Arabidopsis *Vip* genes, At3g01310 (referred to as *AtVip1*), and At5g15070 (referred to as *AtVip2*). While the AtVIP1 and AtVIP2 predicted proteins are 94% similar to each other, they are only 50% similar to the ScVIP1 protein and 59% similar to the HsVIP1 protein. However, both AtVIP proteins are predicted to contain an N-terminal RimK/ATP-Grasp domain and a C-terminal histidine acid phosphatase domain (**Figure 3.4A**), which are conserved in all eukaryotic VIP proteins (*28*). Our phylogenetic analysis supports the tentative identification of AtVIP1 and AtVIP2 as paralogues of the yeast and human VIPs when compared to all other known or predicted inositol kinases from Arabidopsis (**Figure 3.4B**). Our BLAST analyses also indicate that several other plant species contain conserved *Vip* genes, indicating that these genes have likely retained their function during evolution in complex organisms.

While transcripts for both *AtVip* genes were detected in all plant tissues assayed, each gene exhibits distinct patterns of expression across the different tissues. *AtVip1* expression is higher in vegetative compared to reproductive tissue, while *AtVip2* expression is higher in roots and reproductive tissues (**Figure 3.4C**). This suggests that the two genes may have non-redundant functions. Querying of expression databases, including the Expression Fluorescent Pictograph Browser from U. Toronto indicates that *AtVip1* may be the more highly expressed form in most plant tissues, with the exception that *AtVip2* is more abundant in mature pollen.

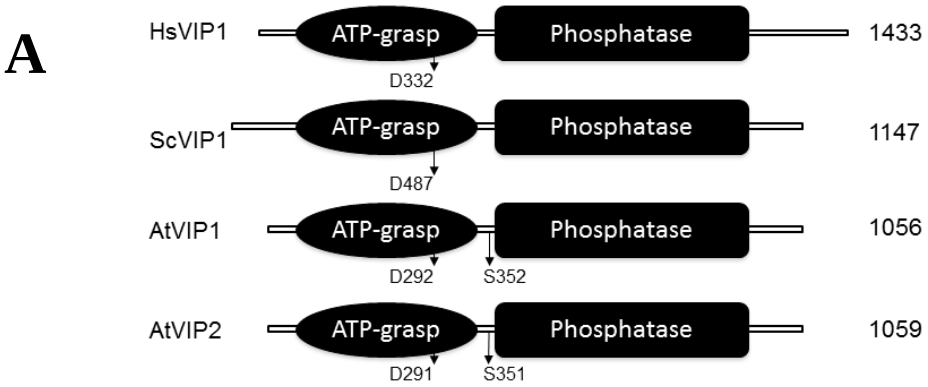
A
HsVIP1
ATP-grasp
Phosphatase
1433
D332
ScVIP1
ATP-grasp
Phosphatase
1147
D487
AtVIP1
ATP-grasp
Phosphatase
1056
D292
S352
AtVIP2
ATP-grasp
Phosphatase
1059
D291
S351

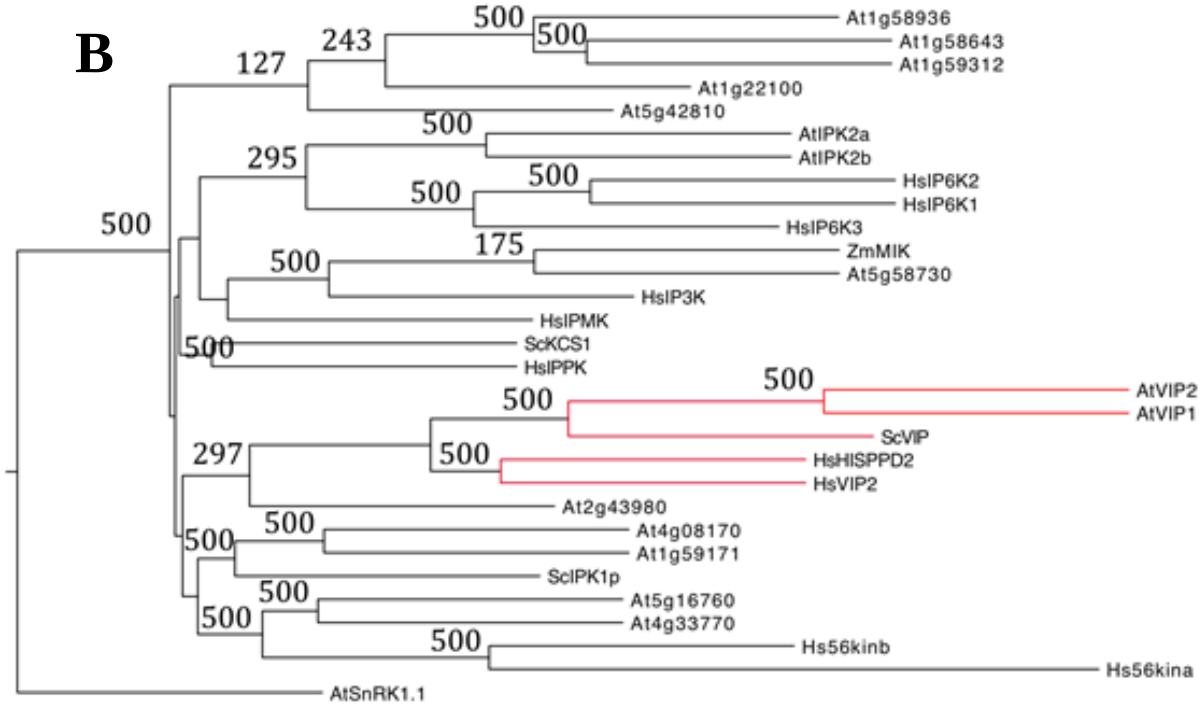
B
500
243
500
At1g58936
127
500
At1g58643
At1g59312
At1g22100
At5g42810
500
AtIPK2a
AtIPK2b
295
500
500
HsIP6K2
HsIP6K1
500
HsIP6K3
175
ZmMIK
500
At5g58730
HsIP3K
HsIPMK
500
ScKCS1
HsIPPK
500
500
AtVIP2
AtVIP1
ScVIP
297
500
HsHISPPD2
HsVIP2
At2g43980
500
At4g08170
500
At1g59171
ScIPK1p
500
At5g16760
500
At4g33770
500
Hs56kinb
Hs56kina
AtSnRK1.1

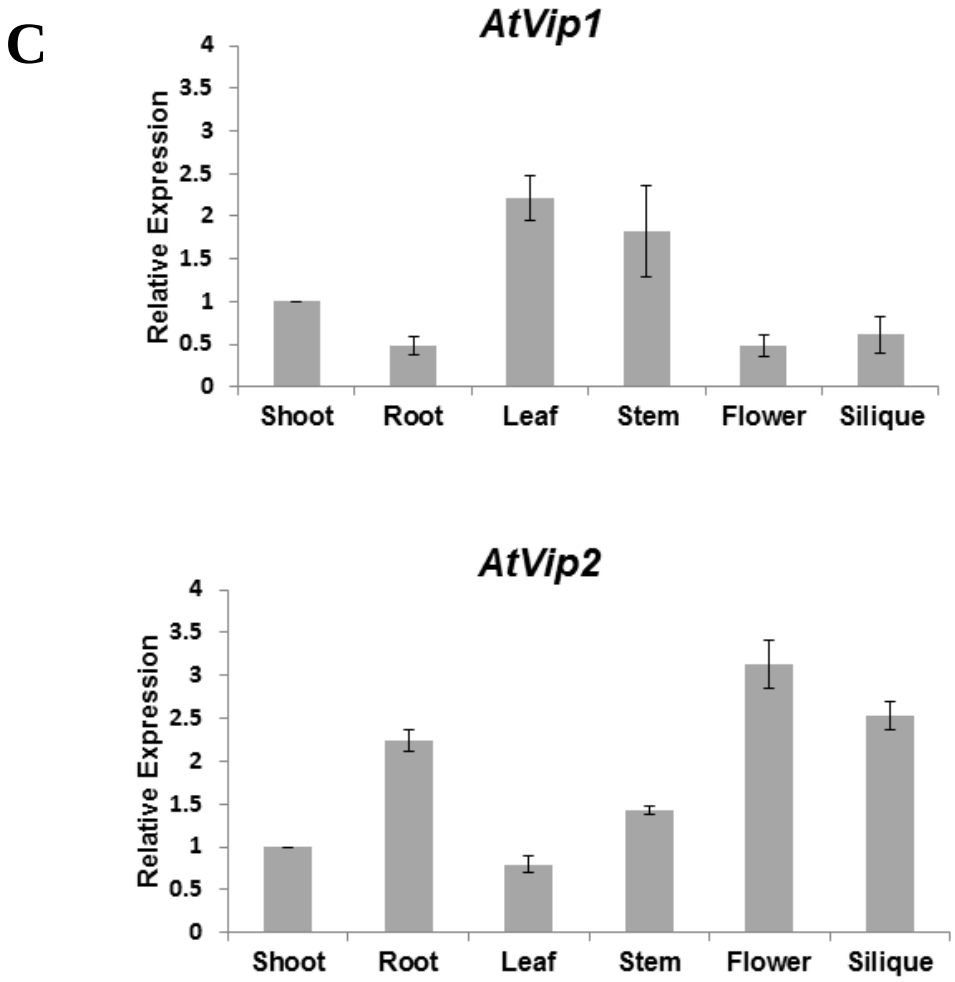

Figure 3.4. Domain Organization, Phylogenetic Analysis and Expression of the AtVIP Kinases

(A) Schematic alignment of the ATP grasp/RimK/ kinase and the histidine acid phosphatase domains within the VIP proteins from *Homo sapiens* (Hs: Genbank AAH57395), *Saccharomyces cerevisiae* (Sc: NP_013514) and *Arabidopsis thaliana* (*AtVip1* Gene ID: 821297; *AtVip2* Gene ID: 831359). Arrows note the conserved aspartic acid residue (D) required for kinase activity and the known phosphorylated serine residues within the Arabidopsis VIPs.
(B) Phylogenetic Analysis of Plant VIP proteins. Amino acid sequences were aligned with Clustal W, and ProtDist was used to infer phylogeny. The Arabidopsis SnRK1.1 protein kinase was used as the outgroup. Total number of bootstraps (500 total) is shown for branches with greater than 50% support.
(C) Q-PCR of *AtVip1* and *AtVip2* in shoot and root tissue from 2 week old seedlings grown on agar plates, leaf, stem, flower and siliques from 10 week old mature plants. Gene expression was measured by quantitative PCR with gene specific primers for *AtVip1* and *AtVip2*. PP2a was used as the reference gene. Expression levels are shown relative to shoot tissue and are the average (+SE) of 3 biological replicates analyzed during independent experiments.

The AtVIPs Restore $InsP_7$ Synthesis to Yeast Mutants

To determine whether *AtVip* genes encode kinases capable of phosphorylating $InsP_6$, we tested whether these genes can function in the synthesis of $InsP_7$ in a yeast triple null mutant. The yeast Δ*kcs1*Δ*ddp1*Δ*vip* mutant lacks $InsP_7$ synthesis due to mutations in both types of $InsP_6$ kinases, but possesses a high intracellular concentration of $InsP_6$ (*28*). Mutation of diphosphoinositol phosphate phosphatase (*ddp1*; also known in humans as DIPP) (*40*) in this mutant results in high steady state levels of $InsP_7$ when a functional *Vip* gene is supplied (*28, 41*). Full-length cDNAs for *AtVip1* and *AtVip2* were cloned and expressed in the Δ*kcs1*Δ*ddp1*Δ*vip* mutant under control of a galactose-inducible promoter. These yeast lines were radiolabeled with ^{3}H-*myo*-inositol and InsP accumulation was analyzed by HPLC. A Δ*kcs1*Δ*ddp1*Δ*vip* mutant overexpressing the human *Vip1* kinase domain (*41*) was used as a control for restoration of $InsP_7$ synthesis (**Figure 3.5**). Production of $InsP_7$ could also be restored by introduction of a plasmid encoding either the AtVIP1 protein or the AtVIP2 protein (**Figure 3.6**).

To test whether the predicted kinase domains of AtVIP1 and AtVIP2 are active in $InsP_7$ synthesis, we expressed the putative kinase domains (KD) of each gene, which includes the ATP grasp domain, in the same yeast system. The KDs from both genes were able to restore partial $InsP_7$ synthesis (**Figure 3.6**), however, we consistently measured less $InsP_7$ accumulation with the KDs alone as compared to when the intact AtVIPs were expressed (**Figure 3.6**). We also examined the importance of a critical aspartic acid residue (D292) in AtVIP1 by expressing the native and a mutant version (D292A) of the putative AtVIP1 kinase domain (*AtVip1KD$_m$*), which we predicted would render the AtVIP1 kinase domain inactive (*28, 41*). Our results (**Figure 3.6B**) show that D292 is critical for activity of the kinase domain as $InsP_7$ synthesis is not

restored by expression of the KD mutant (**Figure 3.6B**). We conclude that the AtVIP1 and AtVIP2 proteins encode functional $InsP_6$ kinases, and that D292 is required for activity. However, since the kinase domains alone did not restore $InsP_7$ to same levels as the intact AtVIPs, we conclude that amino acid sequences outside of the predicted AtVIP kinase domains impact activity in this heterologous system.

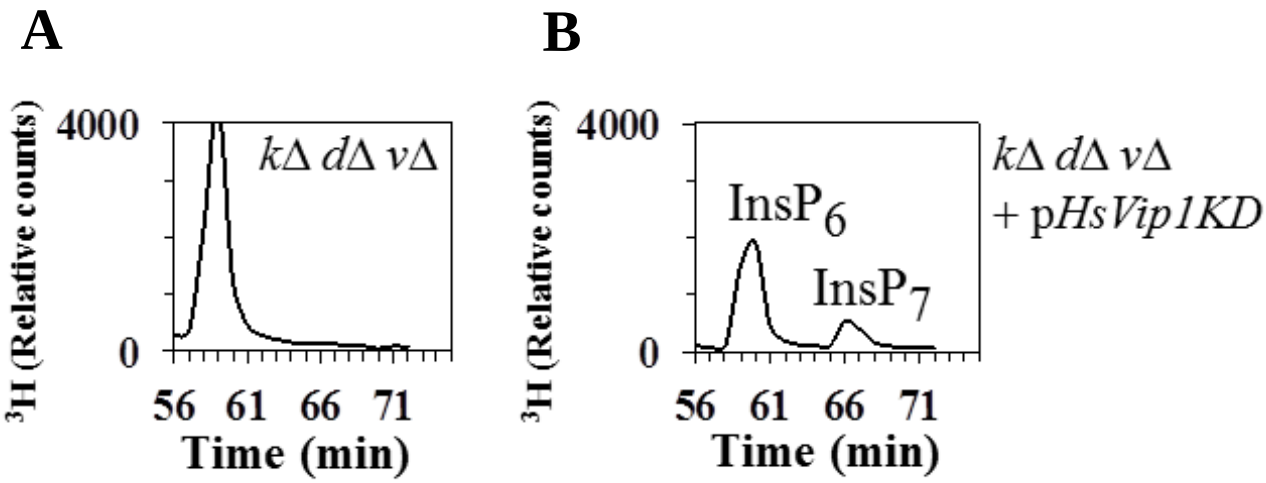

Figure 3.5. Complementation of a Yeast Triple Mutant with a Human *Vip* gene.

(A) A yeast triple mutant defective in the KCS1, VIP and DDP1 (*k*Δ*d*Δ*v*Δ) was transformed with empty vector and were labeled with ^{3}H-*myo*-inositol. Soluble InsPs were isolated and resolved by HPLC and scintillation counting. The data are representative of 2 biological replicates.
(B) The *k*Δ*d*Δ*v*Δ mutant was transformed with the human *Vip1* kinase domain (*HsVip1KD*) and analyzed as described in (A). The data are representative of 2 biological replicates.

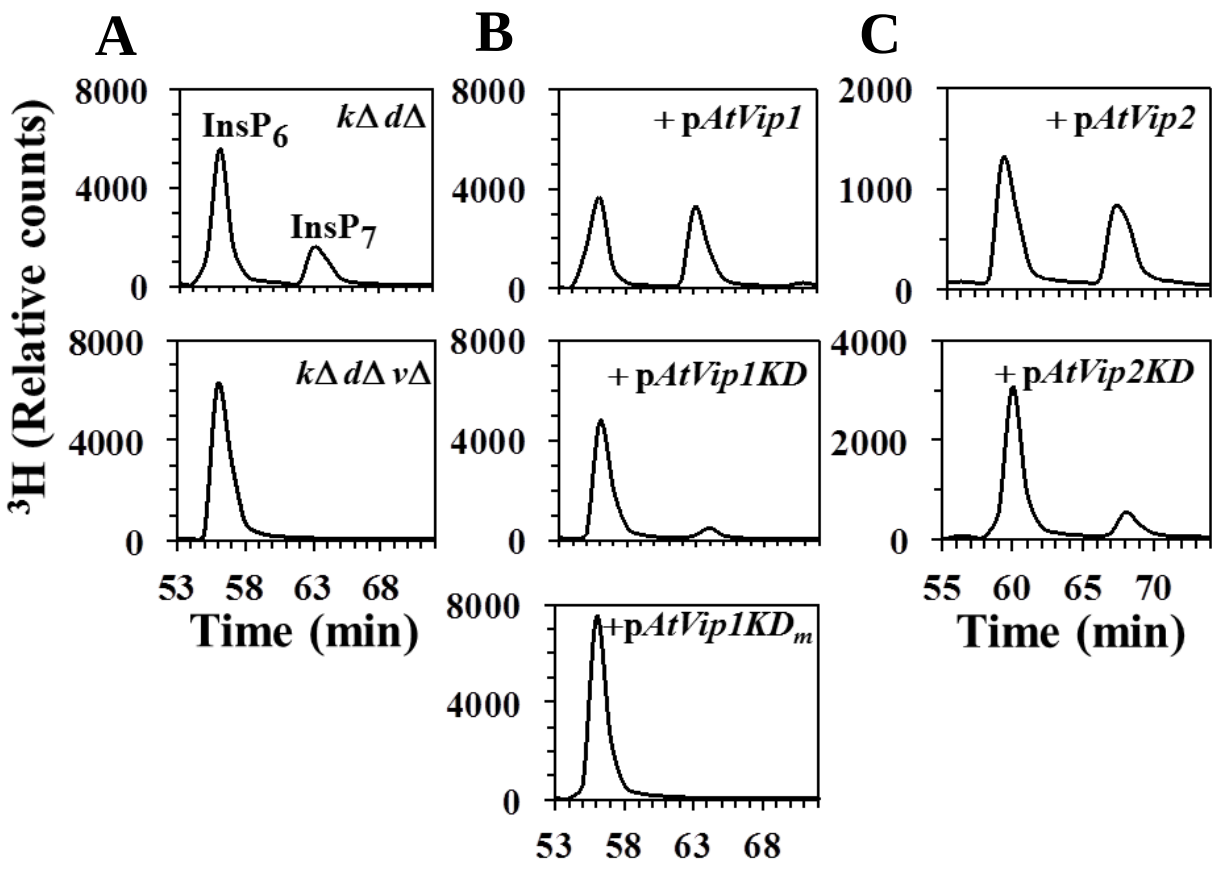

Figure 3.6. *AtVip1* and *AtVip2* Restore InsP$_7$ Synthesis in Yeast

(A) A yeast double mutant (*k*Δ*d*Δ) and triple mutant (*k*Δ*d*Δ*v*Δ) were labeled with ^{3}H-*myo*-inositol, and the soluble InsPs were isolated and resolved by HPLC and scintillation counting. (B) The *k*Δ*d*Δ*v*Δ mutant was transformed with expression constructs for *AtVip1*, the kinase domain of *AtVip1* (p*AtVip1KD*) and a mutated version of the *AtVip1* kinase domain (*AtVip1KDmut*) and analyzed as in (A).
(C) The *k*Δ*d*Δ*v*Δ mutant was transformed with expression constructs for *AtVip2*, or *AtVip2* kinase domain (*AtVip2KD*) construct. All data are representative of 3-5 biological replicates.

The AtVIPs Complement Growth in Yeast Mutants

When starved for one or more nutrients, yeast can alter its growth pattern to produce elongated cells that grow invasively as filaments. This type of invasive filamentous growth requires the *Vip1* gene, and involves the formation of elongated cells called pseudohyphae that allow for the adhesion of cells to surfaces such as agar (*42*). We tested whether the *AtVips* could complement yeast *vip1* mutants that are defective in invasive growth and pseudohyphae formation. Yeast *vip1* mutant cells complemented with the *Saccharomyces cerevisiae Vip1* gene (*ScVip1)*, or *AtVip1* or *AtVip2* were spotted on rich media. After 20 days of incubation at 30°C (**Figure 3.7A**, top), we tested if cells could penetrate the agar by rinsing them with water, and vigorously rubbing cells off the agar (**Figure 3.7A**, middle), and allowing for re-growth at 30°C for one day (**Figure 3.7A**, bottom). We found that complementation with the *ScVip1*, *AtVip1* and *AtVip2* genes, but not the pYES vector alone, allowed cells to penetrate the agar (**Figure 3.7A**, middle), and more subsequent re-growth resulted one day afterwards (**Figure 3.7**, bottom). Microscopic analysis of invasively growing cells confirmed the presence of elongated cells in all the complemented lines, but not in the mutant transformed with the pYES vector alone (**Figure 3.7B**). Quantification of yeast form (round) versus filamentous form (i.e. elongated) cells in these cultures indicated that *AtVip1* and *AtVip2* genes restored the ability to grow invasively at the same degree as the *ScVip1* gene (**Figure 3.7C**). Together, these data indicate that the *AtVip1* and *AtVip2* genes are functional in restoring invasive growth by providing VIP activity.

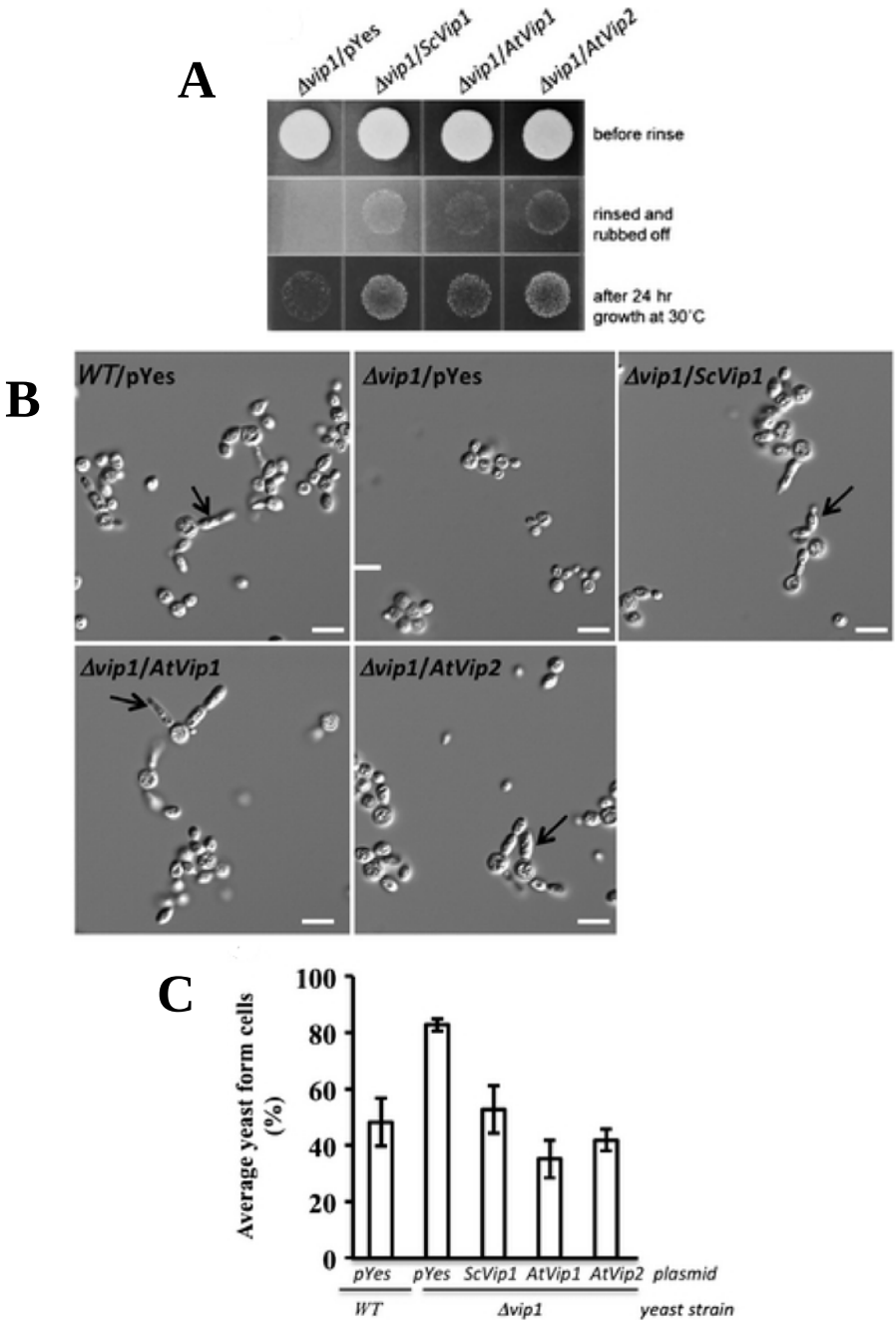
A
Δvip1/pYes
Δvip1/ScVip1
Δvip1/AtVip1
Δvip1/AtVip2
before rinse
rinsed and rubbed off
after 24 hr growth at 30˚C
B
WT/pYes
Δvip1/pYes
Δvip1/ScVip1
Δvip1/AtVip1
Δvip1/AtVip2
C
Average yeast form cells (%)
100
80
60
40
20
0
pYes
pYes
ScVip1
AtVip1
AtVip2
plasmid
WT
Δvip1
yeast strain

Figure 3.7. *AtVip1* and *AtVip2* Restore Invasive Growth to a *vip1* Mutant.

(A) A total of 10^5 Δ*vip1*/pYES, Δ*vip1*/ScVip1, and Δ*vip1* with *AtVip1* and *AtVip2* cells were spotted on SLAHD medium and incubated for 20 days at 30°C (top), and the plates were rinsed with water and cells were rubbed off (middle). Subsequently the plate was incubated at 30°C for 24 hr (bottom). The data are representative of two independent biological replicates.
(B) DIC image showing morphological alterations in invasively growing complemented strains described above. The indicated strains were grown in liquid selective medium for 20 days at 30°C. Bar is equal to 20 μm. Arrows indicate the elongated cells. The data are representative of three independent biological replicates.
(C) Average yeast cell form cells were determined by examining microscope images of cells (N = ~ 180 cells). Standard error is presented. The data are representative of two independent biological replicates.

DISCUSSION

$InsP_7$ and $InsP_8$ are "energy-rich" molecules having one or more energy-rich pyrophosphate moieties that have a free energy of hydrolysis comparable to that of ATP (*13*). Besides roles in controlling telomere length and modulating insulin signaling, these molecules have recently been shown to be critical for metabolic reprogramming by influencing ATP homeostasis and mitochondrial function (*10, 11, 39, 43-45*). Surprisingly, these molecules have not been the subject of investigation in plants even though plants produce large amounts of their precursor and most abundant InsP in nature, $InsP_6$. The observation of compounds with PAGE mobility and HPLC elution similar to $InsP_7$ and $InsP_8$ (**Figures 3.2, 3.3**), and the identification of plant genes that restore $InsP_7$ synthesis to yeast mutants (**Figures 3.6, 3.7**), clearly demonstrates that higher plants possess the metabolic machinery to synthesize these molecules.

Our observation of $InsP_7$ and $InsP_8$ was enhanced via the discovery that seed produced by Arabidopsis and maize (*mrp*) mutants have elevated levels of $InsP_7$ and $InsP_8$ (**Figure 3.2**, **Table 3.1**, **Figure 3.8**). Multidrug resistance proteins (MRP)s are a subfamily of the ATP-binding cassette (ABC) transporters that transport anions across membranes of cells and organelles. *AtMRP5* is highly expressed in seeds (*46*) and has been shown to be a high affinity $InsP_6$ transporter (*35*). $InsP_6$ accumulates in developing seeds as a means for sequestering and storing phosphorus required for seed germination and early seedling growth. *Atmrp5* mutants produce seeds with decreased amounts of $InsP_6$ and increased amounts of inorganic phosphate (*35, 37, 47, 48*). One possible explanation for elevated $InsP_7$ and $InsP_8$ in these $InsP_6$ transporter mutants is that a block in the transporter function results in an elevated $InsP_6$ pool *accessible to the* plant VIP kinases. Alternatively, synthesis and accumulation of $InsP_6$ in seeds could involve $InsP_7$ and

$InsP_8$ *intermediates* that provide the high-energy phosphate bonds for $InsP_6$ transporter activation/transport and the substrate (i.e. $InsP_6$) for transport. Further studies are required to test these hypotheses.

We show here that different plants and plant issues accumulate detectable levels of $InsP_7$ and $InsP_8$ (**Table 3.1** and Results). Surprisingly, levels of $InsP_7$ and $InsP_8$ were similar in both developing seeds and vegetative tissues although plant seeds accumulate roughly two orders of magnitude more $InsP_6$ than plant vegetative tissues (*49*); this suggests a role for these molecules even in tissues where the substrate $InsP_6$ is not extremely abundant. The binding of $InsP_6$ and $InsP_5$ to auxin (*50*) and jasmonic acid (*51, 52*) receptors, respectively, has spurred interest in the potential signaling roles of $InsP_6$, and our identification of $InsP_7$ and $InsP_8$ extends the scope of $InsP_6$ function.

We also show here that plants have two $InsP_6$ kinase genes that are functional in yeast systems. Key to this finding was the ability to show that both *AtVip* genes restore the production of $InsP_7$ in a budding yeast triple mutant (**Figure 3.6**). As well, both *AtVip* genes are capable of restoring invasive growth in a yeast *vip1* mutant (**Figure 3.7**). Invasive growth is considered to be an adaptation to low nutrients that allows for scavenging of nutrients (*53*). Our full complementation of a nutrient response phenotype and restoration of $InsP_7$ synthesis supports that *AtVip* genes are paralogous to the yeast and animal *Vips*, with conserved roles as active $InsP_6$ kinases.

Genome searches show that *Vip* genes are conserved throughout higher plants, and contain the widely-conserved dual domain structure, an N-terminal ATP grasp (i.e. kinase) domain and a C-terminal histidine acid phosphatase domain (**Figure 3.4**). We predicted that the AtVIP kinase domains alone would support $InsP_7$ synthesis in budding yeast mutants, but found that the AtVIP kinase domain alone does not function as well as the full-length VIP proteins. This suggests that the plant VIPs have sequences outside the conserved kinase domain that influence activity. In contrast, the yeast and human VIP kinase domains are more active than the full-length proteins in assays both *in vitro* and *in vivo*. Recent data indicated that recombinant human VIP phosphatase domain alone is inactive and instead binds to PtdIns(3,4,5)P_3, which regulates the subcellular location of the enzyme (*54*). We note here that phosphoprotemics work has shown both AtVIP1 and AtVIP2 proteins are phosphorylated at serine 352 and 351, respectively, which is positioned between the kinase and phosphatase domains (**Figure 3.4**) (http://phosphat.mpimp-golm.mpg.de). This residue has not been identified as a phosphorylation target in the yeast and human VIPs, thus it may be a unique regulatory site for the plant VIPs where it could influence catalytic activity.

We could find no evidence of plant genes encoding the second type of conserved $InsP_6$ kinase, exemplified by the yeast KCS1 and the three human IP6K genes, which function in synthesis of 5PP-$InsP_5$ (**Figure 3.1**) (*27*). Our phylogenetic analyses support the idea that either the KCS1/IP6K genes are missing in plants or that another plant inositol kinase has a unique ability to synthesize 5PP-$InsP_5$. If true, this would be surprising as the architecture of the catalytic sites in the KCS1/IP6K and VIP enzymes dictates the 5-position and 1/3-position phosphorylation, respectively (*11*). Since 5PP-Ins(1,2,3,4,6)P_5 and 1/3PP-Ins(2,3,4,5,6)P_5 are indistinguishable

during HPLC separation, the identity of the newly identified plant $InsP_7$ isomer awaits further structural studies requiring NMR. We also detected $InsP_8$ in both *Atmrp5* and maize *mrp4* mutants by PAGE (**Figure 3.2**, **Figure 3.8**), and in Arabidopsis and other plants by using HPLC (**Figure 3.3**, **Table 3.1**). The existence of $InsP_8$ in plants is intriguing and the enantiomeric configuration of this molecule is also likely to yield insight into the plant synthetic pathway (**Figure 3.1**). Since the best characterized $InsP_8$ enantiomer in any organism is 1,5PP_2-Ins(2,3,4,6)P_4, (*29, 55*) and plants may not contain an enzyme that phosphorylates the 5-position of $InsP_6$, we speculate that the $InsP_8$ we measured is either 1,3PP_2-Ins(2,4,5,6)P_4 or 1/3PPP-$InsP_5$ (**Figure 3.1**). It is important to note that we did not observe a molecule consistent with the identity of PP-$InsP_4$ in any of our work, suggesting that the plants we examined were not using a KCS1-like enzyme to phosphorylate $InsP_5$, as is the case in yeast (*25*).

Our results also expand our knowledge of the impact of important "low phytate" mutations (*23, 56*), which we show here can include increases in seed $InsP_7$ and $InsP_8$ in addition to decreases in $InsP_6$. This is important as the maize *MRP4* locus is the target of breeding and engineering efforts to develop low-phytate crops in multiple food crop species. Mutations in orthologs in soybean (*57*), rice (*48*) and common bean (*58*) have also been isolated and are currently being used in the breeding and bioengineering of the low phytate trait, which is expected to decrease phosphate pollution from run-off and to enhance animal nutrition.

EXPERIMENTAL PROCEDURES

Plant Materials

Arabidopsis thaliana ecotype Columbia, *Camelina sativa*, *Gossypium hirsutum* (cotton; Deltapine 90) and maize (*Zea mays* L.) hybrid seed were used. The maize *mrp4* mutant has been described (*37*). The wild-type and *mrp4* hybrids were near-isogenic except for the *mrp4* gene, and were produced by crossing two public sector inbred lines (A632 and A619), and were grown in the same field nursery in Kimberly, ID. The Arabidopsis *ipk2β*, *ipk1*, At3g45090 and *mrp5* mutants have been described (*34*-*37*).

PAGE Analyses of PPx-InsPs from Seeds

PPx-InsPs were extracted from maize and Arabidopsis seed by homogenization in 10 volume/dry weight 0.4 N HCl + 10% (w/v) Na_2SO_4. Extracts were neutralized with 2N NaOH, centrifuged, and aliquots (20 μL) of supernatant were fractionated using PAGE as described (*59*). Under our conditions, $InsP_6$ had an Rf value relative to Orange G of ~1.35. Gels were stained with Toluidine Blue as described (*59*). $InsP_6$ was prepared using Sigma phytic acid dodecasodium salt hydrate (prepared from rice), while 5PP-$InsP_5$, 1/3PP-$InsP_5$ and (1/3), $5PP_2$-$InsP_5$ (called $InsP_8$) was kindly provided by Drs. A. Saiardi, Univ. College London and J. York, Vanderbilt Univ.).

Detailed method of PAGE Analyses of PPx-InsPs from Seeds

F_2 seed produced by a maize (*Zea mays* L.) hybrid, that was either homozygous wild-type or homozygous for a recessive allele of the *mrp4* gene, which encodes an $InsP_6$-specific member of the ABC transporter gene family (*35, 37*), were tested using PAGE. The wild-type and *mrp4*

hybrids were near-isogenic except for the *mrp4* gene, and were produced by crossing two public sector inbred lines (A632 and A619), that were either wild-type or homozygous mutant, and were grown in the same field nursery located in Kimberly, ID. The initial source seed of *Arabidopsis thaliana* genotypes were provided by Dr. T. Tai, USDA-ARS, Davis CA. These were then propagated in the greenhouse using standard cultural practices.

Maize seed was first milled to pass 40 mesh, whereas for *Arabidopsis thaliana*, whole seed were homogenized. Extraction was in a 1.5 mL eppendorf microfuge tube on ice: tissue aliquots or whole seed were homogenized for 1.0 min in 10 volume/dry weight 0.4 N HCl + 10% (w/v) Na_2SO_4, immediately neutralized with 2N NaOH, and extracts centrifuged (12,000 RPM, 20 min in an eppendorf microfuge at 4^o C). Aliquots (20 μL) of supernatant were fractionated using PAGE as describe (*59*): prior to loading, 10 μL of 6x Dye (10 mM TrisHCl pH 7.0; 1 mM EDTA; 30% glycerol; 0.1% Orange G) was added to each aliquot; these were fractionated on a 24 x 16 x 0.1 cm gel using 33.3% polyacrylamide in TBE (31.7 mL 40% Acr/Bis (19:1); 3.8 mL 10X TBE; 2.2 mL H_2O; 270 μL 10% APS; 30 μL TEMED); gels were pre-run for 20 min at 300 volts; after loading, gels were run at 300 volts overnight at 4^oC. Under our conditions, Ins P_6 had an Rf value relative to Orange G of ~1.35, and we typically ran gels until the Orange G migrated 6 to 8 cm. Gels were stained with Toluidine Blue as follows: they were agitated in staining solution (20% methanol; 2% glycerol; 0.05% Toulidine Blue) then distained for 2 hrs with three changes of the staining solution without dye. Photographs were taken using a white-light transilluminator.

Standards were: 1) 0.5 mM $InsP_6$ prepared using Sigma phytic acid dodecasodium salt hydrate (prepared from rice), which we confirmed had a dodecasodium salt formula weight of 923.8, a water content of 5.5 moles H_2O per mole, and a phytic acid dodecasodium•H_2O of formula weight of 1022.8; 1/3 PP-Ins P_7 generated by a yeast recombinant VIP1 catalytic domain; 5PP-$InsP_5$ generated by a mouse recombinant $InsP_6$ kinase; (1/3),5 PP-$InsP_5$ produced by the mouse recombinant $InsP_6$ kinase (kindly provided by Dr. A. Saiardi, Univ. College London and J. York, Vanderbilt Univ.).

For follow-up tests of the InsPs in *At mrp5* seed, a seed sample (450 mg) confirmed to be homozygous for *Atmrp5* was extracted in 10 mL 0.4 N HCl + 10% (w/v) Na_2SO_4 at 4^oC. Following centrifugation (10 min, 10,000 RPM), a 100 μL aliquot of supernatant was neutralized with 20 μL 2 N NaOH, and then used as a "crude extract" control. Supernatant InsPs were first obtained as a ferric precipitate (*31*), as follows. Five mL of supernatant was transferred to a 30 mL Corex centrifuge tube, to which was added 5 mL ddH_2O and 2.5 mL of 15 mM $FeCl_3$:0.2 M HCl:5% Na_2SO_4. This solution was then heated in a boiling water bath for 30 min, cooled, and centrifuged (10 min, 7,000 RPM). A 10 X concentration was then achieved via re-suspension of the ferric precipitate in 1 N NaOH (using 1/10 of the original supernatant volume), which converts the ferric Ins phosphates to soluble sodium Ins phosphates. The resulting solution was then neutralized with 6 N H_2SO_4.

Plant ^{3}H-*myo*-Inositol Labeling for HPLC Analysis

For labeling, we followed methodology described in (*38*) with the following modifications. For analysis of developing seeds, green siliques of similar developmental stage were chosen, and clipped with the pedicel. Six to eight siliques were used for each labeling experiment. For seedling analysis, 15 4-day old Arabidopsis seedlings were collected from 0.5x MS + 0.8 % agar plates grown in chambers with 100 µE light with a 16 hour day/8 hour night cycle after stratification at 4°C for three days. The samples were incubated with 50 µl of 1x MS + 1% sucrose (pH 5.7) and 100 µl of aqueous *myo* [2-^{3}H(N)]-inositol (100 µCuries, American Radiolabeled Chemicals Cat. #ART 0116A, specific activity 20 Ci/mmol) was added to each tube. The tubes were incubated with supplemental light for 4 days. Seed were removed from labeled siliques and used for InsP extraction. A similar method was used for *Camelina sativa* seedlings, except fewer seedlings were used for each extraction. For labeling of cotton, a single three-day old seedling was labeled for 4 days and divided into root and shoot portions prior to extraction. Leaf punches from Arabidopsis and cotton were made on developing leaves with a standard hole punch and labeled for four days as described (*60*). Extraction of InsPs (*61*) involved grinding tissue in extraction buffer (25mM EDTA, 10 mg/ml $InsP_6$ and 1M Perchloric acid ($HClO_4$), adding glass beads, vortexing, and neutralization to pH 6 to 8 with 250 mM EDTA, 1M K_2CO_3. Samples were dry-extracted to a volume of 70 µl.

HPLC Separation of InsPs and Analysis

A binary HPLC pump (Beckman Coulter) equipped with a Partisphere SAX 4.6 X 125 mm column and connected through a guard cartridge was used. Elution gradient for HPLC was set up

as per (*61*) using Buffer A (1mM EDTA) and Buffer B (1.3M Ammonium Phosphate, pH 3.8). The flow rate was set to 1ml/min, and an in-line IN/US radiation detector was used to generate chromatograms. Four ml of Ultima-Flo AP scintillation cocktail (Perkin Elmer, Waltham, MA) was added to each 1 ml eluted fraction post-detector to quantify the radioactivity of the eluted fractions using the ^{3}H window of a Beckman Coulter LS6500 Scintillation Counter. Scintillation counts were graphed using MicroSoft Excel. The ^{3}H-*myo*-Ins cpm incorporated into InsPs (total InsPs) was calculated by taking the sum of cpm of all fractions and subtracting the ^{3}H-Ins peak cpm. The amount of each InsP was calculated as follows: [(Σ cpms in peak) / (total InsPs)]*100]. Results from HPLC experiments were independently validated in two different laboratories.

Phylogenetic Analyses

Amino acid sequences for Arabidopsis, human and yeast VIPs and related inositol kinase proteins were aligned using ClustalW. The Arabidopsis SnRK1.1 protein kinase was used as an outgroup. Phylogenetic trees were constructed with ProtDist and bootstrapped 500 times. Figtree1.4 was used to draw phylogenetic trees.

RNA Preparation and qRT-PCR

RNA was isolated from 2 week-old seedlings grown on plates (shoot and root) and 10 week-old plants (leaf, stem, flower and silique). For mature plants tissue was pooled from 10 plants. RNA was isolated using the Plant RNeasy kit (Qiagen) with on-column DNAse treatment. Reverse transcription was carried out using 1µg of total RNA and Omniscript Reverse Transcriptase (Qiagen). The equivalent of 20 ng of cDNA was used for quantitative PCR using gene specific

primers for *AtVip1* and *AtVip2* and SYBRgreen. Reactions were carried out in triplicate with PP2A as the reference gene. Primer efficiencies for both *AtVip1* and *AtVip2* and PP2A were determined and found to be comparable. Relative expression was calculated by the ΔΔCT method (*62*).

Construction of Yeast Expression Plasmids

Saccharomyces cerevisiae strains used in this study are found in Supp. **Table 3.2** and were kindly provided by the York and Fleig laboratories. The full-length cDNA coding sequences of *AtVip1* and *AtVip2* were amplified from RNA purified from 3-week old light grown seedlings (ecotype Col-0) with a Qiagen kit and specific primer pairs (Supp. **Table 3.3**. cDNA was prepared using an RT-Kit (Improm-II^{TM}, Promega) and Phusion polymerase and subsequently cloned into pENTR/D-TOPO (Invitrogen), and confirmed by DNA sequencing. The coding sequence of *S. cerevisiae Vip1p* was amplified from yeast DNA using the indicated primers. *AtVip1*, *AtVip2*, and *YVip1* were cloned into pYES 2.0, a multi-copy, galactose-inducible yeast expression vector carrying the URA3 auxotrophic marker. A similar strategy was used to clone the first 1086 bp of *AtVip1* and 1036 bp of *AtVip2* genes resulting in kinase domain gene sequences that were transformed into pYes2.0. The D292A kinase-dead mutation (*AtVip1*^{D292A}) was introduced into the full-length *AtVip1* cDNA using PCR (http://www.methodbook.net/pcr/pcrmut.html). Yeast mutants were transformed with the *AtVip* and *ScVip* constructs or empty vectors using an EZ-transformation kit following the manufacturer's protocol (Clontech). For general growth, cells were grown in synthetic minimal medium lacking uracil containing 2% glucose at 30°C after spotting onto selective synthetic

minimal medium plates lacking uracil and containing 2% galactose plus 1% raffinose, unless otherwise indicated. The expression of *AtVips* was verified by RT-PCR analysis of cDNA prepared from strains harboring these constructs, induced with galactose-containing medium. Yeast RNA was prepared with an RNeasy Mini Kit, Qiagen, following the manufacturer's instructions. RNA was eluted with warm water and 2 µg of RNA was utilized for cDNA preparation. The cDNA was prepared using a RT-Kit (Improm-II^{TM}, Promega).

Steady-State Labeling of Yeast for HPLC Analysis

Freshly-grown yeast colonies were used to inoculate SD/2% glucose-Ura medium with 110 nM inositol. The culture was grown overnight to an OD_{600} >1, centrifuged, washed with sterile water, and resuspended in SD/2% galactose/1% raffinose –Ura medium without inositol. The culture was diluted in 10 ml of the same medium to OD_{600} of 0.01 to 0.02. Aqueous *myo* [2-^{3}H(N)]-inositol (20 µCuries, American Radiolabeled Chemicals Cat. #ART 0116A, 20 Ci/mmol) was added. Duplicate unlabeled cultures containing 110 nM inositol were grown side-by-side to verify OD_{600}. The culture was grown at 30^{o} C with shaking in a 50 ml flask to OD_{600} of 0.5 to 1.2. The culture was centrifuged, washed three times with water, and frozen at -80^{o} C. Perchloric acid extraction of InsPs was performed as in (*61*). When needed, extracts were concentrated under $N_{2(g)}$ to 65 µL volume. Samples were either loaded onto the HPLC immediately or frozen at -80^{o}C.

Functional Complementation of Yeast

Yeast transformants were grown in liquid media overnight and normalized by resuspending in sterile water to 0.1 OD at 600 nm. An equal volume (15 µl) of the normalized culture was used spotted onto SLAHD-URA with galactose and raffinose, followed by drying before transferring the plate for incubation at 30°C for 20 days. The occurrence of yeast form (yf) and filamentous form (ff) cells was assessed by microscopic examination with a Zeiss Axioimager. A cell was designated yf if the cell was round, and if no unipolar buds were observed, and ff if the cell was elongated.

Acknowledgements

We thank John York and Ursula Fleig for providing yeast mutants. We also thank John York for inositol phosphate standards, and Adolfo Saiardi for helpful advice on protocols. We thank Peter Svizeny for assistance with the yeast assays.

APPENDIX TO CHAPTER III

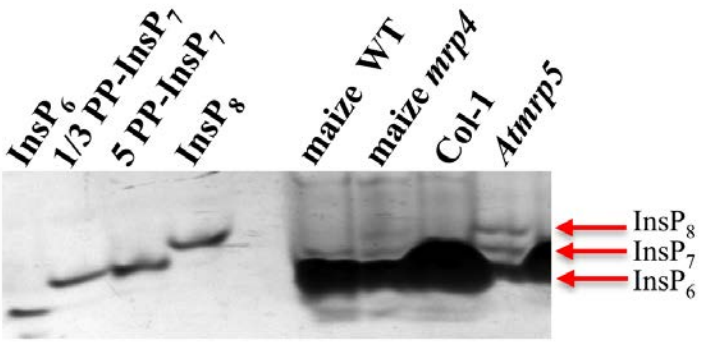

Figure 3.8. Supplemental Data: PAGE Analyses of Inositol Pyrophosphates in Maize and Arabidopsis Seeds

InsPs from mature dry seeds of maize wildtype and *mrp4* mutants, and *Arabidopsis thaliana* wildtype (Col-1) and *mrp5* mutants were extracted and analyzed via PAGE as described in the methods. Gels were stained with toluidine blue. Standards lanes contain 2.5 nmoles of each indicated compound. The positions of $InsP_8$, $InsP_7$ and $InsP_6$ are marked. Note that wildtype seed contain high levels of $InsP_6$ that can obscure endogenous $InsP_7$ and $InsP_8$.

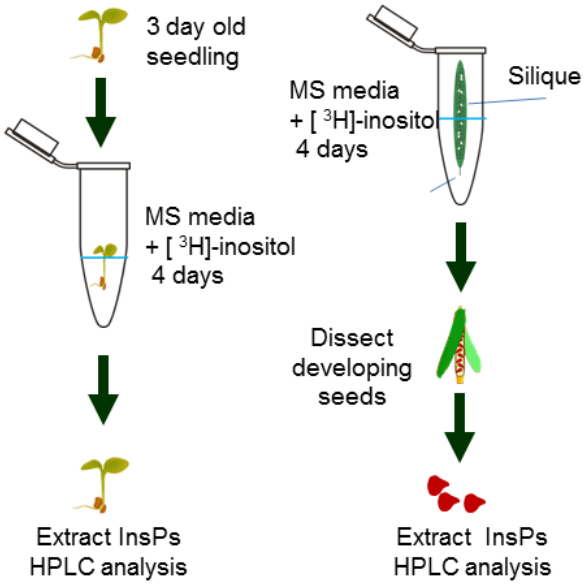

Figure 3.9. Supplemental Data: Diagram of ^{3}H-*myo*-inositol Labeling Method

Left: Germinated seedlings were incubated in ^{3}H-*myo*-inositol solution for 4 days, then removed, washed and inositol phosphates were extracted as described in the methods. Right: Developing siliques were incubated in ^{3}H-*myo*-inositol solution for 6 days, then removed and washed. Developing seed were dissected and inositol phosphates were extracted from seed as described in the methods.

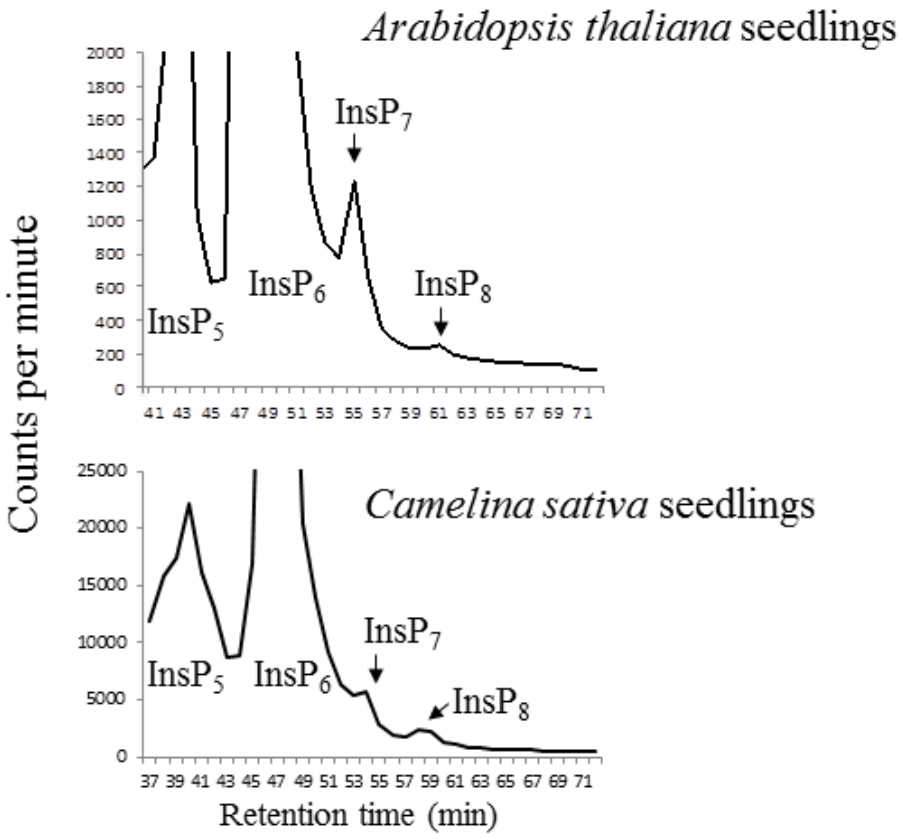

Figure 3.10. Supplemental Data: Detection of $InsP_8$ in Seedlings

Radiolabeling of Arabidopsis (top) and *Camelina* (bottom) seedlings followed by InsP extraction and analysis of extracts by HPLC was performed as described. Scintillation counting of HPLC fractions was performed and the counts per minute of each fraction were plotted versus the fraction number. Enlargement of the $InsP_7$ and $InsP_8$ peaks results in the loss of the top portion of the $InsP_6$ and $InsP_5$ peaks from Arabidopsis and the $InsP_6$ peak from *Camelina sativa*.

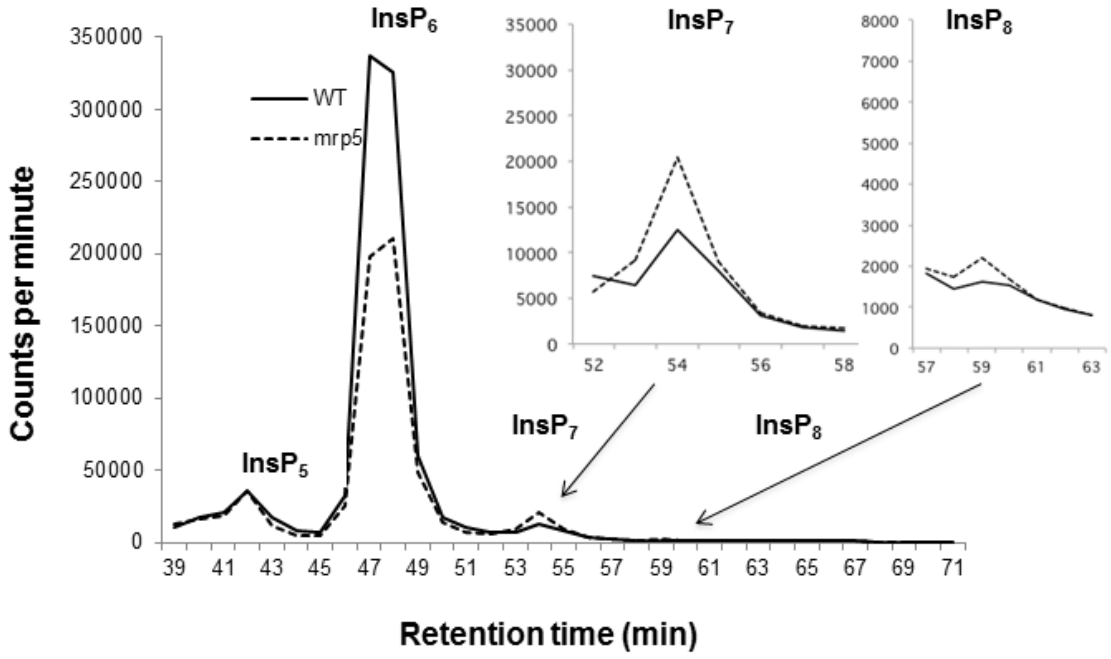

Figure 3.11. Supplemental Data: Detection of Higher InsPs in *mrp5* and Wildtype Siliques.

Radiolabeling of siliques from wildtype (solid line) and *mrp5* mutants (dashed line) followed by InsP extraction and analysis of extracts by HPLC was performed as described. Scintillation counting of HPLC fractions was performed and the counts per minute of each fraction were plotted versus the fraction number. The insets show enlargement of the $InsP_7$ and $InsP_8$ fractions from the indicated positions. Five biological replicates of each tissue type were analyzed.

Table 3.2. *S. cerevisiae* Strains Used in this Study

Strain	Genotype	Source
JYY105 (w303)	*MATα ade2-1 ura3-1 his3-11,15 trp1-1 leu2-3,112 can1-100*	(*28*)
JYY911	*MATα kcs1::HIS3 ddp1::HIS3 vip1::kanMX4*	(*28*)
LSY525	*MATα kcs1::HIS3/ddp1::HIS3*	(*28*)
JYY1141	*MATα kcs1::HIS3/ddp1::HIS3/vip1::kanMX4 pRS426-cup1-GFP-myc3-hVip1-KD(1-373)*	(*28*)
JYY918	*MATα vip1::HIS3 las17::LEU2*	(*28*)
UFY1780	*MAT***a***/MATα ura3-52/ura3-52 vip1Δ*::Kan^r*/Vip1*	(*42*)
UFY1781	*MAT***a***ura3-52 vip1Δ*::Kan^r	(*42*)
YUG94	*MAT***a***ura3-52*	(*42*)

Table 3.3. Primers Used this Study

Type of Construct	Gene ID	Primer name	Primer sequence
pENTR-AtVip1	At3g01310	pE-Vip1FW	CACCATGGAGATGGAAGAAGGAGCAAGTG
		pE-Vip1RE	TTAGCTCCTTCCATTAGAAGAAGAGTTCTTATAG
		pE-Vip1KDRE	TTATTCTGACTGCCCAAAAGTGCCGAT
		pE-Vip1KDmFW	ATGTTTGTGCTGTCAATGGATG
		pE-Vip1KDmRE	TACAAACACGACAGTTACCTAC
pENTR-AtVip2	At5g15070	pE-Vip2FW	CACCATGGGGGTGGAAGAAGGAGCTGGTG
		pE-Vip2RE	TTAGCTTTTGCCATTAGAGGTGTTCTTGTGG
		pE-Vip2KDRE	TTACTCTGACTGCCCAAAAGTTCCGATGATGCC
pYES2-YVip1	YLR410W	pYYVip1*BamHI*W	CGCGGATCCATGAGTGGGATAAAGAAGG
		pYYVip1*XhoI* RE	CCGCTCGAGCTAATCTAATGTCTTGTTAAC
pENTR-AtVip2	At5g15070	pE-Vip2FW	CACCATGGGGGTGGAAGAAGGAGCTGGTG
		pE-Vip2RE	TTAGCTTTTGCCATTAGAGGTGTTCTTGTGG
		pE-Vip2KDRE	TTACTCTGACTGCCCAAAAGTTCCGATGATGCC
pYES2-AtVip2	At5g15070	pYVip2*BamHI* FW	CGCGGATCCATGGGGGTGGAAGAAGGAGCTGGTG
		pYVip2*EcoRI* RE	CCGGAATTCTTAGCTTTTGCCATTAGAGGTGTTCTTG
		pYVip2KD*XbaI*RE	GCTCTAGATTACTCTGACTGCCCAAAAGTTCCGATGATGCC
pYES2-AtVip1	At3g01310	pYVip1*BamHI*FW	CGCGGATCCATGGAGATGGAAGAAGGAGCAAGTG
		pY-Vip1*EcoRI* RE	CCGGAATTCTTAGCTCCTTCCATTAGAAGAAGAGTTC
		pYVip1KD*XbaI*RE	GCTCTAGATTATTCTGACTGCCCAAAAGTGCCGAT

qRT-PCR AtVIP1	At3g01310	qRTAtVip1F	CACCATGGAGATGGAAGAAGGAGCAAGTG
		qRTAtVip1R	GCAGCATATGCCTGAGCCTTCTC
qRT-PCR AtVIP2	At5g15070	qRTAtVip2F	CAAGAGGTTGGTTCATGTTTGACCCTC
		qRTAtVip2R	GTGGAAGGGCCAAAGTTTAACAAGACG
qRT-PCR PP2AA3	At1g13320	qRTPP2AF	TAACGTGGCCAAAATGATGC
		qRTPP2AR	GTTCTCCACAACCGCTTGGT

REFERENCES

1. G. E. Gillaspy, The role of phosphoinositides and inositol phosphates in plant cell signaling. *Adv Exp Med Biol* **991**, 141 (2013).
2. C. J. Barker, P. O. Berggren, New horizons in cellular regulation by inositol polyphosphates: insights from the pancreatic beta-cell. *Pharmacol Rev* **65**, 641 (Apr, 2013).
3. S. B. Shears *et al.*, Defining signal transduction by inositol phosphates. *Subcell Biochem* **59**, 389 (2012).
4. M. M. Tsui, J. D. York, Roles of inositol phosphates and inositol pyrophosphates in development, cell signaling and nuclear processes. *Adv Enzyme Regul* **50**, 324 (2010).
5. T. Munnik, J. E. Vermeer, Osmotic stress-induced phosphoinositide and inositol phosphate signalling in plants. *Plant Cell Environ* **33**, 655 (Apr, 2010).
6. I. Y. Perera, I. Heilmann, S. C. Chang, W. F. Boss, P. B. Kaufman, A role for inositol 1,4,5-trisphosphate in gravitropic signaling and the retention of cold-perceived gravistimulation of oat shoot pulvini. *Plant Physiol* **125**, 1499 (Mar, 2001).
7. I. Y. Perera, C. Y. Hung, S. Brady, G. K. Muday, W. F. Boss, A universal role for inositol 1,4,5-trisphosphate-mediated signaling in plant gravitropism. *Plant Physiol* **140**, 746 (Feb, 2006).
8. I. Y. Perera, C. Y. Hung, C. D. Moore, J. Stevenson-Paulik, W. F. Boss, Transgenic Arabidopsis plants expressing the type 1 inositol 5-phosphatase exhibit increased drought tolerance and altered abscisic acid signaling. *Plant Cell* **20**, 2876 (Oct, 2008).
9. N. M. Perera, R. H. Michell, S. K. Dove, Hypo-osmotic stress activates Plc1p-dependent phosphatidylinositol 4,5-bisphosphate hydrolysis and inositol Hexakisphosphate accumulation in yeast. *J Biol Chem* **279**, 5216 (Feb 13, 2004).
10. A. Saiardi, Cell signalling by inositol pyrophosphates. *Subcell Biochem* **59**, 413 (2012).
11. S. B. Shears, J. D. Weaver, H. Wang, Structural insight into inositol pyrophosphate turnover. *Adv Biol Regul* **53**, 19 (Jan, 2013).
12. M. S. Wilson, T. M. Livermore, A. Saiardi, Inositol pyrophosphates: between signalling and metabolism. *Biochem J* **452**, 369 (Jun 15, 2013).
13. C. E. Hand, J. F. Honek, Phosphate transfer from inositol pyrophosphates InsP5PP and InsP4(PP)2: a semi-empirical investigation. *Bioorg Med Chem Lett* **17**, 183 (Jan 1, 2007).
14. Z. Szijgyarto, A. Garedew, C. Azevedo, A. Saiardi, Influence of inositol pyrophosphates on cellular energy dynamics. *Science* **334**, 802 (Nov 11, 2011).
15. J. H. Choi, J. Williams, J. Cho, J. R. Falck, S. B. Shears, Purification, sequencing, and molecular identification of a mammalian PP-InsP5 kinase that is activated when cells are exposed to hyperosmotic stress. *J Biol Chem* **282**, 30763 (Oct 19, 2007).
16. A. Chakraborty *et al.*, Inositol pyrophosphates inhibit Akt signaling, thereby regulating insulin sensitivity and weight gain. *Cell* **143**, 897 (Dec 10, 2010).
17. A. Burton, C. Azevedo, C. Andreassi, A. Riccio, A. Saiardi, Inositol pyrophosphates regulate JMJD2C-dependent histone demethylation. *Proc Natl Acad Sci U S A* **110**, 18970 (Nov 19, 2013).
18. R. S. Jadav, M. V. Chanduri, S. Sengupta, R. Bhandari, Inositol pyrophosphate synthesis by inositol hexakisphosphate kinase 1 is required for homologous recombination repair. *J Biol Chem* **288**, 3312 (Feb 1, 2013).

19. V. Raboy, myo-Inositol-1,2,3,4,5,6-hexakisphosphate. *Phytochemistry* **64**, 1033 (Nov, 2003).
20. V. Raboy, Approaches and challenges to engineering seed phytate and total phosphorus. *Plant Sci.* **177**, 281 (2009).
21. V. Raboy, D. Bowen, Genetics of inositol polyphosphates. *Subcell Biochem* **39**, 71 (2006).
22. H. Brinch-Pedersen, L. Sørensen, P. Holm, Engineering crop plants: getting a handle on phosphate. *Trends Plant Sci* **7**, 118 (2002).
23. V. Raboy, Progress in breeding low phytate crops. *J Nutr* **132**, 503S (Mar, 2002).
24. C. Azevedo, Z. Szijgyarto, A. Saiardi, The signaling role of inositol hexakisphosphate kinases (IP6Ks). *Adv Enzyme Regul* **51**, 74 (2011).
25. A. Saiardi, J. J. Caffrey, S. H. Snyder, S. B. Shears, The inositol hexakisphosphate kinase family. Catalytic flexibility and function in yeast vacuole biogenesis. *J Biol Chem* **275**, 24686 (Aug 11, 2000).
26. A. Saiardi, E. Nagata, H. R. Luo, A. M. Snowman, S. H. Snyder, Identification and characterization of a novel inositol hexakisphosphate kinase. *J Biol Chem* **276**, 39179 (Oct 19, 2001).
27. A. Saiardi, H. Erdjument-Bromage, A. M. Snowman, P. Tempst, S. H. Snyder, Synthesis of diphosphoinositol pentakisphosphate by a newly identified family of higher inositol polyphosphate kinases. *Curr Biol* **9**, 1323 (Nov 18, 1999).
28. S. Mulugu *et al.*, A conserved family of enzymes that phosphorylate inositol hexakisphosphate. *Science* **316**, 106 (Apr 6, 2007).
29. P. Draskovic *et al.*, Inositol hexakisphosphate kinase products contain diphosphate and triphosphate groups. *Chem Biol* **15**, 274 (Mar, 2008).
30. H. Lin *et al.*, Structural analysis and detection of biological inositol pyrophosphates reveal that the family of VIP/diphosphoinositol pentakisphosphate kinases are 1/3-kinases. *J Biol Chem* **284**, 1863 (Jan 16, 2009).
31. J. A. Dorsch *et al.*, Seed phosphorus and inositol phosphate phenotype of barley low phytic acid genotypes. *Phytochemistry* **62**, 691 (Mar, 2003).
32. C. C. Smart, S. Flores, Overexpression of D-myo-inositol-3-phosphate synthase leads to elevated levels of inositol in Arabidopsis. *Plant Mol Biol* **33**, 811 (Mar, 1997).
33. C. A. Brearley, D. E. Hanke, Pathway of synthesis of 3,4- and 4,5-phosphorylated phosphatidylinositols in the duckweed Spirodela polyrhiza L. *Biochem J* **290 (Pt 1)**, 145 (Feb 15, 1993).
34. S. I. Kim, T. H. Tai, Identification of genes necessary for wild-type levels of seed phytic acid in Arabidopsis thaliana using a reverse genetics approach. *Mol Genet Genomics* **286**, 119 (Aug, 2011).
35. R. Nagy *et al.*, The Arabidopsis ATP-binding cassette protein AtMRP5/AtABCC5 is a high affinity inositol hexakisphosphate transporter involved in guard cell signaling and phytate storage. *J Biol Chem* **284**, 33614 (Nov 27, 2009).
36. J. Stevenson-Paulik, R. J. Bastidas, S. T. Chiou, R. A. Frye, J. D. York, Generation of phytate-free seeds in Arabidopsis through disruption of inositol polyphosphate kinases. *Proc Natl Acad Sci U S A* **102**, 12612 (Aug 30, 2005).
37. J. Shi *et al.*, Embryo-specific silencing of a transporter reduces phytic acid content of maize and soybean seeds. *Nat Biotechnol* **25**, 930 (Aug, 2007).

38. J. Stevenson-Paulik *et al.*, Inositol phosphate metabolomics: merging genetic perturbation with modernized radiolabeling methods. *Methods* **39**, 112 (Jun, 2006).
39. M. P. Thomas, B. V. Potter, The enzymes of human diphosphoinositol polyphosphate metabolism. *Febs J* **281**, 14 (Jan, 2014).
40. S. T. Safrany *et al.*, A novel context for the 'MutT' module, a guardian of cell integrity, in a diphosphoinositol polyphosphate phosphohydrolase. *Embo J* **17**, 6599 (Nov 16, 1998).
41. P. C. Fridy, J. C. Otto, D. E. Dollins, J. D. York, Cloning and characterization of two human VIP1-like inositol hexakisphosphate and diphosphoinositol pentakisphosphate kinases. *J Biol Chem* **282**, 30754 (Oct 19, 2007).
42. J. Pohlmann, U. Fleig, Asp1, a conserved 1/3 inositol polyphosphate kinase, regulates the dimorphic switch in Schizosaccharomyces pombe. *Mol Cell Biol* **30**, 4535 (Sep, 2010).
43. C. J. Barker, C. Illies, G. C. Gaboardi, P. O. Berggren, Inositol pyrophosphates: structure, enzymology and function. *Cell Mol Life Sci* **66**, 3851 (Dec, 2009).
44. M. Bennett, S. M. Onnebo, C. Azevedo, A. Saiardi, Inositol pyrophosphates: metabolism and signaling. *Cell Mol Life Sci* **63**, 552 (Mar, 2006).
45. A. Saiardi, A. C. Resnick, A. M. Snowman, B. Wendland, S. H. Snyder, Inositol pyrophosphates regulate cell death and telomere length through phosphoinositide 3-kinase-related protein kinases. *Proc Natl Acad Sci U S A* **102**, 1911 (Feb 8, 2005).
46. M. Klein, B. Burla, E. Martinoia, The multidrug resistance-associated protein (MRP/ABCC) subfamily of ATP-binding cassette transporters in plants. *FEBS Lett* **580**, 1112 (Feb 13, 2006).
47. S. M. A. Maroof , N. M. Glover, R. M. Biyasheva, G. R. Buss, E. A. Grabau, Genetic Basis of the Low-Phytate Trait in the Soybean Line CX1834. *Crop Science* **49**, 69 (2009).
48. X. H. Xu *et al.*, Mutations of the multi-drug resistance-associated protein ABC transporter gene 5 result in reduction of phytic acid in rice seeds. *Theor Appl Genet* **119**, 75 (Jun, 2009).
49. L. Bentsink, K. Yuan, M. Koornneef, D. Vreugdenhil, The genetics of phytate and phosphate accumulation in seeds and leaves of Arabidopsis thaliana, using natural variation. *Theor Appl Genet* **106**, 1234 (May, 2003).
50. X. Tan *et al.*, Mechanism of auxin perception by the TIR1 ubiquitin ligase. *Nature* **446**, 640 (Apr 5, 2007).
51. A. Mosblech, C. Thurow, C. Gatz, I. Feussner, I. Heilmann, Jasmonic acid perception by COI1 involves inositol polyphosphates in Arabidopsis thaliana. *The Plant journal : for cell and molecular biology* **65**, 949 (Mar, 2011).
52. L. B. Sheard *et al.*, Jasmonate perception by inositol-phosphate-potentiated COI1-JAZ co-receptor. *Nature* **468**, 400 (Nov 18, 2010).
53. P. J. Cullen, G. F. Sprague, Jr., Glucose depletion causes haploid invasive growth in yeast. *Proc Natl Acad Sci U S A* **97**, 13619 (Dec 5, 2000).
54. N. A. Gokhale, A. Zaremba, S. B. Shears, Receptor-dependent compartmentalization of PPIP5K1, a kinase with a cryptic polyphosphoinositide binding domain. *Biochem J* **434**, 415 (Mar 15, 2011).
55. T. Wundenberg, G. W. Mayr, Synthesis and biological actions of diphosphoinositol phosphates (inositol pyrophosphates), regulators of cell homeostasis. *Biol Chem* **393**, 979 (Sep, 2012).

56. V. Raboy, The ABCs of low-phytate crops. *Nat Biotechnol* **25**, 874 (Aug, 2007).
57. J. Gillman, V. Pantalone, K. Bilyeu, The low phytic acid phenotype in soybean line CX1834 is due to mutations in two homologs of the maize low phytic acid gene. *Plant Genome* **2**, 179 (2009).
58. D. Panzeri *et al.*, A defective ABC transporter of the MRP family, responsible for the bean lpa1 mutation, affects the regulation of the phytic acid pathway, reduces seed myo-inositol and alters ABA sensitivity. *New Phytol* **191**, 70 (Jul, 2011).
59. O. Losito, Z. Szijgyarto, A. C. Resnick, A. Saiardi, Inositol pyrophosphates and their unique metabolic complexity: analysis by gel electrophoresis. *PLoS One* **4**, e5580 (2009).
60. D. E. Hanke, P. N. Parmar, S. E. Caddick, P. Green, C. A. Brearley, Synthesis of inositol phosphate ligands of plant hormone-receptor complexes: pathways of inositol hexakisphosphate turnover. *Biochem J* **444**, 601 (Jun 15, 2012).
61. C. Azevedo, A. Saiardi, Extraction and analysis of soluble inositol polyphosphates from yeast. *Nat Protoc* **1**, 2416 (2006).
62. T. D. Schmittgen, K. J. Livak, Analyzing real-time PCR data by the comparative C(T) method. *Nat Protoc* **3**, 1101 (2008).

CHAPTER IV

Distribution of PPx-InsP Synthesis and Degradation Enzymes Across Cell Compartments

Sarah P. Williams and Glenda Gillaspy

Contributions of Authors: SPW performed all experiments and wrote the manuscript, GG edited the manuscript.

ABSTRACT

Inositol pyrophosphates (PPx-InsP) are unique signaling molecules, recently identified in plants. Current work is underway to identify their signaling role but in other organisms they are important for energy and nutrient sensing as well as metabolic response. Here we focus on when and where the PPx-InsPs are synthesized both in the whole plant as well as within the plant cell. We report all tissue express the enzymes in the known pathway to synthesis PPx-InsPs and then the enzyme directly responsible for their synthesis (AtVIP2) is greatly upregulated in pollen. We examined the subcellular localization of the enzymes most proximal to InsP6 and PPx-InsP synthesis. We concluded from this analysis that InsP6 and PPx-InsP could be synthesized in the nucleus and ER suggesting a new organelle component to InsP signaling pathway.

INTRODUCTION

The *myo*-inositol phosphate (InsP) signaling pathway is critically important in eukaryotes, functioning in a wide array of processes such as hormonal signaling, stress responses, phosphorus sensing, homeostasis and storage (*1-4*). A new frontier for InsP signaling is the study of unique signaling roles for a novel group of InsPs containing diphospho- or triphospho- moieties (PPx) at one or more positions on the inositol ring. In some ways, these PPx-InsPs are analogous to ATP in that they contain high-energy pyrophosphate bonds, and in addition, have been linked to communicating the energy status of the cell in other organisms. These so-called inositol pyrophosphates are produced from other InsPs, with inositol hexakisphosphate or $InsP_6$, as the proximal precursor (**Figure 4.1**). One conundrum of plant PPx-InsP synthesis is the fact that a seemingly key enzyme, the $InsP_6$ Kinase (called KCS1 in yeast), is missing from all examined plant genomes (*5*). Other eukaryotes have two types of enzymes that allow for synthesis of $InsP_7$ and $InsP_8$, with $InsP_8$ production requiring both the $InsP_6$ Kinase and an $InsP_7$ Kinase named VIP (Very Important Protein kinase) **(Figure 4.1)**. We previously developed and described methods to detect PPx-InsPs in plant tissues, identified and cloned genes encoding the VIP kinases that are responsible for inositol pyrophosphate production in plants, and developed genetic resources to examine function of the plant VIP genes (*5*). Our preliminary work with *vip* loss of function mutants suggests that inositol pyrophosphates are required for regulation of growth under low energy conditions (unpublished data, Gillaspy lab). Other recent work has delineated that $InsP_8$ is a ligand for the Jasmonic Acid (JA) receptor, which is important for plant defense signaling pathways. Further, a *vip1* mutant is not able to elevate $InsP_8$ in response to added JA, and this mutant is deficient in its response to insects that trigger the JA pathway (*6*).

Thus, on-going work with genetic mutants and inositol profiling of these mutants, is likely to reveal functions of the inositol pyrophosphates in plants.

One key element in understanding how InsPs and PPx-InsPs function in plants is the spatial regulation and restriction of the synthesis and degradation pathways shown in **Figure 4.1**. There are several enzymes in the pathway that have known and well-characterized catalytic roles (*7*). The InsP kinases are a large group, defined by their specific InsP substrates and the position on the inositol ring they phosphorylate. Many InsP kinases are capable of performing secondary reactions in addition the major role ascribed to them. Along with the well-characterized enzymes, there are also enzymes predicted to be involved at specific points in the pathway, based on the presence of a conserved InsP kinase or phosphatase domain (*8*). Lastly, there are enzymes identified from low phytic acid (LPA) genetic screens, that can often be associated at a specific step in the pathway, based on the predicted encoded gene product (*9*). In many cases, enzymes in the pathway are encoded by multi-gene families, complicating genetic approaches to understanding function.

A further complication in the pathway is the probable existence of two separate routes of $InsP_6$ synthesis. These are called the lipid-dependent and lipid-independent pathways (*7*). These two synthesis pathways differ in their starting points, with the lipid-dependent pathway starting with $Ins(1,4,5)P_3$ produced via phospholipase C (PLC) action on phosphatidylinositol 4,5-bisphosphate ($PtdIns(4,5)P_2$) and the lipid independent beginning with the phosphorylation of myo-inositol by the *myo*-inositol kinase (MIK). Both pathways share an Inositol-Pentakisphosphate 2-Kinase (IPK1) which phosphorylates $InsP_5$ at the 2-position to synthesize

$InsP_6$. While direct experimental evidence is lacking, it has been speculated that $InsP_6$ synthesis in developing embryos utilizes the lipid-independent route of synthesis. In contrast, other plant cells known to be active in PLC signaling, such as guard cells, are generally considered to primarily use the lipid-dependent pathway of $InsP_6$ synthesis.

Equally important are the enzymes that transport or dephosphorylate $InsP_6$ and PPx-InsPs. Multidrug Resistant Protein 5 (MRPS) is an ABC transporter that acts to transport and sequester $InsP_6$ in the vacuole (*10*). This allows for the safe storage and ability to accumulate this highly charged molecule. The hydrolysis of $InsP_6$ is carried out by a group of enzymes collectively called Phytases. Diversity within this group allows for dephosphorylation at specific sites on the inositol ring (*11*). To date the PPx-InsP phosphatases have yet to be determined, but in other eukaryotes members of the Nudix family catalyze the removal of a phosphate from PPx-InsP. Thus through the action of these enzymes signaling PPx-InsPs are degraded and the signaling information they convey is terminated.

It has been proposed that regulation of PPx-InsP synthesis maybe specific for particular developmental stages and/or takes place in different subcellular compartments within the cell. We sought to understand which tissues in the model plant, *Arabidopsis thaliana*, express genes that encode enzymes that can recapitulate the entire pathway to PPx-InsPs. In addition, we sought to understand the spatial nature of the pathway in terms of subcellular compartmentation. While it is generally accepted that InsP synthesis occurs in the cytosol, two pieces of data suggest that the animal cell nucleus also contains signaling InsPs. First, recent work has identified a small pool of human homology of VIP (PPIP5K2) in the nucleus (*12*). Second,

PtdInsP signaling pathway molecules are also found in the nucleus (*13*). Because the subcellular localization of individual InsPs and PPx-InsPs would require a complex and very sensitive assay, and this information does not exist for any eukaryote, we examined the subcellular localization of key enzymes in the pathway, focusing on enzymes implicated in the lipid-dependent pathway. We report here that the kinases needed to synthesis $InsP_6$ and PPx-InsPs are localized to the nucleus and ER, while Nudix phosphatases are localized to the nucleus as well as ER, chloroplast and cytoplasm. Understanding the spatial restrictions on the PPx-InsP synthesis pathway informs us as to where PPx-InsP may be acting and what roles they might play in the plant. Given the diverse connections of other InsPs in plants to drought, salt and light signaling pathways, it is likely that understanding the roles of inositol pyrophosphates will facilitate future engineering of plant responses and adaption to many different environmental stresses.

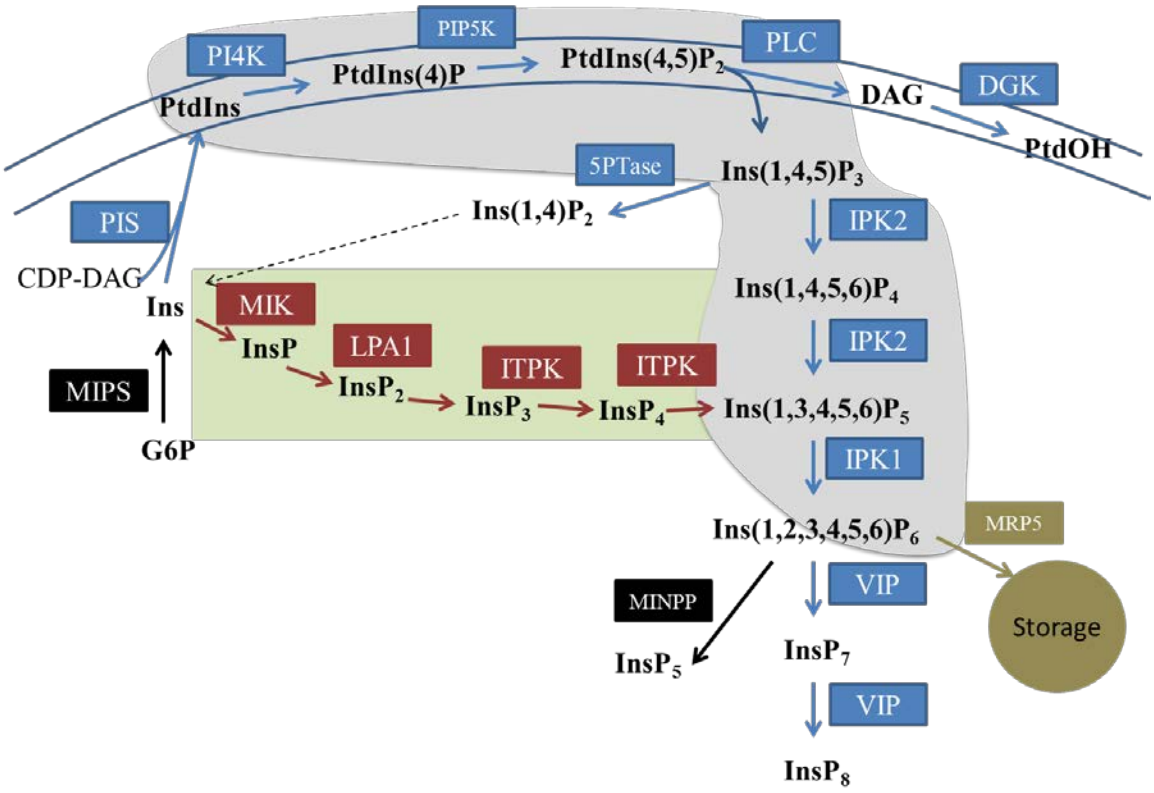

Figure 4.1. InsP Signaling Pathway

There are two pathways to $InsP_6$ production, the lipid-dependent is delineated by the blue shading and the lipid-independent by the green shading. Enzymes are indicated by boxes. Abbreviations are defined in the text. Once synthesized, $InsP_6$ has a number of fates: it can be hydrolyzed by phosphatases, including MINPP, sequestered in the vacuole by MRP5, or further phosphorylated producing the PPx-InsPs. The rate-limiting step in Ins synthesis is catalyzed by *myo*-inositol phosphate synthase (MIPS), which acts on glucose-6-phosphate (G6P). This is also the first step shown for synthesis of PtdInsPs.

RESULTS AND DISCUSSION

Overview of Genes in the Pathway

We assembled gene sequences for all enzymes involved in InsP and PPx-InsP synthesis and degradation (**Table 4.1**). We took as the start of the pathway the rate-limiting enzyme in *myo*-inositol synthesis, the *myo*-inositol phosphate synthase (MIPS) enzyme, which is encoded by three MIPS genes in Arabidopsis (*14*). In the lipid-dependent pathway *myo*-inositol is converted into phosphatidylinositol (PtdIns) and the PtdInsPs through the action of the PtdIns synthase (PIS), PtdIns 4-kinase (PI4K), and the PtdInsP5-kinases (PIP5K). We did not include these lipid-modifying enzymes in our analyses, as these have other signaling functions not linked to the PPx-InsPs. We do include the five genes encoding PLC, which cleaves PtdIns(4,5)P_2 into the soluble molecule, Ins(1,4,5)P_3, and the lipid diacylglycerol (DAG). In animals, Ins(1,4,5)P_3 is the second messenger which releases calcium ($Ca^{2+)}$ from internal stores. Ins(1,4,5,)P_3 signaling is terminated via dephosphorylation of Ins(1,4,5)P_3, which is catalyzed by the *myo*-inositol polyphosphate 5-phosphatases (5PTases). Our analysis includes the 5PTase13 gene (Table 1). Two Inositol Polyphosphate kinase 2 (IPK2) enzymes can phosphorylate Ins(1,4,5)P_3 to Ins(1,4,5,6)P_4 and Ins(1,3,4,5,6)P_5. Finally, a single expressed gene encoding the afore-mentioned IPK1 can phosphorylate Ins(1,3,4,5,6)P_5 to InsP_6.

We also include genes encoding enzymes from the lipid-independent pathway, including the *myo*-inositol kinase (MIK), which phosphorylates *myo*-inositol to InsP (*15*). The kinase or kinases responsible for conversion of InsP to InsP_2 and InsP_3 has yet to be determined, but the homologues of rice Low Phytic acid (LPA)1 gene encode kinases that might catalyze these

reactions (*8*). This pathway could continue with four genes encoding the Inositol (1,3,4)-trisphosphate 5/6-kinase (ITPK), which synthesizes $InsP_4$ and $InsP_5$ from $InsP_3$ (*16*). The penultimate phosphorylation step to $InsP_6$ requires the IPK1 gene product. Also included in this analysis is Multidrug Resistance-associated Protein 5 (MRP5), an ABC transporter responsible for sequestering $InsP_6$ in the vacuole (*10*).

Once $InsP_6$ is synthesized, the two VIP gene products could act to catalyze sequential phosphorylation reactions, leading to production of $InsP_7$ and $InsP_8$. In non-plant eukaryotes, the phosphatases that hydrolyze InsP7 and InsP8 are members of the large Nudix hydrolase family, which act on substrates that have a nucleoside diphosphate linked to some other moiety, X (Nudix). Substrates for the Nudix enzymes include (d)NTPs, dinucleoside polyphosphates, nucleotide sugars, NADH, FAD, co-enzyme A, and other compounds containing pyrophosphates (*17*). In this larger family, the human DIPP (Diphosphoinositol polyphosphate phosphohydrolase) subfamily acts on PPx-InsPs (*18*). The Nudix homologue in *Saccharomyces cerevisiae* is DDP1(Diadenosine and Diphosphoinositol Phosphohydrolase) (*19, 20*) and in *Schizosaccharomyces pombe* is APS1(diadenosine 5',5'''-p1,p6-hexaphosphate hydrolase) (*21-23*) . The Arabidopsis genome contains 29 genes encoding putative Nudix hydrolases, all containing the Gx_5Ex_7REUXEEXGU motif, where U is a bulky hydrophobic amino acid (*17*).

A sequence homology search of Arabidopsis using ScDDP1 and HsDIPP identified several Nudix family members. BLAST searches using ScDDP1 as a query identified Arabidopsis Nudix 21, 4, 18, 17 as strong candidates (e value < 1e-04). Nudix 16 was also identified with a slightly less significant e value (0.003). BLAST search using HsDIPP identified Nudix 12, 21, and 4 with

e values < 1e-04, and Nudix 13, 17 and 16 also share amino acid identity. SpAPS1 identified Nudix 21, 18,17,4,12, 13, and 16 as containing strong homology (e value > 1e-04). The Nudix domains of Nudix 4, 12, 13, 16, 17, and 18, have an additional glycine rich C-terminal (X_2GX_6G), which points to the PPx-InsPs or di-adenosine polyphosphates as possible substrates (*17*) (**Figure 4.2**). Another possible candidate for a plant PPx-InsP phosphatase is a yeast SIW14 orthologue (At1g05000); ScSIW14, a predicted protein tyrosine phosphatase, has recently been identified as having 5PP-$InsP_5$ hydrolase activity (personal communication, Rhonda Rolfes). In Arabidopsis, Plant and Fungi Atypical Dual-Specificity Phosphates (ATPFA-DSP1) has been annotated as a protein tyrosine kinase with a dual domain structure of SIW14 (*24*).

Figure 4.2. Alignment of Nudix Predicted Proteins

Putative PPx-InsP hydrolases from the Nudix family were aligned using Cluster Omega (*25*). The Nudix domain is indicated with a blue line and the glycine rich C-terminus is indicated with a red line. This glycine rich domain is predictive of PPx-InsP substrates. Amino acids are colored based on chemical properties (red=small, blue=acidic, pink=basic, green= contains a hydroxyl, sulfhydryl, amine or is a glycine). Stars beneath the alignment indicate conserved residues, while dots indicate conservative substitutions.

Spatial Analysis of Expression of Genes in the InsP Pathway

Understanding the spatial nature of regulation of InsP pathway enzymes can help elucidate where PPx-InsP signaling is occurring. To determine which tissues in Arabidopsis contain PPx-InsP synthesis, we used a publically available database and queried this database for developmental expression patterns of all genes in the pathway. Genes in the InsP pathway are listed in **Table 4.1**, which includes their unique gene identifier. The Electronic Fluorescence Pictograph (eFP) Browser contains microarray data from large-scale data sets generated by many groups and this data is mapped onto pictographic representations of the experimental samples used to generate the data sets (*26*). This analysis revealed three main patterns of expression (**Figures 4.3-4.8**).

The first pattern contains Group 1 genes that have in common their up-regulation in pollen (**Figures 4.3, 4.4**). The upregulation of PLC(PI), PLC4, and PLC3 which generate Ins(1,4,5)P_3, and 5PTase13, which dephosphorylates Ins(1,4,5)P_3, in Group 1, suggests the importance of $InsP_3$ signaling in mature pollen (**Figure 4.4**). Surprisingly, LPA1a, whose loss of function decreases $InsP_6$ in the seed (*8*) was upregulated in pollen. VIP2 and a number of Nudix family members (13, 16, 17, 21) are also found in Group 1 suggesting a role for VIP2 catalyzed production of PPx-InsPs in pollen (**Figure 4.4**).

Group 2 genes are upregulated in embryo and seed development (**Figures 4.5, 4.6**). This group consists of multiple genes encoding enzymes spanning the entire pathway to $InsP_6$ beginning with MIPS1 and MIPS2, MIK, IPK2α, IPK2β, ITPK1 and ITPK3. Multiple inositol polyphosphate phosphatase (MINPP), an $InsP_6$ phosphatase, is upregulated in early seed

development, though notably reduced in the late stages of maturation. The potential PPx-InsP hydrolase, SIW14, is also included in this group. LPA1b and MRP5 are also upregulated in seed. LPA1b, MIP2 and MIPS1 had the highest absolute expression values in seed. Surprisingly, Group 2 does not contain a PLC, which suggests that the lipid dependent pathway to $InsP_6$ production is not the driving factor in seed synthesis of $InsP_6$. However, the contribution from the lipid dependent pathway should not be dismissed, as PLC2 is expressed in high levels in during seed development.

Group 3 genes have less restricted expression, and this group contains genes expressed in various vegetative and reproductive tissues (**Figures 4.7, 4.8**). Group 3 genes include PLC1, PLC2, PLC8, PLC9, ITPK2, ITPK4, and VIP1 and Nudix 12, suggesting roles for the genes in basal InsP production or signaling. It also indicates that PPx-InsPs are likely synthesized in almost all tissues in the plant.

All tissues queried had at least one member of the most proximal enzymes for PPx-InsP synthesis, namely, ITPK, IPK2, IPK1, and a VIP. In addition, high levels of expression of VIP2 in pollen indicate that this tissue likely has high levels of PPx-InsP. However, the importance of PPx-InsP signaling in vegetative tissue should not be discounted given the more ubiquitous expression of VIP1. VIP1 expression is notably down in seeds, indicating synthesis of PPx-InsP might be less abundant. However we have been able to detect PPx-InsP in seeds(*5*) where PPx-InsPs might serve as potential storage molecules for the germinating seed.

Table 4.1. Genes Included in Expression Analyses

Gene abbreviation	Gene name/function	Gene ID
MIPS2	*myo*-Inositol Phosphate Synthase	At2g22240
MIPS1	*myo*-Inositol Phosphate Synthase	At4g39800
PLC1	Phospholipase C – PI specific	At5g58670
PLC2	Phospholipase C– PI specific	At3g08510
PLC3	Phospholipase C– PI specific	At4g38530
PLC4	Phospholipase C– PI specific	At5g58700
PLC8	Phospholipase C– PI specific	At3g47290
PLC9	Phospholipase C– PI specific	At5g47220
PLC (PI)	Phospholipase C– PI specific	At3g55940
PLC (PI) – no data	Phospholipase C– PI specific	At2g40116
5PTase13	Inositol Polyphosphate 5-Phosphatases	At1g05630
IPK2α	Inositol Polyphosphate Kinase Inositol Polyphosphate Multikinase	At5g07370
IPK2β	Inositol Polyphosphate Kinase Inositol Polyphosphate Multikinase	At5g61760
IPK1	Inositol Polyphosphate Kinase	At5g42810
MIK	*myo*-Inositol Kinase	At5g58730
ITPK1	*myo*-Inositol-Trisphosphate 3-kinase	At5g16760
ITPK2	*myo*-Inositol-Trisphosphate 3-kinase	At4g33770
ITPK3	*myo*-Inositol-Trisphosphate 3-kinase	At4g08170
ITPK4	*myo*-Inositol-Trisphosphate 3-kinase	At2g43980
MINPP	Multiple Inositol Polyphosphate Phosphatase	At1g09870
MRP5	Multidrug Resistance-Associated Protein	At1g04120
LPA1a	Low Phytic Acid – Proposed Kinase	At3g45090
LPA1b	Low Phytic Acid – Proposed Kinase	At5g60760
VIP1	$InsP_{6/7}$ Kinase	At3g01310
VIP2	$InsP_{6/7}$ Kinase	At5g15070

Nudix 4 - No data	Nudix hydrolase	At1g18300
Nudix 12	Nudix hydrolase	At1g12880
Nudix 13	Nudix hydrolase	At3g26690
Nudix 16	Nudix hydrolase	Atg312600
Nudix 17	Nudix hydrolase	At2g01670
Nudix 18 - No data	Nudix hydrolase	At1g14860
Nudix 21	Nudix hydrolase	At1g73540
SIW14	Protein Tyrosine Phosphatase	At1g05000

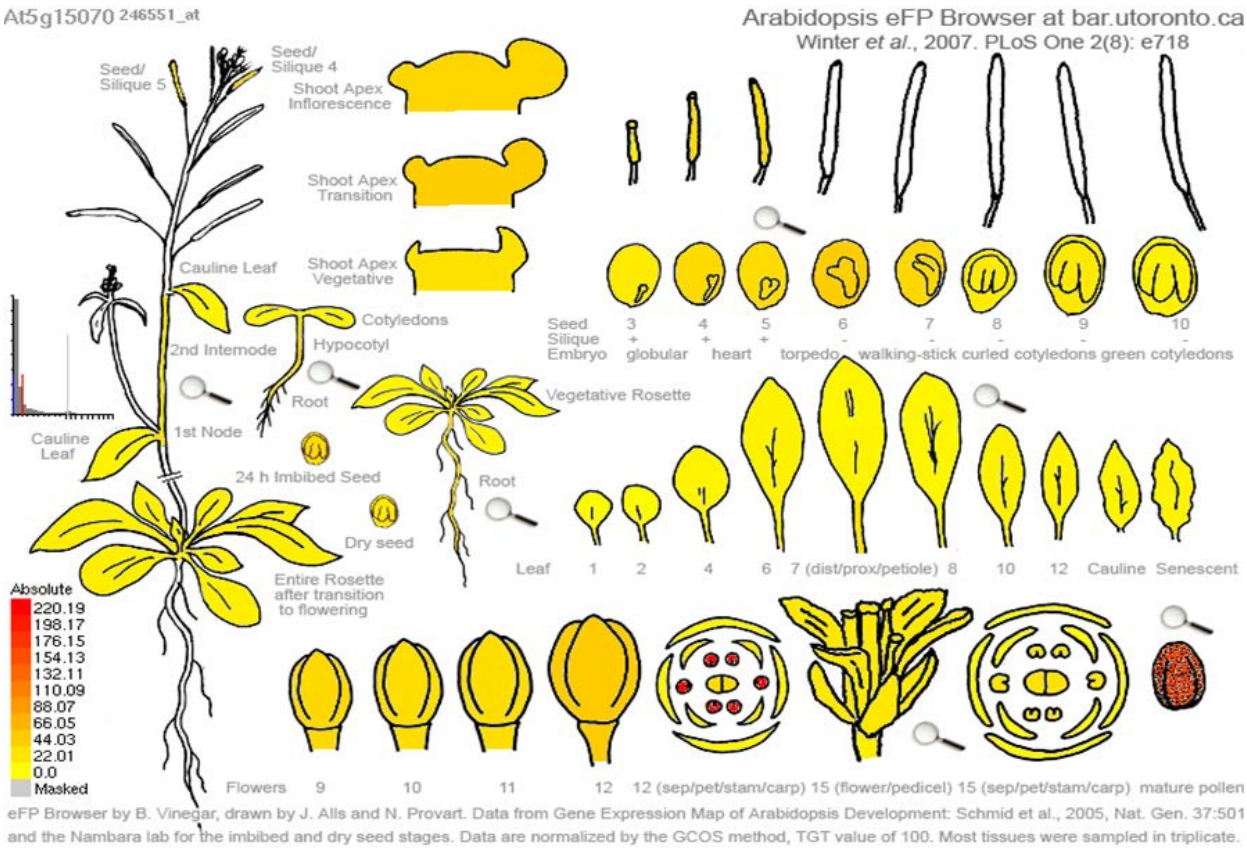

Figure 4.3. Representative Image of Group 1 Expression Pattern

Representative image of Group 1 gene expression profile from eFP Browser (http://bar.utoronto.ca/efp/cgi-bin/efpWeb.cgi). Gene expression levels are indicated by color, with low expression in yellow and highest expression levels indicated by red. Group 1 genes have high expression in pollen and lower expression in other tissues. Shown is expression of AtVIP2 (At5g15070).

	Group 1									
Tissue	PLC (PI)	Nudix 16	PLC4	Nudix 13	Nudix 21	LPA1a	VIP2	5ptase13	Nudix 17	PLC3
Vegetative Rosette	13.51	122.08	47.35	62.9	52.66	32.46	10.35	47.7	229	23.98
1st Node	27.43	148.85	50.7	20.95	137.75	69.28	24.6	23.26	143.4	55.73
Cauline Leaf	12.01	50.41	19.15	11.81	193.1	8.88	10.25	31.61	581.63	41.95
Cotyledon	7.96	58.56	21.85	7.01	473.7	11.66	10.46	26.81	391.91	30.3
Root	22.2	257.83	127.41	118.08	866.08	57.65	30	22.56	417.76	49.83
Rosette post bolting	14.58	82.71	42.63	26.01	34.73	22.73	14.26	38.85	346.31	33.4
Flower Stage 9	7.34	165.26	71.69	76.91	38.76	80.65	32.83	41.41	70.73	29.68
Flower Stage 10/11	8.45	164.55	53.18	90.18	52.28	70.36	28.88	39	114.81	18.23
Flower Stage 12	12.26	164.05	74.85	67.39	127.53	57.3	44.06	46.79	123.48	22.53
Flower Stage 15	9.33	135.54	83.01	41.28	90.73	25.2	20.28	27.48	238.86	24.41
Flower Stage 12, Carpels	14.56	140.43	80.98	59.04	337.63	68.36	31.8	27.5	190.35	18.21
Flower Stage 12, Petals	16.38	71.03	83.96	56.48	376.25	34.48	22.38	21.89	272.61	15.55
Flower Stage 12, Sepals	7.34	49.8	41.15	64.96	422.15	19.66	8.81	18.8	291.95	20.68
Flower Stage 15, Carpels	8.79	136.23	108.05	56.85	184.4	42.76	23.78	27.48	237.5	22.1
Flower Stage 15, Petals	9.88	64.68	51.53	16.18	272.91	18.78	3.31	12.95	235.73	21.88
Flower Stage 15, Sepals	6.91	86.11	43.41	28.93	208.18	11.81	7.83	20.61	405.81	17.73
Flowers Stage 15, Pedicels	32.28	58.46	62.08	28.51	97.05	35.31	13.93	64.91	231.35	30
Flower Stage 12, Stamens	58.9	452.16	112.78	294.51	957.41	118.71	220.2	186.55	142.79	25.08
Flower Stage 15, Stamen	18.85	296.98	162.63	102.09	351.85	39.08	22.73	22.78	190.9	20.1
Mature Pollen	95.6	1917.43	1132.9	645.61	1785.18	272.95	165	281.85	700.18	63.81
Leaf 1 + 2	12.25	70.35	28.2	24.41	466.61	9.91	4.5	38.76	242.56	32.58
Leaf 7, Petiole	16.58	105.7	55.93	28.23	175.26	29.76	27.45	31.96	264.95	39.08
Leaf 7, Distal Half	18.81	83.73	19.76	14.8	214.61	20.66	8.35	50.31	387.73	27.3
Leaf 7, Proximal Half	13.56	67.55	25.06	17.31	202.61	20.16	11.14	54.16	372.55	32.06
Hypocotyl	12.16	193.38	98.15	80.6	208.38	49.2	31.96	23.26	320.93	57.28
Root	21.73	280.41	153.76	151.26	451.23	57.36	28.7	25.25	376.51	42.53
Rosette Leaf 2	14.66	101.98	25.64	7.58	146.96	8.74	3.91	29.96	375.91	49.79
Rosette Leaf 4	11.23	97.03	23.5	16.8	199.51	16.11	10.3	41.73	321.71	28.33
Rosette Leaf 6	14.71	76.36	33.78	17.73	266.33	16.51	11.9	52.5	374.75	39.15
Rosette Leaf 8	16	67.56	30.41	20.48	315.84	19.43	8.15	55.43	315.04	26.76
Rosette Leaf 10	13.15	73.71	36.18	26.36	336.33	18.84	12.5	70.45	325.84	33.68
Rosette Leaf 12	14.31	87.09	44.88	38.3	395.2	26.18	11.25	76.61	312.88	29.55
Senescing Leaf	8.65	78.95	13.61	3.7	141.08	14.53	10.03	27.03	641.85	50.01
Shoot Apex, Inflorescence	7.3	207.8	79.53	85.26	42.83	87.91	35.5	49.9	49.88	17.96
Shoot Apex, Transition	7.4	256.55	80.58	86.46	26.16	88.36	42.55	44.13	31.18	18.45
Shoot Apex, Vegetative	9.38	206.56	74.51	69.51	178.9	63.4	24.88	32.66	138.38	36.65
Stem, 2nd Internode	29.05	114.05	28.39	12.18	84.38	32.61	20.73	27.15	254.75	43.46
Seeds Stage 3 w/ Siliques	17.91	153.53	114.7	50.9	85.86	45.35	18.03	29.7	138.78	24.61
Seeds Stage 4 w/ Siliques	12.44	109.71	45.4	16.33	195.9	45.7	31.88	20.2	163.48	17.84
Seeds Stage 5 w/ Siliques	7.73	97.8	34.25	20.21	66.8	50.81	29.43	18.01	85.66	17.58
Seeds Stage 6 w/o Siliques	2.98	125.3	28.58	36.58	77.7	65.56	42.4	14.5	32.46	20.9
Seeds Stage 7 w/o Siliques	4	119.13	34.11	45.08	62.13	55.45	34	13.48	43.53	26.28
Seeds Stage 8 w/o Siliques	12.56	64.93	14.68	102.51	352.61	21.68	17.25	10.86	39.65	28.15
Seeds Stage 9 w/o Siliques	13.03	57.43	25.33	94.83	173.01	9.78	19.55	5.68	40.83	29.91
Seeds Stage 10 w/o Siliques	14.16	44.26	22.75	78.16	229.1	6.63	12	17.41	44.38	36.08
Dry seed	4.1	37.52	12.85	200.26	112.55	14.73	17.62	4.41	5.51	9.89
Imbibed seed, 24 h	1.44	210.38	33.53	43.05	30.72	22.92	30.91	9.77	54.68	10.1

Figure 4.4. Group 1 Expression Table

Table of expression values from eFP Browser for all genes included in Group 1. Each column contains data for one gene. Within each column, yellow indicates low expression, red indicates higher expression. Rows contain data from different plant tissues/stages. The relative expression values for each data point are included.

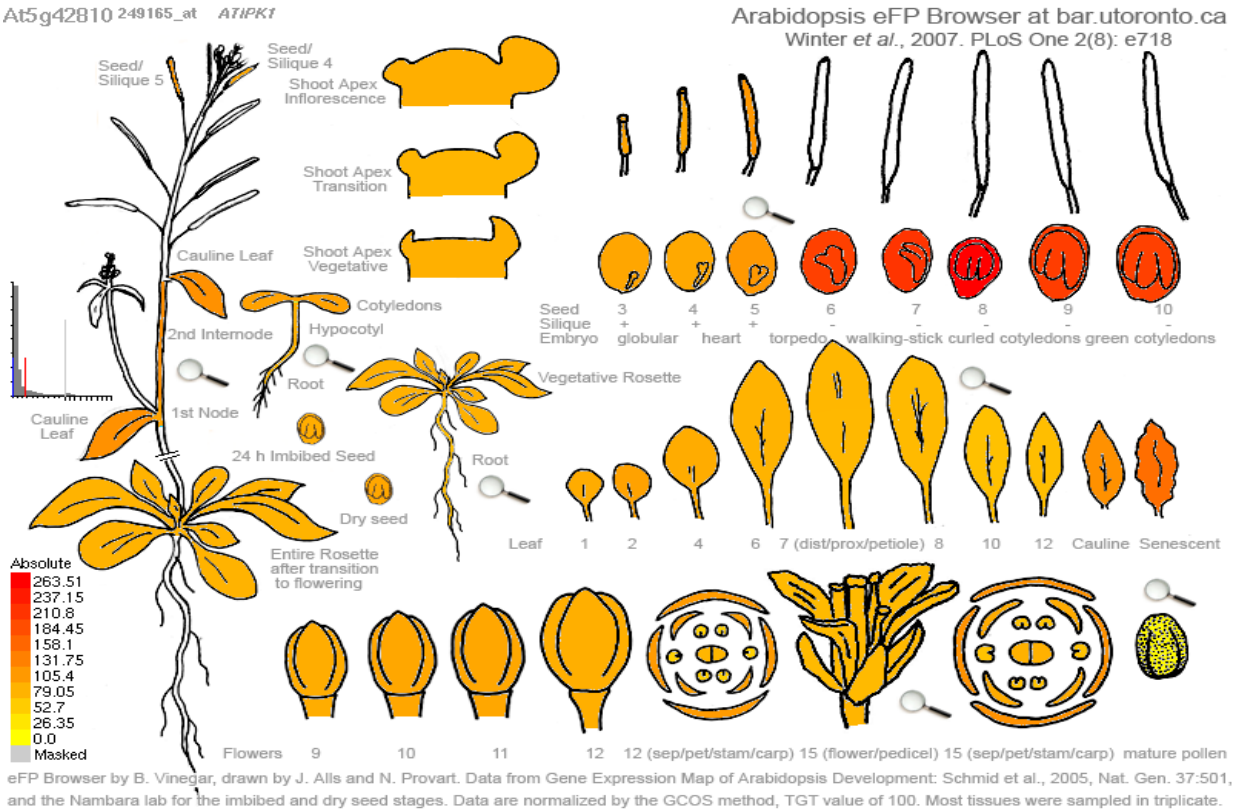

Figure 4.5. Representative Image of Group 2 Expression Pattern

Representative image of Group 2 gene expression profile from eFP Browser (http://bar.utoronto.ca/efp/cgi-bin/efpWeb.cgi). Gene expression levels are indicated by color, with low expression in yellow and highest expression levels indicated by red. Group 2 genes have high expression in developing seeds. Shown is expression of IPK1 (At5g2810).

	Group 2											
Tissue	**ITPK3**	**LPA1b**	**MIPS2**	**IPK2α**	**SIW14**	**IPK1**	**MRP5**	**MIPS1**	**MIK**	**IPK2β**	**MINPP**	**ITPK1**
Vegetative Rosette	91.45	1.18	191.16	220.3	8.11	81.63	97.43	365.55	35.26	40.11	122.08	225.86
1st Node	100.5	0.63	630.61	217.6	28.15	94.5	308.78	890.5	91.21	103.1	115.21	253.91
Cauline Leaf	50.68	1.9	188.93	280.2	30.16	114.2	123.88	1063.9	102.6	102.8	92.53	257.76
Cotyledon	59.75	1.71	68.48	330.1	68.58	97.01	85.05	468.23	78.61	66.36	85.63	184.16
Root	54.53	86.36	53.33	161.6	39.3	67.11	197.31	257.34	121.5	55.1	187.88	278.01
Rosette post bolting	61.01	2.6	106.48	261.8	22.83	79.55	96.01	743.86	66.96	64.96	96.46	194.2
Flower Stage 9	93.88	43.88	499.28	135.4	12.75	84.9	261.16	342.93	56.51	83.13	158.08	294.43
Flower Stage 10/11	94.45	40.98	667.3	150.7	17.31	91.34	274.7	432.61	55.9	73.46	140.75	253.6
Flower Stage 12	96.11	37.78	361.86	160.3	26.5	83.13	222.26	488.6	72.5	72	162.05	249.44
Flower Stage 15	82.55	15.3	254.53	224.8	45.7	72.21	190.15	356.61	129.5	93.9	126.2	232.61
Flower Stage 12, Carpels	124.5	27.73	303.09	140.9	5.51	75.63	216.23	461.95	64.41	94.18	168.23	219.05
Flower Stage 12, Petals	152	47.26	258.61	195.3	10.33	97.18	233.33	896.33	52.93	97.13	177.58	210.56
Flower Stage 12, Sepals	72.5	8.83	197.28	238.8	21.03	104	217.98	631.58	128.5	70.64	120.01	211.61
Flower Stage 15, Carpels	101.7	26.96	608.35	159	10.43	81.01	215.35	653.75	66.23	89.66	142.29	214.76
Flower Stage 15, Petals	134.2	3.6	82.38	365.6	86.63	86.35	214.89	289.78	185.7	126.4	119.25	360.31
Flower Stage 15, Sepals	63.23	2.85	51.98	292.5	142.18	113.2	230.9	309.38	319.1	98.61	123.76	318.33
Flowers Stage 15, Pedicels	95.5	4.61	133.98	194.8	13.5	76.81	160.46	1014.3	58.45	37.19	134.68	188.4
Flower Stage 12, Stamens	208.7	135.85	146.13	179.5	67.33	47.76	223.95	590.63	268.5	73.83	195.98	353.15
Flower Stage 15, Stamen	109.2	20.31	68.95	190.7	41.25	62.58	186.68	203.88	302.6	90.4	89.18	281.93
Mature Pollen	155.1	141.2	196.36	68.88	12.13	5.43	81.28	186.03	540.6	54.76	88.03	559.61
Leaf 1 + 2	61.48	4.98	60.15	292.7	24.3	86.21	74.11	608.75	35.26	34.2	88.45	184.46
Leaf 7, Petiole	142.6	0.96	55.96	247.8	20.23	71.9	99.95	350.25	64.2	83.11	106.31	166.66
Leaf 7, Distal Half	90.18	0.8	50.21	388.9	65.33	75.26	70.71	673.85	75.03	70.55	87.91	192.58
Leaf 7, Proximal Half	80.56	1.09	50.8	335.9	50	74	72.14	712.65	55.46	73.35	86.45	188.41
Hypocotyl	72.28	3.53	254.43	235.9	43.81	79.7	165.48	142.88	124.6	128.8	126.1	231.4
Root	61.06	173.68	65.58	185.8	42.15	71.91	212.71	236	118.3	65.64	191.28	302.03
Rosette Leaf 2	70.11	0.88	67.66	374.9	77.56	96.71	79.41	550.3	84.03	65.83	79.58	212.93
Rosette Leaf 4	72.88	0.9	50.25	383.2	64.45	86.26	64.05	639.83	72.26	80	93.95	193.18
Rosette Leaf 6	71.08	0.86	46.85	392.3	59.7	79.31	72.03	722.36	76.1	71.86	95.73	170.8
Rosette Leaf 8	67.56	0.73	33.68	340.4	45.5	71.88	67.89	650.56	53.16	62.43	84.23	198.08
Rosette Leaf 10	66.98	1.9	42.98	345.1	39.98	64.85	75.45	531.51	57.91	45.61	95.18	183.98
Rosette Leaf 12	60.15	2.45	47.48	267.9	20.28	67.36	88.46	362.06	42.83	38.31	101.03	190.33
Senescing Leaf	44.43	1.41	130.71	188.8	68.3	150.6	152.6	906.83	123	92.38	118.85	310.25
Shoot Apex, Inflorescence	107.3	41.3	316.18	169.8	13.7	83.31	246.93	271.75	62.51	91.56	161.06	328.48
Shoot Apex, Transition	94.98	20.96	215.15	200.7	11.83	75.85	222.9	145.08	83.6	108.2	155.2	314.3
Shoot Apex, Vegetative	82.71	3.71	90.96	183.6	16.95	82.36	154.53	222.65	76.03	86	151.28	308.81
Stem, 2nd Internode	65.13	1.31	350.71	237.1	12.68	115.9	134.33	617.81	94.48	76.76	113.03	186.81
Seeds Stage 3 w/ Siliques	76.63	11.76	728.98	146.9	16.01	92.03	183.85	752.78	92.28	86.96	171.25	253.19
Seeds Stage 4 w/ Siliques	68.01	49.4	284.75	145.4	52.48	89.58	256.11	1132.4	184.5	79.88	180.41	301.31
Seeds Stage 5 w/ Siliques	78.73	81.55	299	147	69.46	107.2	364.9	1376.1	266.6	71.73	189.2	313.01
Seeds Stage 6 w/o Siliques	97.65	301.38	445.68	146	92.03	197.7	804.5	2052.9	557.9	97.8	254.98	445.45
Seeds Stage 7 w/o Siliques	133	469.36	565.16	183.3	115.96	210.1	887.41	2345	660.9	84.9	199.03	534.66
Seeds Stage 8 w/o Siliques	218.2	2019.4	1452.2	238.3	90.55	263.5	1012.5	1177.8	522	65.23	100.98	653.51
Seeds Stage 9 w/o Siliques	294	2222.4	2675.3	303.1	118.31	201.2	1031.8	1523.8	457.1	73.56	105.86	840.13
Seeds Stage 10 w/o Siliques	277.7	2411.2	2340.9	295	109.23	198	960.56	1040.4	351.2	82.05	95.75	611.94
Dry seed	303.9	1979.4	2476.1	299.6	20.41	91.85	331.55	501.58	93.08	135	133.03	1121.9
Imbibed seed, 24 h	53.92	87.66	19.82	286.4	51.3	85.51	155.73	62.66	88.98	120.7	206.45	432.64

Figure 4.6. Group 2 Expression Table

Table of expression values from eFP Browser for all genes included in Group 2. Each column contains data for one gene. Within each column, yellow indicates low expression, red indicates higher expression. Rows contain data from different plant tissues/stages. The relative expression values for each data point are included.

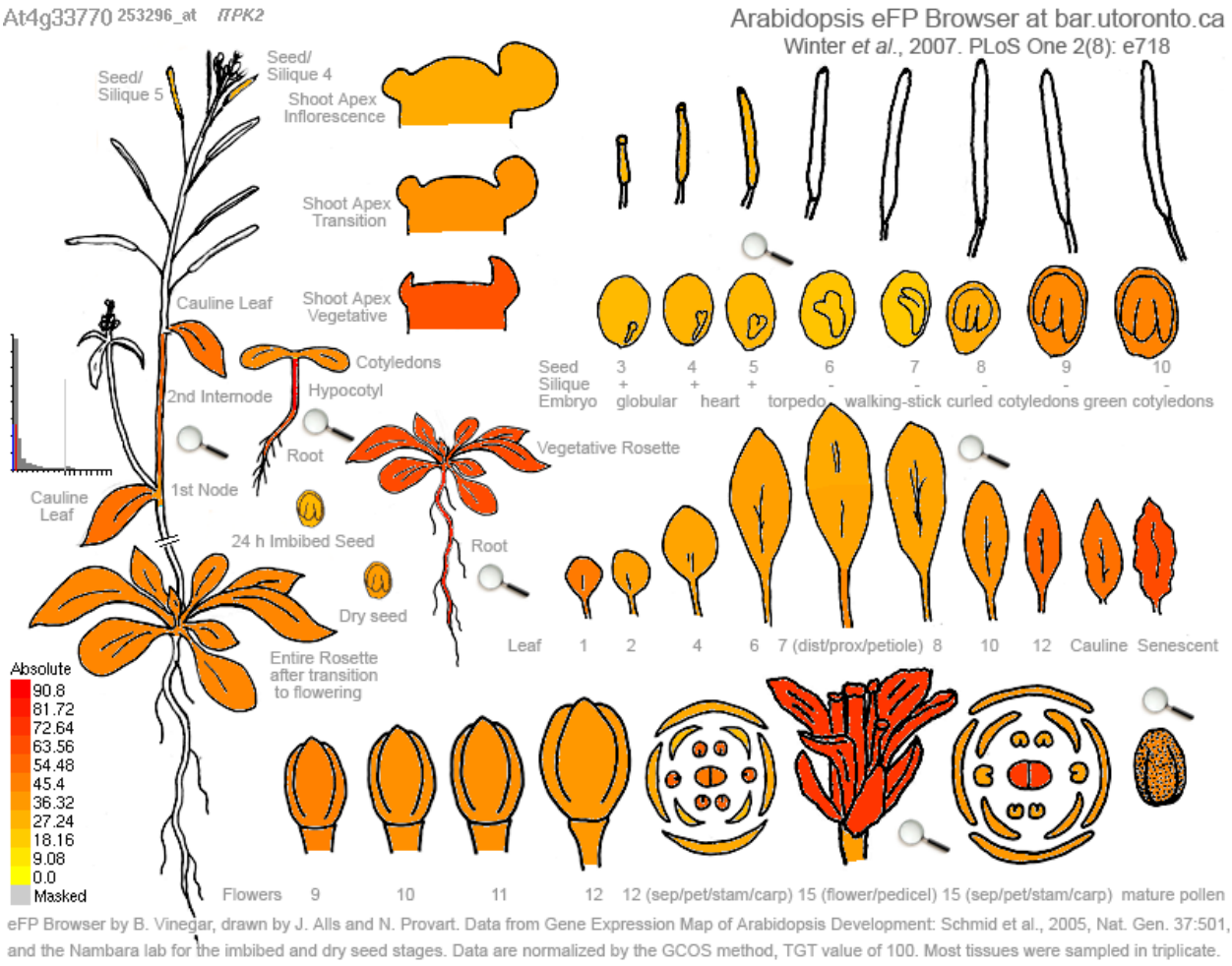

Figure 4.7. Representative Image of Group 3 Expression Profile

Representative image of Group 3 gene expression profile from eFP Browser (http://bar.utoronto.ca/efp/cgi-bin/efpWeb.cgi). Gene expression levels are indicated by color, with low expression in yellow and highest expression levels indicated by red. Group 3 genes are ubiquitously expressed at moderate levels. Shown is expression of ITPK2 (At4g33770).

	Group 3							
Tissue	ITPK4	VIP1	ITPK2	PLC2	PLC9	PLC8	PLC1	Nudix 12
Vegetative Rosette	50.01	271.1	64.78	425.8	126.5	126.5	100.6	11.23
1st Node	64.61	203	37.43	495	79.86	79.86	78.15	37.21
Cauline Leaf	76.56	301.2	51.03	418.7	101.1	101.1	161.7	76.76
Cotyledon	70.61	244.9	40.81	376.5	109.3	109.3	181.2	109.11
Root	76.85	244.8	79.8	284.2	152	152	110.6	30.45
Rosette post bolting	65.14	224	43.41	453.9	106.7	106.7	216.3	57.86
Flower Stage 9	97.36	151	45	297.1	80.68	80.68	16.26	52.04
Flower Stage 10/11	73.74	139.5	39.68	356.1	99.11	99.11	16.45	89.8
Flower Stage 12	83.16	195.9	37	297.2	103.6	103.6	24.95	101.1
Flower Stage 15	84.38	251.2	72.14	420.4	106.9	106.9	38.76	106.84
Flower Stage 12, Carpels	102.4	180.8	47.98	314.5	98.83	98.83	24.58	202.16
Flower Stage 12, Petals	102.7	265.9	23.39	378.7	102.2	102.2	12.33	11.53
Flower Stage 12, Sepals	85.93	346.7	30.45	372	85.73	85.73	24.43	97.4
Flower Stage 15, Carpels	89.43	235.2	70.21	357.5	97.3	97.3	16.15	126.31
Flower Stage 15, Petals	98.83	352.4	36.61	883.1	113.4	113.4	8.71	72.64
Flower Stage 15, Sepals	102.6	226.4	36.8	269.1	90.76	90.76	43.58	112.23
Flowers Stage 15, Pedicels	68.41	230.9	34.8	486.1	120.4	120.4	29.16	32.4
Flower Stage 12, Stamens	90.23	313.1	56.26	134.8	77.09	77.09	55.53	115.46
Flower Stage 15, Stamen	67.2	398.8	32.35	590	163.3	163.3	98.08	58.1
Mature Pollen	54.68	24.48	43.35	199.9	83.2	83.2	16.7	142.13
Leaf 1 + 2	58.35	186.7	47.7	307.2	105.4	105.4	101.3	51.86
Leaf 7, Petiole	53.83	227.4	42.41	486.7	84.48	84.48	247.2	41.16
Leaf 7, Distal Half	54.83	221.6	30.55	386.6	103.1	103.1	453.7	119.66
Leaf 7, Proximal Half	52.7	244	32.65	390	108.9	108.9	352.7	102.68
Hypocotyl	76.61	132.1	90.8	370.1	72.86	72.86	76.19	36.55
Root	84.8	182.2	61.91	265.6	103.1	103.1	120.1	29.46
Rosette Leaf 2	69.98	258.6	34.43	445.5	104.1	104.1	400.1	116.63
Rosette Leaf 4	58.16	247.8	32.71	462.9	73.75	73.75	451.5	91.2
Rosette Leaf 6	69.11	191	34.45	384	96.61	96.61	433.3	81.85
Rosette Leaf 8	58.8	188.5	32.28	350.8	97.48	97.48	348.3	78.81
Rosette Leaf 10	64.39	206.5	39.15	381.2	103.9	103.9	276.1	41.03
Rosette Leaf 12	61.36	230.8	54.46	363.8	105.7	105.7	144.4	30
Senescing Leaf	94.23	415.6	64.1	401.4	76.38	76.38	95.71	42.73
Shoot Apex, Inflorescence	91.1	165.2	30.16	295.3	90.8	90.8	39.36	54.96
Shoot Apex, Transition	103	187.1	38.91	356.9	104.2	104.2	30.1	32.75
Shoot Apex, Vegetative	93.4	163.7	61.9	361.5	114.6	114.6	24.83	9.6
Stem, 2nd Internode	64.86	282.5	55.13	813.8	96.53	96.53	45.66	18.75
Seeds Stage 3 w/ Siliques	56.71	100.7	24.9	293.4	102.6	102.6	26.76	76.56
Seeds Stage 4 w/ Siliques	76.64	149.9	26.76	513.2	57.73	57.73	15.23	28.5
Seeds Stage 5 w/ Siliques	82.81	131.2	25.28	462.2	48.65	48.65	24.51	11
Seeds Stage 6 w/o Siliques	91.8	63.38	21.03	238.7	42.83	42.83	15.8	9.2
Seeds Stage 7 w/o Siliques	84.41	72.06	19.51	301.9	44.21	44.21	19.64	8.83
Seeds Stage 8 w/o Siliques	67.01	112.4	30.2	268.3	18.18	18.18	25.45	11.66
Seeds Stage 9 w/o Siliques	63.38	159.2	42.66	287.8	20.3	20.3	31.45	6.83
Seeds Stage 10 w/o Siliques	80.93	110.1	44.8	292.3	11.28	11.28	25.48	8.7
Dry seed	99.56	359.5	35.22	460.1	13.64	13.64	9.8	3.22
Imbibed seed, 24 h	143.5	147.7	25	214.7	88.8	88.8	6.02	56.3

Figure 4.8. Group 3 Expression Table

Table of expression values from eFP Browser for all genes included in Group 3. Each column contains data for one gene. Within each column, yellow indicates low expression, red indicates higher expression. Rows contain data from different plant tissues/stages. The relative expression values for each data point are included.

Subcellular Localization

While the subcellular localization of PPx-InsPs has not been determined to date, the localization of the kinases and phosphatases responsible for PPx-InsP synthesis and degradation may help us to understand where PPx-InsPs are acting. To investigate the subcellular location of the kinases and phosphatases in the InsP signaling pathway, we generated C-terminal GFP-tagged constructs for each gene, with the exception of the N-terminal GFP tagged VIP2PD construct. C-terminal GFP-tagged construct were used to prevent the tag from obscuring native localization signals. We then transiently expressed each construct in *N. benthamiana* leaves. To ensure the patterns observed were not due to overexpression and off-target accumulation, we used confocal microscopy to image cells at 12, 36, 24, 48 and 72 hours after infiltration. GFP fluorescence is not detectable at 12 hours post infiltration under our conditions, and at the 72 hour time point signal from many of the GFP constructs is beginning to decrease (**Figures 4.26-4.39).** We found each construct was expressed and stably accumulated as measured by protein blotting (**Figure 4.25).** To further investigate the subcellular localization, we co-expressed constructs with an Endoplasmic Reticulum (ER) mCherry organelle marker (*27*) or collected chlorophyll emission spectra. The 48 hour time point was used for co-localization studies to optimize the expression of the gene-GFP protein and the mCherry ER marker. **Table 4.3** includes genes used in this analysis, protein size and known localizations. The 48 hour time point was observed in three separate experiments to confirm reproducibility of pattern. Infiltrated *N. benthamiana* leaves were imaged using confocal microscopy and the same range of settings used to image transient GFP fusion and mCherry proteins to determine autofluorescence (see **Figure 4.24)** Notably,

chloroplast autofluorescence is possible under settings for GFP imaging at higher laser strengths used to image GFP fusion proteins with low expression levels.

IPK1/IPK2

IPK1 and IPK2 are required for the lipid-depended pathway synthesis of $InsP_5$ and $InsP_6$. IPK1- and IPK2-GFP fusion proteins were observed in the nucleus and ER when transiently expressed in *N. benthamiana* leaf epidermis (**Figure 4.9-4.11)**. We localized IPK2α-GFP and IPK2β-GFP and IPK1-GFP to the nucleus and found all three protein were excluded from the nucleolus (**Figures 4.9A, 4.10A, 4.11A**). These IPK2α-GFP and IPK2β-GFP and IPK1-GFP fusion proteins were co-expressed with the ER mCherry marker protein and co-localization was observed in both the ER cisternae surrounding the nucleus as well as the reticulate cortical ER (*28*) (**Figure 4.9B-D, 4.10B-D, 4.11B-D**). The pattern of nuclear and ER localization is consistent over a time course of 24-72 hours post infiltration (**Figure 4.26**). These data suggest $InsP_6$ synthesis occurs in the nucleus, consistent with the known nuclear roles of $InsP_5$ and $InsP_6$ in binding to plant hormone receptors (*29, 30*) and the role of $InsP_6$ in mRNA export in yeast (*31*). Previous work has identified nuclear IPK2β-GFP in protoplasts and native nuclear IPK2β in leaf guard and mesophyll cells (*32*). Thus, our data reported here identify the ER as a second potential site for $InsP_6$ production.

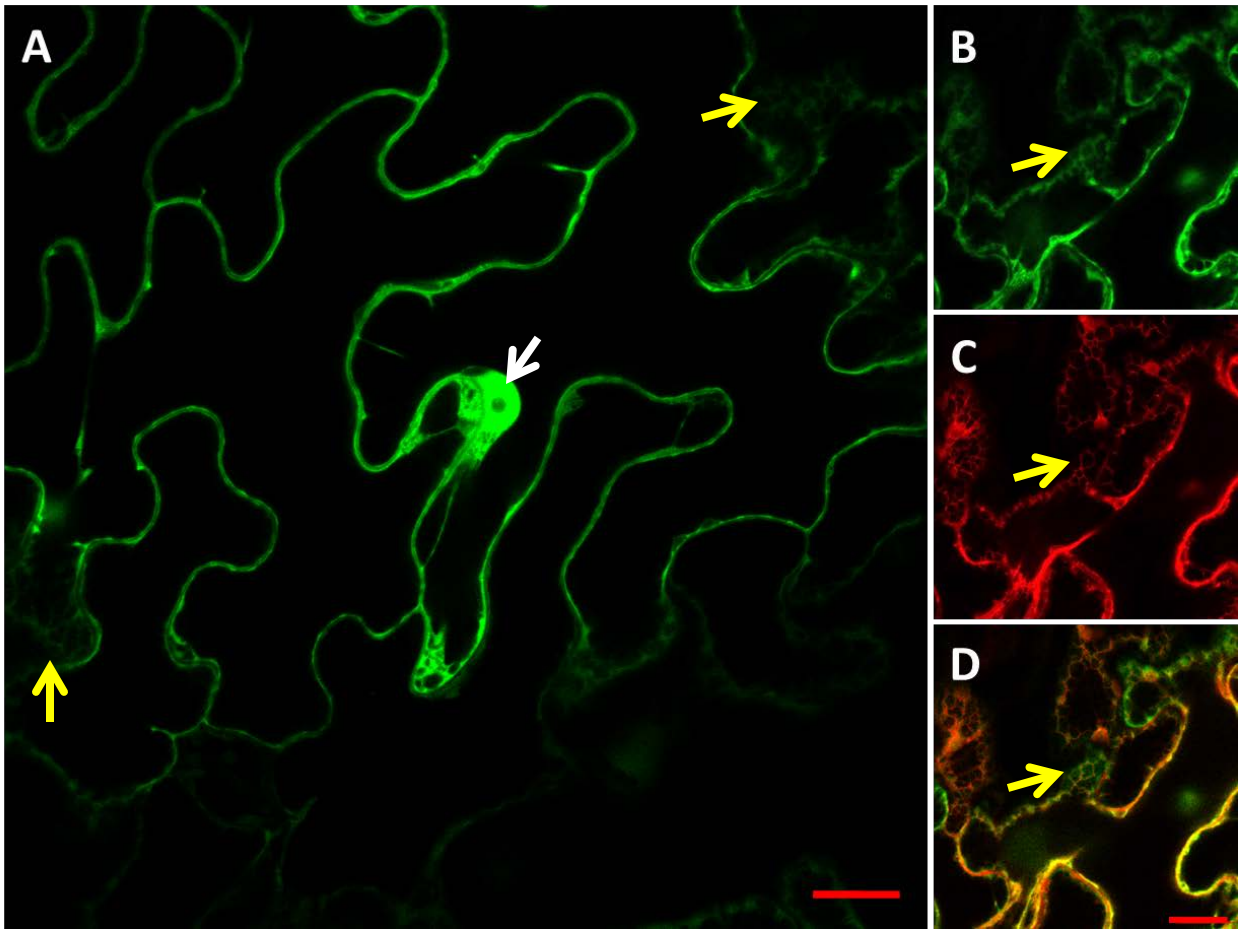

Figure 4.9. Subcellular Localization of IPK1-GFP

IPK1-GFP fusion protein was transiently co-expressed with mCherry ER marker protein in *N. benthamiana* epidermal cells. Data shown are from 48 hours post infiltration. (A) IPK1-GFP fluorescence is detected in the nucleus (white arrow) and ER (yellow arrow). (B-D) Higher magnification of cortical ER, (B) IPK1-GFP (C) mCherry ER marker (D) B and C merged image, yellow indicates co-localization. Scale bar = 20 µm.

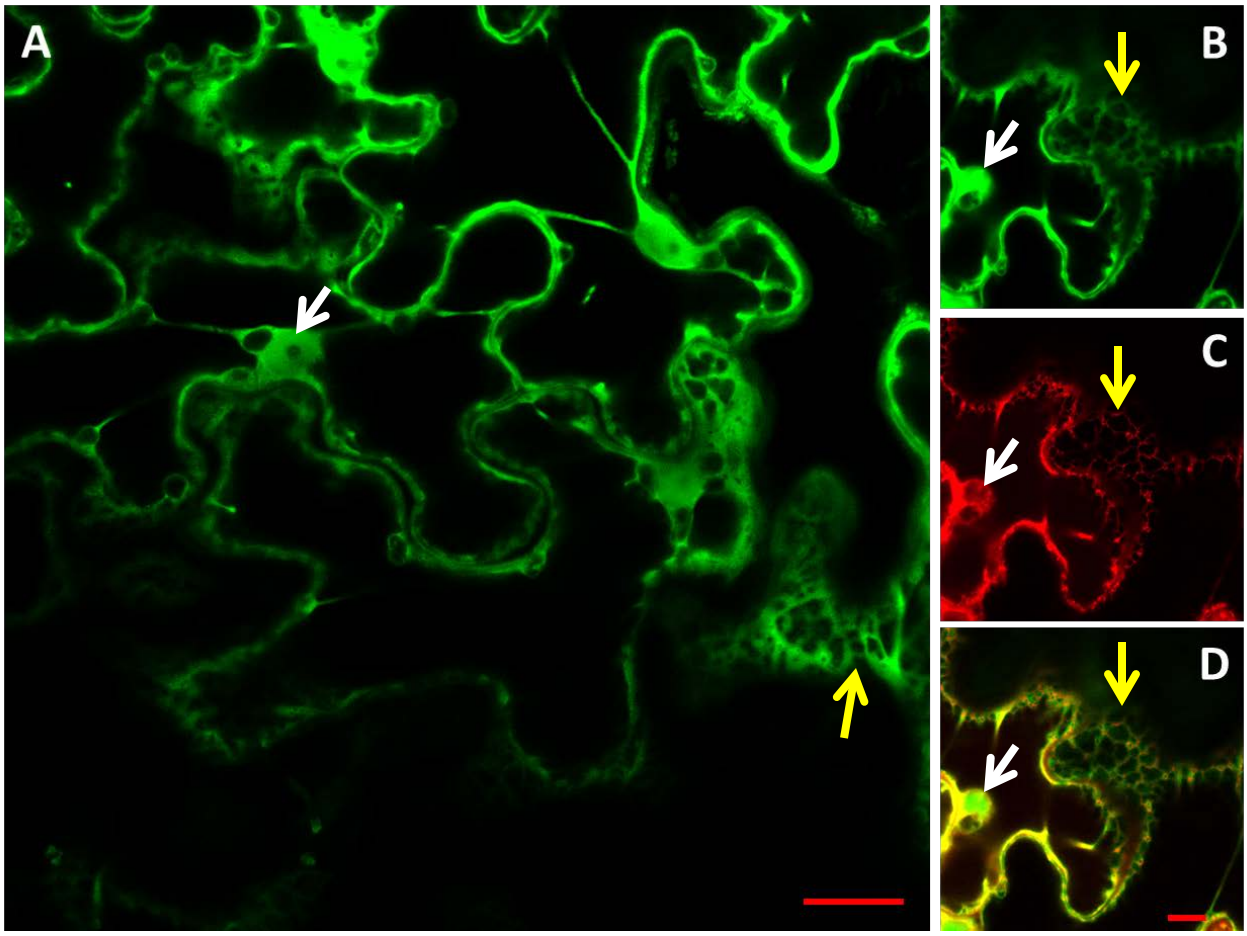

Figure 4.10. Subcellular Localization of IPK2α-GFP

IPK2α-GFP fusion protein was transiently co-expressed with mCherry ER marker protein in *N. benthamiana* epidermal cells. Data shown are from 48 hours post infiltration. (A) IPK2α-GFP fluorescence is detected in the nucleus (white arrow) and ER (yellow arrow).. (B-D) Higher magnification of cortical ER, (B) IPK2α-GFP (C) mCherry ER marker Note: ER outlines the nucleus (D) B and C merged image, yellow indicates co-localization. Scale bar = 20 µm.

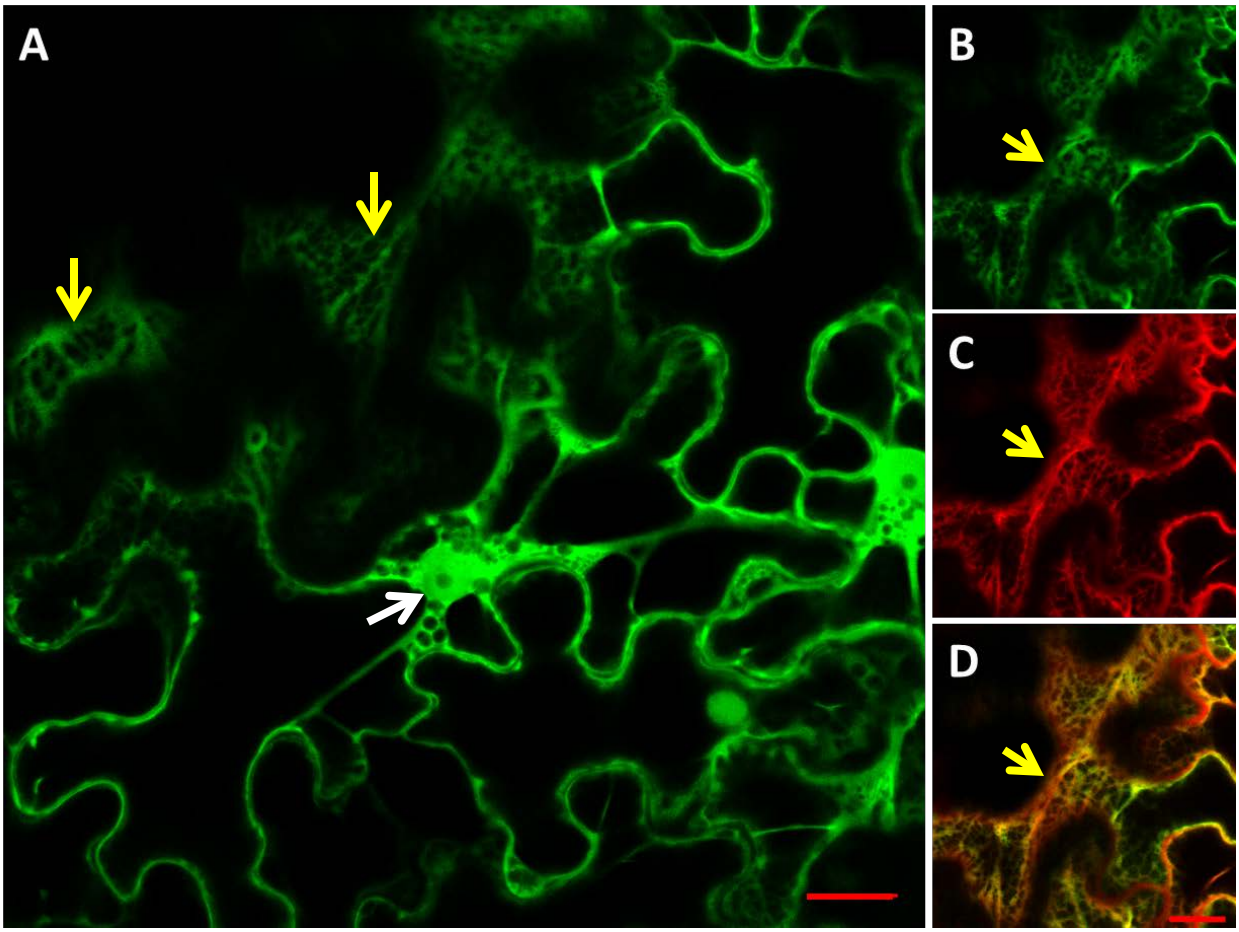

Figure 4.11. Subcellular Localization of IPK2β-GFP

IPK2β-GFP fusion protein was transiently co-expressed with mCherry ER marker protein in *N. benthamiana* epidermal cells. Data shown are from 48 hours post infiltration. (A) IPK2β-GFP fluorescence is detected in the nucleus (white arrow) and ER (yellow arrow). Note: the ER surrounds the nucleus and adjacent chloroplasts, seen as spherical voids in the GFP signal. (B-D) Higher magnification of cortical ER, (B) IPK2β-GFP (C) mCherry ER marker (D) B and C merged image, yellow indicates co-localization. Scale bar = 20 µm.

MINPP

MINPP is an $InsP_6$ phosphatase (phytase). MINPP-GFP fusion protein was found to populate the ER in transformed *N. benthamiana* leaves. MINPP-GFP and mCherry ER marker signals co-localize, though overall expression levels were relatively low (**Figure 4.12**). Only the ER cisternae surrounding the nucleus and signal at the plasma membrane is apparent in epidermal cells expressing MINPP-GFP, however due to the low expression, MINPP-GFP in the cortical ER may simply be below the levels of detection. The pattern was consistent over a time course from 12 to 72 hours (**Figure 4.25**). This is consistent with the ER localization of MINPP in mammals, birds and fruit flies, where each contains a KDEL ER retention signal at the C-Terminus (*33*). Arabidopsis has a corresponding DTEL at C-terminus. It has been suggested that this localization to the ER is indicative of a specialized role in $InsP_6$ signaling versus generalized $InsP_6$ catabolism (*33*).

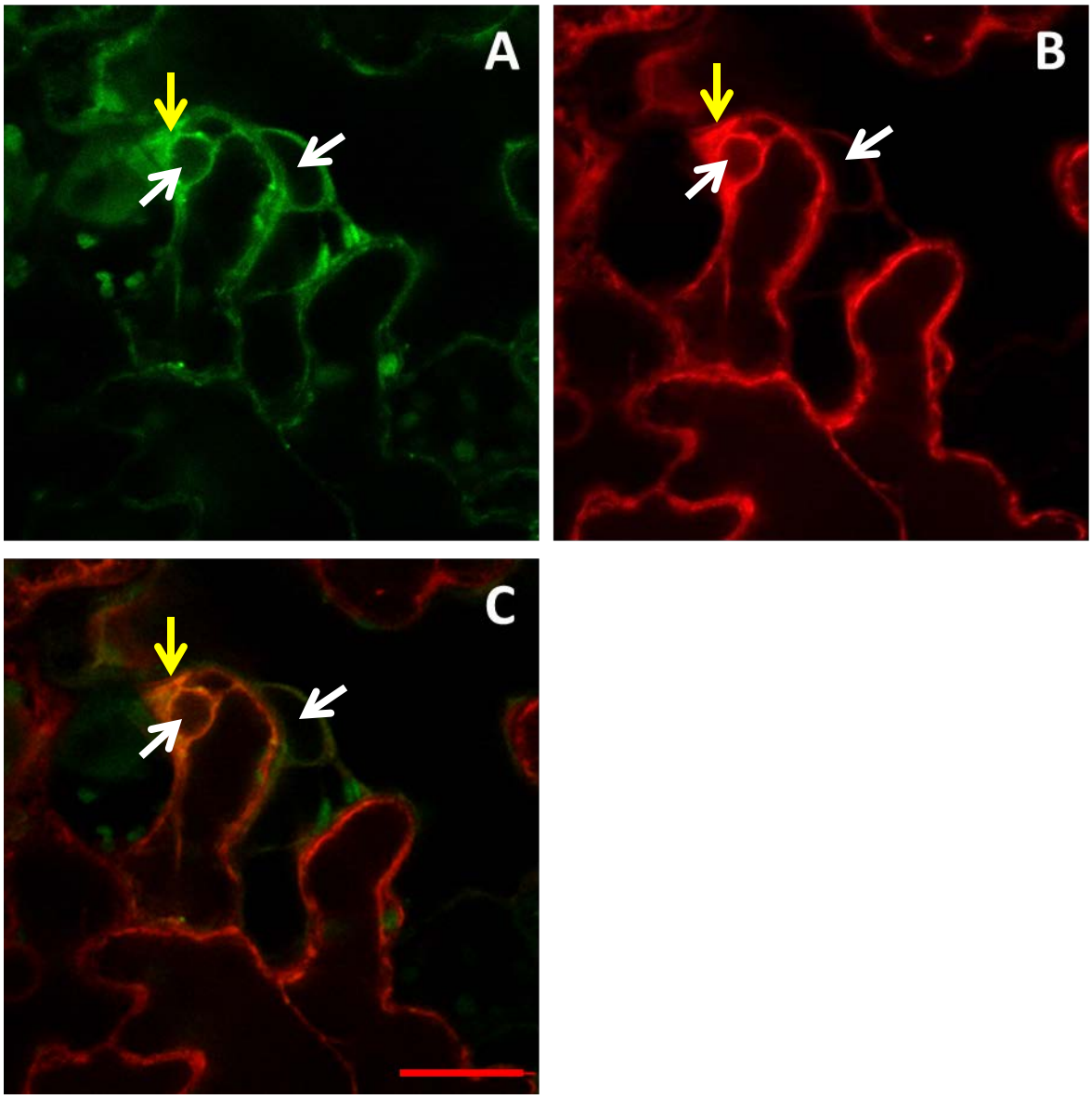

Figure 4.12. Subcellular Localization of MINPP-GFP

MINPP-GFP fusion protein was transiently co-expressed with mCherry ER marker protein in *N. benthamiana* epidermal cells. Data shown are from 48 hours post infiltration. Protein expression level is low for this construct. (A) MINPP-GFP fluorescence is detected in the ER (yellow arrow). Note: The ER surrounds the nucleus (white arrow), and green spheres are autofluorescence from chloroplasts. (B) mCherry ER marker (C) A and B merged image, yellow indicates co-localization. Scale bar = 20 µm.

VIP

VIP2 is a kinase that can synthesis PPx-InsP from an $InsP_6$ precursor (*5*). VIP2FL-GFP fusion protein was co-expressed with the mCherry ER marker in *N. benthamiana* leaves. While VIP2FL-GFP signal is low, it co-localizes with mCherry in the ER cisterna surrounding the nucleus and it is notably absent from the nucleus itself (**Figure 4.13**). When the N-terminal 361 amino acids containing the VIP2 Kinase Domain (KD) were fused to GFP (VIP2KD-GFP) we noted differences in localization from that of the full length VIP2FL-GFP. VIP2KD-GFP localizes to the nucleus (**Figure 4.14**). Co-expression with the mCherry ER does not result in co-localization indicating that VIP2KD-GFP is not in the ER (**Figure 4.14B-D**). The more diffuse pattern is consistent with cytoplasmic localization. This nuclear and cytoplasmic pattern of localization was also found when VIP1KD-GFP (first 284 amino acids) was transiently expressed in *N. benthamiana* (**Figure 4.15**). Non-authentic nuclear localization is possible with small proteins (<60 kDa) and high cytoplasmic expression (*34*). We feel that passive diffusion of the 63 kDa VIP2KD-GFP and the 59kDa VIP1KD-GFP proteins into the nucleus is not likely, as the nuclear signal for each of these constructs appears early in the time course (**Figure 4.27**). Given the unexpected difference in localization between VIP2FL-GFP and VIP2KD-GFP, we generated a GFP-VIP2PD expression construct consisting of the last 1739 amino acids from VIP2 which contains the phosphatase domain (PD) fused to GFP. In transient expression assays in *N. benthamiana*, GFP-VIP2PD has a reticulate pattern consistent with ER and co-localizes with the mCherry ER marker protein (**Figure 4.16)**. Time courses for the expression of VIP2FL-GFP, VIP2KD-GFP, and GFP-VIP2PD indicate that these expression patterns are consistent 24-72 hours post infiltration (**Figure 4.27**)

Recent work with human homologue of VIP, PPIP5K2, has revealed that it contains a cryptic nuclear localization signal (NLS) in the phosphatase domain (PD)(*35*). This NLS consists of 5 R residues and while the location and specific sequence is not conserved in AtVIPs, it is possible that another highly acidic portion of AtVIP2 could be responsible for the nuclear localization that we see in these transient expression assays. The ER localization of AtVIP2FL-GFP is surprising as the human homologue PPIP5K is a cytosolic and plasma membrane associated protein. The normally cytosolic PPIP5K will translocate to the plasma membrane upon activation of the PLC signaling pathway by a Pleckstrin Homology (PH) domain that binds PtdInsPs (*36*). Analysis the C-terminus of AtVIP1 and AtVIP2 does not predict ER localization using the Prediction tool pSORT II (*37*). In addition, neither AtVIP1 nor AtVIP2 contain the canonical KDEL ER retention sequence. Further analysis is needed to determine the mechanism of ER localization of these proteins. Potentially the putative PH domain in AtVIP2 could bind phospholipids in the ER (*5*). The data presented here suggests that VIP2 is located in two compartments: the ER and the nucleus, and thus both of these compartments are predicted to contain PPx-InsPs.

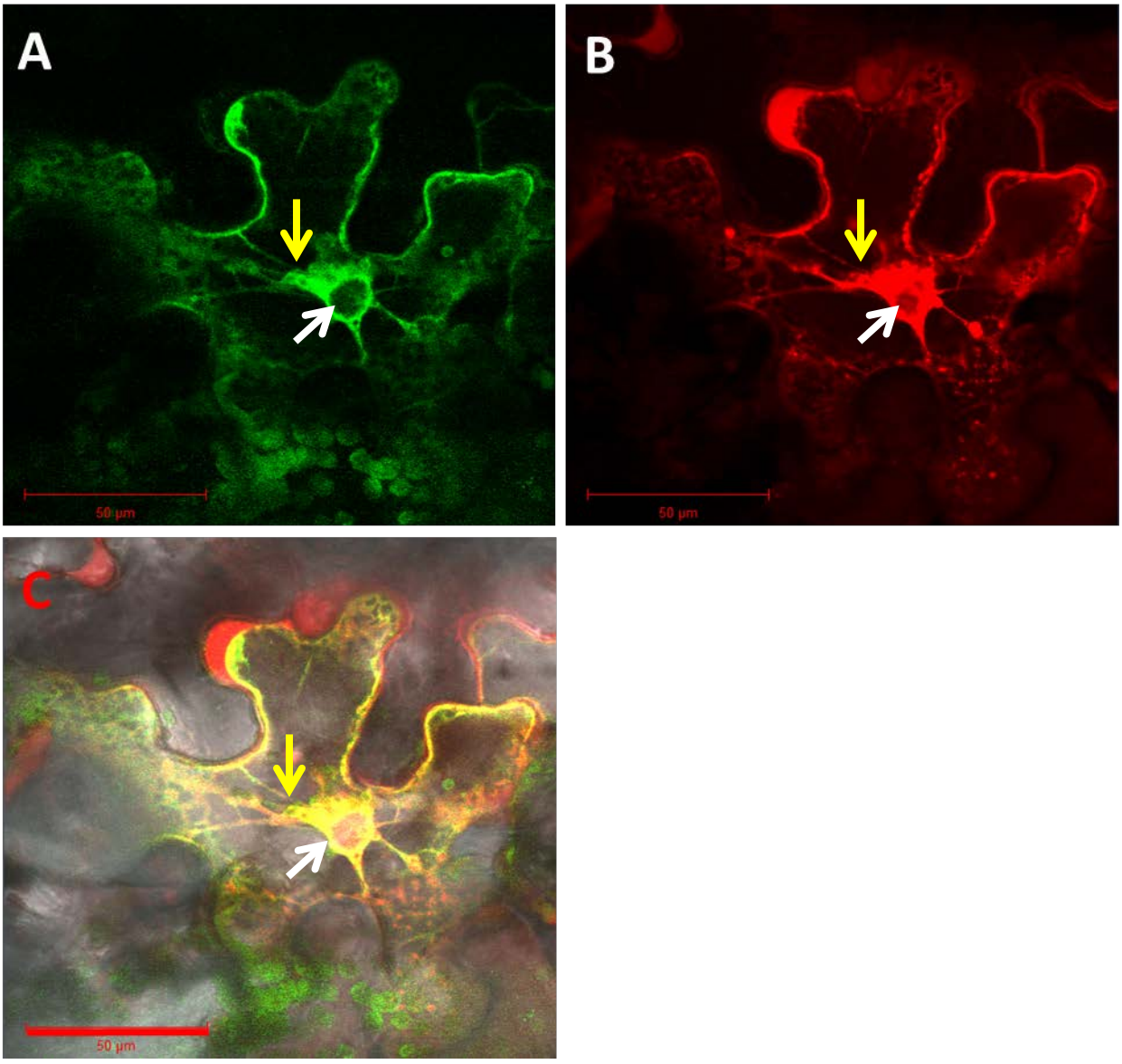

Figure 4.13. Subcellular Localization of VIP2FL-GFP

VIP2FL-GFP fusion protein was transiently co-expressed with mCherry ER marker protein in *N. benthamiana* epidermal cells. Data shown are from 48 hours post infiltration. (A) VIP2FL-GFP fluorescence is detected in the ER cisterna (yellow arrow). Note: no signal in the nucleus (white arrow) (B) mCherry ER marker (D) A and B florescence images merged with the bright field image, yellow indicates co-localization. Scale bar = 50 µm.

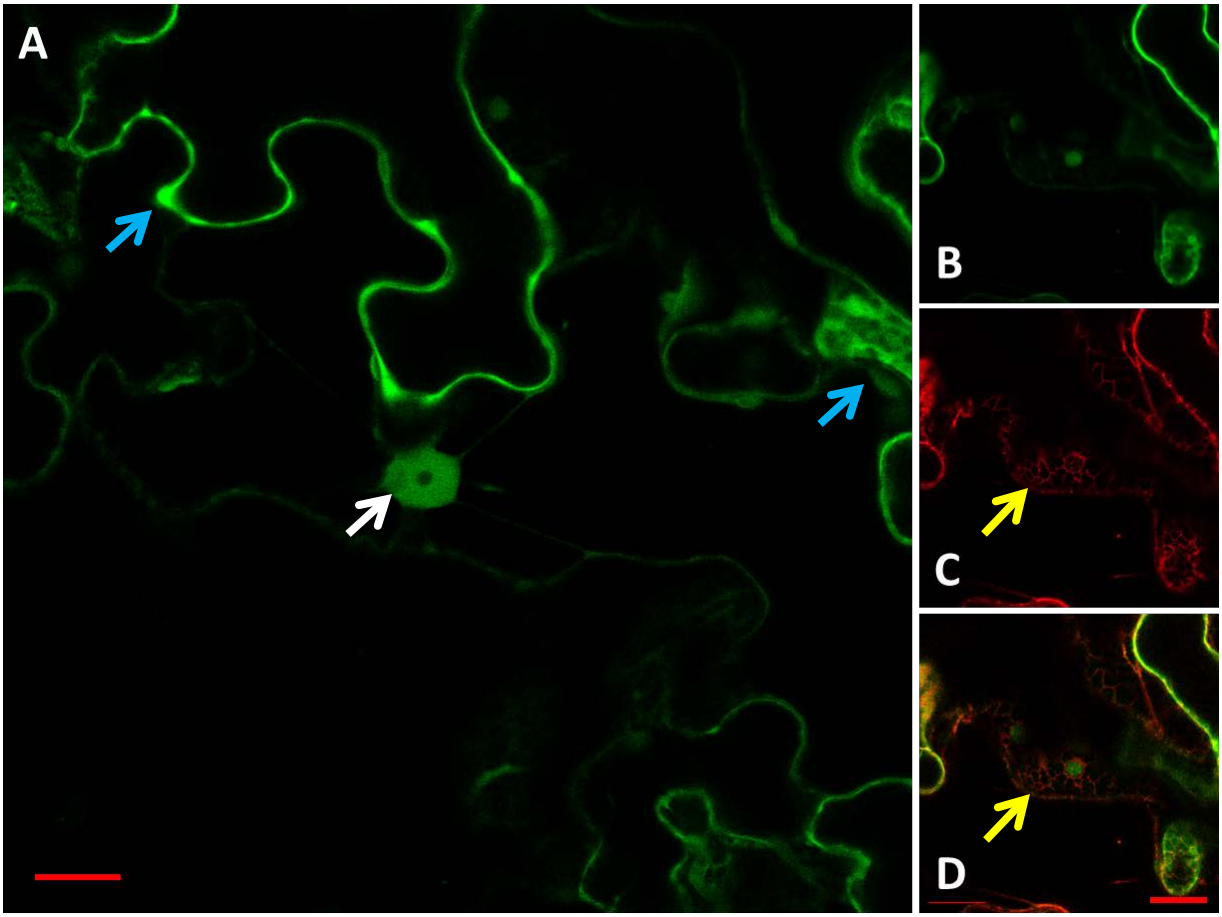

Figure 4.14. Subcellular Localization of VIP2KD-GFP

VIP2KD-GFP fusion protein was transiently co-expressed with mCherry ER marker protein in *N. benthamiana* epidermal cells. Data shown are from 48 hours post infiltration. (A) VIP2KD-GFP fluorescence is detected in the nucleus (white arrow) and cytoplasm (blue arrow). (B-D) Higher magnification of cortical ER (yellow arrow), (B) VIP2KD-GFP (C) mCherry ER marker (D) B and C merged image, lack of yellow indicates no co-localization. Note: ER surrounds the chloroplast (small green sphere). Scale bar = 20 µm.

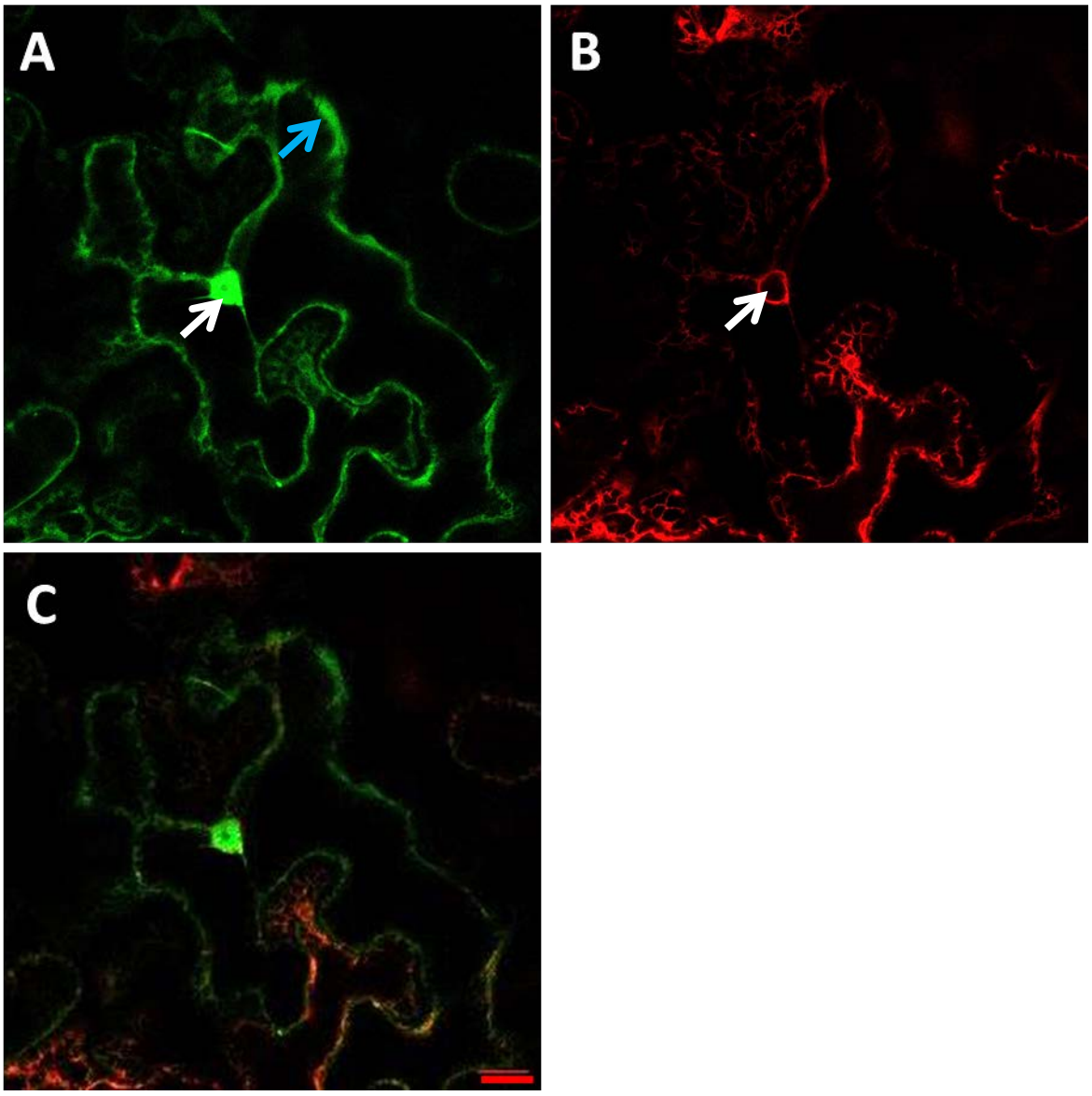

Figure 4.15. Subcellular Localization of VIP1KD-GFP

VIP1KD-GFP fusion protein was transiently co-expressed with mCherry ER marker protein in *N. benthamiana* epidermal cells. Data shown are from 48 hours post infiltration. (A) VIP1KD-GFP fluorescence is detected in the nucleus (white arrow) and cytoplasm (blue arrow) (B) mCherry ER marker (D) A and B merged image, lack of yellow indicates no co-localization. Scale bar = 20 µm.

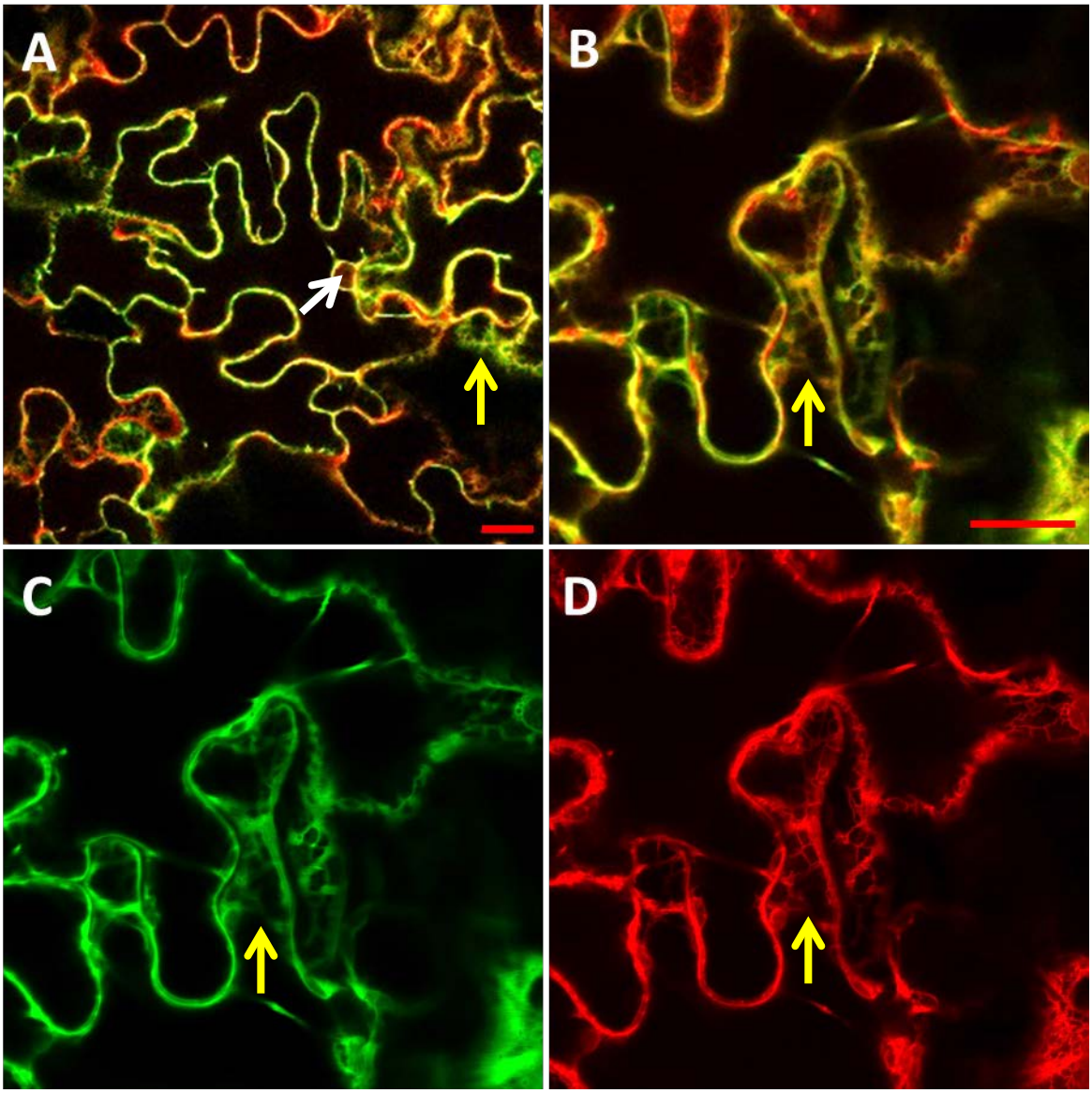

Figure 4.16. Subcellular Localization of GFP-VIP2PD

GFP-VIP2PD fusion protein was transiently co-expressed with mCherry ER marker protein in *N. benthamiana* epidermal cells. Data shown are from 48 hours post infiltration. (A) Merged image of GFP-VIP2PD and mCherry ER marker, yellow indicates co-localization. GFP-VIP2PD fluorescence is detected in the ER (yellow arrow) and absence from nucleus (white arrow) (B-D) Higher magnification of cortical ER, (B) C and D merged image, yellow indicated co-localization (C) GFP-VIP2PD (D) mCherry ER marker. Scale bar = 20 µm.

NUDIX

Seven members of the Nudix hydrolase family are predicted to dephosphorylate PPx-InsPs. GFP fusion proteins for Nudix 4, 12, 13, 16, 17, 18, and 21 were transiently expressed in *N. benthamiana* to determine the subcellular location of these proteins and potential sites of PPx-InsP hydrolysis. A striking feature of these particular Nudix family members is the diverse subcellular localization patterns obtained in this experiment. We will first discuss the similarity in the expression patterns, followed the unique features of each Nudix.

NUDIX4-, NUDIX12-, NUDIX13-, NUDIX16-, NUDIX17-, NUDIX18- and NUDIX21-GFP signals were present in the nucleus (**Figures 4.17-4.23**). One concern is the passive diffusion of highly expressed small cytosolic protein into the nucleus. The classic estimation for the nuclear exclusion limit is 60 kDa (*34*). The Nudix-GFP fusion proteins are under this limit at approximately 50 kDa (**Table 4.3**). In this case, the time course of expression can be a useful tool. The nuclear signal from all NUDIX-GFP fusion proteins was observed at earliest time point with detectable GFP signal (24 hours) (**Figures 4.28, 4.29**). This early localization to the nucleus supports that the localization is not due to the over-accumulation of the protein and passive diffusion into the nucleus. Nuclear signal can also result if the GFP is cleaved from the fusion protein, with an expected molecular mass of 27 kDa. To determine the integrity of the gene-GFP protein was verified by protein blotting. Although some degradation products are detected, the major band with an SDS-PAGE analysis has a molecular mass close to the theoretical size of the fusion protein (**Figure 4.25, Table 4.3**).

The localization of all seven potential PPx-InsP hydrolases to the nucleus suggests the potential of specialized regulation of PPx-InsP degradation in this organelle. A closer look at the expression patterns of NUDIXs reveal that although they are all up regulated in pollen, they differ in the other time and place of high expression. Nudix 21 is highly expressed in root, while Nudix 17 is highly expressed in cauline leaves. During seed development their levels of expression are also different, with Nudix 16 and 17 highly expressed in early embryo development, while Nudix 13 and 21 are highly expressed in late seed development and Nudix 12 is expression very low in seeds (**Figures 4.4, 4.6, 4.8)**).

In addition to the nuclear localization, NUDIX12-, NUDIX13-, and NUDIX16-GFP localize in a diffuse pattern in the cell (**Figures 4.17A, 4.18, 4.19**). Voids in GFP signal correspond to chloroplasts as determined by the collection of chloroplast autofluorescence spectra. This pattern is consistent with cytoplasm localization. In addition to voids for chloroplasts, smaller voids can be seen outlining other organelles (**Figure 4.17 B,C**). The combination of the voids in GFP signal can give the appearance of a reticulate pattern, however imaging at higher magnification helps to resolve the pattern of voids versus fine meshwork of the ER. The center of the cell is filled with the vacuole, therefore no signal from cytosol localized proteins is expected. The vacuole pushes the cytosol to the edges of the cell, resulting in an apparent plasma membrane signal, however the cytosol signal appears as a thick and often uneven outline of the cell. The pattern of nuclear and cytosol localization for NUDIX12-, NUDIX13-, and NUDIX16-GFP was constant over the 24-72 hour time course (**Figure 4.28**)

NUDIX17-GFP and NUDIX18-GFP were observed in a reticulate pattern consistent with ER localization in addition to the nuclear localization previous discussed. NUDIX17- and NUDIX18-GFP were co-localized with the mCherry ER in a transient expression assay in *N. benthamiana* to confirm this localization (**Figure 4.20-21**). GFP fluorescence was observed in the cortical ER and the ER cisternae. This pattern was consistent in the 24-72 hour time course (**Figure 4.28-29**). The localization of NUDIX17- and NUDIX18-GFP to the ER suggested they function to turn over PPx-InsP synthesized there by VIP2.

The localization of Nudix 12, 13, 16, 17, and 18 to the nucleus, cytoplasm and ER was unexpected, as they are predicted to be mitochondrial proteins and previous work has localized Nudix 13 to the mitochondria in protoplasts (*38*). Transient expression of these proteins was allowed to continue for 72 hours to ensure that a localization to the mitochondria did not occur (**Figure 4.28-4.29**). At this point, no puncta were observed to suggest localization to the mitochondria. We used mMDH-GFP (mitochondrial Malate Dehydrogenase) fusion protein to ensure that in this system gene-GFP fusion proteins can be localized to the mitochondria (**Figure 4.30**).

In addition to some nuclear localization, Nudix4-GFP and Nudix21-GFP fusion proteins co-localize with the chloroplast autofluorescence when transiently expressed in *N. benthamiana* epidermal cells. Chloroplast localization was determined though co-localization of GFP fluorescence and chlorophyll autofluorescence. Interestingly over the time course, 24, 48, 72, hours post infiltration, trafficking of NUDIX4-GFP and NUDIX21-GFP to the chloroplast was observed (**Figure 4.30**). At 24 hours, NUDIX4-GFP localized to the nucleus and the cytoplast

outlining the chloroplasts and by 48 hours, the protein has moved inside the chloroplast (**Figure 4.22, 4.29**). In contrast, at 24 hours post infiltration, Nudix21-GFP localizes to puncta within the cytoplasm (**Figure 4.29)**. Many of the puncta appear to co-localize the chloroplast. The ER cortical surrounds the chloroplast in a fine meshwork as seen in **Figure 4.14** and co-expression of NUDIX21-GFP and the mCherry ER marker was used to determine if the puncta were sites of ER/chloroplast connections 48 hours post infiltration. It does not appear that the GFP puncta and ER co-localize in this assay (**Figure 4.23A**). At the 48 hour time point, NUDIX21-GFP localizes to both puncta and as well as interior of the chloroplast (**Figure 4.23 A-D)** and by 72 hours the puncta pattern has disappeared and Nudix21-GFP is localized inside the chloroplasts (**Figure 4.23 E-H)**). Both Nudix4 and Nudix21 have a Chloroplast localization signal as predicted by ChloroP 1.1 (*39*), however, they are not found in published chloroplast proteome data bases AT_CHLORO (*40*) and plptro (*41*). It is interesting to speculate on the role of Nudix 4 and Nudix 21in the chloroplast. As potential PPx-InsP hydrolases, this is a potential link between PPx-InsP signaling and energy homeostasis, as the chloroplast is the site of photosynthesis, where light energy is converted into chemical energy and sugars for the plant.

Our data reported here identify the nucleus as a site of PPx-InsP hydrolysis. Additional sites of PPx-InsPs are the cytoplasm, ER and chloroplasts. The overlapping subcellular expression patterns of Nudix 4, 12, 13, 16, 17,18, and 21 may appear redundant, however these genes have different expression patterns across tissue and development of the plant (**Figure 4.4, 4.6, 4.8**), suggesting hydrolysis of PPx-InsP is controlled in a tissue and time specific manor.

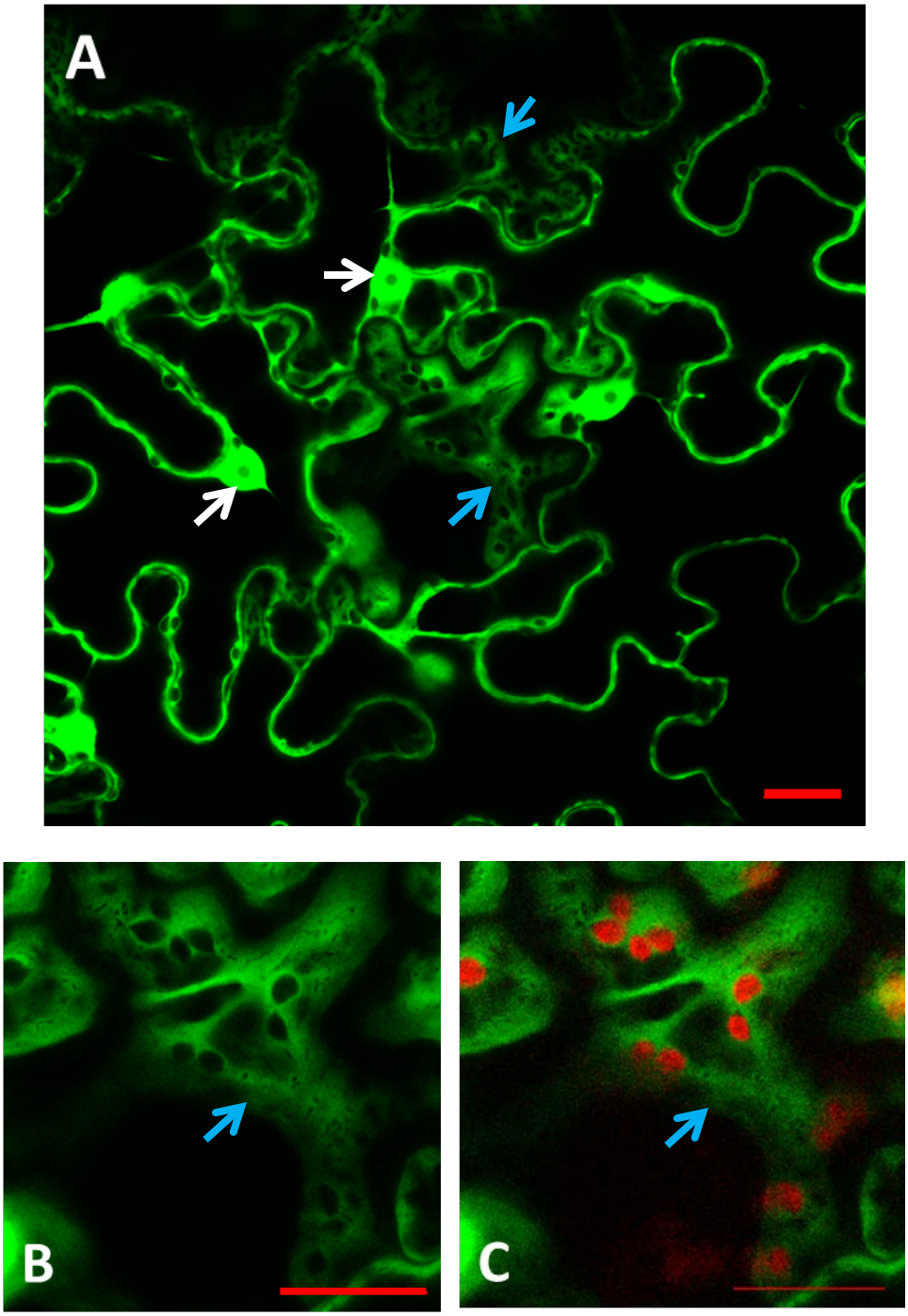

Figure 4.17. Subcellular Localization of NUDIX12-GFP

NUDIX12-GFP fusion protein was transiently expressed in *N. benthamiana* epidermal cells. Data shown are from 48 hours post infiltration. (A) NUDIX12-GFP fluorescence is detected in the nucleus (white arrow) and cytoplasm (blue arrow). (B-C) Higher magnification of cytoplasm, (B) NUDIX12-GFP, Note: Void in GFP signal outlines chloroplasts and other small organelles, (C) Merged image of A and chloroplast autofluorescence (red). Scale bar = 20 µm.

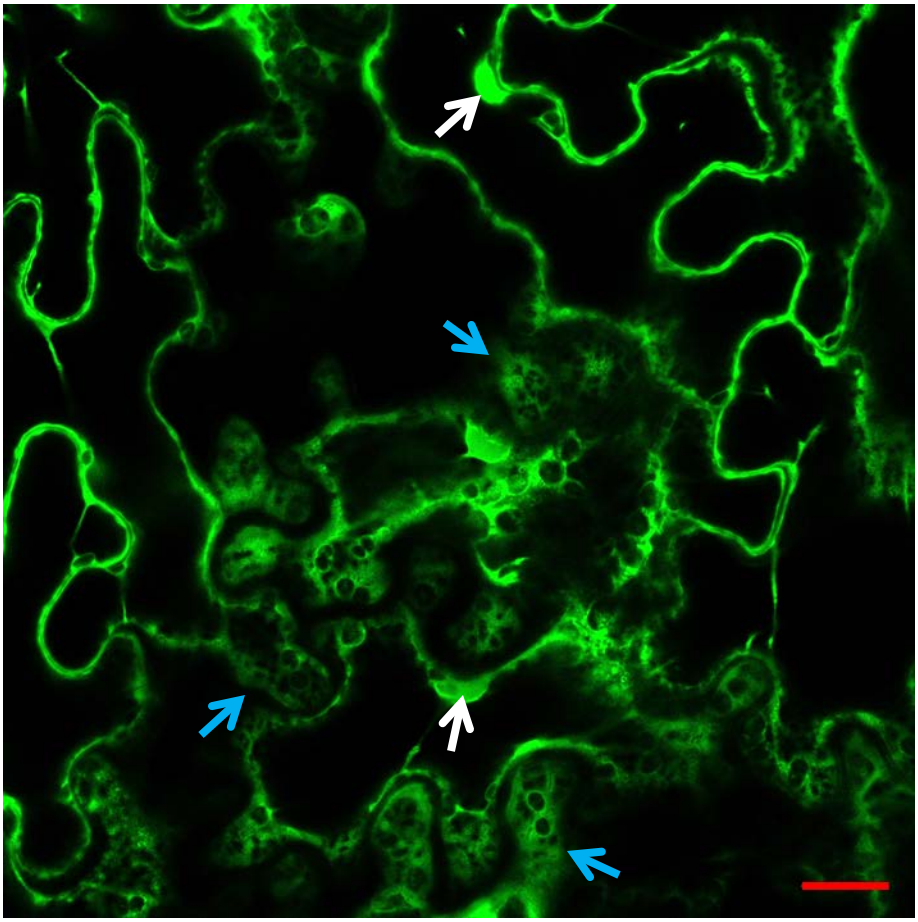

Figure 4.18. Subcellular Localization of NUDIX13-GFP

NUDIX13-GFP fusion protein was transiently expressed in *N. benthamiana* epidermal cells. Data shown are from 48 hours post infiltration. NUDIX13-GFP fluorescence is detected in the nucleus (white arrow) and cytoplasm (blue arrow). Note: Small voids in GFP signal outlines chloroplasts and other small organelles. Scale bar = 20 µm.

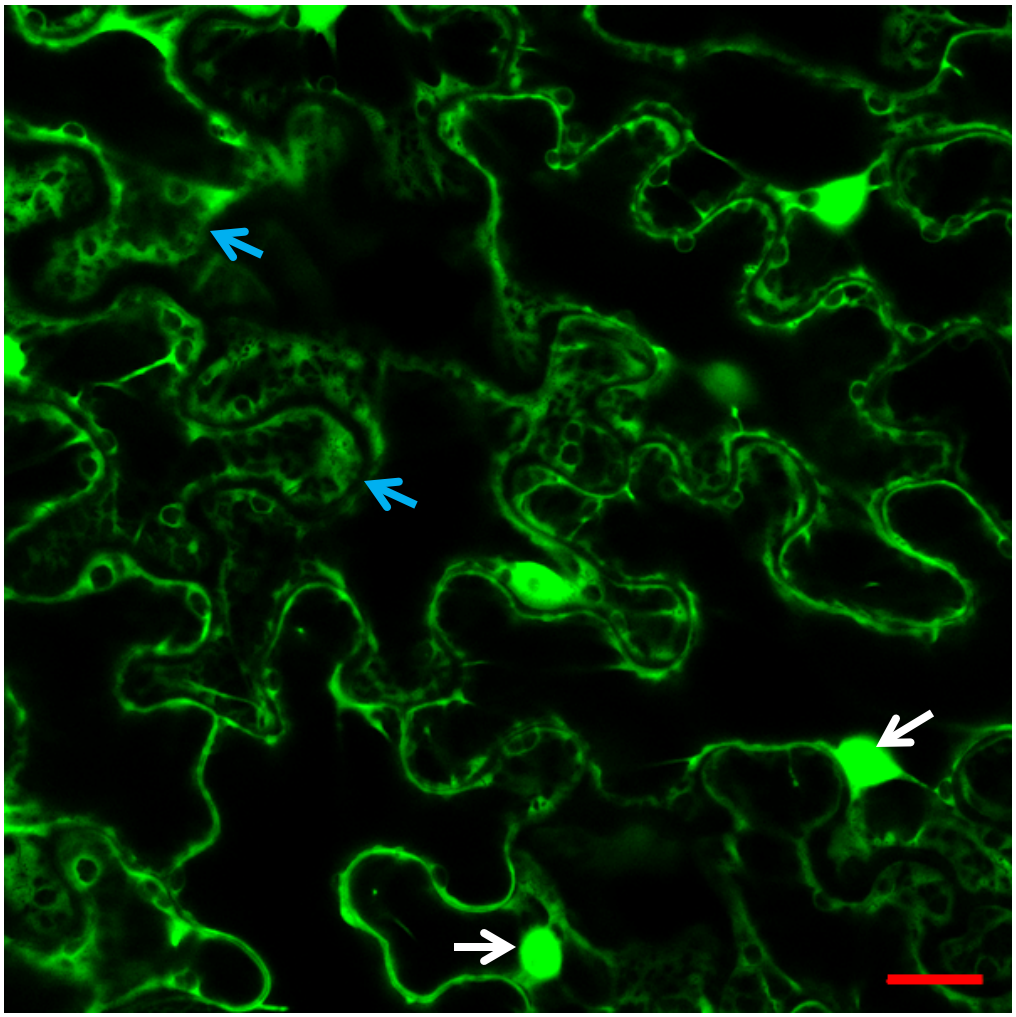

Figure 4.19. Subcellular Localization of NUDIX16-GFP

NUDIX16-GFP fusion protein was transiently expressed in *N. benthamiana* epidermal cells. Data shown are from 48 hours post infiltration. NUDIX16-GFP fluorescence is detected in the nucleus (white arrow) and cytoplasm (blue arrow). Note: Small voids in GFP signal outlines chloroplasts and other small organelles. Scale bar = 20 µm.

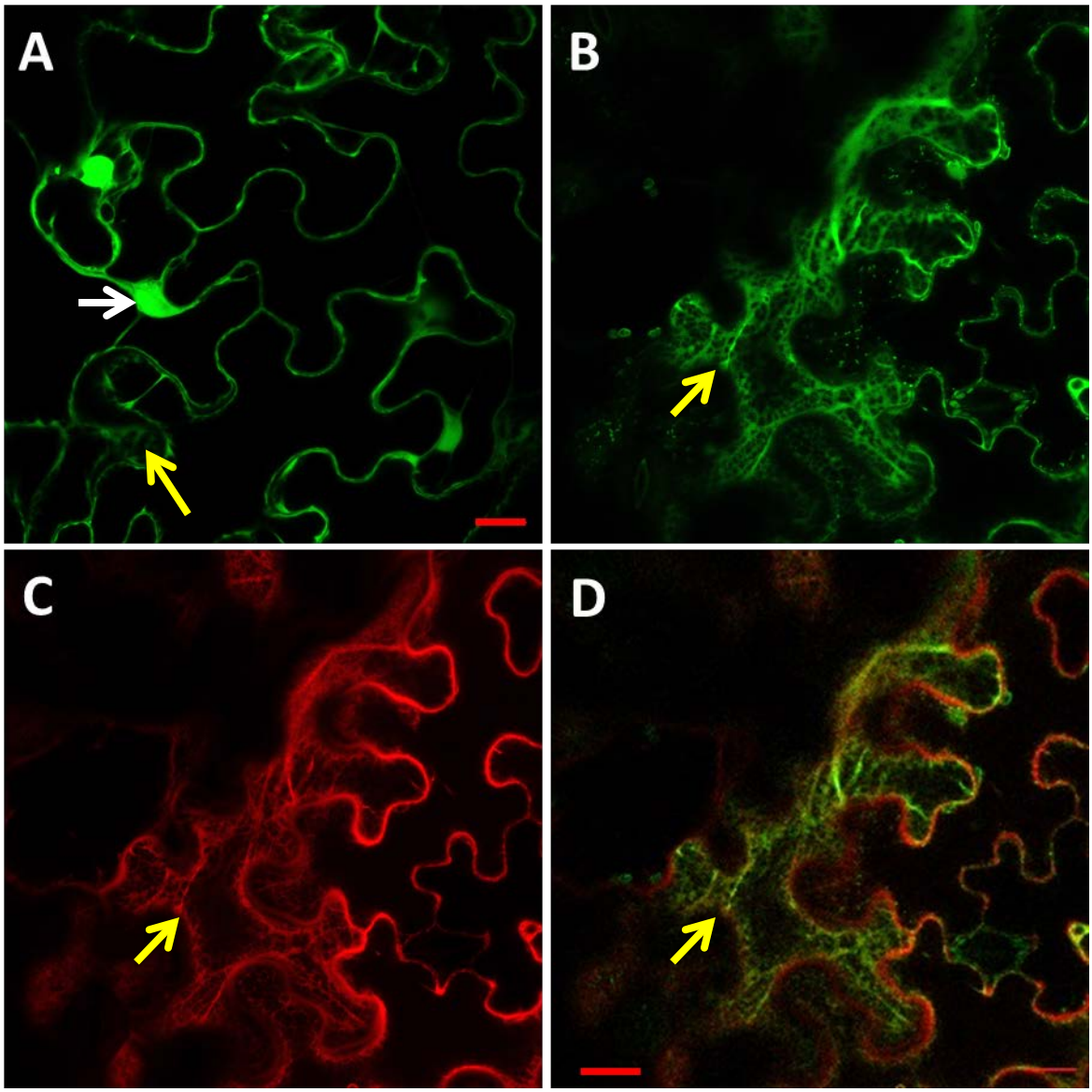

Figure 4.20. Subcellular Localization of NUDIX17-GFP

NUDIX17-GFP fusion protein was transiently co-expressed with mCherry ER marker protein in *N. benthamiana* epidermal cells. Data shown are from 48 hours post infiltration. (A) NUDIX17-GFP fluorescence is detected in the nucleus (white arrow) and ER (yellow arrow). (B-D) Higher magnification of cortical ER, (B) NUDIX17-GFP (C) mCherry ER marker (D) B and C merged image, yellow color indicates co-localization. Scale bar = 20 µm.

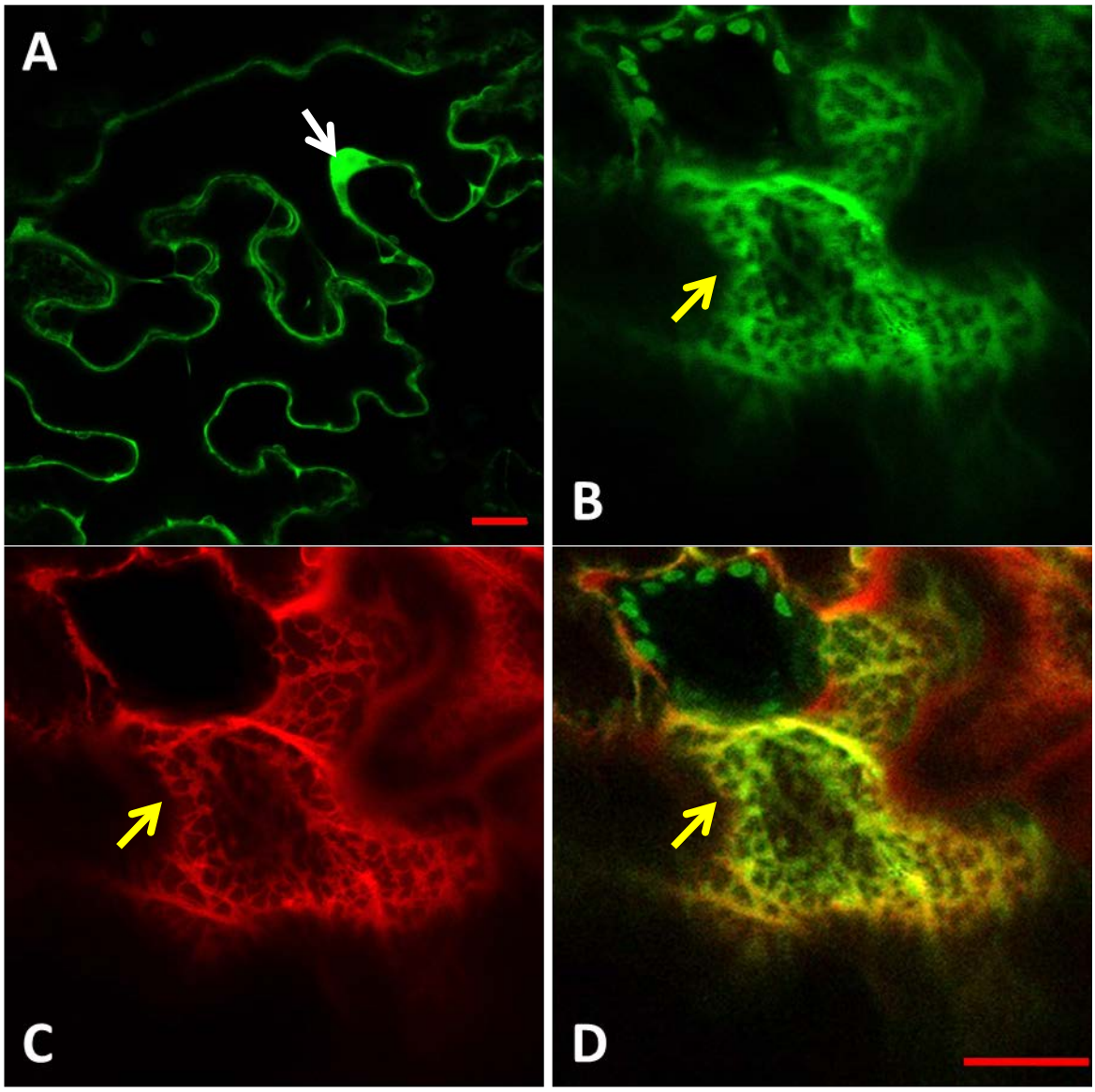

Figure 4.21. Subcellular Localization of NUDIX18-GFP

NUDIX18-GFP fusion protein was transiently co-expressed with mCherry ER marker protein in *N. benthamiana* epidermal cells. Data shown are from 48 hours post infiltration. (A) NUDIX18-GFP fluorescence is detected in the nucleus (white arrow) and ER (yellow arrow). (B-D) Higher magnification of cortical ER, (B) NUDIX18-GFP Note: Small green spheres are chloroplast autofluorescence in the guard cells (C) mCherry ER marker (D) B and C merged image, yellow color indicates co-localization. Scale bar = 20 µm.

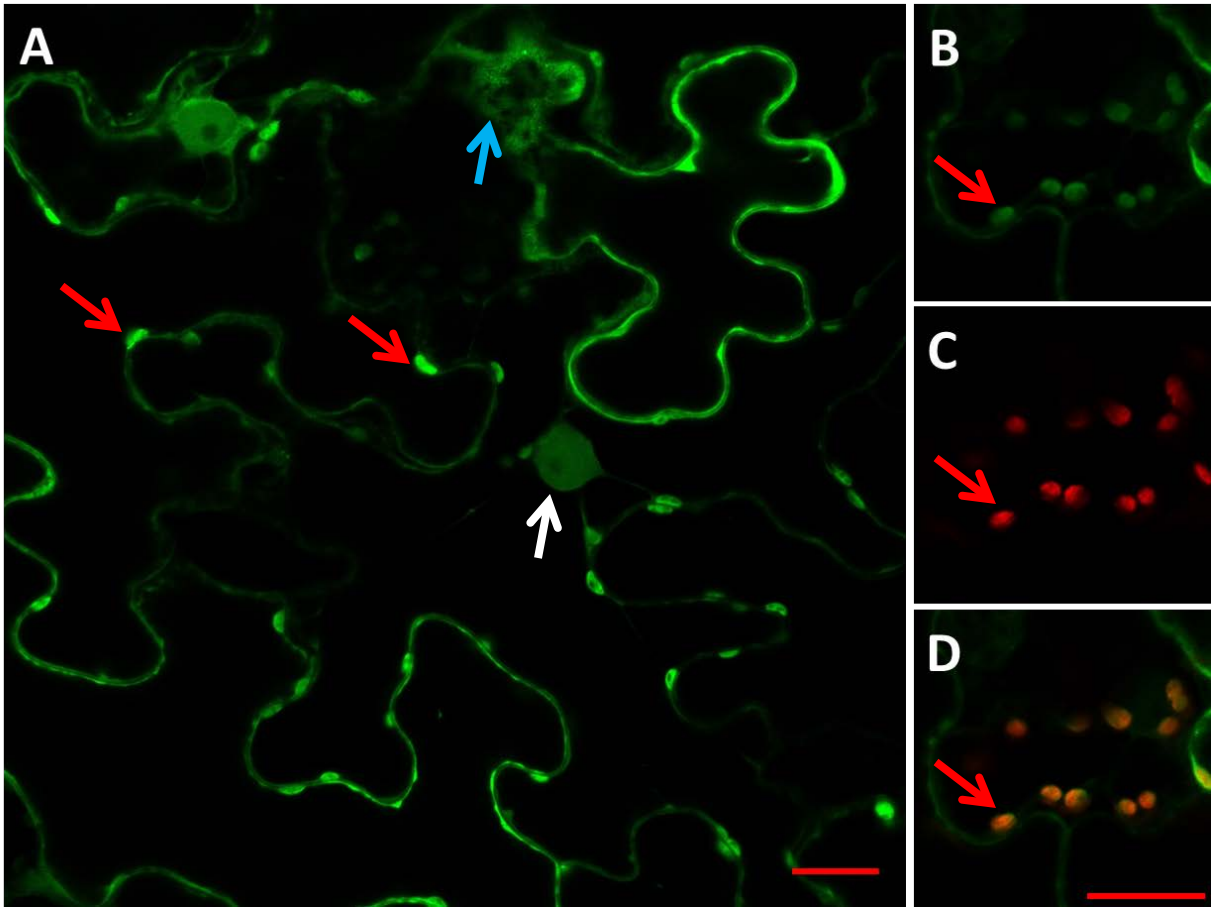

Figure 4.22. Subcellular Localization of NUDIX4-GFP

NUDIX4-GFP fusion protein was transiently expressed in *N. benthamiana* epidermal cells. Data shown are from 48 hours post infiltration. (A) NUDIX4-GFP fluorescence is detected in the nucleus (white arrow), cytoplasm (blue arrow) and chloroplasts (red arrow). (B-D) Higher magnification of chloroplasts, (B) NUDIX4-GFP (C) chloroplast autofluorescence (D) B and C merged image, yellow color indicates co-localization. Scale bar = 20 µm.

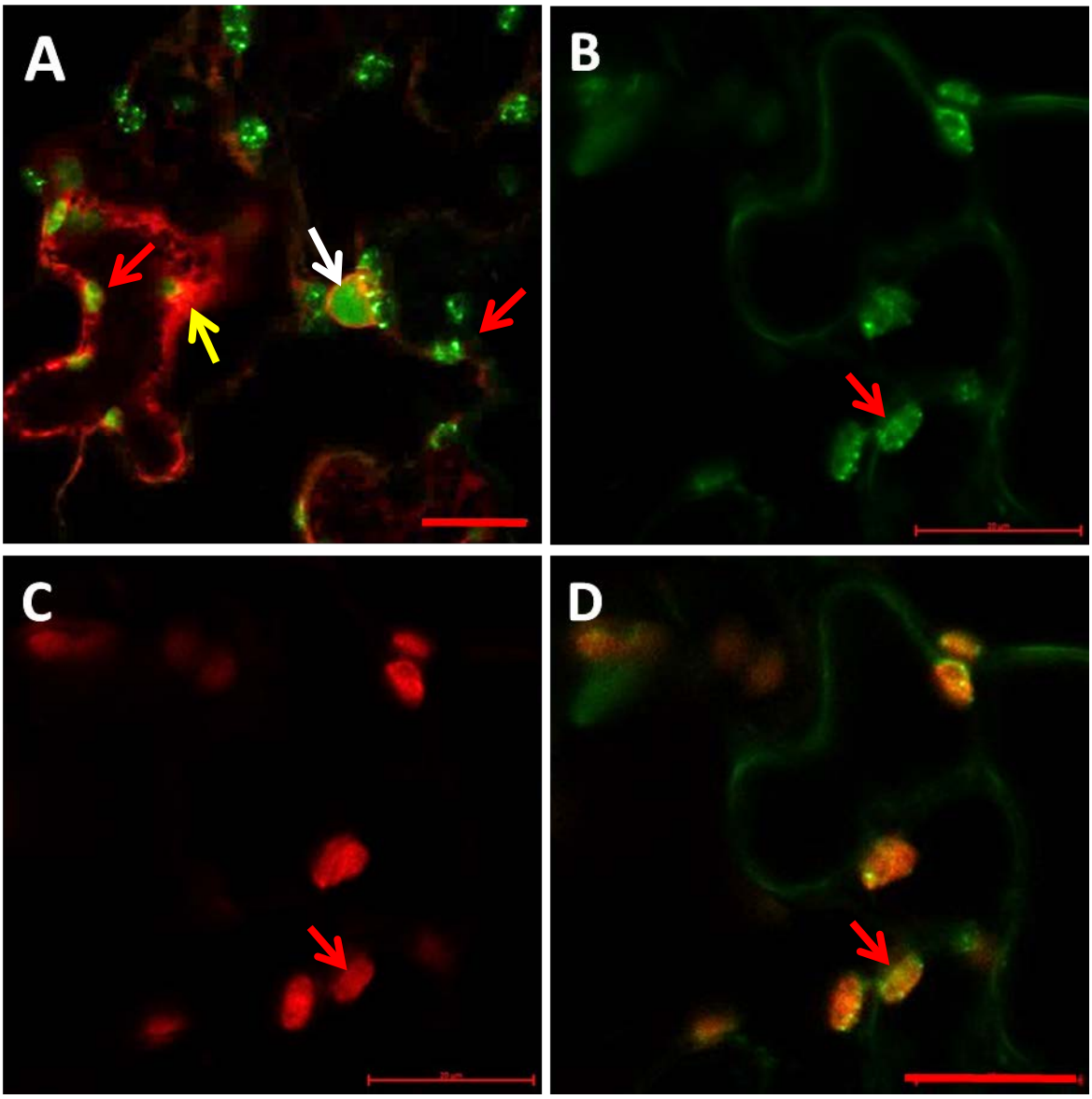
A
B
C
D

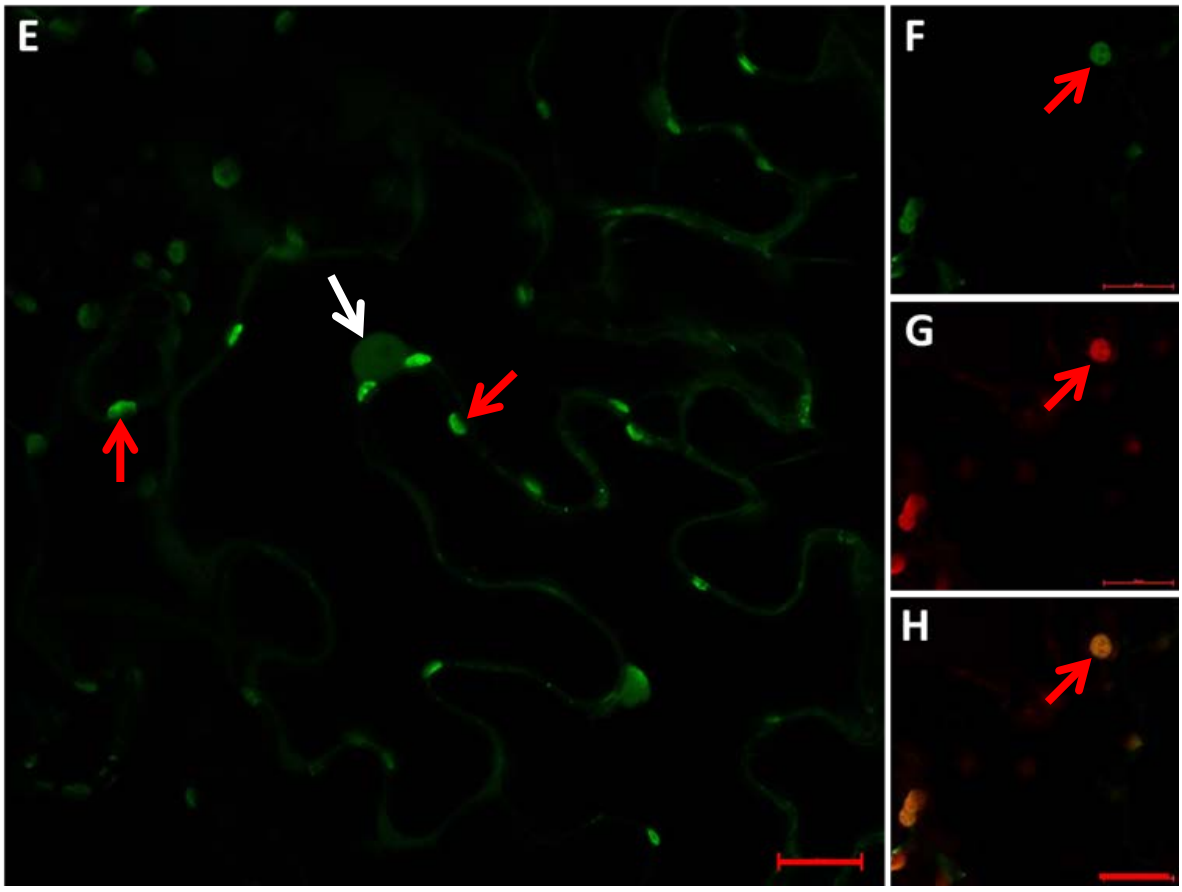

Figure 4.23. Subcellular Localization of NUDIX21-GFP

NUDIX21-GFP fusion protein was transiently expressed in *N. benthamiana* epidermal cells. Data shown are from 48 (A-D) and 72 (E-H) hours post infiltration.

(A) Merged image of mCherry ER marker and NUDIX21-GFP fluorescence. NUDIX21-GFP is detected in the nucleus (white arrow) and cytoplasmic puncta associated with the chloroplasts (red arrow). ER indicated by yellow arrow. Puncta are not associated with ER/chloroplast interface. (B-D) Higher magnification of chloroplast, (B) NUDIX21-GFP (C) chloroplast autofluorescence (D) B and C merged image, yellow color indicates co-localization. Scale bar = 20 µm.

(E) After 72 hours, NUDIX21-GFP fluorescence is detected in the nucleus (white arrow) and chloroplasts (red arrow). (F-H) Higher magnification of chloroplast, (F) NUDIX21-GFP (G) chloroplast autofluorescence (H) F and G merged image, yellow color indicates co-localization. Scale bar = 20 µm.

From the transient expression of Gene-GFP fusion protein in *N. benthamiana* leaves, we conclude that the kinases needed to synthesis $InsP_6$ are found in the nucleus (IPK1, IPK2α/β). The many members of the Nudix family (12,13,16,17,18) found there could dephosphorylate PPx-InsPs. Surprisingly, subcellular localization data also indicates the ER contains the kinases needed to synthesize $InsP_6$ and PPx-InsPs (IPK1, IPK2α, and VIP2), as well as the phosphatase MINPP. The Nudix genes are localized to the nucleus as well as other organelles (ER and chloroplasts) and the cytoplasm indicating potential sites of PPx-InsP hydrolysis. These data suggest a role for PPx-InsP signaling in the nucleus as well as an organelle based component to PPx-InsP signaling which may be unique to plants.

Acknowledgement:

We would like to thank John York and Imara Perera for supplying some clones and Joonho Park, Mihir Mandal, and Janet Donahue for construction of some GFP plasmids.

MATERIALS AND METHODS

eFP Browser Analyses

The table of expression values for plant development data was downloaded from eFP browser for each gene in **Table 4.1** (http://bar.utoronto.ca/efp/cgi-bin/efpWeb.cgi). Spreadsheet software (excel) was used to generate a table from this data and conditional formatting of each column individually generated a heat map for expression of each gene, with yellow being the lowest expression and red the highest. This recapitulates the color used by eFP browser. To generate the global expression table, conditional formatting was applied across all columns, with blue indicating the lowest number and red the highest.

Nudix Alignments

The coding sequences for Nudix 4, 12, 13, 16, 17, 18 and 21 were obtained from TAIR and aligned using Cluster Omega. The sequences are colored based on the biochemical properties of the amino acid. The symbols beneath the alignment denote conservation or conservative substitutions.

Cloning of GFP constructs

The coding regions of IPK1, IPK2α, IPK2β, VIP1, VIP2, Nudix 4, Nudix 12, Nudix 13, Nudix 16, Nudix 17, Nudix 18, Nudix 21 and MINPP were amplified from plasmids, WT Arabidopsis genomic or cDNA using the primers indicated in **Table 1**. The PCR product corresponding to the full length coding sequence without the stop codon was cloned into pENTR™\D-TOPO® (Invitrogen Corp., Carlsbad, CA) and sequenced before recombining either VIP2PD into

pK7WGF2(N-terminus GFP)or all others into pK7FWG2(C-Terminus GFP) (Karimi et al. 2002) containing the 35S Cauliflower Mosaic virus promoter and e*GFP* gene using the Gateway® LR Clonase™ II kit (Invitrogen Corp., Carlsbad, CA). A single colony was used to amplify the [Gene-pK7FW2/pK7WGF2] plasmid and it was sequenced before transforming Agrobacterium (strain GV3101) for transient expression in *N. benthamiana*. Cloning and expression plasmids were amplified in *Escherichia coli* One Shot®Top10 cells (Invitrogen Corp., Carlsbad, CA) and purified from an overnight culture using DNA Mini prep kit (Qiagen Co., Valencia Ca).

GFP Localization and Imaging

N. benthamiana plants were agro-infiltrated as previously described (*42*). Briefly, Agrobacterium cultures were grown over night in liquid media. Cells were pelleted and suspended in MMA (1x MS, 10 mM MES, 200 µM acetosyringone) to an optical density of 1.0, A_{600nm}. Cultures were allowed to incubate at room temperature 2-4 hours before infiltration. *N. benthamiana* plants were grown under long day conditions (16 hours light) and 150 µE light. Leaf sections were imaged 12, 24,36, 48, or 72 hours post infiltration as indicated using a Zeiss LSM 880 (Carl Zeiss). Slides were examined with a 40x C-Apochromat water immersion lens. A set of mCherry tagged organelle markers were used for co-localization experiments (*43*). GFP was excitation using a 488-nm argon laser and its fluorescence was detected at 500- to 550-nm. mCherry was imaged using excitation with a 594-nm laser and fluorescence was detected at 600-650-nm. Chlorophyll signal was collected using a 594-nm laser and emission above 650 nm was collected. A Zeiss LSM 510 laser-scanning microscope (Carl Zeiss) with an inverted Axio

Observer Z1 base was also used for confocal imaging. GFP was excited using a 488-nm argon laser and fluorescence detected using 505- to 550-nm band-pass emission filter. Slides were examined with x40 C-Apochromat water immersion lens.

Protein Blot Analyses

Conditions have been previously reported (*44*). Briefly, tissues were ground in liquid nitrogen, homogenized, cellular debris was pelleted and SDS-bromophenol blue loading dye added to the supernatant. The supernatant was boiled, centrifuged, and the subsequent supernatant was loaded onto a polyacrylamide gel for separation. Equal amounts of protein were loaded onto gels. SDS-PAGE was followed by western blotting with a 1:10,000 dilution of rabbit anti-GFP antibody (Invitrogen Molecular Probes, Eugene, OR). A secondary goat anti-rabbit horseradish peroxidase antibody (Bio-Rad Laboratories, Hercules, CA) was used at a 1:2,500 dilution. Immunoreactive bands were detected using an ECL™ Prime Western Blotting Detection Reagent (Amersham, Buckinghamshire, UK). Ponceau S staining of blots was performed to ensure that equal amounts of protein within extracts were analyzed.

APPENDIX TO CHAPTER VI

Table 4.2. Supplemental Data: Primer Table for GFP Fusion Proteins

Gene Name	Source	Primers (listed 5' to 3')
Vip1-KD	Clone Perera Lab, UNC	Forward - CACCATGGAGATGGAAGAAGGAGCAAG
		Reverse - CCCACAGACCGCTTGCCT
Vip2-FL	Clone #104767 ABRC	Forward - CACCATGGGGGTGGAAGAAGGAGCTG
		Reverse - GCTTTTGCCATTAGAGGTGTTCTTGTGG
Vip2-KD	Clone #104767 ABRC	Forward - CACCATGGGGGTGGAAGAAGGAGCTG
		Reverse - CTCTGACTGCCCAAAAGTTCC
Vip2-PD	Clone #104767 ABRC	Forward - CACCTATTACGACGATGCTGCTTGTG
		Reverse - TTAGCTTTTGCCATTAGAGGTGTTCTTGTGG
IPK1	Clone JY308, York Lab IPK1-GST-pGEXKG (*45*)	Forward - CACCATGGAGATGATTTTGGAGGAGGAAA
		Reverse - GCTGTGGGAAGGTTTTGAGTTGCC
IPK2α	Clone # JYB897, York Lab (*46*)	Forward - CAAATGCAGCTCAAAGTCCCTGA
		Reverse - AGAATCTGCATACTCATCTGGG
IPK2β	cDNA, Col 60,000	Forward - CACCATGCTCAAGGTCCCTGAACACC
		Reverse - GCGCCCGTTCTCAAGTAG
Nudix4	Clone # U22579, ABRC	Forward - CACCATGGACAGGGTTCTCTGTG
		Reverse - GTTCCCACTTTCATCATCGTC
Nudix12	cDNA, Col 60,000	Forward - CACCATGTCGGTTCTTTCTTCTCGGACA
		Reverse - GTTAACTACAAAACAGTACCAAGG
Nudix13	cDNA, Col 60,000	Forward - CACCATGTCGAATCTTTCTGCAAGAACA
		Reverse - GACTACAAAGCAGTACGAGGCTCA
Nudix16	cDNA, Col 60,000	Forward - CACCATGTGTGATTTGGTCGCGCGTACG
		Reverse - ATGTTCACCAGTTATCTCCTCTCC
Nudix17	cDNA, Col 60,000	Forward - CACCATGGGTGTTGAGAAAATGGTGTGT
		Reverse - ACACATTGTTTCAATAGAGATTGA
Nudix18	cDNA, Col 60,000	Forward - CACCATGGTGTGTTGGTCTCCCGTACG
		Reverse - GTAGATAGAGATCAGTGGAAGGTT
Nudix21	Clone #U17545 ABRC	Forward - CACCATGATTTCTCTATTCATCTCAAACTTTTCAAACTTATC
		Reverse - TTGGGTCTGGCATTTCCGGTTAATG
MINPP	Clone # BX837947 CNRGV	Forward - CACCATGGCGACGAAGACTGTTTGGAT
		Reverse - GAGCTCGGTATCGTGGCTTGA

Table 4.3. Supplemental Data: Size of GFP Fusion Proteins

Gene Name	Gene ID	GFP Fusion Protein size	Subcellular Localization
IPK1	At5g42810	77 kDa	
IPK2α	At5g07370	59 kDa	
IPK2β	At5g61760	61 kDa	Nucleus (*32*)
MINPP	At1g09870	82 kDa	
Vip1-KD	At3g01310	59 kDa	
Vip2-KD	At5g15070	67 kDa	
Vip2-FL	At5g15070	146 kDa	
Nudix4	At1g18300	51 kDa	
Nudix12	At1g12880	51 kDa	
Nudix13	At3g26690	51 kDa	Mitochondria (*38*)
Nudix16	At3g12600	47 kDa	
Nudix17	At2g01670	48 kDa	
Nudix18	At1g14860	47 kDa	
Nudix21	At1g73540	49 kDa	

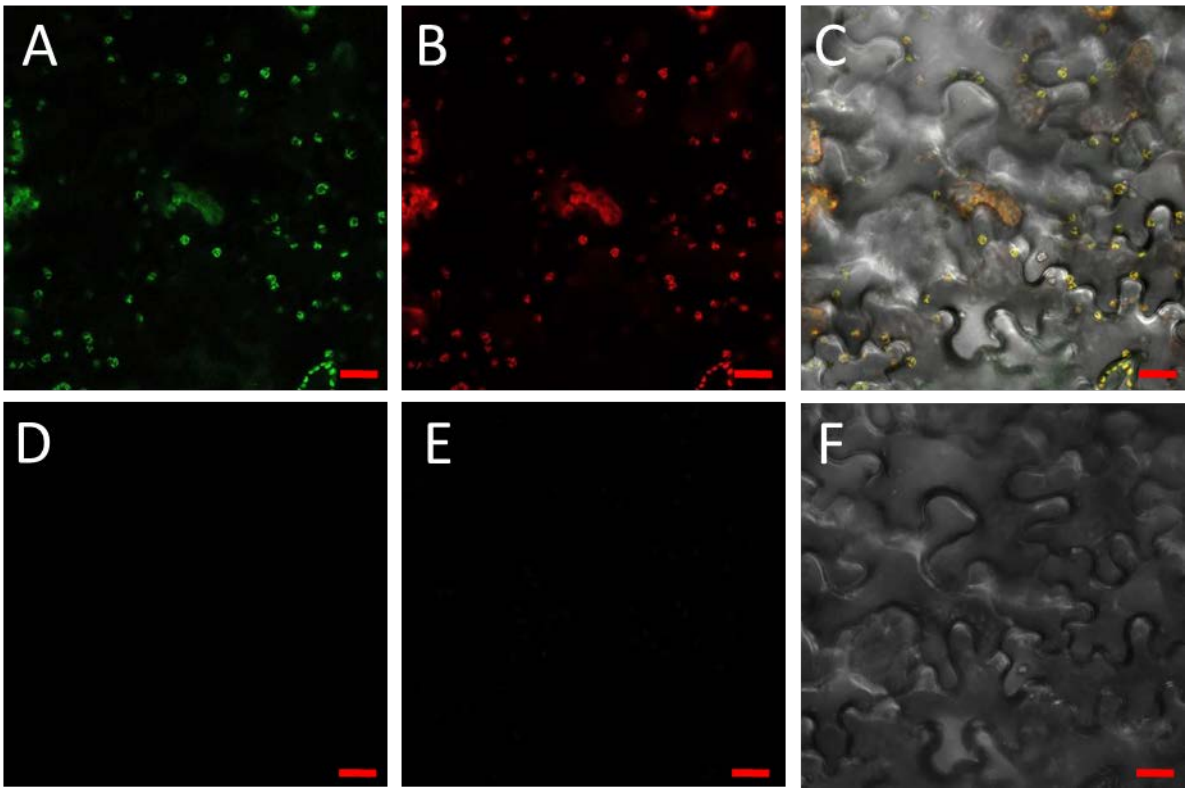

Figure 4.24. Supplemental Data: Imaging Controls

Confocal imaging of uninfiltrated *N. benthamiana*.

(A) Setting for GFP detection (excitation: 488nm argon laser 10%, 500-550 nm emission), chloroplast autofluorescence is detected
(B) Setting for chloroplast autofluorescence (excitation: 594 nm laser, 650-700 nm emission)
(C) Overlay of panels A and B and bright field image, yellow color indicates co-localization
(D) Setting for GFP detection (excitation: 488 nm argon laser 3%, 500-550 nm emission), no chloroplast autofluorescence detected
(E) Settings for mCherry detection (594 nm laser 60%, 605-650 emission) no chloroplast autofluorescence detected
(F) Bright field image of field of view

Scale bar = 20 µm

Using GFP imaging setting (488nm excitation), chloroplast autofluorescence can be seen when 10% laser strength is used (A) however at lower levels, (D) 3% laser strength, this autofluorescence is minimal. (B) Chloroplasts can also be detected using the 594nm laser with emission of 650-700nm. (C) The merge of (A) and (B) show co-localization (yellow color). The settings for imaging mCherry (594 nm excitation, 605-650nm emission) are stringent enough that even with high laser power, 60%, autofluorescence is not detected. (F) bright field image of leaf section used.

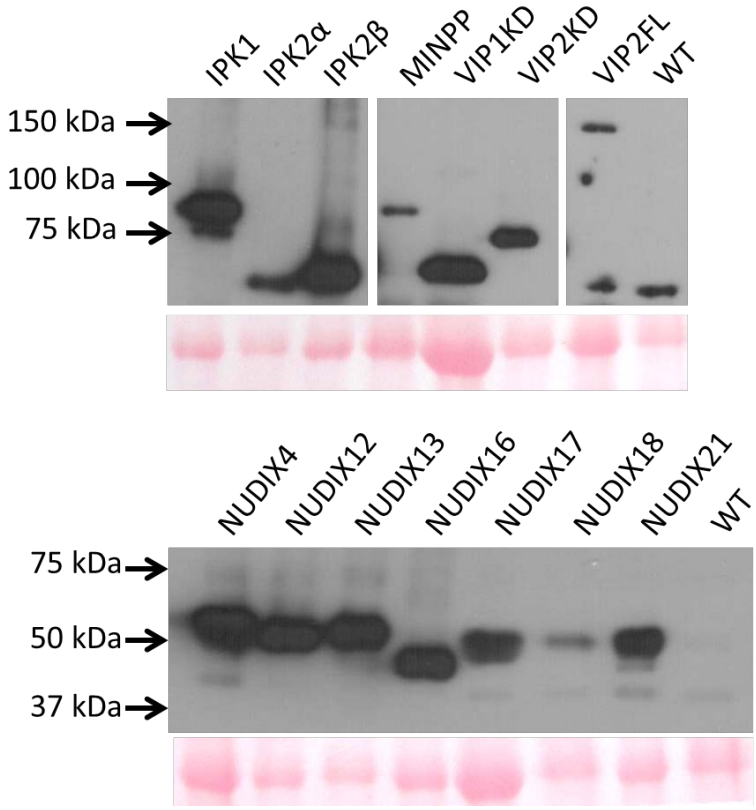

Figure 4.25. Supplemental Data: Western Blot of *N. benthamiana* Leaves Expressing GFP Fusion Proteins

Proteins were extracted from *N. benthamiana* leaves transiently expressing the indicated GFP fusion proteins for 48 hours or uninfiltrated (WT) leaves, and analyzed by western blotting with anti-GFP antibody. Ponceau S staining filters are shown as controls for loading. Top panel: Multiple exposure times were needed to visualize fusion proteins on one western blot (from left to right, 1 sec, 10 sec, and 5 min)

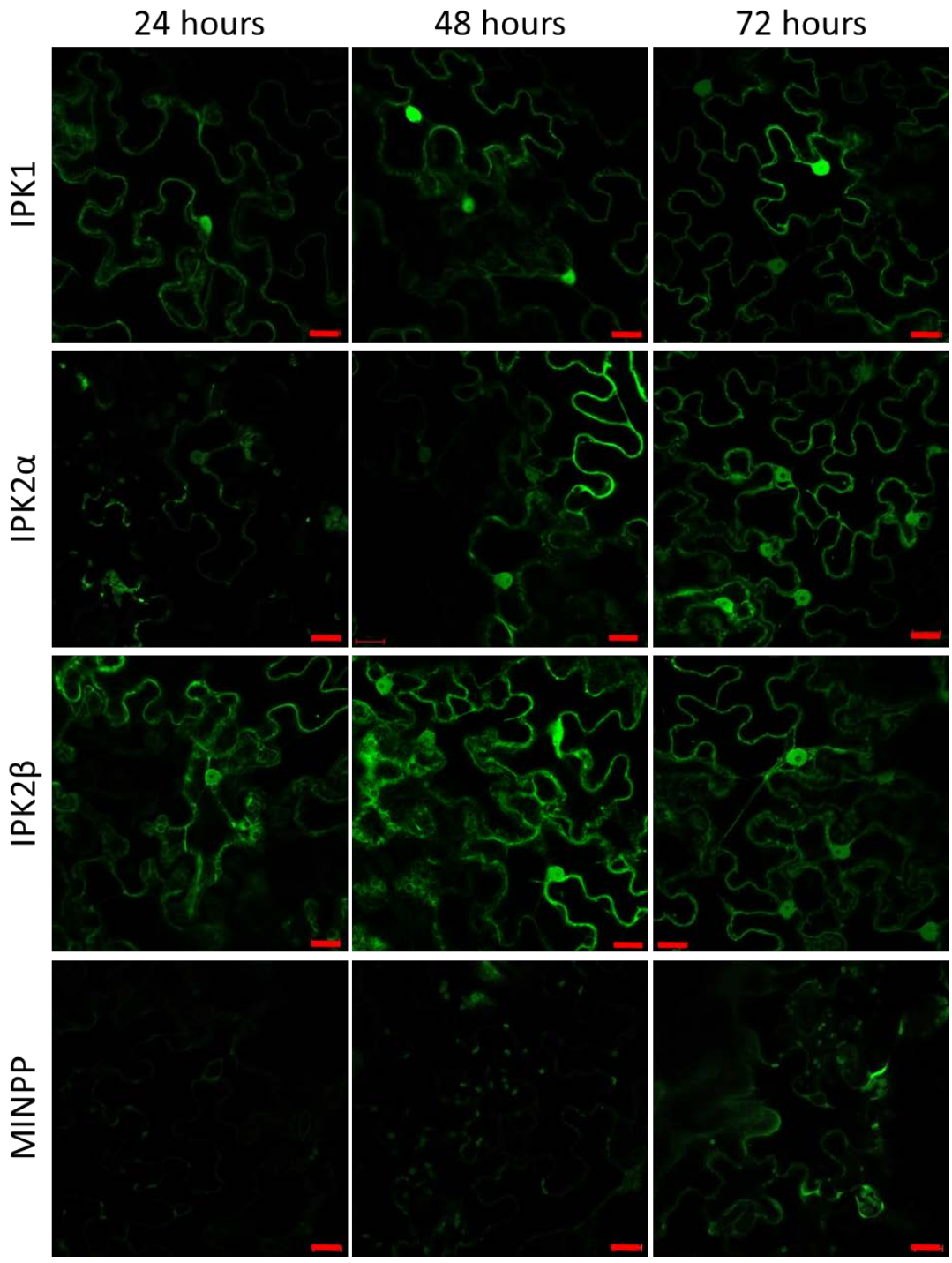

Figure 4.26. Supplemental Data: Time Course IPK1-, IPK2α-, IPK2β-, MINPP-GFP

IPK1-, IPK2α-, IPK2β-, MINPP-GFP fusion proteins were transiently expressed in *N. benthamiana* epidermal cells. Data was collected at 24, 48, and 72 hours post infiltration using confocal microscopy. No signal was detected at 12 hours post infiltration. Scale bar = 20 µm.

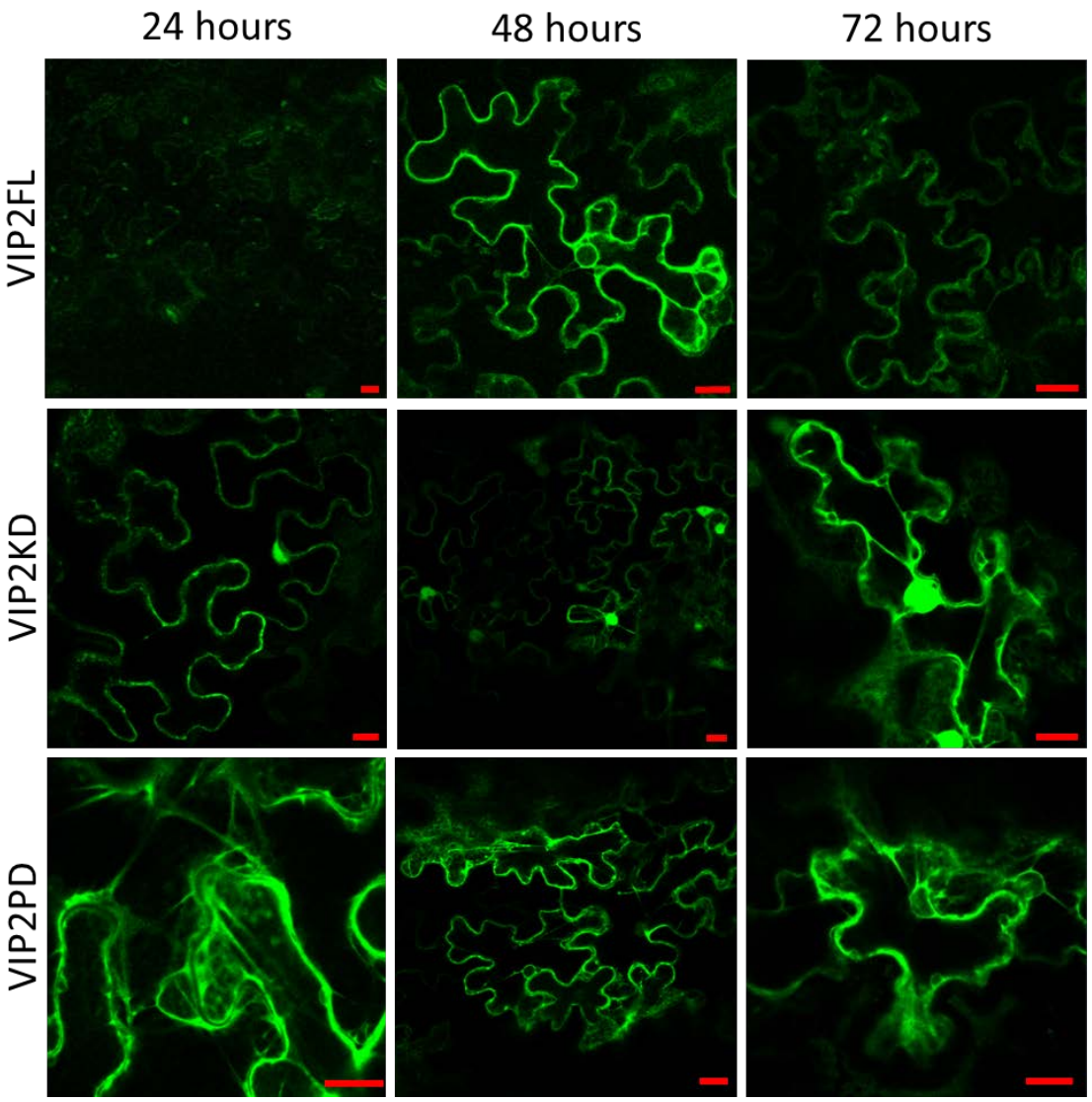

Figure 4.27. Supplemental Data: Time Course VIP2FL-GFP, VIP2KD-GFP, GFP-VIP2PD

VIP2FL-GFP, VIP2KD-GFP, GFP-VIP2PD fusion proteins were transiently expressed in *N. benthamiana* epidermal cells. Data was collected at 24, 48, and 72 hours post infiltration using confocal microscopy. No signal was detected at 12 hours post infiltration. Scale bar = 20 µm.

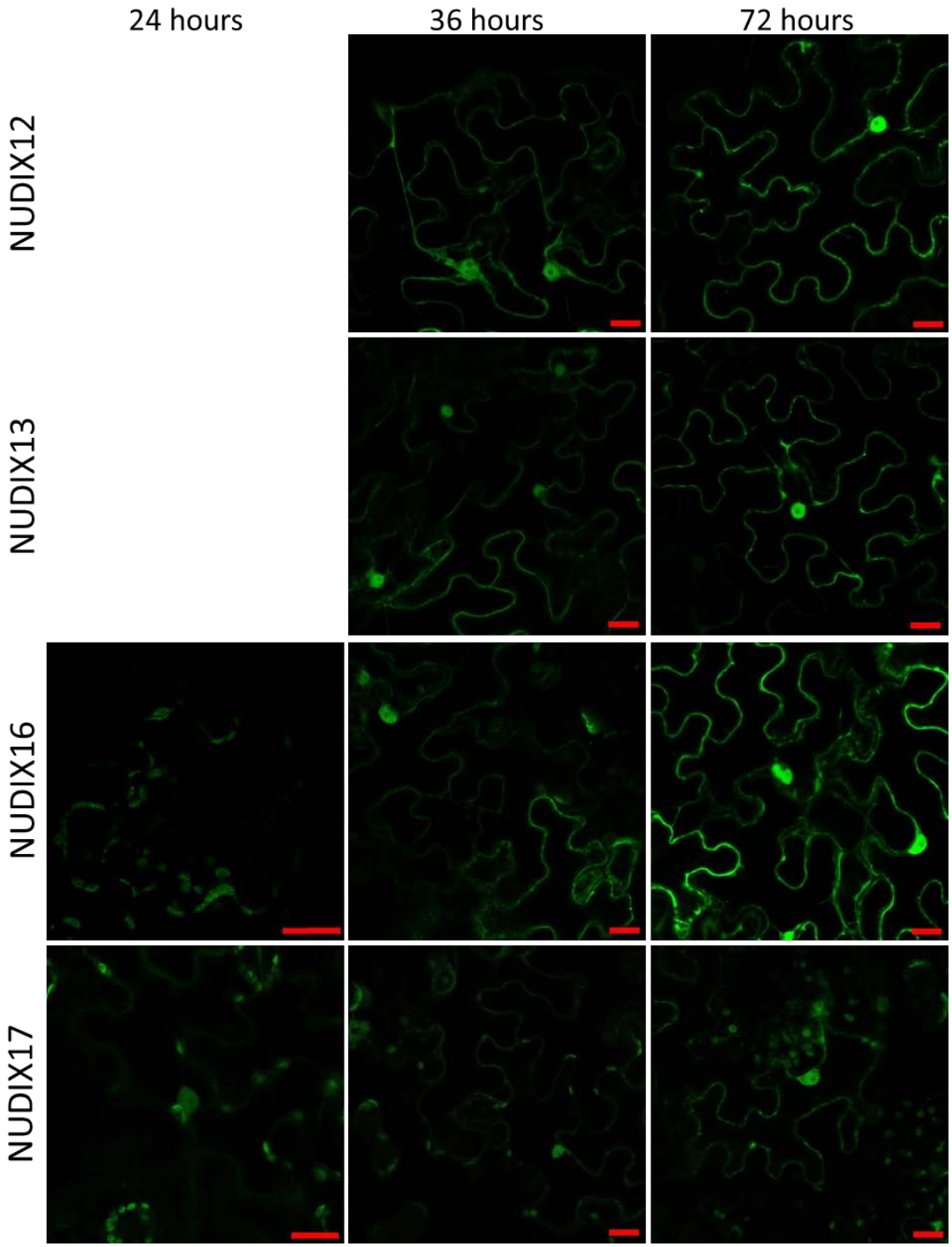

Figure 4.28. Supplemental Data: Time Course NUDIX12-, NUDIX13-, NUDIX16-, NUDIX17-GFP

NUDIX12-, NUDIX13-, NUDIX16-, NUDIX17-GFP fusion proteins were transiently expressed in *N. benthamiana* epidermal cells. Data was collected at 24, 36 and 72 hours post infiltration using confocal microscopy. No signal was detected at 12 hours post infiltration and 24 hours post infiltration for NUDIX12- and NUDIX13-GFP. Scale bar = 20 µm.

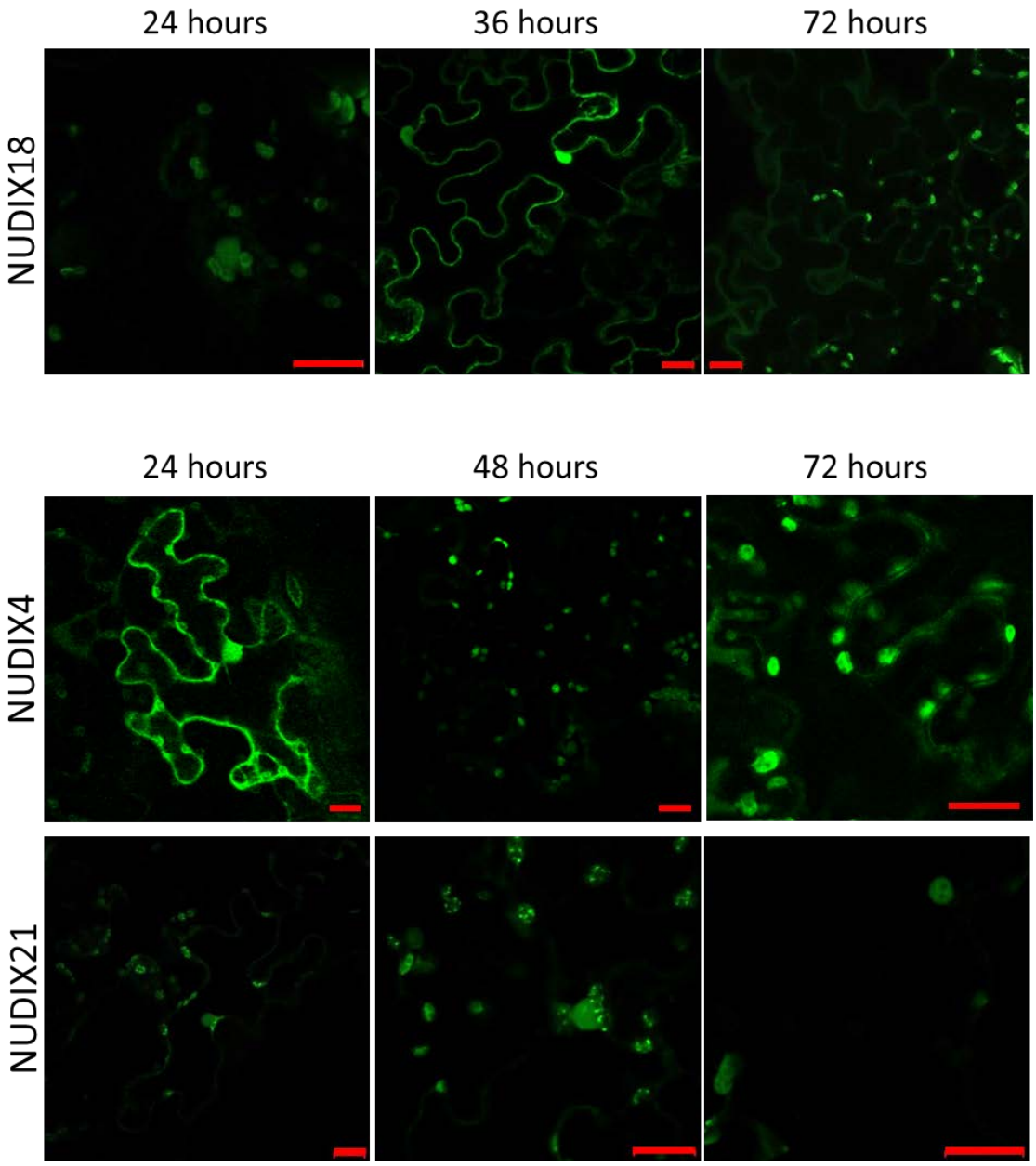

Figure 4.29. Supplemental Data: Time Course NUDIX18-, NUDIX4-, NUDIX21-GFP

NUDIX18-, NUDIX4-, NUDIX21-GFP fusion proteins were transiently expressed in *N. benthamiana* epidermal cells. Data was collected at 24, 36 or 48 and 72 hours post infiltration using confocal microscopy. No signal was detected at 12 hours post infiltration. Scale bar = 20 µm.

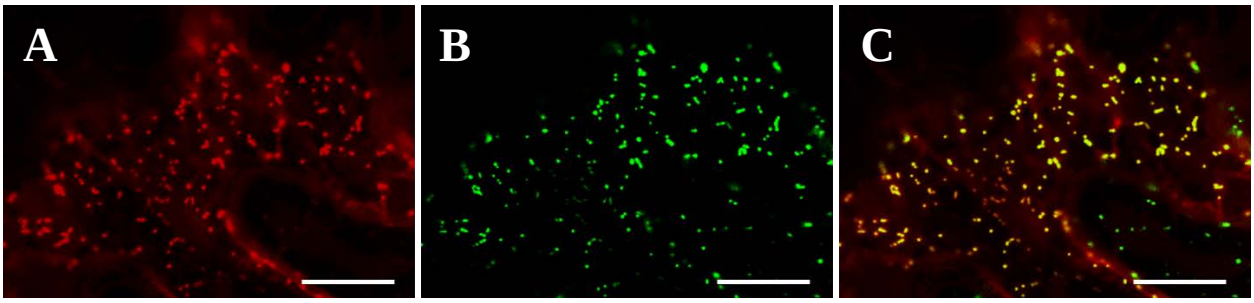

Figure 4.30. Supplemental Data: Subcellular Localization of mMDH-GFP

Mitochondrial Malate Dehydrogenase (mMDH)-GFP fusion protein was transiently co-expressed with mCherry mitochondrial marker protein in *N. benthamiana* epidermal cells. Data shown is from 48 hours post infiltration. (A) mitochondria mCherry marker (B) mMDH-GFP (C) A and B merged image, yellow indicates co-localization

REFERENCES

1. G. E. Gillaspy, The role of phosphoinositides and inositol phosphates in plant cell signaling. *Adv Exp Med Biol* **991**, 141 (2013).
2. C. J. Barker, P. O. Berggren, New horizons in cellular regulation by inositol polyphosphates: insights from the pancreatic beta-cell. *Pharmacol Rev* **65**, 641 (Apr, 2013).
3. S. B. Shears *et al.*, Defining signal transduction by inositol phosphates. *Subcell Biochem* **59**, 389 (2012).
4. M. M. Tsui, J. D. York, Roles of inositol phosphates and inositol pyrophosphates in development, cell signaling and nuclear processes. *Adv Enzyme Regul* **50**, 324 (2010).
5. M. Desai *et al.*, Two Inositol Hexakisphosphate Kinases Drive Inositol Pyrophosphate Synthesis in Plants. *Plant J*, (Sep 17, 2014).
6. D. Laha *et al.*, VIH2 Regulates the Synthesis of Inositol Pyrophosphate InsP8 and Jasmonate-Dependent Defenses in Arabidopsis. *Plant Cell* **27**, 1082 (Apr, 2015).
7. G. E. Gillaspy, The cellular language of myo-inositol signaling. *New Phytol* **192**, 823 (Dec, 2011).
8. S. I. Kim, C. B. Andaya, S. S. Goyal, T. H. Tai, The rice OsLpa1 gene encodes a novel protein involved in phytic acid metabolism. *Theor Appl Genet* **117**, 769 (Sep, 2008).
9. V. Raboy, The ABCs of low-phytate crops. *Nat Biotechnol* **25**, 874 (Aug, 2007).
10. R. Nagy *et al.*, The Arabidopsis ATP-binding cassette protein AtMRP5/AtABCC5 is a high affinity inositol hexakisphosphate transporter involved in guard cell signaling and phytate storage. *J Biol Chem* **284**, 33614 (Nov 27, 2009).
11. L. Bohn, A. S. Meyer, S. K. Rasmussen, Phytate: impact on environment and human nutrition. A challenge for molecular breeding. *Journal of Zhejiang University. Science. B* **9**, 165 (02/18/2008).
12. S. T. Yong *et al.*, Identification of a functional nuclear translocation sequence in hPPIP5K2. *BMC Cell Biology* **16**, 17 (06/18/2015).
13. C. B. Dieck, W. F. Boss, I. Y. Perera, A Role for Phosphoinositides in Regulating Plant Nuclear Functions. *Frontiers in plant science* **3**, 50 (03/16/2012).
14. J. L. Donahue *et al.*, The Arabidopsis thaliana Myo-Inositol 1-Phosphate Synthase1 Gene Is Required for Myo-inositol Synthesis and Suppression of Cell Death. *The Plant Cell* **22**, 888 (03/09/2010).
15. J. Shi, H. Wang, J. Hazebroek, D. S. Ertl, T. Harp, The maize low-phytic acid 3 encodes a myo-inositol kinase that plays a role in phytic acid biosynthesis in developing seeds. *Plant J* **42**, 708 (Jun, 2005).
16. A. R. Stiles, X. Qian, S. B. Shears, E. A. Grabau, Metabolic and signaling properties of an Itpk gene family in Glycine max. *FEBS Lett* **582**, 1853 (Jun 11, 2008).
17. E. Kraszewska, The plant Nudix hydrolase family. *Acta Biochim Pol* **55**, 663 (2008).
18. S. T. Safrany *et al.*, A novel context for the 'MutT' module, a guardian of cell integrity, in a diphosphoinositol polyphosphate phosphohydrolase. *EMBO J* **17**, 6599 (Nov 16, 1998).
19. N. R. Leslie, A. G. McLennan, S. T. Safrany, Cloning and characterisation of hAps1 and hAps2, human diadenosine polyphosphate-metabolising Nudix hydrolases. *BMC biochemistry* **3**, 20 (Jul 16, 2002).

20. K. Hidaka *et al.*, An adjacent pair of human NUDT genes on chromosome X are preferentially expressed in testis and encode two new isoforms of diphosphoinositol polyphosphate phosphohydrolase. *J Biol Chem* **277**, 32730 (Sep 6, 2002).
21. S. W. Ingram, S. T. Safrany, L. D. Barnes, Disruption and overexpression of the Schizosaccharomyces pombe aps1 gene, and effects on growth rate, morphology and intracellular diadenosine 5',5'''-P1,P5-pentaphosphate and diphosphoinositol polyphosphate concentrations. *Biochem J* **369**, 519 (Feb 1, 2003).
22. S. T. Safrany *et al.*, The diadenosine hexaphosphate hydrolases from Schizosaccharomyces pombe and Saccharomyces cerevisiae are homologues of the human diphosphoinositol polyphosphate phosphohydrolase. Overlapping substrate specificities in a MutT-type protein. *J Biol Chem* **274**, 21735 (Jul 30, 1999).
23. S. W. Ingram, S. A. Stratemann, L. D. Barnes, Schizosaccharomyces pombe Aps1, a diadenosine 5',5' ''-P1, P6-hexaphosphate hydrolase that is a member of the nudix (MutT) family of hydrolases: cloning of the gene and characterization of the purified enzyme. *Biochemistry* **38**, 3649 (Mar 23, 1999).
24. D. Kerk *et al.*, The complement of protein phosphatase catalytic subunits encoded in the genome of Arabidopsis. *Plant Physiol* **129**, 908 (Jun, 2002).
25. F. Sievers *et al.*, Fast, scalable generation of high-quality protein multiple sequence alignments using Clustal Omega. *Molecular systems biology* **7**, 539 (2011).
26. D. Winter *et al.*, An "Electronic Fluorescent Pictograph" browser for exploring and analyzing large-scale biological data sets. *PLoS One* **2**, e718 (2007).
27. B. K. Nelson, X. Cai, A. Nebenfuhr, A multicolored set of in vivo organelle markers for co-localization studies in Arabidopsis and other plants. *Plant J* **51**, 1126 (Sep, 2007).
28. D. Zhang, A. Vjestica, S. Oliferenko, Plasma membrane tethering of the cortical ER necessitates its finely reticulated architecture. *Current biology : CB* **22**, 2048 (Nov 6, 2012).
29. L. B. Sheard *et al.*, Jasmonate perception by inositol phosphate-potentiated COI1-JAZ co-receptor. *Nature* **468**, 400 (10/06, 2010).
30. X. Tan *et al.*, Mechanism of auxin perception by the TIR1 ubiquitin ligase. *Nature* **446**, 640 (Apr 5, 2007).
31. C. S. Weirich *et al.*, Activation of the DExD/H-box protein Dbp5 by the nuclear-pore protein Gle1 and its coactivator InsP6 is required for mRNA export. *Nature cell biology* **8**, 668 (Jul, 2006).
32. H. J. Xia *et al.*, Arabidopsis inositol polyphosphate 6-/3-kinase is a nuclear protein that complements a yeast mutant lacking a functional ArgR-Mcm1 transcription complex. *Plant Cell* **15**, 449 (Feb, 2003).
33. H. Chi *et al.*, Multiple inositol polyphosphate phosphatase: evolution as a distinct group within the histidine phosphatase family and chromosomal localization of the human and mouse genes to chromosomes 10q23 and 19. *Genomics* **56**, 324 (Mar 15, 1999).
34. C. Dingwall, R. A. Laskey, Protein import into the cell nucleus. *Annual review of cell biology* **2**, 367 (1986).
35. H. Wang *et al.*, Asp1 from Schizosaccharomyces pombe Binds a [2Fe-2S] Cluster Which Inhibits Inositol Pyrophosphate 1-Phosphatase Activity. *Biochemistry*, (Oct 9, 2015).

36. N. A. Gokhale, A. Zaremba, S. B. Shears, Receptor-dependent compartmentalization of PPIP5K1, a kinase with a cryptic polyphosphoinositide binding domain. *Biochem J* **434**, 415 (Mar 15, 2011).
37. K. Nakai, P. Horton, PSORT: a program for detecting sorting signals in proteins and predicting their subcellular localization. *Trends Biochem Sci* **24**, 34 (Jan, 1999).
38. K. Olejnik, M. W. Murcha, J. Whelan, E. Kraszewska, Cloning and characterization of AtNUDT13, a novel mitochondrial Arabidopsis thaliana Nudix hydrolase specific for long-chain diadenosine polyphosphates. *FEBS J* **274**, 4877 (Sep, 2007).
39. O. Emanuelsson, H. Nielsen, G. von Heijne, ChloroP, a neural network-based method for predicting chloroplast transit peptides and their cleavage sites. *Protein science : a publication of the Protein Society* **8**, 978 (May, 1999).
40. M. Ferro *et al.*, AT_CHLORO, a comprehensive chloroplast proteome database with subplastidial localization and curated information on envelope proteins. *Molecular & cellular proteomics : MCP* **9**, 1063 (Jun, 2010).
41. T. Kleffmann *et al.*, The Arabidopsis thaliana chloroplast proteome reveals pathway abundance and novel protein functions. *Current biology : CB* **14**, 354 (Mar 9, 2004).
42. J. Kapila, R. DeRycke, M. Van Montagu, G. Angenon, An Agrobacterium-mediated transient gene expression system for intact leaves. *Plant Sci* **122**, 101 (1997).
43. B. K. Nelson, X. Cai, A. Nebenfuhr, A multicolored set of in vivo organelle markers for co-localization studies in Arabidopsis and other plants. *Plant J* **51**, 1126 (Sep, 2007).
44. R. N. Burnette, B. M. Gunesekera, G. E. Gillaspy, An Arabidopsis inositol 5-phosphatase gain-of-function alters abscisic acid signaling. *Plant Physiol* **132**, 1011 (Jun, 2003).
45. J. Stevenson-Paulik, R. J. Bastidas, S. T. Chiou, R. A. Frye, J. D. York, Generation of phytate-free seeds in Arabidopsis through disruption of inositol polyphosphate kinases. *Proc Natl Acad Sci U S A* **102**, 12612 (Aug 30, 2005).
46. J. Stevenson-Paulik, A. R. Odom, J. D. York, Molecular and biochemical characterization of two plant inositol polyphosphate 6-/3-/5-kinases. *J Biol Chem* **277**, 42711 (Nov 8, 2002).

SUMMARY AND FUTURE WORK

Through this work, I have explored connections between inositol phosphate (InsP) signaling and energy responses in plants. I examined two aspects of these connections, the low energy sensor SnRK1 and the PPx-InsPs, a new class of InsP signaling molecules.

The first study examined differential expression of SnRK1.1 and SnRK1.2 in plants and investigated how different SnRK1 isoforms reprogram growth and development. Interactions between SnRK1 and the InsP signaling pathway is already known as SnRK1 and 5PTase13 are part of a protein complex. Since preliminary data from the Gillaspy lab suggests that there is a protein interaction between SnRK and VIP, future work should address the nature of this interaction and the role of PPx-InsPs in low energy responses in plants. Specifically, is VIP a target of SnRK phosphorylation and do SnRK mutant plants have altered PPx-InsP profiles?

The second part of this work examines a new group of InsPs. It quantifies PPx-InsPs in plants, and characterizes a family of kinases (AtVIPs) capable of catalyzing synthesis of PPx-InsPs, along with an examination of the subcellular localization of PPx-InsP synthesis. I identified the nucleus, ER and chloroplasts as potential locations of PPx-InsPs. Future work should confirm the presence of $InsP_6$ and PPx-InsPs in these organelles. Current experiments are underway to use Titanium oxide (TiO) beads to pull down InsPs from purified nuclei and chloroplasts. A very recent publication illustrated how this approach can be used to purify $InsP_6$ and PPx-InsPs from *Dictyostelium discoideum* cells, and animal tissues including human blood and urine (*1*). After purification with TiO beads, InsPs could be separated and identified by both PAGE (*2*) and Mass Spectrometry (MS) analysis. Preliminary results from our lab suggest that this technique

can be applied to seed and leaf tissue. Purified nuclei were also tested and a preliminary trial suggests that at least one higher InsP is found in this organelle. Based on the migration of this InsP, it is most likely $InsP_6$. Recent work has suggested a nuclear role of $InsP_8$ as a cofactor in the Jasmonic acid receptor (*3*).

A separate approach that is likely to advance the connection between PPx-InsPs and energy sensing is to profile InsPs produced under various energy conditions. AtVip double mutants have been generated and preliminary data indicates they are smaller and bolt later under low energy, suggesting that PPx-InsP are important to responses to low energy conditions.

REFERENCES

1. M. S. Wilson, S. J. Bulley, F. Pisani, R. F. Irvine, A. Saiardi, A novel method for the purification of inositol phosphates from biological samples reveals that no phytate is present in human plasma or urine. *Open Biol* **5**, 150014 (Mar, 2015).
2. O. Losito, Z. Szijgyarto, A. C. Resnick, A. Saiardi, Inositol pyrophosphates and their unique metabolic complexity: analysis by gel electrophoresis. *PLoS One* **4**, e5580 (2009).
3. D. Laha *et al.*, VIH2 Regulates the Synthesis of Inositol Pyrophosphate InsP8 and Jasmonate-Dependent Defenses in Arabidopsis. *Plant Cell* **27**, 1082 (Apr, 2015).